Confidential

Establishing and improving a liver abscess model for future mitigation experimentation in beef-on-dairy crossbred cattle

Final Study Report

Study Number: GJC-LHB-3

Principal Investigator: Lance H. Baumgard, PhD
baumgard@iastate.edu
515-294-3615

Associate Principal Investigator: Johana Mayorga, PhD
jmayorga@iastate.edu
515-291-4867

Graduate Student: Gaelan Combs
gcombs@iastate.edu
608-293-3726

Study Location: Iowa State University
Ames, Iowa 50011

Study Start Date: February 11th, 2025

Study End Date: June 12th, 2025

Liver Abscess Induction Model
Study Number: GJC-LHB-3

Signature Page

Primary Investigator:

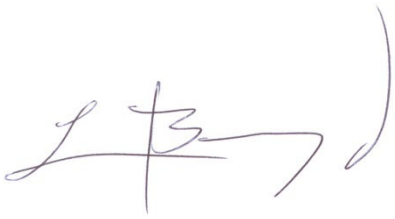

_____ _____

Lance H. Baumgard Date

Sponsor monitor / Person responsible:

_____ _____

Iowa Beef Industry Center Date

Kemin Industries Date

Table of Contents

List of Tables

List of Figures

Liver Abscess Induction Model
Study Number: GJC-LHB-3

Abstract

Objectives were to create a repeatable liver abscess (**LA**) induction model to identify phenotypic indicators and proteomic signatures of LA formation. Beef × dairy calves (n=32; 114.0 ± 13.9 kg) were enrolled across 2 replicates (**Rep**; n=16/rep) and assigned to either control (**CON**; n=14) or LA induction protocol (**LAIP**; n=18) for 42 d. CON calves received a low starch (**LS**; 29% NSC) diet *ad libitum* throughout the study. Starting on d 1, LAIP calves received 4 rumen acidosis cycles consisting of 3 d of a high-starch (**HS**; 50% NSC) diet followed by 2 d of LS. After acidotic cycles, LAIP calves were fasted for 16 h on d 20 and 22 with a ruminal inoculation (**RI**) of *Fusobacterium necrophorum* subsp. *necrophorum* and *Salmonella* Lubbock (10^{10} CFU/calf) on d 23. Following the RI, LAIP calves received the HS diet and were fasted again on d 24 and 26, followed by 3 d of LS, and received a second RI on d 30. After the 2nd RI, LAIP-fed calves remained on HS and all calves were euthanized on d 42. Data were analyzed using PROC MIXED of SAS and hepatic proteins were analyzed using the ClusterProfiler package in R. In Rep 1, 4 of 8 LAIP calves developed LA (Fisher's P=0.04), but no Rep 2 calves developed LA. LAIP calves tended to consume less feed than CON from the 2nd RI until euthanasia (1.3 kg; P=0.06) and had decreased ADG (P<0.01), leading to reduced live weight at d 42 in both Rep (15 kg; P<0.01). At euthanasia, LAIP calves developed eosinophilia (24%; P<0.01) and tended to have increased basophil counts from RI to euthanasia (9%; P=0.09). Rep 1 LAIP calves developed a transient pyretic response to both RI (0.2°C vs CON; P<0.01), but Rep 2 LAIP calves did not develop a febrile response to either RI. *Post hoc* analysis of successful (**LAIP-Y**; n=4) vs. unsuccessful (**LAIP-N**; n=4) LA formation in Rep 1 revealed neutrophilia in LAIP-Y vs. LAIP-N (54%; P<0.01). LAIP-Y steers had increased liver weight compared to LAIP-N (2.4 vs. 2.0% of BW). There were no differences in circulating liver health enzymes or acute phase proteins following either RI (P>0.15) between LAIP-Y and LAIP-N. Proteomic analysis of liver proteins identified that LAIP upregulated cellular immunity (i.e. neutrophil extracellular trap formation; P<0.01) and downregulated amino acid (Gly, Ser, Thr, and Trp) metabolism, thermogenesis, and oxidative phosphorylation (P<0.05). The 'mineral absorption' pathway was upregulated in LAIP-Y relative to CON (P<0.01) and tended to be upregulated in LAIP-Y relative to LAIP-N (P<0.08), driven by increased (13-fold) abundance of metallothioneins in LAIP-Y vs LAIP-N. Complement and coagulation cascades tended to be upregulated in LAIP-Y vs LAIP-N and were upregulated in LAIP-Y vs CON, driven by increased abundance (>2.5-fold; P≤0.04) of complement factor D, von Willebrand factor, and cathelicidins. LAIP-Y, but not LAIP-N, increased pathway enrichment of Fc-γ R-mediated phagocytosis, integrin signaling, and natural killer cell-mediated cytotoxicity relative to CON (P<0.10). Abundance of proteins involved in cytochrome P450, endocannabinoid, PPAR signaling, and bile metabolism decreased in LAIP-Y vs CON (<0.5-fold; P≤0.04). Reasons for the inconsistency in the LA induction model are not clear and there appears to be very few differences in variables measured herein, other than LAIP-Y appearing to have more of an immune response to the RI at the hepatic and systemic level.

Liver Abscess Induction Model
Study Number: GJC-LHB-3

1.0 Introduction

Liver abscesses (**LA**) compromise animal health productivity and are a concern for the beef industry at large. LA are associated with decreased average daily gain pre-harvest as well as increased viscera loss at the abattoir, which ultimately decreases feedlot productivity and profitability for beef producers (Amachawadi and Nagaraja, 2016).

While described in the literature for over 80 years (Smith, 1944), considerable uncertainty remains regarding the formation of LA, and thus reliable models to generate LA remain elusive (Saginala et al., 1997; McDaniel et al., 2023, 2024). Furthermore, increased use of Angus × Holstein calves in the beef supply chain over the last 15 years has increased the prevalence of liver abscesses at abattoirs (Amachawadi and Nagaraja, 2016). Taken together, the incomplete understanding of LA and increased risk with crossbred calves necessitates further research into the causes of abscess formation, especially in at-risk groups.

Conventional theories regarding LA etiology implicate ruminal permeability to *Fusobacterium necrophorum* as the primary etiologic agent of LA formation (Scanlan and Hathcock, 1983, Amachawadi et al., 2017). The passage of *F. necrophorum* across the ruminal epithelia and into portal circulation presumably allows for abscess formation in the liver as they overwhelm host defenses (Nagaraja and Lechtenberg, 2007). Recently, however, the potential role of hindgut permeability in LA formation has received attention (Jennings et al., 2021; McDaniel et al., 2024) as the hindgut separates luminal contents from portal circulation by a singular layer of columnar epithelia, compared to four layers of tissue in the rumen (Steele et al., 2016). Our laboratory has implicated the role of hindgut permeability in a host of on-farm stressors for dairy cattle, including feed restriction (Horst et al., 2020; Goetz et al., 2023b), hindgut acidosis (Abeyta et al., 2023a,b,c), heat stress (Sanz Fernandez et al., 2014; Opgenorth et al., 2021), and the transition to lactation (Goetz et al., 2023a). However, the role of the hindgut in LA formation is yet unknown.

A current strategy to reduce LA incidence is dietary antibiotic supplementation with Tylosin Phosphate for all animals upon entry to the feedlot (Brown et al., 1975). Due to changing consumer perception and increased risk of antibiotic resistance, however, these strategies are under greater scrutiny. LA identification via blood or ultrasound is currently not reliable *in vivo,* and thus, more research is warranted into potential predictive biomarkers of LA progression pre-harvest to select animals for targeted therapeutic treatment.

2.0 Study objectives

Objectives were to develop a repeatable and reliable model of liver abscess induction in growing steers and identify biomarkers in blood and/or feces associated with the development of a liver abscess to detect abscess progression *in vivo.*

3.0 Overview of experimental design

3.1 Study live phase start and end dates:

Live phase started on: February 11th, 2025
Live phase completed on: June 12th, 2025
Laboratory analysis completed on: February 24th, 2026

3.2 Animals

Thirty-two weaned Angus × Holstein calves (31 steers and 1 heifer; 114.0 ± 13.9 kg initial BW) were purchased from a commercial farm in South Dakota and brought to the Animal Metabolism Room in Kildee Hall (Ames, IA), where they were placed in individual metabolism crates (1.37 x 0.91 m). The room maintained a constant temperature and humidity (17.0 ± 0.6°C; 56.4 ± 10.0% relative humidity) and was subjected to 12.5 h light cycles daily. Due to space constraints, the experiment was divided into two replicates. Steers began a 3-d electrolyte therapy following transit (Bluelite; Techmix, LLC, Stewart, MN), and animals in replicate 2 (n = 16) were started on a 5-d oral gavage of amprolium suspension (Corid 9.6% solution; Huvepharma, Inc., Peachtree, GA). Within 24 h of arrival, all animals were administered a metaphylactic dose of florfenicol (Nuflor; Merck Animal Health, Rahway, NJ) subcutaneously at a rate of 40 mg/kg of body weight to alleviate the risk of bovine respiratory disorder (**BRD**). Two animals with symptoms of BRD shortly after arrival were given florfenicol i.m. and administered flunixin meglumine (Banamine; Merck Animal Health, Rahway, NJ) to alleviate pyrexia instead of the aforementioned subcutaneous dose.

Calves were stratified by body weight and assigned to one of two treatments: 1) a low-starch, high fiber control diet (**CON**; n = 14), or 2) a liver abscess induction protocol (**LAIP**; n = 18). Animals were given 5 d of acclimation before treatment periods began. Diets were formulated to meet or exceed the predicted requirements (NASEM, 2016) of energy, protein, minerals, and vitamins (Table 1). All procedures were approved by the Iowa State University Institutional Animal Care and Use Committee and Institutional Biosafety Committee (IACUC # 24-165; IBC # 24-122).

3.3 Experimental phase

The data collection phase of the trial consisted of two experimental periods. Period 1 (**P1**) lasted 4 d, during which all calves were fed a low-starch (**LS**) diet and served as the baseline. Period 2 (**P2**) lasted 42 d and marked the beginning of interventions for LAIP to induce gastrointestinal hyperpermeability.

Briefly, CON calves were fed a low-starch, high-fiber diet *ad libitum* throughout P1 and P2. At the beginning of P2, LAIP were abruptly switched from a LS diet to a high starch (HS) ration with low effective fiber for 3 d, followed by 2 d of recovery on a LS ration. This cycle of HS and LS was repeated 4 times, and following the fourth acidotic cycle, LAIP were given 4 d of the LS diet prior to intraruminal inoculation (**RI**) of *Fusobacterium necrophorum* (100 mL; 10^{10} CFUs/calf) and *Salmonella enterica* serovar Lubbock (100 mL; 10^{10} CFUs/calf). Immediately following inoculation, LAIP were switched to a HS ration for 4 d, followed by 3 d of LS and a second RI of *F. necrophorum* and *S. enterica*. Surrounding the initial RI, LAIP were fasted for 16 h on d –3, -1, 2, and 4 relative to the first ruminal inoculation (i.e. fasting occurred on d

20, 22, 24, and 26 of P2) and LAIP returned to *ad libitum* feeding at 2300 h. Following the second RI, LAIP remained on the HS ration for 13 d until euthanasia.

Following d 42 of P2, steers were transported at 0700 h to the ISU Livestock Infectious Disease Isolation Facility (Ames, IA), humanely euthanized via captive bolt technique followed by exsanguination, and immediately necropsied. Wet weights of liver, lung, and spleen were collected, and gross pathology of the rumen, jejunum, ileum, colon, lung, spleen, and liver was assessed by a veterinary pathologist in a semiquantitative fashion based on modified scoring systems from published literature (See Table 1; Brown et al., 1975; Mansfield and Urban, 1996; Rezac et al., 2014; Tennant et al., 2014; Offersen et al., 2024).

3.3.1 Preparation of live bacteria

Live cultures of *Fusobacterium necrophorum* subsp. *necrophorum* (strain 8L1) and *Salmonella enterica* (serovar Lubbock; strain 2016-13-36) were prepared from frozen cultures prior to inoculation. *F. necrophorum* was inoculated into prereduced, anaerobically sterilized Brain Heart Infusion broth (PRAS-BHI; Becton-Dickinson, Franklin Lakes, NJ) for the entire culturing process, while *S. enterica* was cultured into Tryptic soy broth. Briefly, *F. necrophorum* and *S. enterica* were thawed, streaked onto separate blood agar plates, and incubated at 37°C for 48 h for colony growth. A single colony of each bacterium was inoculated into 10 mL of their respective broth and incubated overnight at 37°C. Following incubation, 3 mL of culture was inoculated into 100 mL of broth in serum bottles and incubated for 6 h at 37°C. This step was repeated once more, and the culture was incubated for an additional 14-16 h to achieve the final inoculation dose.

3.3.1 Inoculation procedure

All cattle in the LAIP treatment were inoculated at 0900 on d 23 and 30 of P2. Steers were restrained in a body chute, and a Fick speculum was inserted into the mouth to the oropharynx. Flexible tubing fitted with a rounded bulb and funnel was inserted into the speculum, and passage into the esophagus was confirmed by a veterinarian. Tubing was fed into the reticulorumen where one bottle each of *S. enterica* and *F. necrophorum* (10^{10} CFU/calf) were slowly poured into the esophageal tube. A final rinse of 300 mL of sterile phosphate buffered saline (**PBS**) followed dosing to ensure passage of inoculum into the rumen. Feed was withheld from 0700 until following inoculation (~0930) to ensure adequate rumen pH for bacterial survival.

Table 1. Scoring systems used in gross tissue pathology.

Organ	Adapted from	Scale	Comments
Liver[1]	Brown et al., 1975	0, A-, A, A+	0: No abscesses or scar tissue. A-: ≤ 2 abscesses present and all ≤ 2 cm in diameter. A: 2-4 abscesses present 2-4 cm in diameter. A+: ≥ 1 abscess > 4 cm in diameter or > 4 abscesses > 2 cm in diameter.
Lung	Tennant et al., 2014	0-5	0: No lesions observed. 1: Fibrin tag formation or interlobular adhesions between lobes. 2: Consolidation of lung lobes or mycoplasma-like lesions affecting < 5% of tissue. 3: Consolidation of lung lobes or mycoplasma-like lesions affecting 5-15% of tissue. 4: Multiple adhesions or portions of lung missing affecting 15-50% of tissue. 5: Multiple adhesions or portions of lung missing affecting > 50% of tissue and active bronchial lymph nodes.
Spleen	-	0-3	0: Normal size and appearance, no nodules or congestion. 1: Slight enlargement, capsule thickening, mild fibrosis, mild dark red or purple discoloration. 2: Moderate enlargement, darkening and blood pooling present, 2-5 mm nodules and local fibrosis. 3: Enlargement >50% of normal size, severe discoloration with purple/black color, nodules > 5 mm and extensive fibrosis with hardening of the organ.
Rumen	Rezac et al., 2014	0-2	0: Healthy; thick, lush papillae, no inflammation or ulceration. 1: Consolidated portions of denuded papillae. 2: Acute lesions across the rumen, ulcerations present either as circular, depressed red foci or ulceration scars star-shaped and devoid of papillae.
Jejunum & Ileum	Offersen et al., 2024	0-3	1: Hyperemia or local hemorrhage. 2: Extensive hemorrhage. 3: Necrosis present and/or pneumatosis intestinalis. 3: Necrosis present and/or pneumatosis intestinalis.
Colon	Mansfield and Urban, 1996	0-3	0: Healthy; unaffected by parasites or bacteria, smooth, tan. 0.5-1.5 mm thick with lymphoid tissue. 1: Patchy areas of hemorrhage (< 50% of area) and slightly roughened surface. 1.51-2.5 mm thick with minor immune cell infiltration to lymphoid tissue. 2: Hemorrhagic (> 50% of surface) and markedly roughened. >2.50 mm thickness with pus and debris within the lymphoid tissue. 3: Fibronecrotic pseudomembrane covers the colon. >2.50 mm thickness with sloughing of mucosa and pus within the lymphoid tissue.

[1]Subsclassification of livers with scaration but no active abscess (0Sc) and A+ livers either with open abscess (A+Open) or abscesses adhered to the abdomen (A+Adhesion) were also noted.

3.4 Diet mixing and administration

Diets were mixed at the ISU Beef Nutrition farm and stored indoors in covered totes until feeding. Six batches of LS and three batches of HS were milled, and samples were collected. Following study completion, batches were composited into a single representative sample and sent for wet chemistry analysis (Dairyland Laboratories, Arcadia, WI) for carbohydrate, lipid, protein, and ash content.

3.5 Daily measurements

3.5.1 Vitals

During P1 and P2, respiration rate (**RR**) and rectal temperature (**Tr**) were measured daily at 0700 and 1800 h. RR was determined by observing flank movements over a 15 sec interval, and this measurement was multiplied by 4 to obtain breaths per minute (breaths/min). Rectal temperatures were measured using a standard digital thermometer (GLA M700 Digital Thermometer, San Luis Obispo, CA).

3.5.2 Dry matter intake (DMI), body weight, and productivity

Feed was offered once daily during P1 and P2 (0700 h) following RR and Tr data collection unless animals were feed restricted. Orts were collected, weighed, and feed delivery was adjusted to achieve a 10% refusal rate. Body weights were obtained on a livestock scale (Tru-Test 700 Series scale; Mount Wellington, Auckland, New Zealand) immediately before blood samples collection at the ends of acclimation, P1, and on d 3, 8, 13, 18, 20, 22, 24, 26, 30, and 42 during P2. Between the end of acclimation and P1, P1 and d 18 of P2, d 20 and d 26 of P2, d 30 and d 42 of P2, and from end of P1 through the end of P2, the change in body weight over time was used to calculate average daily gain (**ADG**) and ADG was then divided by feed intake to calculate gross feed efficiency (GFE; ADG:DMI).

3.6 Serum, plasma, and fecal analysis

Blood and fecal samples were collected at 0600 h at the ends of acclimation, P1, and on d 3, 8, 13, 18, 20, 22, 24, 26, 30, and 42 during P2. All fecal collections were obtained through manual stimulation immediately prior to blood sample analysis. Fecal pH was determined using a 1:1 dilution of fecal matter with distilled water and homogenized using a laboratory blender (Lab-Blender Stomacher 80, Seward Ltd, West Sussex, UK). Following sample homogenization, fecal pH was assessed using a portable pH meter (Orion Star A121, Thermo Fisher Scientific, Waltham, MA). Feces was aliquoted into a 15mL conical tube for storage at -20°C for further analysis, or into a 2mL microtube for storage at -80°C until further analysis for bacterial 16S DNA sequencing at Kemin Industries (Des Moines, IA).

Animals were briefly restrained and skin was cleaned with an ethanol wipe prior to jugular venipuncture for blood collection. Blood was collected from the right jugular vein directly into disposable tubes containing a clot activator for serum analysis (BD®, Franklin Lakes, NJ) or K_2EDTA for plasma harvest and complete blood cell (**CBC**) count (BD®, Franklin Lakes, NJ) at the end of P1 and on d 18, 22, 30, and 42 of P2. Serum samples were allowed to clot at room temperature for 1 h prior to centrifugation. Plasma and serum were harvested following centrifugation at 2,000 × *g* for 15 min at 4°C and were subsequently frozen at -20°C until analysis. An additional set of serum and plasma (150 µL each) were stored at -80°C until analysis. Samples for CBC were stored at 4°C with regular agitation for up to 48 h until submission to Iowa State University's Department of Veterinary Pathology (Ames, IA).

Serum glucose, blood urea nitrogen (**BUN**), creatinine, total protein (**TP**), albumin, globulin, alanine aminotransferase (**ALT**), alkaline phosphatase (**ALP**), aspartate aminotransferase (**AST**), total bilirubin (**Tbil**), total calcium (**Ca**), sodium (**Na**), potassium (**K**), chloride (**Cl**), and total CO_2 (**tCO_2**) were measured using the VETSCAN VS2 (model 3.3.1) with the Preventative Care Profile Plus rotor (Zoetis; Parsippany, New Jersey).

Samples collected on d 18 and 42 of P2 were analyzed in CON (n = 8) while d 18, 22, 24, 26, 30, and 42 were analyzed in LAIP steers (n = 12). Samples were thawed from -20°C, briefly centrifuged, and 100 µL of serum was dispensed into the rotor for analysis.

Plasma insulin, lipopolysaccharide binding protein (**LBP**), serum amyloid A (**SAA**), and haptoglobin (**Hp**) were determined using commercially available kits validated for use in our laboratory on a subset of animals (n=20; insulin, Mercodia AB, Uppsala, Sweden; LBP, Hycult Biotech, Uden, the Netherlands; SAA, Tridelta Development Ltd., Kildare, Ireland; Hp, Life Diagnostics, Inc., West Chester, PA). Samples were analyzed at the conclusion of P1 and on d 3, 18, 22, 30, and 42 of P2. The intra- and inter-assay coefficients of variation for insulin, LBP, SAA, and Hp assays were 1.1 and 3.2%, 3.3 and 4.4%, 3.0 and 15.2%, and 3.9 and 5.6%, respectively.

3.7 Feed analysis

Feed was mixed in a standing mixer by the Iowa State University Beef Nutrition unit (Ames, IA) and stored in totes prior to feeding. Samples of each feed mix were obtained and composited into a representative sample. Samples were submitted to Dairyland Laboratories. Inc. (Arcadia, WI) and analyzed via wet chemistry methods.

Table 2. Ingredients and composition of nutrients, DM%

Ingredient, %	**LS[1]**	**HS[2]**
Beet Pulp, Shredded	45.7	-
Soybean Meal	28.7	30.9
Corn Grain, cracked	21.3	-
Corn Grain, finely ground	-	59.7
Molasses	-	5.3
Mineral Premix[3]	3.6	4.1
Sodium Bicarbonate	0.6	-
Nutrients, %		
DM, %	88.0	87.7
CP, %	19.58	21.54
ADF, %	14.65	5.05
aNDF, %	25.74	12.08
aNDFom, %	20.43	11.77
Lignin (sulfuric acid), %	1.40	2.04
Lignin (%NDF), %	6.85	0.24
ADICP (%CP), %	3.58	2.74
NDICP (%CP), %	8.48	4.50
Prot Sol (%CP), %	11.91	19.37
EE, %	2.21	4.25
Ash, %	5.73	5.32
Ca, %	0.84	0.58
P, %	0.40	0.36
Mg, %	0.26	0.15
K, %	0.97	0.84
S, %	0.28	0.21

[1]Low-Starch Ration
[2]High-Starch Ration
[3]Formulated for 39.683 mg/kg Cu. 62.500 mg/kg Mn, 50.000 mg/kg Se, 84.507 mg/kg Zn, 6.793 mg/kg I, and 0.303 mg/kg Co. Vit A & E premix included at 0.20% of premix DM.

3.8 Post-mortem tissue collection and DNA isolation

At the conclusion of d 42 of P2, steers were transported to the Iowa State Livestock Infectious Disease Isolation Facility and euthanized by a licensed veterinarian with a CASH Special captive bolt gun (Accles & Shelvoke Ltd., Sutton Coldfield, West Midlands) using a large animal charge. The liver, lungs, spleen, and intestinal tissues were harvested posthaste following euthanasia, and wet weights of liver, lungs, and spleen were recorded (within 15 minutes). Ruminal samples were harvested from the ventral sac. A single 30-40 cm jejunal sample was collected 80 cm distal to the pyloric sphincter. One segment of the ileum, approximately 40-50 cm, was collected about 15 cm proximal to the ileocecal junction. One segment of descending colon, circa 20-30 cm, was collected approximately 30 cm proximal to the pelvic inlet. Duodenum, jejunum, ileum, and colon segments were flushed with cold saline to remove intestinal contents, fixed in 10% neutral buffered formalin for 24 h, and transferred to 70% ethanol for histological analysis. Liver samples were collected from the caudate lobe proximal to the portal triad and from the caudal portion of the right lobe. Lung samples were collected from the right caudal lobe. Splenic samples were collected from the distal portion of the organ. Visceral adipose tissue (**VAT**) was collected from the exterior of the kidneys. Urine was collected directly from the bladder via syringe postmortem. All tissue samples were snap-frozen in liquid nitrogen and stored at -80˚C until later analysis.

Prior to tissue sample collection, intestinal segments, liver, lung, spleen, and VAT were swabbed for bacterial DNA isolation. Dry transport swabs (Fischer Scientific, Waltham MA; During replicate 2, lung, ileum, jejunum, colon, and VAT were collected on swabs from Puritan Medical Products Co., Guilford, ME) were swabbed on the epithelial surface of intestinal segments immediately prior to cold saline flush to determine bacterial contents at the mucosal surface. Lung, liver, spleen, and VAT were opened, and swabs were collected from internal tissue for microbiome analysis. All swabs were taken in triplicate and stored on dry ice until storage at -80 °C. Swabs were analyzed for 16S DNA content at Kemin Industries (Des Moines, IA).

3.9 Protein isolation and proteome analysis

Snap-frozen liver samples from the right caudate lobe were homogenized in 50 µ*M* Tris HCl and 1 m*M* EDTA lysis buffer for 30 seconds following initial thaw. Samples were cooled on ice for 30 minutes and spun at 10,000 revolutions per minute (**rpm**) at 4°C for 15 minutes to separate supernatant from infranatant. Supernatant was spun again to further clarify the solution, and the final supernatant was used for protein quantification and proteomics analysis.

Protein content was assessed in clarified supernatant using commercially available bicinchoninic acid (**BCA**) assay (Pierce BCA Assay; Thermo Fisher Scientific, Waltham, MA). Protein concentration was diluted to 1000 µg/mL with Tris buffer within each sample following BCA analysis. A pooled sample of all tissues (n = 12) was made from diluted samples and frozen at -80°C until proteomic analysis for standardization between runs.

Label-free liquid chromatography-tandem mass spectrometry (**LC-MS/MS**) was performed using an Orbristrap Astral Mass Spectrometer (Thermo Fisher Scientific, Waltham, MA) at the Iowa State University Protein Core Facility (Ames, IA). Briefly, proteins were separated using gel electrophoresis, excised from gel fragments, and digested with trypsin/Lys-c on an automated digester (Investigator ProGest; Genomic Solutions; Ann Arbor, MI). Digested peptides were spiked with Peptide Retention Time Calibration (**PRTC**; Thermo Fischer Scientific, Waltham, MA) for internal control prior to column elution. Fragmentation patterns from LC-MS/MS (Agilent Zorbax SB-C18, 0.5 mm x 150 mm, 5 µm) were compared to theoretical fragmentation patterns for protein identification. Each sample was analyzed separately, and common chromatographic features were aligned across runs. PRTC peptides were excluded from downstream differential abundance analysis after normalization. Raw data were analyzed using Proteome Discoverer (Thermo Fisher Scientific, Waltham, MA) and searched against

publicly available databases using MASCOT. Protein expression was analyzed as pairwise comparisons between treatments in the *post hoc* statistical model (discussed below).

Identified protein sequences from MASCOT were catalogued by Uniprot ID within treatment, and *ad hoc* pairwise comparisons were made between treatment groups in untargeted analysis. Upper-quartile scaling normalization was taken on each pair of treatment groups, following initial normalization via PRTC peptide standardization. Normalized data were tested using Student's t-test and Shapiro-Wilk test for normality. Results were expressed as fold-change (**FC**) differences to interpret the magnitude of change using Python v. 3.10.2 running pandas 2.2.3, numpy 2.1.3, statsmodels 0.14.4, scipy 1.14.1, and sklearn 1.6.1. Significance was determined in untargeted analysis using log-transformed FC ≥ 1 and $P \leq 0.05$.

Gene-set enrichment analysis (**GSEA**; Subramanian, 2005) was performed on all pairwise comparisons to elucidate up or down-regulated pathways. Briefly, enrichment scores (**ES**) were assigned to all proteins by multiplying $\log_2$ FC and the respective negative log-transformed *P*-value within each pairwise comparison. Proteins with a valid NCBI gene ID were filtered, sorted by ES, and compared against Bos taurus pathways within the Kyoto Encyclopedia of Genes and Genomes (**KEGG**) for pathway enrichment. Proteins with valid gene symbols were filtered, sorted by ES, and compared against Bos taurus pathways within gene ontology (**GO**) biological processes (**BP**) and molecular function (**MF**) categories for pathway enrichment. GSEA was conducted on 12/27/2025 using the clusterProfiler package in R (v 4.10.1 and v 4.3.2) with gseKEGG and gseGO functions, respectively. Gene set sizes were limited to 5-500 genes and significance was declared at $P < 0.05$, with a tendency for significance at $0.05 < P \leq 0.10$. Benjamini-Hochberg adjustments were utilized to adjust for multiple comparisons.

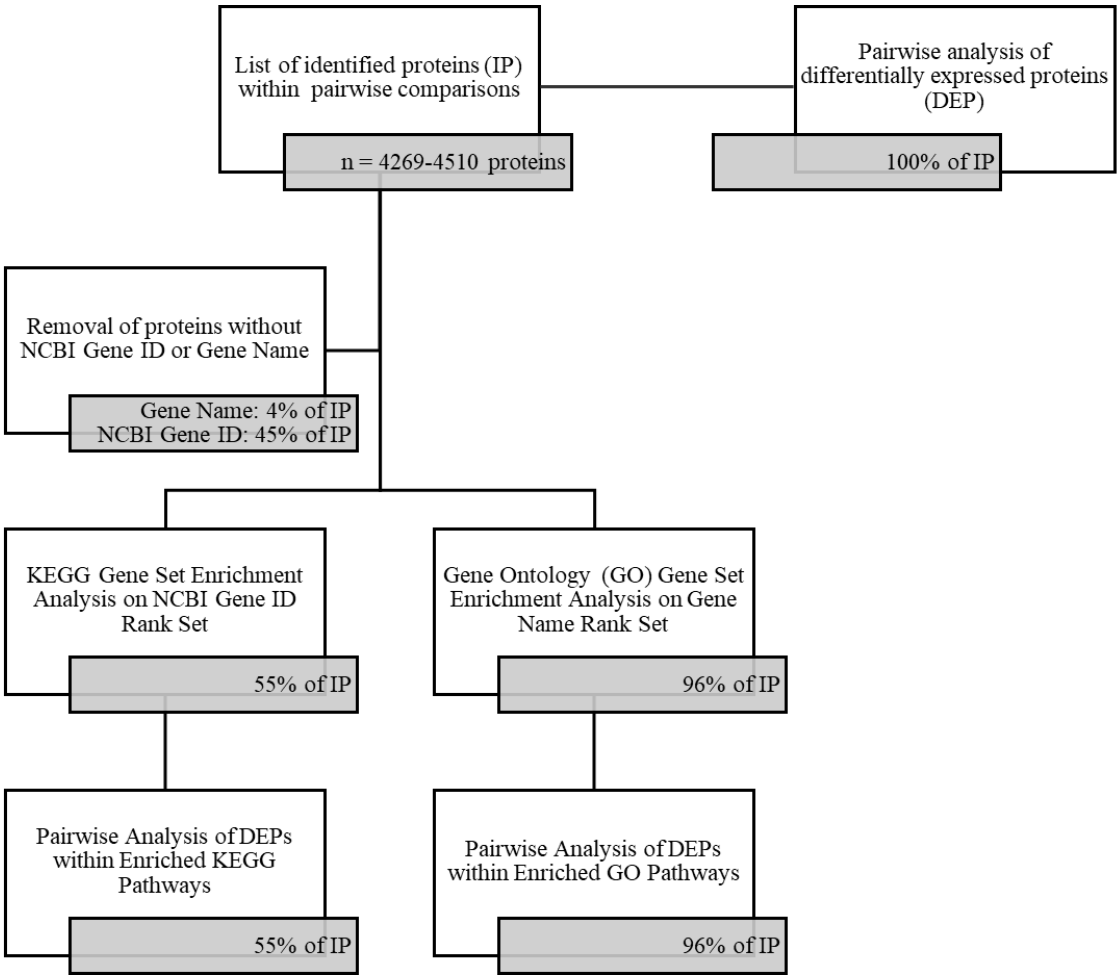

Figure 1. Flowchart of the analysis of liver proteome data.

3.10 Histology

For histological analysis, 10% neutral buffered formalin-fixed ileum, jejunum, and colon samples were submitted to the Iowa State University Veterinary Diagnostic Laboratory for sectioning and staining. Tissues were mounted and stained with hematoxylin and eosin (**H&E**) for tissue structure, periodic acid-Schiff (**PAS**) staining for goblet cell area quantification, and myeloperoxidase immunohistochemistry staining as a marker of neutrophil infiltration. For each stain, one slide per tissue was generated. Using a microscope (Leica® DMI3000 B Inverted Microscope, Bannockburn, IL) with an attached camera (Leica® K5C CMOS, Bannockburn, IL), five images per section of intestine were obtained at specified magnification. All image processing and quantification were done using ImageJ 1.54g (National Institutes of Health, USA).

3.10.1 Histological morphology

Villus height was measured by the segmented line tool at 5X magnification and marking the enterocyte brush border of the villus tip to the level of the villus-crypt interface along midline of the villus as we have previously described (Sanz Fernandez, 2014). Villus width was measured using a single line at mid-villus height, marking from the enterocyte brush border margin of one lateral edge to the enterocyte brush border of the other. Crypt depth was measured with a single line from a point at the level of the villus-crypt interface to the level of the junction of laminae propria and muscularis mucosa. Results of the five pictures were condensed into a single average per steer.

3.10.2 Goblet cell area quantification

Using a microscope (Leica® DMI3000 B Inverted Microscope, Bannockburn, IL) with an attached camera (Leica® K5C CMOS, Bannockburn, IL), five images per section of intestine were obtained at 5x magnification. Images were processed and goblet cell area of the epithelium was determined after subtracting luminal area. The results of the five pictures were condensed into a single average per steer.

3.10.3 Neutrophil Infiltration

Using a microscope (Leica® DMI3000 B Inverted Microscope, Bannockburn, IL) with an attached camera (Leica® K5C CMOS, Bannockburn, IL), five images per section of intestine were obtained at 50x magnification. Images of myeloperoxidase-stained tissue were processed and stain of the epithelium was determined after subtracting luminal area. The results of the five pictures were condensed into a single average per steer and expressed as a percentage of epithelial area.

4.0 Statistical analysis

Effects of replicate, treatment (CON or LAIP), days, and treatment by day interaction were assessed using PROC MIXED (SAS 9.4 Inst. Inc., Cary, NC). Period 1 and P2 were run as separate models. Each specific variable's P1 value (when available) served as a covariate for P2. Covariance structure, within repeated measures statements, was chosen based on the lowest AIC criterion for each variable within each period. Logarithmic transformation was performed when necessary, and data were back transformed for interpretation.

Plasma metabolites were unequally analyzed across treatments by study design. Therefore, treatment effects compare global means across all times, time effects compare changes across time (ergo, LAIP over time, and CON between d 18 and 42), and treatment × time compares multiple treatments represented across time (ergo, d 18 vs. d 42 for all treatments, as well as intermediate timepoints between LAIP-N and LAIP-Y in *post hoc* comparisons discussed below). Period 2 means of CON (when unequally sampled) represent the average of available timepoints for comparison to LAIP.

Due to unexpected differences in LA outcomes between replicate 1 and 2, a second *post hoc* model was utilized within replicate 1 data where a subset of steers were classified as control (**CON**; n =4), LAIP diet with a successful liver abscess induction (**LAIP-Y**; n = 4), or LAIP diet with a failed liver abscess induction (**LAIP-N**; n = 4). LAIP-N and LAIP-Y were combined into a single group (**LAIP**) for pairwise comparison within analysis of proteomics data, and pairwise comparisons of all 4 treatment groups were used to assess differences in hepatic proteome. CON was chosen at random from all control animals in replicate 1 (n = 8). Effects of treatment (CON, LAIP, LAIP-Y, or LAIP-N), days, and treatment by day interaction were analyzed as explained previously. Results are reported as least squares means, and means are considered different when $P \leq 0.05$ and tend to differ if $0.05 < P \leq 0.10$.

5.0 Results

5.1 Feed intake

During P2, DMI was similar between LAIP and CON during HS feeding prior to fasting, but resumption of LS feeding following 3 d of HS on d 4, 9, 14, and 19 decreased DMI in LAIP relative to CON (23%; $P < 0.01$; Figure 2). By design, fasting decreased DMI, but fasting pre-RI on the LS ration resulted in more moderate DMI decline than fasting post-RI on the HS ration (32 vs. 44%; $P < 0.01$; Figure 2). Overall, DMI was depressed in LAIP from the induction of fasting through euthanasia (Figure 2). *Post hoc* analysis revealed that DMI was depressed in LAIP-N, but not LAIP-Y, following both RI relative to CON (55% vs. CON; $P < 0.01$; Figure 3). LAIP-N consumed less feed from 2nd RI to euthanasia compared to CON ($P < 0.01$; Figure 3), while LAIP-Y was intermediate and

statistically not different than CON. Patterns of energy intake (accounting for dissimilar dietary energy between HS and LS) revealed subtler differences than those observed for DMI when diets were dissimilar between LAIP and CON. Post-fast energy intake of the HS ration decreased in LAIP on d 24 and 26 (29%; $P < 0.01$; Figure 4), but dietary energy intake was largely similar in LAIP relative to CON from 2nd RI through euthanasia aside from a transient decline on d 41 (10%; Figure 4). *Post hoc* analysis of energy consumption revealed LAIP-N decreased energy consumption from d 33 to 38 (3 to 8 d following 2nd RI; 36%; $P < 0.01$) while LAIP-Y was not different from CON from 2nd RI to euthanasia (Figure 5).

5.2 Body weight, average daily gain, and feed efficiency

Overall, LAIP weighed less than CON during P2 (5%; $P < 0.01$; Table 4). LAIP were modestly lighter than CON following acidosis cycles (6.8 kg; Figure 6); however, fasting decreased BW in LAIP relative to CON (12.0 kg; Figure 5), and differences became more pronounced at slaughter (15.0 kg at euthanasia; $P < 0.01$; Figure 5). *Post hoc* analysis indicated LAIP-Y and LAIP-N were similar in BW throughout P2, and both weighed less than CON at euthanasia ($P < 0.01$; Figure 6). Similarly, ADG was depressed in LAIP across P2 (26%; $P < 0.01$; Table 4). In the *post hoc* analysis, LAIP-N tended to have decreased ADG across P2 relative to CON, while LAIP-Y was not different than either treatment ($P = 0.07$; Table 6). During the fasting period from d 20 to d 26, LAIP-Y increased ADG relative to LAIP-N, but decreased ADG relative to CON (1.87, 0.31, and – 0.09 kg/d for CON, LAIP-Y, and LAIP-N, respectively; $P < 0.01$; Table 6). GFE was largely similar to ADG, with GFE decreased in LAIP vs. CON in primary analysis across P2 (19%; $P < 0.01$; Table 4) and acute differences during fasting (1.6-fold difference in LAIP vs. CON; $P < 0.01$; Table 4). GFE tended to decrease in LAIP-N relative to CON, while LAIP-Y was not different than either treatment during P2 within *post hoc* models ($P = 0.07$; Table 6).

5.3 Body temperature indices and fecal pH

Respiration rate decreased in LAIP relative to CON following the first RI (7 bpm; $P < 0.01$; Figure 12) but was overall not different across P2. Likewise, there was a weak tendency for a treatment × time interaction in the *post hoc* model ($P = 0.10$; Figure 13), but no clear pattern was established. There was a treatment × time interaction in the main model for Tr where LAIP had increased Tr relative to CON on d 26 and 34 of P2 (i.e. 3 and 4 d post-RI; 0.1 °C; Figure 14). *Post hoc* assessment indicated LAIP-Y had increased Tr relative to CON and LAIP-N from d 30 through 36 (0.3 °C; $P < 0.01$; Figure 15). Fecal pH was highly variable in both CON and LAIP, with no overall P2 differences in main or *post hoc* models ($P > 0.61$; Tables 4 & 6).

5.4 Plasma metabolites

5.4.1 Energy metabolites and serum proteins

Glucose decreased in LAIP overall following fasting (10% from d 18 to d 22; $P < 0.01$; Figure 18) but was not affected by abscess result ($P > 0.90$; Figure 19). No treatment differences were observed between CON and LAIP or within *post hoc* treatments ($P > 0.67$; Table 8). Insulin tended to increase on d 42 in CON (76%; $P = 0.07$; Figure 20) but these changes were not observed in the *post hoc* model ($P > 0.91$; Figure 21). BUN tended ($P = 0.08$) to be increased in CON across P2 in the main model (32%; Table 8). Within the *post hoc* comparisons, BUN increased in both LAIP-N and LAIP-Y from d 24 to 26 (82%; $P < 0.01$; Figure 23). Creatinine tended ($P = 0.09$) to be increased in CON vs. LAIP during P2 (7%; Table 8; Figure 24).

Albumin was decreased in LAIP across P2 (5%; $P < 0.01$; Table 8) while globulin was increased (7%; $P = 0.03$; Table 8), leading to decreased A:G in LAIP (10%; $P = 0.01$; Table 8). Likewise, in *post hoc* analysis, albumin was decreased in LAIP treatments ($P = 0.03$; Table 9) while globulin was numerically ($P > 0.13$) increased in LAIP-N and LAIP-Y, leading to a tendency toward decreased A:G ($P = 0.06$; Table 9).

5.4.2 Hepatobiliary and mineral metabolites

ALT increased from d 18 to d 42 in LAIP and CON (22%; $P < 0.01$; Figure 34) and similar results were observed in the *post hoc* analysis. ALP was not different from d 18 to 42 but decreased in LAIP from d 22 through 2nd RI (19%; $P < 0.01$; Figure 36). AST was nominally greater in P2 in LAIP (2%; $P = 0.05$; Table 8; Figure 38) but was not different across treatment groups in a *post hoc* comparison ($P > 0.25$; Table 9).

Total calcium and sodium were not different between treatment, time, or their interaction in the main or *post hoc* models ($P > 0.14$; Figures 42-45). Potassium tended ($P = 0.09$) to be augmented by treatment in *post hoc* comparison ($P = 0.09$; Table 9; Figure 47). Chloride increased during P2 in LAIP ($P < 0.01$; Table 8) driven by a tendency for a difference at d 18 between treatments (6%; $P = 0.09$; Figure 46). Total CO_2 decreased in LAIP on d 18 (8%; $P < 0.01$; Figure 50) but was not different within *post hoc* treatments or treatment × time ($P > 0.25$; Figure 51).

5.4.3 Inflammatory Metabolites

No differences in LBP, SAA, or Hp were observed in the main effects model between LAIP and CON across time, treatment, or their interaction ($P > 0.21$; Table 8). *Post hoc* analysis of LAIP-Y indicated numerical increases in LBP (1.3-fold; Figure 53), SAA (1.3-fold; Figure 55), and Hp (1.6-fold; Figure 57) relative to LAIP-N at euthanasia, but no treatment, time, or treatment × time interactions were observed ($P > 0.15$; Table 9).

5.5 Hematology

Red blood cells were nominally decreased at euthanasia in LAIP (0.5×10^6 cells/mL; $P < 0.01$; Figure 58) and within *post hoc* treatments, LAIP-N was decreased relative to LAIP-Y on d 22 of P2 (1.0×10^6 cells/mL; $P = 0.01$), while CON was not different than either (Figure 59). White blood cells tended to be increased within a pairwise comparison at euthanasia relative to LAIP, driving an overall treatment by time interaction (11%; $P = 0.04$; Figure 60), and this was accentuated in LAIP-Y relative to LAIP-N and CON within *post hoc* comparisons (23 and 38%, respectively; $P = 0.05$; Figure 61). Similar patterns were observed in neutrophils, where LAIP tended to increase neutrophils at euthanasia therefore influencing overall treatment by time interaction (25%; $P < 0.01$; Figure 62), especially within *post hoc* comparisons of LAIP-Y versus LAIP-N and CON (54 and 84%, respectively; $P < 0.01$; Figure 63). Eosinophils also increased in LAIP at d 42 (67%; $P < 0.01$; Figure 64), with LAIP-Y greater than CON (88%; $P < 0.01$; Figure 67) and LAIP-N not different than either treatment. A treatment × time interaction was detected in *post hoc* assessment of monocytes ($P = 0.02$), but no pairwise differences were elucidated (Figure 69). Basophils were decreased in LAIP-Y relative to LAIP-N on d 22 (49%; $P = 0.05$; Figure 73) but no differences at euthanasia were detected. Hemoglobin tended ($P = 0.07$) to be nominally increased in CON during P2 (0.4 g/dL; Table 12) driven by pairwise differences at d 42 (Figure 74). The *post hoc* models indicated LAIP-N had decreased hemoglobin relative to CON across P2, with LAIP-Y having an intermediate value ($P = 0.03$; Table 14). Hematocrit followed identical patterns to hemoglobin, with decreased hematocrit in LAIP across P2 ($P = 0.03$; Table 12) and *post hoc* treatment effects driven by a difference between CON and LAIP-N ($P = 0.04$; Table 14).

5.6. Post-mortem measurements

5.6.2 Organ Pathology

Across both models, all spleens and colons were scored as the least severe rank (i.e. score 0), therefore they were not statistically analyzed. No CON developed LA, and there was a tendency for LAIP to be associated with liver abscess scoring in the main model, with 22% of LAIP developing LA ($P = 0.09$; Table 17). No association between lung scoring and treatment was indicated ($P = 0.11$), but treatment was significantly associated with

rumen scoring (7% in CON vs 94% in LAIP with score >0; $P < 0.01$; Table 17) as well as jejunum scoring (0% in CON vs 50% in LAIP with score >0; $P < 0.01$; Table 17).

By design, *post hoc* analysis of organ pathology using Fisher's exact test showed associations of liver score by treatment ($P < 0.01$; Table 18). Lung scores were associated with treatment (0% in CON vs. 25% in LAIP-N vs. 75% in LAIP-Y with score >0; $P < 0.01$; Table 19). Rumen scores were significant within the *post hoc* model (25% in CON vs. 100% in LAIP-N vs. 100% in LAIP-Y with score >0; $P = 0.02$; Table 19) while jejunum scores tended to be significant ($P = 0.07$). Ileum scores were all 0 in the *post hoc* model, so no statistics were performed.

5.6.2 Organ Weights

Following euthanasia, LAIP-Y tended ($P = 0.08$) to have increased liver weight relative to LAIP-N (0.9 kg; Table 16; Figure 79), with CON not different from either LAIP treatment. Adjusting for body weight at euthanasia revealed LAIP-Y had increased liver weight relative to both CON and LAIP-N (0.3 and 0.4%, respectively; $P = 0.05$; Table 16; Figure 81). Lung and spleen weights were not different across either the main model or *post hoc* model, either on a kilogram basis or after adjustment for body weight ($P > 0.15$).

5.6.3 Intestinal measurements

Intestinal morphology did not differ between LAIP and CON in jejunum, ileum, or colon villus height, width, or crypt depth ($P > 0.37$; Table 19). Ileal goblet cell area was decreased in LAIP (51%; $P < 0.01$; Table 19) but jejunal and colonic GCA was not different ($P > 0.18$). Likewise, myeloperoxidase area was similar between LAIP and CON across all intestinal segments ($P > 0.50$).

Post hoc analysis observed decreased ileal GCA in LAIP-N relative to CON (85%; $P = 0.03$; Table 20) while LAIP-Y was not different than CON or LAIP-Y. All other intestinal measurements were similar between treatments ($P > 0.17$).

5.7 Proteomic analysis

5.7.1 KEGG Pathway Enrichment

A total of 69 KEGG pathways with differential enrichment were identified between pairwise comparisons of LAIP-N, LAIP-Y, and CON. Of these 69 pathways, 29% and 26% are classified under 'Metabolism' or 'Environmental information processing/Cellular processes/Organismal systems', respectively, and were subject to acute inquiry. Within pairwise comparisons of either LAIP-N or LAIP-Y versus CON, five pathways, including neutrophil extracellular trap formation ($P < 0.07$) and tuberculosis ($P \leq 0.02$), were upregulated in both comparisons. Twenty-two pathways were downregulated in both LAIP-N and LAIP-Y relative to CON, including steroid hormone biosynthesis, oxidative phosphorylation, arachidonic acid metabolism, tryptophan metabolism, drug metabolism - other enzymes, retinol metabolism, drug metabolism – cytochrome P450, metabolism of xenobiotics by cytochrome P450, and thermogenesis ($P \leq 0.05$). Pentose and glucuronate interconversions tended ($P = 0.07$) to be downregulated in LAIP-N versus CON, but were significantly upregulated ($P < 0.01$) in LAIP-Y versus CON.

Analysis of differential KEGG pathway expression in steers with successful liver abscesses relative to failed abscess formation may offer insight into the biochemical fingerprints of liver abscess formation. Mineral absorption and complement and coagulation cascade pathways tended to be upregulated in LAIP-Y relative to LAIP-N ($P \leq 0.08$) and were significantly upregulated in LAIP-Y relative to CON, but not different in LAIP-N versus CON ($P > 0.10$). Additionally, three immune system pathways (Fc-γ R-mediated phagocytosis, integrin signaling, and natural killer cell-mediated cytotoxicity) tended to be upregulated in LAIP-Y relative to CON ($P < 0.10$). Thirteen metabolic and immune pathways tended to be or were downregulated in LAIP-Y relative to control, including porphyrin

metabolism, fatty acid degradation, primary bile acid synthesis, ascorbate and aldarate metabolism, cholesterol metabolism, retrograde endocannabinoid signaling, peroxisome, non-alcoholic fatty liver disease, bile secretion, fatty acid metabolism, and the PPAR signaling pathway ($P < 0.07$). However, these pathways did not differ between LAIP-Y versus LAIP-N ($P > 0.10$).

5.7.2 Protein expression within KEGG pathways

Within pathway analysis of mineral absorption in LAIP-Y relative to CON and LAIP-N, metallothionein proteins (MT1A, MT1E, and MT2A) tended to be enriched in LAIP-Y (all 12.8-fold; $P < 0.08$). Five differentially expressed proteins (**DEP**) were classified under 'metabolic pathways' using KEGG mapper (**CYP7A1**, **DPYS**, **CERS6**, **OCRL**, and **ACOX3**), but the pathway was not significantly enriched. Other DEPs were classified into many pathways with less than 2 proteins per path.

Protein enrichment in LAIP-Y versus CON led to the identification of 78 proteins with differential abundance ($P < 0.05$; $|\text{Log}_2 \text{FC}| \geq 1$). Of these proteins, UDP-glucosyltransferases (**LOC540544**, **LOC781988I**, and **LOC100138004**) were unenriched in LAIP-Y versus CON ($P \leq 0.04$) and drove the downregulation of ascorbate and aldarate metabolism, drug metabolism – other enzymes, pentose and glucoronate interconversions, bile secretion, and porphyrin metabolism. Additionally, decreased abundance of cytochrome P450 1A (**CYP1A1** and **CYP1A2**) with changes to UDP-glucosyltransferase abundance led to downregulation of three chemical carcinogenesis pathways (DNA adducts, reactive oxygen species, and receptor activation). Additionally, these decreases led to downregulation of cytochrome P450 drug metabolism and xenobiotic metabolism, decreasing steroid hormone biosynthesis and retinol metabolism. Conversely, increased abundance of antimicrobial cathelicidins (**CATHL1**, **CATHL2**, and **CATHL3**) in LAIP-Y led to upregulation of tuberculosis and staphylococcus aureus infection pathways. Increased abundance of complement cascade proteins von Willebrand factor (**VWF**) and complement factor D (**CFD**) led to upregulation of pathways including of human papilloma virus, integrin signaling, coronavirus disease – COVID 19, and the complement/coagulation cascade.

Pairwise comparison of protein expression in LAIP-N versus CON led to similar observations as LAIP-Y versus CON, with CATHL1, CATHL2, CATHL3, VWF, and CFD increased relative to CON. Increased protein abundance led to upregulation of pathways including salivary secretion, tuberculosis, human papilloma virus, coronavirus disease – COVID 19, staphylococcus aureus infection, and neutrophil extracellular trap formation. The absolute change in log-fold change abundance of CYP1A1 and CYP1A2 was <1, and therefore pairwise differences were not statistically different. However, increased abundance of nucleoporin 153 (**NUP153**) and transportin 3 (**TNPO3**) led to upregulation of nucleocytoplasmic transport and viral life cycle -HIV I pathways.

5.7.3 GO Pathway Enrichment

A total of 28 BP and 8 MF pathways were differentially regulated within pairwise comparisons. No differences were found between LAIP-N versus LAIP-Y in either BP or MF categories ($P > 0.10$). Generation of precursor metabolites and energy was downregulated in LAIP-N relative to CON (-1.77 NES; $P = 0.04$) but not different in LAIP-Y vs CON. Several immunological pathways were upregulated in LAIP-Y versus CON but not in LAIP-N versus CON, including defense response to other organisms, response to biotic stimulus, defense response, biological process involved in interspecies interaction between organisms, immune system process, and response to external stimulus ($P \leq 0.03$). Metabolic processes including aminoglycan metabolic process as well as glycosaminoglycan metabolic process were also upregulated ($P = 0.02$). Downregulation of oxidative phosphorylation, cellular respiration, alcohol metabolic process, steroid metabolic process, and proton transmembrane transport was evident in LAIP-Y versus CON ($P \leq 0.05$).

LAIP-N and LAIP-Y downregulated molecular function of oxidoreductase activity in both groups relative to CON ($P < 0.01$) and tended to decrease transporter activity in LAIP-N versus CON ($P = 0.06$). Meanwhile, LAIP-Y increased zinc ion binding, molecular function regulator activity, nucleic acid binding, and enzyme inhibitor activity versus CON ($P \leq 0.01$).

5.7.4 Protein Expressions within GO Pathways

Similarly to KEGG analysis, upregulation of defense response pathways in LAIP-Y was driven by pairwise differences in CFD, CATHL1, and CATHL3 (log FC > 1.63; $P \leq 0.04$). Additionally, lactoferrin (**LTF**) was increased in LAIP-Y versus CON (log FC = 1.69; $P = 0.04$) but not in LAIP-N versus CON. Changes to metabolic processes were driven mainly by an increase in the abundance of inter-alpha trypsin heavy chain H3 (**ITIH3**), which was upregulated in both LAIP-N and LAIP-Y versus CON ($P \leq 0.02$). Increases in both ITIH3 and LTF also led to the enrichment of MF molecular function regulator activity and enzyme inhibitor activity pathways in LAIP-Y versus CON.

Downregulation of oxidative phosphorylation and cellular respiration in LAIP-Y was driven by a subtle, but significant decreased abundance of electron transport proteins Cytochrome C oxidase subunit 7A2 (**COX7A2**; log FC = -0.88; $P = 0.05$) and proteins involved in complex I of the mitochondrial electron transport chain (**NDUFB8** and **NDUFS8**; log FC < -0.72; $P \leq 0.04$). In MF pathways, zinc ion binding was increased by upregulation of MT1A and MT2A, along with increased enrichment of ubiquitin-like modifier activating enzyme 5 (**UBA5**; log FC = 1.26, $P < 0.01$). Upregulation of nucleic acid binding was driven by increased abundance of DNA replication factors 5 and 7 in LAIP-Y (**MCM5** & **MCM7**; $P \leq 0.05$).

6.0 Take home messages

- LA induction protocol:
  - Induced abscesses in 50% of LAIP in replicate 1, but 0% of LAIP in replicate 2.
  - Decreased DMI, growth, and ADG and GFE when fed a HS diet, especially for prolonged periods of time.
  - Decreased glucose and increased BUN following fasting bouts.
  - Decreased albumin:globulin ratio across period 2.
  - Increased ALT across period 2.
  - Treatment was associated with rumen and jejunum pathology scores at harvest.
- Successful LA induction:
  - Increased ADG versus unsuccessful LAIP following rumen inoculations.
  - Caused transient pyretic response from 3-5 d post-inoculation.
  - Increased neutrophil and eosinophil concentrations in blood at slaughter.
  - Induced numerical increases in acute phase proteins at slaughter.
  - Increased liver weights adjusted for body weight at slaughter.
  - Altered hepatic proteome to increase mineral sequestration and increase humoral immunity through the complement cascade.
  - Decreased hepatic proteins relating to fatty acid oxidation and PPAR pathways vs. CON.

7.0 Conclusion

Results herein suggest limited repeatability in a fasting and acidosis-based model for induction of LA in growing steers. However, LA formation coincides with transient pyrexia, neutrophilia, and increased defense-oriented proteins in the liver, leaving subtle indications of abscess formation. Future studies should investigate differences between replicate 1 and 2, including the use of coccidiostats, in the mitigating LA formation.

8.0 Summary of Coccidiosis Analysis

- February 2025: Steers enrolled in replicate 1 and given no coccidiostat upon arrival to ISU. Multiple steers had reported diarrhea throughout P1 around 18-22 d post arrival. All steers sourced from a farm feeding lasalocid as a coccidiostat prior to enrollment.
- March 31st, 2025: Fecal floats from diarrhetic steers returned positive for *Eimeria* spp. In 3/6 samples.
- April 2025: GJC and LB agree to treat all steers for coccidiosis upon arrival to ISU for replicate 2. PG advises using a 5-day regimen of oral amprolium suspension (9.6%).
- April/May 2025: Diarrhea is less apparent throughout replicate 2, especially in CON steers.
- July 25th, 2025: Matt Brewer, PG, LB, and GJC meet to discuss failure of LA induction and rep 2. MB suggests fecal floats for frozen feces on hand, but damage to oocytes can occur following freeze/thaw cycles.
- July 29th, 2025: Fecal floats from both replicates return no observed coccidiosis pressure.
- February 12th, 2026: GJC and DM coordinate jejunal, ileal, and colonic H&E slide analysis for histopathological analysis. DM reports no coccidia present in tissue, indicating a) no coccidia present or b) adequate lag time between oocyte maturation and slaughter for epithelial repair.

9.0 References

Abeyta, M. A., B. M. Goetz, E. J. Mayorga, S. Rodriguez-Jimenez, J. Opgenorth, A. D. Freestone, J. M. Lourenco, T. R. Callaway, and L. H. Baumgard. 2023a. Effects of abomasally infused rumen fluid from corn-challenged donor cows on production, metabolism, and inflammatory biomarkers in healthy recipient cows. J. Dairy Sci. 106(6):4336-4352.

Abeyta, M. A., E. A. Horst, B. M. Goetz, E. J. Mayorga, S. Rodriguez-Jimenez, M. Caratzu, and L. H. Baumgard. 2023b. Effects of hindgut acidosis on production, metabolism, and inflammatory biomarkers in feed-restricted lactating dairy cows. J. Dairy Sci. 106(4):2890-2903.

Abeyta, M. A., E. A. Horst, B. M. Goetz, S. Rodriguez-Jimenez, E. J. Mayorga, M. Al-Qaisi, and L. H. Baumgard. 2023c. Effects of hindgut acidosis on inflammation, metabolism, and productivity in lactating dairy cows fed a high-fiber diet. J. Dairy Sci. 106(4):2879-2889.

Amachawadi, R. G. and T. G. Nagaraja. 2016. Liver abscesses in cattle: A review of incidence in Holsteins and of bacteriology and vaccine approaches to control in feedlot cattle12. J. Anim. Sci. 94(4):1620-1632.

Amachawadi, R. G., T. J. Purvis, B. V. Lubbers, J. W. Homm, C. L. Maxwell, and T. G. Nagaraja. 2017. Bacterial flora of liver abscesses in crossbred beef cattle and Holstein steers fed finishing diets with or without tylosin1,2. J. Anim. Sci. 95(8):3425-3434.

Brown, H., R. F. Bing, H. P. Grueter, J. W. McAskill, C. O. Cooley, and R. P. Rathmacher. 1975. Tylosin and Chlortetracycline for the Prevention of Liver Abscesses, Improved Weight Gains and Feed Efficiency in Feedlot Cattle. J. Anim. Sci. 40(2):207-213.

Goetz, B. M., M. A. Abeyta, S. Rodriguez-Jimenez, E. J. Mayorga, J. Opgenorth, G. M. Jakes, A. D. Freestone, C. E. Moore, D. J. Dickson, J. E. Hergenreder, and L. H. Baumgard. 2023a. Effects of Bacillus subtilis PB6 supplementation on production, metabolism, inflammatory biomarkers, and gastrointestinal tract permeability in transition dairy cows. J. Dairy Sci. 106:9793–9806

Goetz, B. M., M. A. Abeyta, S. Rodriguez-Jimenez, J. Opgenorth, J. L. McGill, K. A. Bryan, and L. H. Baumgard. 2023b. Effects of a multispecies direct-fed microbial on gastrointestinal permeability during feed restriction in a growing heifer model. JDS Comm. 2024 (5):167–171

Horst, E. A., E. J. Mayorga, M. Al-Qaisi, S. Rodriguez-Jimenez, B. M. Goetz, M. A. Abeyta, P. J. Gorden, S. K. Kvidera, and L. H. Baumgard. 2020. Evaluating effects of zinc hydroxychloride on biomarkers of inflammation and intestinal integrity during feed restriction. J. Dairy Sci. 103(12):11911-11929.

Jennings, J. S., R. G. Amachawadi, S. K. Narayanan, T. Nagaraja, L. O. Tedeschi, W. N. Smith, and T. E. Lawrence. 2021. Effects of corn stalk inclusion and tylosin on performance, rumination, ruminal papillae morphology, and gut pathogens associated with liver abscesses from finishing beef steers. Livest. Sci. 251:104623.

Mansfield, L. S. and J. F. Urban. 1996. The pathogenesis of necrotic proliferative colitis in swine is linked to whipworm induced suppression of mucosal immunity to resident bacteria. Vet. Immunol. Imunopathol. 50(1):1-17.

McDaniel, Z. S., K. E. Hales, T. G. Nagaraja, T. E. Lawrence, R. G. Amachawadi, J. A. Carroll, N. C. Burdick Sanchez, M. L. Galyean, T. M. Smock, M. A. Ballou, V. S. Machado, and P. R. Broadway. 2023. Short communication: evaluation of an endotoxin challenge and intraruminal bacterial inoculation model to induce liver abscesses in Holstein steers. J. Anim. Sci. 101:1-7.

McDaniel, Z. S., K. E. Hales, H. Salih, A. Deters, X. Shi, T. G. Nagaraja, T. E. Lawrence, T. C. Tennant, R. G. Amachawadi, J. A. Carroll, N. C. Burdick Sanchez, M. L. Galyean, T. M. Smock, M. A. Ballou, V. S. Machado, E. Davis, and P. R. Broadway. 2024. Development of an experimental model for liver abscess induction in Holstein steers using an acidotic diet challenge and bacterial inoculation. J. Anim. Sci. 102.

Nagaraja, T. and K. F. Lechtenberg. 2007. Liver abscesses in feedlot cattle. Veterinary Clinics of North America: Food Anim. Pract. 23(2):351-369.

National Academies of Sciences, Engineering, and Medicine. 2016. *Nutrient Requirements of Beef Cattle: Eighth Revised Edition*. Washington, DC: The National Academies Press.

Offersen, S. M., N. L. Henriksen, and A. Brunse. 2024. A weighted and cumulative point system for accurate scoring of intestinal pathology in a piglet model of necrotizing enterocolitis. Exp. and Mol. Path. 140:104936.

Opgenorth, J., M. Abuajamieh, E. A. Horst, S. K. Kvidera, J. S. Johnson, E. J. Mayorga, M. V. Sanz-Fernandez, M. A. Al-Qaisi, J. M. DeFrain, D. H. Kleinschmit, P. J. Gorden, and L. H. Baumgard. 2021. The effects of zinc amino acid complex on biomarkers of gut integrity, inflammation, and metabolism in heat-stressed ruminants. J. Dairy Sci. 104(2):2410-2421.

Rezac, D., D. Thomson, S. Bartle, J. Osterstock, F. Prouty, and C. Reinhardt. 2014. Prevalence, severity, and relationships of lung lesions, liver abnormalities, and rumen health scores measured at slaughter in beef cattle. J. Anim. Sci. 92(6):2595-2602.

Saginala, S., T. Nagaraja, K. Lechtenberg, M. Chengappa, K. Kemp, and P. Hine. 1997. Effect of Fusobacterium necrophorum leukotoxoid vaccine on susceptibility to experimentally induced liver abscesses in cattle. J. Anim. Sci. 75(4):1160-1166.

Sanz Fernandez, M. V., S. C. Pearce, N. K. Gabler, J. F. Patience, M. E. Wilson, M. T. Socha, J. L. Torrison, R. P. Rhoads, and L. H. Baumgard. 2014. Effects of supplemental zinc amino acid complex on gut integrity in heat-stressed growing pigs. Animal. 8(1):43-50.

Scanlan, C. M. and T. L. Hathcock. 1983. Bovine rumenitis - liver abscess complex: a bacteriological review. Cornell Vet. 73(3):288-297.

Smith, H. 1944. Ulcerative lesions of the bovine rumen and their possible relation to hepatic abscesses.

Steele, M. A., G. B. Penner, F. Chaucheyras-Durand, and L. L. Guan. 2016. Development and physiology of the rumen and the lower gut: Targets for improving gut health. J. Dairy Sci. 99(6):4955-4966.

Tennant, T. C., S. E. Ives, L. B. Harper, D. G. Renter, and T. E. Lawrence. 2014. Comparison of tulathromycin and tilmicosin on the prevalence and severity of bovine respiratory disease in feedlot cattle in association with feedlot performance, carcass characteristics, and economic factors. J. Anim. Sci. 92(11):5203-5213.

10.0 Tables and Figures

Table 3: Effects of liver abscess induction protocol (LAIP) or control (CON) on production parameters during P1.

	Diet			*P*						
Parameters	CON	LAIP	SEM	Rep[1]	Trt[2]	Time	Rep × Trt	Rep × Time	Trt × Time	Rep × Trt × Time
Number of animals (n=32)										
DMI[3], kg/d	2.39	2.79	0.12	<0.01	0.02	<0.01	0.23	0.91	0.1	<0.01
Energy Intake, Mcal/d	3.13	3.66	0.15	<0.01	0.02	<0.01	0.23	0.91	0.1	<0.01
Body Weight, kg	118	122	3	<0.01	0.22	-	0.88	-	-	-
ADG[4], kg	1.10	1.89	0.22	0.51	0.02	-	0.02	-	-	-
GFE[5], kg ADG/kg DMI	0.40	0.69	0.10	0.95	0.04	-	0.03	-	-	-
Tr[6], °C	40.10	40.04	0.03	<0.01	0.11	0.13	0.09	0.47	0.87	<0.01
RR[7], bpm	38.81	39.73	1.32	0.02	0.62	<0.01	0.82	0.18	0.45	<0.01
Fecal pH	6.17	6.18	0.12	<0.01	0.93	-	0.74	-	-	-

[1]Replicate
[2]Treatment
[3]Dry matter intake
[4]Average daily gain
[5]Gross feed efficiency
[6]Rectal temperature
[7]Respiration rate

Table 4: Effects of liver abscess induction protocol (LAIP) or control (CON) on production parameters during P2.

	Diet			*P*						
Parameters	CON	LAIP	SEM	Rep[1]	Trt[2]	Time	Rep × Trt	Rep × Time	Trt × Time	Rep × Trt × Time
Number of animals (n=32)										
DMI[3], kg/d	4.23	3.53	0.11	0.17	<0.01	<0.01	0.20	<0.01	<0.01	0.06
Energy Intake, Mcal/d	5.55	5.14	0.14	0.14	0.06	<0.01	0.19	<0.01	<0.01	0.04
Body Weight, kg	151	144	1	0.49	<0.01	<0.01	0.27	0.02	<0.01	0.58
ADG[4], kg										
d 1 to 18, kg	1.46	1.11	0.08	0.21	<0.01	-	0.41	-	-	-
d 20 to 26, kg	1.43	0.18	0.13	0.56	<0.01	-	0.02	-	-	-
d 30 to 42, kg	1.77	1.04	0.11	<0.01	<0.01	-	0.4	-	-	-
P2, kg	1.57	1.21	0.06	0.55	<0.01	-	0.12	-	-	-
GFE[5], kg ADG/kg DMI										
d 1 to 18, kg	0.44	0.34	0.02	0.30	<0.01	-	0.93	-	-	-
d 20 to 26, kg	0.37	0.04	0.04	0.60	<0.01	-	0.20	-	-	-
d 30 to 42, kg	0.38	0.23	0.02	<0.01	<0.01	-	0.98	-	-	-
P2	0.40	0.33	0.01	<0.01	<0.01	-	0.89	-	-	-
Tr[6], °C	40.25	40.27	0.02	0.54	0.43	<0.01	0.15	<0.01	<0.01	<0.01
RR[7], bpm	48.30	45.48	0.66	0.52	<0.01	<0.01	0.51	<0.01	<0.01	<0.01
Fecal pH	6.52	6.47	0.07	0.01	0.61	<0.01	0.14	0.04	<0.01	0.27

[1]Replicate
[2]Treatment
[3]Dry Matter Intake
[4]Average Daily Gain
[5]Gross feed efficiency
[6]Rectal Temperature
[7]Respiration Rate

Table 5: *Post hoc* comparison of the effects of successful liver abscess induction (LAIP-Y), failed liver abscess induction (LAIP-N), or control (CON) on production parameters during P1.

	Diet				*P*		
Parameters	CON	LAIP-N	LAIP-Y	SEM	Trt[1]	Time[2]	Trt × Time
Number of animals (n=12)							
DMI[3], kg/d	2.82	3.03	3.01	0.20	0.73	0.18	0.51
Energy Intake, Mcal/d	3.70	3.98	3.94	0.27	0.73	0.18	0.51
Body Weight, kg	130	134	131	4	0.78	-	-
ADG[4], kg	1.56	1.67	1.53	0.34	0.95	-	-
GFE[5], kg ADG/kg DMI	0.55	0.57	0.50	0.11	0.91	-	-
Tr[6], °C	39.99	39.94	39.88	0.06	0.41	0.70	0.54
RR[7], bpm	40.50	40.25	43.50	2.12	0.50	0.49	0.30
Fecal pH	5.63	5.91	5.88	0.22	0.62	-	-

[1]Replicate
[2]Treatment
[3]Dry Matter Intake
[4]Average Daily Gain
[5]Gross feed efficiency
[6]Rectal Temperature
[7]Respiration Rate

Table 6: *Post hoc* comparison of the effects of successful liver abscess induction (LAIP-Y), failed liver abscess induction (LAIP-N), or control (CON) on production parameters during P2**.**

	Diet				*P*		
Parameters	CON	LAIP-N	LAIP-Y	SEM	Trt[1]	Time	Trt × Time
Number of animals (n=12)							
DMI[2], kg/d	4.53	3.33	3.82	0.11	<0.01	<0.01	<0.01
Energy Intake, Mcal/d	5.95	4.82	5.55	0.15	<0.01	<0.01	<0.01
Body Weight, kg	166	153	157	5	0.18	<0.01	<0.01
ADG[3], kg							
d 1 to 18, kg	1.62	1.05	1.20	0.20	0.17	-	-
d 20 to 26, kg	1.87[a]	-0.31[c]	0.29[b]	0.18	<0.01	-	-
d 30 to 42, kg	1.59	0.59	0.85	0.30	0.11	-	-
P2, kg	1.65[x]	1.00[y]	1.24[xy]	0.17	0.08	-	-
GFE[4], kg ADG/kg DMI							
d 1 to 18, kg	0.45[x]	0.32[y]	0.32[y]	0.04	0.07	-	-
d 20 to 26, kg	0.43[a]	-0.09[b]	0.08[b]	0.05	<0.01	-	-
d 30 to 42, kg	0.31	0.14	0.17	0.06	0.18	-	-
P2	0.38[x]	0.29[y]	0.[31xy]	0.03	0.07	-	-
Tr[5], °C	40.14	40.14	40.29	0.02	<0.01	<0.01	<0.01
RR[6], bpm	47.86	45.66	48.65	1.38	0.34	<0.01	0.10
Fecal pH	6.16	6.30	6.18	0.17	0.81	<0.01	0.11

[1]Treatment
[2]Dry Matter Intake
[3]Average Daily Gain
[4]Gross feed efficiency
[5]Rectal Temperature
[6]Respiration Rate
[a, b, c] denotes pairwise differences where $P < 0.05$
[x, y, z] denotes tendency for pairwise differences where $0.05 \leq P < 0.10$

Table 7: Effects of liver abscess induction protocol (LAIP) or control (CON) on blood metabolites during P1.

Parameters	Diet		SEM	*P*		
	CON	LAIP		Rep[1]	Trt[2]	Rep × Trt
Number of animals (n=20)						
Insulin, µg/L	0.40	0.42	0.06	0.10	0.79	0.35
Inflammatory Metabolites						
LBP[3], µg/mL	3.74	4.18	0.80	0.41	0.70	0.06
SAA[4†], µg/mL	26.16	16.08	0.98	0.77	0.30	0.06
Haptoglobin[†], µg/mL	1.73	1.59	0.19	0.29	0.87	0.50

[1]Replicate
[2]Treatment
[3]Lipopolysaccharide binding protein
[4]Serum amyloid A
[†]Values were log-transformed for statistical analysis and back transformed for interpretation

Table 8: Effects of liver abscess induction protocol (LAIP) or control (CON) on blood metabolites during P2.

Parameters	Diet		SEM	*P*						
	CON	LAIP		Rep[1]	Trt[2]	Time	Rep × Trt	Rep × Time	Trt × Time	Rep × Trt × Time
Number of animals (n=20)										
Energy Metabolites										
Glucose, mg/dL	106.13	102.67	2.29	0.79	0.67	<0.01	0.57	0.82	0.31	0.97
Insulin, µg/L	0.89	0.64	0.11	0.91	0.07	0.12	0.53	0.50	0.07	0.13
BUN[3], mg/dL	11.81	8.52	0.65	0.72	0.08	<0.01	0.85	0.52	0.41	0.53
Creatinine, mg/dL	0.99	0.92	0.05	0.37	0.09	0.22	0.76	0.19	0.81	0.81
Total Protein, g/dL	6.44	6.60	0.13	0.90	0.16	0.25	0.59	0.11	0.07	0.20
Albumin, g/dL	2.56	2.44	0.04	0.77	<0.01	0.13	0.20	0.59	0.50	0.38
Globulin, g/dL	3.88	4.15	0.13	0.87	0.03	0.02	0.29	<0.01	0.01	0.03
A:G[4]	0.66	0.60	0.02	0.88	0.01	<0.01	0.28	0.22	0.10	0.11
Hepatobiliary Metabolites										
ALT[5], U/L	19.88	18.68	0.56	0.67	0.16	<0.01	0.13	0.59	0.78	0.04
ALP[6], U/L	191.8	189.8	14.8	0.33	0.32	<0.01	0.11	0.47	0.56	0.79
AST[7], U/L	75.9	77.4	3.5	0.8	0.05	<0.01	0.83	0.97	0.31	0.36
Total Bilirubin, mg/dL	0.23	0.23	0.01	0.82	0.32	0.05	<0.01	<0.01	0.62	<0.01
Mineral Metabolites										
Calcium, mg/dL	11.01	11.15	0.10	0.79	0.25	0.23	0.43	0.67	0.77	0.94
Sodium, mmol/L	143.6	143.3	0.7	0.22	0.6	0.15	0.83	0.51	0.29	0.46
Potassium, mmol/L	5.19	5.33	0.10	0.15	0.31	0.73	0.07	0.24	0.63	0.84
Chloride, mmol/L	95.4	97.8	0.7	0.41	<0.01	<0.01	0.52	0.30	0.09	0.67
Total CO_2, mmol/L	29.19	29.04	0.38	0.55	0.14	<0.01	0.57	0.23	<0.01	0.85
Inflammatory Metabolites										
LBP[8], µg/mL	3.60	5.30	0.73	0.41	0.31	0.25	0.83	0.40	0.58	0.79
SAA[9†], µg/mL	2.81	3.39	0.81	0.77	0.29	0.29	0.68	0.16	0.65	0.93
Haptoglobin[†], µg/mL	0.27	1.06	0.19	0.51	0.32	0.21	0.58	0.17	0.61	0.71

[1]Replicate
[2]Treatment
[3]Blood Urea Nitrogen
[4]Albumin-to-globulin ratio
[5]Alanine aminotransferase
[6]Alkaline phosphatase
[7]Aspartate aminotransferase
[8]Lipopolysaccharide binding protein
[9]Serum amyloid A
[†]Values were log-transformed for statistical analysis for analysis and back-transformed for interpretation

Table 9: *Post hoc* comparison of the effects of successful liver abscess induction (LAIP-Y), failed liver abscess induction (LAIP-N), or control (CON) on blood metabolites during P1.

	Diet				
Parameters	CON	LAIP-N	LAIP-Y	SEM	*P*
Number of animals (n=12)					
Insulin, µg/L	0.51	0.56	0.34	0.10	0.28
Inflammatory Metabolites					
LBP[1], µg/mL	4.41	1.91	3.19	1.00	0.26
SAA[2†], µg/mL	38.86	10.38	8.58	0.90	0.02
Haptoglobin[†], µg/mL	1.55	0.94	1.06	0.05	0.54

[1]Lipopolysaccharide binding protein
[2]Serum amyloid A
[†]Values were log-transformed for statistical analysis and back transformed for interpretation

Table 10: *Post hoc* comparison of the effects of successful liver abscess induction (LAIP-Y), failed liver abscess induction (LAIP-N), or control (CON) on blood metabolites during P2.

	Diet				*P*		
Parameters	CON	LAIP-N	LAIP-Y	SEM	Trt[1]	Time	Trt × Time
Number of animals (n=12)							
Energy Metabolites							
Glucose, mg/dL	101.1	100.8	102.4	3.4	0.93	<0.01	0.90
Insulin, µg/L	0.70	0.66	0.79	0.27	0.76	0.39	0.91
BUN[2], mg/dL	13.32	9.90	7.98	1.00	0.19	<0.01	0.18
Creatinine, mg/dL	1.03	0.97	0.93	0.08	0.59	0.72	0.22
Total Protein, g/dL	6.60	6.60	6.65	0.22	0.47	0.02	0.45
Albumin, g/dL	2.56	2.44	2.40	0.05	0.03	0.09	0.67
Globulin, g/dL	3.99	4.14	4.26	0.21	0.13	<0.01	0.10
A:G[3]	0.65	0.60	0.58	0.04	0.06	<0.01	0.25
Hepatobiliary Metabolites							
ALT[4], U/L	17.38	18.09	18.15	0.88	0.12	<0.01	0.72
ALP[5], U/L	185.0	165.8	167.3	25.2	0.91	0.02	0.91
AST[6], U/L	73.25	75.75	81.20	5.36	0.25	<0.01	0.54
Total Bilirubin, mg/dL	0.23	0.23	0.22	0.01	0.27	0.17	0.06
Mineral Metabolites							
Calcium, mg/dL	11.13	11.14	11.01	0.15	0.72	0.14	0.95
Sodium, mmol/L	144.1	142.5	143.3	1.1	0.78	0.14	0.73
Potassium, mmol/L	5.21	5.19	5.46	0.15	0.09	0.21	0.17
Chloride, mmol/L	97.50	97.54	98.24	0.95	0.10	<0.01	0.59
Total CO_2, mmol/L	28.50	29.07	28.74	0.39	0.53	<0.01	0.25
Inflammatory Metabolites							
LBP[7], µg/mL	4.56	4.39	6.47	1.12	0.26	0.29	0.15
SAA[8†], µg/mL	20.49	18.92	33.78	1.14	0.40	0.48	0.82
Haptoglobin[†], µg/mL	2.56	2.86	4.39	0.59	0.38	0.33	0.49

[1]Treatment
[2]Blood Urea Nitrogen
[3]Albumin-to-globulin ratio
[4]Alanine aminotransferase
[55]Alkaline phosphatase
[6]Aspartate aminotransferase
[7]Lipopolysaccharide binding protein
[8]Serum amyloid A
[†]Values were log-transformed for statistical analysis and back-transformed for interpretation

Table 11: Effects of liver abscess induction protocol (LAIP) or control (CON) on blood hematology during P1.

Parameters	Diet		SEM	*P*		
	CON	LAIP		Rep[1]	Trt[2]	Rep × Trt
Number of animals (n=32)						
RBC[3], cells×10^6/μL	11.37	10.8	0.2	0.05	0.06	0.05
WBC[4], cells×10^3/μL	10.55	9.67	0.52	0.16	0.23	0.9
Neutrophils, cells×10^3/μL	3.82	3.21	0.26	<0.01	0.11	0.71
Lymphocytes, cells×10^3/μL	6.00	5.80	0.32	0.38	0.66	0.86
Eosinophils, cells×10^3/μL	0.21	0.14	0.02	0.77	0.03	0.82
Monocytes, cells×10^3/μL	0.34	0.34	0.03	<0.01	0.99	0.93
Basophils, cells×10^3/μL	0.13	0.13	0.01	0.27	0.71	0.04
Platelets, cells×10^3/μL	572	593	33	0.14	0.64	0.46
Hemoglobin, g/dL	12.98	11.99	0.27	0.77	0.01	0.55
Hematocrit, %	36.2	34.18	0.7	0.17	0.05	0.54

[1]Replicate
[2]Treatment
[3]Red blood cells
[2]White blood cells

Table 12: Effects of liver abscess induction protocol (LAIP) or control (CON) on blood hematology during P2.

Parameters	Diet		SEM	*P*						
	CON	LAIP		Rep[1]	Trt[2]	Time	Rep × Trt	Rep × Time	Trt × Time	Rep × Trt × Time
Number of animals (n=32)										
RBC[3], cells×10^6/μL	10.23	9.97	0.15	0.05	0.24	<0.01	0.84	0.06	<0.01	0.12
WBC[4], cells×10^3/μL	10.19	10.39	0.39	0.58	0.72	<0.01	0.26	0.02	0.04	0.13
Neutrophils, cells×10^3/μL	3.49	3.58	0.32	0.61	0.83	<0.01	0.32	0.03	<0.01	0.24
Lymphocytes, cells×10^3/μL	6.07	6.14	0.24	0.07	0.84	<0.01	0.68	0.02	0.55	0.15
Eosinophils, cells×10^3/μL	0.16	0.20	0.02	0.87	0.14	<0.01	0.85	<0.01	<0.01	0.09
Monocytes, cells×10^3/μL	0.29	0.26	0.02	0.11	0.19	0.61	0.26	<0.01	0.31	0.26
Basophils, cells×10^3/μL	0.12	0.12	0.01	0.13	0.37	0.39	0.27	0.01	0.09	<0.01
Platelets, cells×10^3/μL	560	583	18	<0.01	0.38	0.1	0.22	<0.01	0.08	0.04
Hemoglobin, g/dL	11.94	11.55	0.14	0.34	0.07	0.61	0.86	0.04	<0.01	0.42
Hematocrit, %	34.05	32.89	0.36	0.16	0.03	0.81	0.81	0.03	<0.01	0.30

[1]Replicate
[2]Treatment
[3]Red Blood Cells
[4]White Blood Cells

Table 13: *Post hoc* comparison of the effects of successful liver abscess induction (LAIP-Y), failed liver abscess induction (LAIP-N), or control (CON) on blood hematology during P1**.**

	Diet				
Parameters	CON	LAIP-N	LAIP-Y	SEM	*P*
Number of animals (n=12)					
RBC[1], cells×10^6/μL	10.98	10.75	10.85	0.37	0.90
WBC[2], cells×10^3/μL	10.15	10.15	10.32	1.14	0.99
Neutrophils, cells×10^3/μL	3.68	3.57	4.2	0.47	0.61
Lymphocytes, cells×10^3/μL	5.68	5.74	5.38	0.75	0.93
Eosinophils, cells×10^3/μL	0.27	0.16	0.12	0.06	0.25
Monocytes, cells×10^3/μL	0.36	0.46	0.43	0.06	0.46
Basophils, cells×10^3/μL	0.12	0.15	0.14	0.02	0.37
Platelets, cells×10^3/μL	511	614	608	55.2	0.37
Hemoglobin, g/dL	12.95	12.18	11.93	0.49	0.35
Hematocrit, %	36.10	34.08	33.53	1.16	0.30

[1]Red blood cells
[2]White blood cells

Table 14: *Post hoc* comparison of the effects of successful liver abscess induction (LAIP-Y), failed liver abscess induction (LAIP-N), or control (CON) on blood hematology during P2**.**

	Diet				*P*		
Parameters	CON	LAIP-N	LAIP-Y	SEM	Trt[1]	Time	Trt × Time
Number of animals (n=12)							
RBC[2], cells×10^6/μL	10.31	9.98	10.31	0.23	0.53	<0.01	0.01
WBC[3], cells×10^3/μL	9.81	10.26	11.03	0.76	0.54	<0.01	0.05
Neutrophils, cells×10^3/μL	3.14	3.40	4.46	0.50	0.19	<0.01	<0.01
Lymphocytes, cells×10^3/μL	6.19	6.46	5.55	0.51	0.48	<0.01	0.50
Eosinophils, cells×10^3/μL	0.15	0.20	0.19	0.03	0.57	0.57	<0.01
Monocytes, cells×10^3/μL	0.28	0.24	0.27	0.03	0.57	0.02	0.02
Basophils, cells×10^3/μL	0.13	0.12	0.12	0.02	0.87	0.05	0.24
Platelets, cells×10^3/μL	527	566	523	37	0.65	0.10	0.05
Hemoglobin, g/dL	12.29	11.36	11.92	0.24	0.05	0.03	0.06
Hematocrit, %	35.23	32.32	33.76	0.66	0.04	0.04	0.06

[1]Treatment
[2]Red Blood Cells
[3]White Blood Cells

Table 15: Effects of liver abscess induction protocol (LAIP) or control (CON) on organ weights at euthanasia.

	Diet			*P*		
Parameters	CON	LAIP	SEM	Rep[1]	Trt[2]	Rep × Trt
Number of animals (n=32)						
Liver weight, kg	4.00	3.77	0.12	0.72	0.27	0.11
Liver, % of BW	2.11	2.21	0.05	0.24	0.18	0.25
Lung, kg	1.92	1.79	0.06	0.10	0.15	0.01
Lung, % of BW	1.00	1.00	0.01	0.03	0.66	0.04
Spleen, kg	0.41	0.40	0.02	0.31	0.75	0.17
Spleen, % of BW	0.22	0.24	0.02	0.12	0.25	0.36

[1]Replicate
[2]Treatment

Table 16: *Post hoc* comparison of the effects of successful liver abscess induction (LAIP-Y), failed liver abscess induction (LAIP-N), or control (CON) on organ weights at euthanasia**.**

	Diet				
Parameters	CON	LAIP-N	LAIP-Y	SEM	*P*
Number of animals (n=32)					
Liver, kg	4.23	3.49	4.39	0.25	0.08
Liver, % of BW	2.07[b]	2.03[b]	2.39[a]	0.09	0.05
Lung, kg	2.10[ab]	1.77[b]	1.96[a]	0.14	0.32
Lung, % of BW	1.05	1.01	1.08	0.06	0.76
Spleen, kg	0.42	0.40	0.46	0.04	0.49
Spleen, % of BW	0.21	0.22	0.26	0.02	0.31

[a, b, c] denotes pairwise differences where $P < 0.05$

Table 17: Comparison of the effects of liver abscess induction protocol (LAIP), or control (CON) on organ pathology scores at euthanasia.

	Diet				
	CON		LAIP		
Organ	Freq.	Percent	Freq.	Percent	*P*
Liver[1]					0.09
0	14/14[†]	100%	14/18[‡]	78%	
A	0/14	0%	1/18	6%	
A+	0/14	0%	3/18	17%	
Lung[2]					0.11
0	12/14	86%	13/18	72%	
1	1/14	7%	4/18	22%	
2	1/14	7%	1/18	6%	
3	0/14	0%	0/18	0%	
4	0/14	0%	0/18	0%	
5	0/14	0%	0/18	0%	
Spleen					-
0	14/14	100%	18/18	100%	
1	0/14	0%	0/18	0%	
2	0/14	0%	0/18	0%	
3	0/14	0%	0/18	0%	
Rumen[3]					<0.01
0	13/14	93%	1/18	6%	
1	1/14	7%	17/18	94%	
2	0/14	0%	0/18	0%	
Jejunum[4]					<0.01
0	14/14	100%	9/18	50%	
1	0/14	0%	9/18	50%	
2	0/14	0%	0/14	0%	
Ileum[4]					0.16
0	14/14	100%	15/18	83%	
1	0/14	0%	3/18	17%	
2	0/14	0%	0/18	0%	
Colon[5]					-
0	14/14	100%	18/18	100%	
1	0/14	0%	0/18	0%	
2	0/14	0%	0/18	0%	
3	0/14	0%	0/18	0%	

[1]Adapted from Brown et al., 1975
[2]Adapted from Tennant et al., 2014
[3]Adapted from Rezac et al., 2014
[4]Adapted from Offersen et al., 2024
[5]Adapted from Mansfield and Urban, 1996
[†]3 Livers in CON (21%) scored as 0 had scar tissue present
[‡]6 Livers in LAIP (33%) scored as 0 had scar tissue present

Table 18: *Post hoc* comparison of the effects of successful liver abscess induction (LAIP-Y), failed liver abscess induction (LAIP-N), or control (CON) on organ pathology scores at euthanasia.

	Diet						
	CON		LAIP-N		LAIP-Y		
Organ	Freq.	Percent	Freq.	Percent	Freq.	Percent	*P*
Liver[1]							<0.01
0	4/4	100%	4/4	100%	0/4	0%	
A	0/4	0%	0/4	0%	1/4	25%	
A+	0/4	0%	0/4	0%	3/4	75%	
Lung[2]							<0.01
0	4/4	100%	3/4	75%	1/4	25%	
1	0/4	0%	0/4	0%	3/4	75%	
2	0/4	0%	1/4	25%	0/4	0%	
3	0/4	0%	0/4	0%	0/4	0%	
4	0/4	0%	0/4	0%	0/4	0%	
5	0/4	0%	0/4	0%	0/4	0%	
Spleen							-
0	4/4	100%	4/4	100%	4/4	100%	
1	0/4	0%	0/4	0%	0/4	0%	
2	0/4	0%	0/4	0%	0/4	0%	
3	0/4	0%	0/4	0%	0/4	0%	
Rumen[3]							0.02
0	3/4	75%	0/4	0%	0/4	0%	
1	1/4	25%	4/4	100%	4/4	100%	
2	0/4	0%	0/4	0%	0/4	0%	
Jejunum[4]							0.07
0	4/4	100%	2/4	50%	2/4	50%	
1	0/4	0%	2/4	50%	2/4	50%	
2	0/4	0%	0/4	0%	0/4	0%	
Ileum[4]							-
0	4/4	100%	4/4	100%	4/4	100%	
1	0/4	0%	0/4	0%	0/4	0%	
2	0/4	0%	0/4	0%	0/4	0%	
Colon[5]							-
0	4/4	100%	4/4	100%	4/4	100%	
1	0/4	0%	0/4	0%	0/4	0%	
2	0/4	0%	0/4	0%	0/4	0%	
3	0/4	0%	0/4	0%	0/4	0%	

[1]Adapted from Brown et al., 1975
[2]Adapted from Tennant et al., 2014
[3]Adapted from Rezac et al., 2014
[4]Adapted from Offersen et al., 2024
[5]Adapted from Mansfield and Urban, 1996

Table 19: Effects of liver abscess induction diet (LAIP) or control (CON) on intestinal morphology at euthanasia**.**

	Diet			
Parameters	CON	LAIP	SEM	*P*
Number of animals (n=20)				
Jejunum				
Height, µm	557.3	491.3	62.1	0.46
Width, µm	155.8	146.0	7.9	0.39
Depth, µm	491.3	534.2	50.1	0.55
H:D[1]	1.18	1.03	0.16	0.51
GCA[2], %	8.07	10.02	1.00	0.18
MPO[3], %	8.55	9.41	0.90	0.50
Ileum				
Height, µm	560.9	597.0	41.5	0.54
Width, µm	147.2	144.0	10.5	0.83
Depth, µm	500.8	576.1	57.8	0.37
H:D[1]	1.16	1.30	0.26	0.70
GCA[2], %	11.50	6.81	1.06	<0.01
MPO[3], %	16.12	17.33	1.64	0.60
Colon				
Depth, µm	589.0	572.5	21.8	0.60
GCA[2], %	29.09	26.48	1.86	0.33
MPO[3], %	7.77	7.70	0.59	0.93

[1]Villus height: crypt depth
[2]Goblet cell area, expressed as a percentage of epithelial area
[3]Myloperoxidase area, expressed as a percentage of epithelial area

Table 20: *Post hoc* comparison of the effects of successful liver abscess induction (LAIP-Y), failed liver abscess induction (LAIP-N), or control (CON) on intestinal morphology at euthanasia.

	Diet				
Parameters	CON	LAIP-N	LAIP-Y	SEM	*P*
Number of animals (n=12)					
Jejunum					
Height, µm	589.0	466.1	688.4	120.0	0.46
Width, µm	152.2	147.4	136.1	14.7	0.75
Depth, µm	465.6	656.1	492.3	93.3	0.32
H:D[1]	1.27	0.85	1.55	0.27	0.25
GCA[2], %	8.64	8.57	8.42	1.43	0.99
MPO[3], %	8.96	8.66	9.32	1.00	0.89
Ileum					
Height, µm	518.3	486.0	606.5	57.3	0.35
Width, µm	151.2	147.6	139.9	17.1	0.88
Depth, µm	443.8	494.3	426.0	77.2	0.82
H:D[1]	1.16	1.03	1.94	0.49	0.40
GCA[2], %	15.12[a]	6.08[b]	9.28[ab]	1.93	0.03
MPO[3], %	18.44	19.17	14.05	2.53	0.34
Colon					
Depth, µm	566.7	610.8	572.8	21.1	0.32
GCA[2], %	30.64	30.02	25.78	2.81	0.44
MPO[3], %	7.48	6.34	8.42	0.71	0.17

[1]Villus height: crypt depth
[2]Goblet cell area, expressed as a percentage of epithelial area
[3]Myloperoxidase area, expressed as a percentage of epithelial area

Table 21: Pairwise comparison of protein abundance in control (CON), successful liver abscess induction protocol (LAIP-Y), or failed liver abscess induction protocol (LAIP-N).

Description	UniProt ID	Gene Symbol	Log_2 Fold-Change				*P*			
			LAIP-N vs. CON	LAIP-Y vs. CON	LAIP vs. CON	LAIP-Y vs. LAIP-N	LAIP-N vs. CON	LAIP-Y vs. CON	LAIP vs. CON	LAIP-N vs. LAIP-Y
Protein ABHD1	Q3T0A0	ABHD1	-	-1.05	-	-	-	0.03	-	-
Acyl-coenzyme A oxidase	A0AAA9SE78	ACOX3	-	-	-	-2.08	-	-	-	0.01
A-kinase anchoring protein 1	E1BMU6	AKAP1	-	-	-	-1.59	-	-	-	0.04
Delta-1-pyrroline-5-carboxylate synthase	Q2KJH7	ALDH18A1	-	1.16	1.11	-	-	0.05	0.05	-
Arachidonate 15-lipoxygenase type B	F1MXW0	ALOX15B	1.19	1.18	1.18	-	0.02	0.03	<0.01	-
ATP synthase subunit F, mitochondrial	A0AAA9THX1	ATP5MF	-	-1.71	-1.18	-	-	<0.01	<0.01	-
Azurocidin 1	A0AAA9RU90	AZU1	1.02	-	1.10	-	0.02	-	0.02	-
Branched-chain alpha-ketoacid dehydrogenase kinase	Q2KJG8	BCKDK	1.23	-	1.04	-	0.04	-	0.04	-
Chromosome 19 C17orf75 homolog	E1BCP5	C19H17orf75	-	1.26	1.22	-	-	0.02	0.01	-
Cathelicidin-1	P22226	CATHL1	1.20	1.63	1.43	-	0.02	0.04	0.02	-
Cathelicidin-2	P19660	CATHL2	-	1.94	1.59	-	-	0.03	0.04	-
Cathelicidin-3	P19661	CATHL3	1.44	2.07	1.79	-	0.03	0.03	0.03	-
Ceramide synthase 6	A0A3Q1MJ30	CERS6	-	-	-	-1.11	-	-	-	0.04
Complement factor D	Q3T0A3	CFD	1.96	2.30	2.14	-	0.01	0.03	0.01	-
2',3'-cyclic-nucleotide 3'-phosphodiesterase	A0AAA9TS26	CNP	1.35	-	1.23	-	0.03	-	0.03	-
Copine 5	A0AAA9U0H7	CPNE5	-	-1.23	-	-	-	<0.01	-	-
Cysteine sulfinic acid decarboxylase	A0AAA9T8U5	CSAD	1.53	-	1.15	-	<0.01	-	0.03	-
Cytochrome P450 1A	F1MM10	CYP1A1	-	-1.74	-1.24	-	-	<0.01	<0.01	-
Cytochrome P450 1A	F1MHN9	CYP1A2	-	-1.14	-	-	-	0.01	-	-
Cytochrome P450 family 2 subfamily C member 23	F1MLV5	CYP2C23	-	-1.06	-	-	-	<0.01	-	-
Cytochrome P450 2E1	A0A3S5ZP79	CYP2C87	-1.13	-	-	-	0.03	-	-	-
Cytochrome P450 family 2 subfamily C member 89	A0AAF6DLR8	CYP2C89	-	-1.03	-	-	-	0.05	-	-
CYP39A1 protein	A6H722	CYP39A1	-1.01	-	-1.07	-	0.04	-	<0.01	-
Cytochrome P450 family 4 subfamily V member 2	F1N3Z7	CYP4V2	-1.50	-1.28	-1.38	-	<0.01	0.03	<0.01	-

Liver Abscess Induction Model
Study Number: GJC-LHB-3

Table 21: Pairwise comparison of protein abundance in control (CON), successful liver abscess induction protocol (LAIP-Y), or failed liver abscess induction protocol (LAIP-N).

Description	UniProt ID	Gene Symbol	Log_2 Fold-Change				*P*			
			LAIP-N vs. CON	LAIP-Y vs. CON	LAIP vs. CON	LAIP-Y vs. LAIP-N	LAIP-N vs. CON	LAIP-Y vs. CON	LAIP vs. CON	LAIP-N vs. LAIP-Y
Cholesterol 7-alpha-monooxygenase	E1BM29	CYP7A1	1.51	-	-	-1.17	0.02	-	-	0.02
RNA helicase	F6R6W2	DDX23	1.12	-	-	-	0.02	-	-	-
24-dehydrocholesterol reductase	A0A3Q1M7E0	DHCR24	-	-1.34	-	-	-	0.04	-	-
Iodothyronine deiodinase	A0AAA9S815	DIO1	-1.10	-	-	-	0.03	-	-	-
Dihydropyrimidinase	E1BFN6	DPYS	-	-	-	1.05	-	-	-	0.03
Nondiscriminating glutamyl-tRNA synthetase EARS2, mitochondrial	G3N260	EARS2	-	1.52	1.37	-	-	0.02	0.04	-
cholestenol Delta-isomerase	A0AAA9SXN0	EBP	-1.36	-	-	-	0.04	-	-	-
Enhancer of mRNA-decapping protein 4	E1BJH1	EDC4	1.06	1.12	1.09	-	0.02	0.03	0.01	-
Receptor protein-tyrosine kinase	A0A3Q1MHB0	EGFR	-	-	-	-1.39	-	-	-	0.02
Elastase, neutrophil expressed	G3MWP1	ELANE	1.65	1.87	1.76	-	<0.01	0.02	<0.01	-
EGFR pathway substrate 8, signaling adaptor	A0A3Q1M2P8	EPS8	1.27	-	-	-1.25	0.01	-	-	<0.01
F-box only protein 6	Q3SX24	FBXO6	1.04	-	-	-	0.03	-	-	-
Flavin-containing monooxygenase	G5E5J8	FMO4	-	-1.47	-	-	-	<0.01	-	-
Glycerol kinase 5	A0AAA9U125	GK5	-	-1.10	-	-	-	<0.01	-	-
D-glucuronyl C5-epimerase	O18756	GLCE	-	1.05	1.09	-	-	0.05	0.03	-
Golgin subfamily A member 5	F6RNZ4	GOLGA5	-	-	1.5	-	-	-	0.03	-
alanine transaminase	E1BF40	GPT2	-	-	-2.51	-	-	-	0.01	-
Ral transcription factor IIi	A0A3Q1MDF7	GTF2I	1.33	-	-	-	0.02	-	-	-
2-Hydroxyacid oxidase 2	Q3ZBW2	HAO2	-	-1.11	-	-	-	0.02	-	-
HECT and RLD domain containing E3 ubiquitin protein ligase 4	A0A3Q1LS42	HERC4	-	1.32	1.24	-	-	0.02	0.02	-
hexokinase	A0A3Q1LR63	HK3	-	1.42	1.21	-	-	0.04	0.03	-
Hook microtubule tethering protein 3	A0A3Q1LF92	HOOK3	2.62	2.58	2.6	-	0.04	0.03	0.01	-
Heat shock factor-binding protein 1	Q3ZC22	HSBP1	-	-	1.35	-	-	-	0.04	-
Heat shock protein beta-6	Q148F8	HSPB6	-	-1.33	-	-	-	0.04	-	-
Heat shock protein 105 kDa	Q0IIM3	HSPH1	-	1.12	-	-	-	0.03	-	-
Interleukin-1	A0A3Q1MKE9	IL1RN	-	1.03	-	-	-	0.01	-	-
Iron-responsive element-binding protein 2	A0A3Q1MUL6	IREB2	1.46	-	-	-	<0.01	-	-	-

Table 21: Pairwise comparison of protein abundance in control (CON), successful liver abscess induction protocol (LAIP-Y), or failed liver abscess induction protocol (LAIP-N).

Description	UniProt ID	Gene Symbol	Log_2 Fold-Change				*P*			
			LAIP-N vs. CON	LAIP-Y vs. CON	LAIP vs. CON	LAIP-Y vs. LAIP-N	LAIP-N vs. CON	LAIP-Y vs. CON	LAIP vs. CON	LAIP-N vs. LAIP-Y
Integrin beta-5	P80747	ITGB5	-	1.27	1.13	-	-	0.03	0.01	-
Inter-alpha-trypsin inhibitor heavy chain H3	Cont_P56652	ITIH3	2.01	1.68	1.86	-	0.02	<0.01	<0.01	-
Intersectin 1	A0A3Q1LQU1	ITSN1	-	1.42	1.2	-	-	<0.01	0.01	-
KN motif and ankyrin repeat domains 1	F1N1B8	KANK1	1.65	-	-	-	0.04	-	-	-
ER lumen protein-retaining receptor	A0AAA9RZW3	KDELR2	-	-	-	1.83	-	-	-	<0.01
Lysine-specific histone demethylase	F1MBS5	KDM1A	-	-	-	-1.31	-	-	-	<0.01
Kinesin family member 13B	A0A3Q1NM85	KIF13B	-	-	-	-1.94	-	-	-	<0.01
La ribonucleoprotein 4	F1MHD9	LARP4	1.28	-	1.07	-	0.05	-	0.03	-
UDP-glucuronosyltransferase	E1BBB3	LOC100138004	-	-1.01	-	-	-	0.04	-	-
Retinol dehydrogenase 16-like	A0A3Q1NIN1	LOC100138638	-	-1	-	-	-	<0.01	-	-
Cathelicidin antimicrobial peptide C-terminal domain-containing protein	A0AAF7AJ81	LOC132342071	-	1.65	1.42	-	-	0.05	0.04	-
Peptidase S1 domain-containing protein	A0AAA9TPH0	LOC505658	2.06	-	2.17	-	<0.01	-	0.01	-
UDP-glucuronosyltransferase	F1MRL5	LOC540544	-	-1.07	-	-	-	<0.01	-	-
UDP-glucuronosyltransferase	A6QPD5	LOC781988	-	-1.02	-	-	-	<0.01	-	-
Lactotransferrin	A0AAA9SUD5	LTF	-	1.69	1.63	-	-	0.04	0.03	-
lysozyme	A0A077S9Q3	LYZF1	-	-	-	-1.03	-	-	-	0.02
alpha-mannosidase	F1MWT0	MAN2C1	-	-	-	1.03	-	-	-	0.03
Microtubule associated protein 1S	F1N1H2	MAP1S	1	-	-	-	0.01	-	-	-
Membrane bound O-acyltransferase domain containing 2	F1MH02	MBOAT2	1.41	-	-	-	0.04	-	-	-
DNA replication licensing factor MCM3	A4FUD9	MCM3	1.31	1.69	1.52	-	0.03	0.03	<0.01	-
DNA replication licensing factor MCM4	A0AAA9S1P6	MCM4	-	-	1.36	-	-	-	0.04	-
DNA replication licensing factor MCM5	A0AAA9TCV3	MCM5	-	3.04	-	-	-	0.05	-	-
DNA replication licensing factor MCM7	A0A3Q1MD98	MCM7	-	1.55	1.38	-	-	0.03	0.04	-
Large ribosomal subunit protein uL30m	A0A140T852	MRPL30	-	1.31	-	-	-	<0.01	-	-

Table 21: Pairwise comparison of protein abundance in control (CON), successful liver abscess induction protocol (LAIP-Y), or failed liver abscess induction protocol (LAIP-N).

Description	UniProt ID	Gene Symbol	Log_2 Fold-Change				*P*			
			LAIP-N vs. CON	LAIP-Y vs. CON	LAIP vs. CON	LAIP-Y vs. LAIP-N	LAIP-N vs. CON	LAIP-Y vs. CON	LAIP vs. CON	LAIP-N vs. LAIP-Y
Mitochondrial ribosomal protein S34	F1MKN3	MRPS34	1.27	-	-	-	0.04	-	-	-
MYB binding protein 1a	E1BKX3	MYBBP1A	1.02	-	-	-	0.03	-	-	-
Unconventional myosin-VI	A0AAA9S4N7	MYO6	1.33	-	-	-	0.04	-	-	-
N-alpha-acetyltransferase 25, NatB auxiliary subunit	E1BDV7	NAA25	1.14	-	-	-	0.02	-	-	-
NADH dehydrogenase [ubiquinone] 1 alpha subcomplex subunit 11	A0AAF6Z6D2	NDUFA11	-	-	-1.16	-	-	-	0.03	-
NADH dehydrogenase [ubiquinone] 1 subunit C1, mitochondrial	A0AAA9TJB9	NDUFC1	-	-1.10	-	-	-	0.04	-	-
Nuclear export mediator factor	A0A3Q1MSI2	NEMF	1.11	-	-	-	0.04	-	-	-
Cytosolic purine 5'-nucleotidase	A0AAF7AMR3	NT5C2	1.41	-	1.23	-	<0.01	-	0.01	-
Nucleoporin 153	A0AAA9TXI1	NUP153	1.61	-	1.36	-	<0.01	-	0.02	-
Ornithine aminotransferase	F1MYG0	OAT	-1.68	-2.06	-1.85	-	<0.01	<0.01	<0.01	-
phosphoinositide 5-phosphatase	A0AAA9U0Y4	OCRL	-	-	-	-1.89	-	-	-	0.02
Olfactomedin 4	F1MVJ8	OLFM4	1.66	-	-	-	0.03	-	-	-
Polyadenylate-binding protein 2	Q28165	PABPN1	-	-	-	-1.05	-	-	-	0.03
PDZ and LIM domain protein 2	Q3T0C8	PDLIM2	1.15	-	1.18	-	<0.01	-	0.01	-
Xaa-Pro dipeptidase	A0AAA9U062	PEPD	-	1.26	1.04	-	-	<0.01	0.02	-
Peptidoglycan recognition protein 1	Cont_Q8SPP7	PGLYRP1	-	-	1.11	-	-	-	0.05	-
PGM2L1 protein	A5PKH8	PGM2L1	-	1.13	-	-	-	0.02	-	-
Phosphatidylinositol-glycan biosynthesis class X protein	A0AAA9TVV6	PIGX	-	-1.01	-	-	-	0.02	-	-
Peroxisomal sarcosine oxidase	Q29RU9	PIPOX	-	-1.04	-	-	-	0.05	-	-
Periostin	Cont_Q2KJC7	POSTN	-	1.92	1.68	-	-	<0.01	<0.01	-
E3 ubiquitin-protein ligase PPP1R11	A0AAA9TT39	PPP1R11	-	-	-	1.57	-	-	-	0.02
Protein phosphatase 1 regulatory subunit 18	A0AAA9SFU7	PPP1R18	-	1.27	1.04	-	-	0.01	0.03	-
Protein phosphatase 1 regulatory subunit 9B	A0A3Q1M3I7	PPP1R9B	1.38	-	1.45	-	0.02	-	0.04	-
Protein phosphatase 6 regulatory subunit 1	A0AAA9RUI1	PPP6R1	2.12	-	-	-	0.03	-	-	-
Proteinase 3	G3MXK8	PRTN3	1.05	-	1.2	-	0.02	-	0.04	-
protein-tyrosine-phosphatase	E1BPU9	PTPRM	1.24	1.85	1.57	-	0.02	0.05	0.03	-

Table 21: Pairwise comparison of protein abundance in control (CON), successful liver abscess induction protocol (LAIP-Y), or failed liver abscess induction protocol (LAIP-N).

Description	UniProt ID	Gene Symbol	Log_2 Fold-Change				*P*			
			LAIP-N vs. CON	LAIP-Y vs. CON	LAIP vs. CON	LAIP-Y vs. LAIP-N	LAIP-N vs. CON	LAIP-Y vs. CON	LAIP vs. CON	LAIP-N vs. LAIP-Y
Rabaptin, RAB GTPase binding effector protein 1	F1MQH8	RABEP1	1.35	-	1.41	-	0.03	-	0.04	-
arginine--tRNA ligase	A0AAA9S3M6	RARS2	-	1.35	1.45	-	-	<0.01	0.03	-
RNA binding motif protein 15	A0AAA9RVE8	RBM15	-	1.06	-	-	-	0.04	-	-
RNA binding motif single stranded interacting protein 1	A0AAA9RYP5	RBMS1	-	1.04	-	-	-	0.05	-	-
Ring finger protein 213	A0A3Q1LV49	RNF213	1.33	-	1.2	-	0.02	-	0.02	-
RUN and FYVE domain containing 3	A0AAA9T5Y4	RUFY3	2.45	2.03	2.25	-	<0.01	<0.01	<0.01	-
Protein S100	A0AAF6YHF0	S100A2	-	2.01	-	-	-	0.04	-	-
Protein S100-A8	P28782	S100A8	-	-	1.28	-	-	-	0.02	-
Protein S100-A9	F1MHS5	S100A9	-	-	1.22	-	-	-	0.04	-
Serum amyloid A protein	A0AAA9RWU0	SAA4	-	-1.04	-	-	-	0.03	-	-
Syndecan binding protein	A0AAA9SP21	SDCBP	-	1.35	1.04	-	-	<0.01	0.02	-
L-serine ammonia-lyase	F1N0R8	SDS	1.06	-	1.29	-	<0.01	-	0.04	-
Nucleoporin SEH1	A7YY75	SEH1L	-	1.02	-	-	-	0.03	-	-
Semaphorin 4B	F1MYZ4	SEMA4B	-	-	-	1.29	-	-	-	0.05
Serpin A3-4	Cont_A2I7N0	SERPINA3-4	-	3.02	2.87	-	-	0.04	0.05	-
SHC-transforming protein 1	E1B716	SHC1	1.02	-	-	-	<0.01	-	-	-
Solute carrier family 38 member 10	A0A3Q1LQW5	SLC38A10	1.04	1.04	1.04	-	0.05	0.04	0.01	-
Transporter	E1BPI1	SLC6A11	-	-	-	-1.36	-	-	-	0.02
Schlafen family member 11	E1B9R8	SLFN11	-	1.49	1.32	-	-	0.05	0.04	-
SWI/SNF related, matrix associated, actin dependent regulator of chromatin, subfamily e, member 1	F6RNR1	SMARCE1	-	-	-	1.01	-	-	-	<0.01
Small integral membrane protein 12	A0AAA9TIC4	SMIM12	-1.09	-	-1.04	-	0.04	-	<0.01	-
Cytospin-A	A0A3Q1MCL9	SPECC1L	-	-	-2.11	-	-	-	0.04	-
Serine and arginine rich splicing factor 5	F6RS73	SRSF5	-	1.08	1.02	-	-	0.02	0.03	-
Syntaxin-binding protein 2	F1MHC2	STXBP2	-	-	1.19	-	-	-	0.05	-
FACT complex subunit	A0AAA9T403	SUPT16H	-	-	1.52	-	-	-	0.05	-
Transcription elongation factor SPT5	A0A3Q1MQ76	SUPT5H	-	1.2	1.04	-	-	0.04	0.02	-
Tyrosine aminotransferase	A0AAA9TG21	TAT	-	-1.09	-	-	-	0.03	-	-

Liver Abscess Induction Model
Study Number: GJC-LHB-3

Table 21: Pairwise comparison of protein abundance in control (CON), successful liver abscess induction protocol (LAIP-Y), or failed liver abscess induction protocol (LAIP-N).

Description	UniProt ID	Gene Symbol	Log_2 Fold-Change				*P*			
			LAIP-N vs. CON	LAIP-Y vs. CON	LAIP vs. CON	LAIP-Y vs. LAIP-N	LAIP-N vs. CON	LAIP-Y vs. CON	LAIP vs. CON	LAIP-N vs. LAIP-Y
Transcription elongation factor A protein-like 4	A0AAA9TRF8	TCEAL4	1.04	1.02	1.03	-	0.04	0.03	0.01	-
L-threonine 3-dehydrogenase, mitochondrial	Q2KIR8	TDH	-	-	-1.04	-	-	-	0.03	-
Calcineurin B homologous protein 3	A0AAA9RW98	TESC	-	-	-	1.89	-	-	-	0.02
Threonine aldolase 1	F1MVX8	THA1	-	1.39	1.19	-	-	0.03	0.05	-
Threonine aldolase 1	A0A3Q1MKR6	THA1	-	1.34	1.1	-	-	0.04	0.05	-
Transmembrane emp24 domain-containing protein 1	Q2TBK5	TMED1	-	1.06	-	-	-	0.04	-	-
TNPO3 protein	A5D7C4	TNPO3	1.08	-	-	-	0.05	-	-	-
Ubiquitin-like modifier-activating enzyme 5	A0AAF6YML4	UBA5	-	1.26	1.27	-	-	<0.01	0.01	-
NEDD8-conjugating enzyme UBE2F	Q1RMW1	UBE2F	-	-	-	-1.32	-	-	-	<0.01
Cytochrome b-c1 complex subunit 8	A0AAA9RXP7	UQCRQ	-1.11	-	-	-	<0.01	-	-	-
Vesicle trafficking 1	F1N318	VTA1	1.13	-	-	-	0.02	-	-	-
von Willebrand factor (Fragment)	Cont_P80012	VWF	1.56	1.38	1.47	-	0.03	<0.01	<0.01	-
von Willebrand factor	A0AAA9SW64	VWF	1.43	1.47	1.45	-	0.03	0.02	<0.01	-
WD repeat-containing protein 37	A0AAA9TTD4	WDR37	-	-	-	-1.08	-	-	-	0.03
WD repeat-containing protein 48	A0A3Q1LQA5	WDR48	1.10	-	1.01	-	0.04	-	0.01	-
WAP four-disulfide core domain protein 2	G3MX65	WFDC2	-	-	-1.6	-	-	-	0.05	-
non-specific serine/threonine protein kinase	E1BN63	WNK1	-	-	-	1.28	-	-	-	0.03
X-ray repair cross complementing 6	F1MMD5	XRCC6	1.14	-	-	-	0.02	-	-	-
Uncharacterized protein	A0AAF7A422	-	1.68	2.29	2.02	-	0.03	0.03	0.02	-
Cathelicidin 4	A0AAF6ZFN1	-	1.14	1.93	1.59	-	0.01	0.03	0.03	-
glucuronosyltransferase	A0A3Q1MIN6	-	-1.09	-1.5	-1.28	-	<0.01	<0.01	<0.01	-
Apolipoprotein B receptor	A0AAA9TS69	-	-	2.22	1.88	-	-	0.02	0.03	-
Ig-like domain-containing protein	A0AAA9TPF4	-	-	1.81	1.58	-	-	0.05	0.04	-
Ig-like domain-containing protein	A0A3Q1MT50	-	-	1.18	-	-	-	<0.01	-	-
Cathelicidin 5	A0A452DIN2	-	-	-	1.77	-	-	-	0.03	-
Serpin domain-containing protein	A0A452DJA9	-	-	-	1.27	-	-	-	0.05	-
Sushi domain-containing protein	G3N0S9	-	-	-	-	1.04	-	-	-	0.01

Table 21: Pairwise comparison of protein abundance in control (CON), successful liver abscess induction protocol (LAIP-Y), or failed liver abscess induction protocol (LAIP-N).

Description	UniProt ID	Gene Symbol	Log_2 Fold-Change				*P*			
			LAIP-N vs. CON	LAIP-Y vs. CON	LAIP vs. CON	LAIP-Y vs. LAIP-N	LAIP-N vs. CON	LAIP-Y vs. CON	LAIP vs. CON	LAIP-N vs. LAIP-Y

Table 22: *Post hoc* gene-set enrichment analysis of select KEGG pathways in control (CON), successful liver abscess induction protocol (LAIP-Y), or failed liver abscess induction protocol (LAIP-N). Proteins with NCBI gene IDs were ranked by log_2 fold change and *P* value within pairwise comparison and ranks were used to compute normalized enrichment.

Pathway Description	Pathway ID	Normalized Enrichment Score				*P*			
		LAIP-N vs. CON	LAIP-Y vs. CON	LAIP vs. CON	LAIP-Y vs. LAIP-N	CON vs. LAIP-N	CON vs. LAIP-Y	CON vs. LAIP	LAIP-N vs. LAIP-Y
Mineral absorption	bta04978	-	1.75	1.53	1.72	-	<0.01	0.08	0.08
Complement and coagulation cascades	bta04610	-	1.71	1.57	1.83	-	<0.01	0.05	0.06
Tuberculosis	bta05152	1.70	1.67	1.70	-	0.02	0.02	<0.01	-
Nucleocytoplasmic transport	bta03013	1.59	1.61	1.63	-	0.06	0.05	0.03	-
Neutrophil extracellular trap formation	bta04613	1.57	1.86	1.73	-	0.07	<0.01	<0.01	-
Human papillomavirus infection	bta05165	1.55	1.55	1.68	-	0.06	0.05	<0.01	-
Coronavirus disease - COVID-19	bta05171	1.53	1.61	1.63	-	0.06	0.02	0.02	-
Huntington disease	bta05016	-1.62	-1.95	-1.89	-	0.02	<0.01	<0.01	-
Chemical carcinogenesis - receptor activation	bta05207	-1.63	-1.67	-1.67	-	0.06	0.03	0.04	-
Alzheimer disease	bta05010	-1.66	-1.90	-1.92	-	<0.01	<0.01	<0.01	-
Glyoxylate and dicarboxylate metabolism	bta00630	-1.72	-1.62	-1.66	-	0.07	0.09	0.07	-
Pentose and glucuronate interconversions	bta00040	-1.72	-1.93	-1.90	-	0.07	<0.01	<0.01	-
Glycine, serine and threonine metabolism	bta00260	-1.74	-1.63	-1.79	-	0.06	0.08	0.03	-
Steroid hormone biosynthesis	bta00140	-1.78	-2.04	-2.08	-	0.05	<0.01	<0.01	-
Diabetic cardiomyopathy	bta05415	-1.79	-1.83	-1.82	-	<0.01	<0.01	<0.01	-
Thermogenesis	bta04714	-1.79	-2.04	-1.97	-	<0.01	<0.01	<0.01	-
Oxidative phosphorylation	bta00190	-1.80	-2.08	-2.12	-	<0.01	<0.01	<0.01	-
Prion disease	bta05020	-1.89	-1.99	-2.02	-	<0.01	<0.01	<0.01	-
Arachidonic acid metabolism	bta00590	-1.90	-1.75	-1.90	-	<0.01	0.02	<0.01	-
Cardiac muscle contraction	bta04260	-1.91	-1.61	-1.77	-	<0.01	0.10	0.03	-
Metabolic pathways	bta01100	-1.92	-2.08	-2.15	-	<0.01	<0.01	<0.01	-
Tryptophan metabolism	bta00380	-1.97	-1.76	-2.01	-	<0.01	0.01	<0.01	-
Drug metabolism - other enzymes	bta00983	-2.08	-1.89	-2.12	-	<0.01	<0.01	<0.01	-

Table 21: Pairwise comparison of protein abundance in control (CON), successful liver abscess induction protocol (LAIP-Y), or failed liver abscess induction protocol (LAIP-N).

Description	UniProt ID	Gene Symbol	Log_2 Fold-Change				*P*			
			LAIP-N vs. CON	LAIP-Y vs. CON	LAIP vs. CON	LAIP-Y vs. LAIP-N	LAIP-N vs. CON	LAIP-Y vs. CON	LAIP vs. CON	LAIP-N vs. LAIP-Y
Parkinson disease	bta05012	-2.11	-2.13	-2.24	-		<0.01	<0.01	<0.01	-
Retinol metabolism	bta00830	-2.13	-2.10	-2.13	-		<0.01	<0.01	<0.01	-
Chemical carcinogenesis - reactive oxygen species	bta05208	-2.19	-2.21	-2.28	-		<0.01	<0.01	<0.01	-
Drug metabolism - cytochrome P450	bta00982	-2.20	-1.97	-2.11	-		<0.01	<0.01	<0.01	-
Chemical carcinogenesis - DNA adducts	bta05204	-2.21	-2.03	-2.18	-		<0.01	<0.01	<0.01	-
Metabolism of xenobiotics by cytochrome P450	bta00980	-2.23	-2.03	-2.16	-		<0.01	<0.01	<0.01	-
Salivary secretion	bta04970	1.59	-	1.62	-		0.06	-	0.04	-
Influenza A	bta05164	1.55	-	1.61	-		0.08	-	0.04	-
Tyrosine metabolism	bta00350	-1.69	-	-1.62	-		0.06	-	0.07	-
Histidine metabolism	bta00340	-1.69	-	-1.63	-		0.06	-	0.06	-
Biosynthesis of cofactors	bta01240	-1.73	-	-1.59	-		<0.01	-	0.02	-
Glutathione metabolism	bta00480	-1.77	-	-1.86	-		0.06	-	<0.01	-
Carbon metabolism	bta01200	-1.65	-	-	-		0.04	-	-	-
Staphylococcus aureus infection	bta05150	-	1.74	1.74	-		-	<0.01	<0.01	-
Herpes simplex virus 1 infection	bta05168	-	1.66	1.54	-		-	0.03	0.07	-
Fc gamma r-mediated phagocytosis	bta04666	-	1.61	1.58	-		-	0.06	0.05	-
Integrin signaling	bta04518	-	1.56	1.53	-		-	0.08	0.07	-
Natural killer cell mediated cytotoxicity	bta04650	-	1.55	1.68	-		-	0.10	0.02	-
Non-small cell lung cancer	bta05223	-	1.54	1.53	-		-	0.10	0.07	-
Spliceosome	bta03040	-	1.48	1.46	-		-	0.10	0.10	-
Amyotrophic lateral sclerosis	bta05014	-	-1.65	-1.43	-		-	<0.01	0.04	-
Porphyrin metabolism	bta00860	-	-1.65	-1.65	-		-	0.06	0.06	-
Pathways of neurodegeneration - multiple diseases	bta05022	-	-1.67	-1.53	-		-	<0.01	<0.01	-
Fatty acid degradation	bta00071	-	-1.68	-1.73	-		-	0.05	0.04	-
Peroxisome	bta04146	-	-1.76	-1.65	-		-	<0.01	0.06	-
Fatty acid metabolism	bta01212	-	-1.76	-1.74	-		-	0.02	0.04	-
Non-alcoholic fatty liver disease	bta04932	-	-1.84	-1.75	-		-	<0.01	<0.01	-
PPAR signaling pathway	bta03320	-	-1.86	-1.76	-		-	<0.01	0.03	-
Bile secretion	bta04976	-	-1.99	-1.78	-		-	<0.01	0.03	-

Table 21: Pairwise comparison of protein abundance in control (CON), successful liver abscess induction protocol (LAIP-Y), or failed liver abscess induction protocol (LAIP-N).

Description	UniProt ID	Gene Symbol	Log_2 Fold-Change				*P*			
			LAIP-N vs. CON	LAIP-Y vs. CON	LAIP vs. CON	LAIP-Y vs. LAIP-N	LAIP-N vs. CON	LAIP-Y vs. CON	LAIP vs. CON	LAIP-N vs. LAIP-Y
Micrornas in cancer	bta05206	-	1.61	-	-		-	0.06	-	-
Cholesterol metabolism	bta04979	-	-1.65	-	-		-	0.07	-	-
Primary bile acid biosynthesis	bta00120	-	-1.71	-	-		-	0.01	-	-
Retrograde endocannabinoid signaling	bta04723	-	-1.75	-	-		-	0.02	-	-
Ascorbate and aldarate metabolism	bta00053	-	-1.77	-	-		-	<0.01	-	-
Sphingolipid signaling pathway	bta04071	-	-	1.60	-		-	-	0.04	-
Glioma	bta05214	-	-	1.58	-		-	-	0.03	-
Focal adhesion	bta04510	-	-	1.56	-		-	-	0.05	-
Hepatitis b	bta05161	-	-	1.56	-		-	-	0.06	-
T-cell receptor signaling pathway	bta04660	-	-	1.52	-		-	-	0.09	-
Breast cancer	bta05224	-	-	1.51	-		-	-	0.06	-
EGFR tyrosine kinase inhibitor resistance	bta01521	-	-	1.51	-		-	-	0.09	-
Human cytomegalovirus infection	bta05163	-	-	1.50	-		-	-	0.09	-
Biosynthesis of unsaturated fatty acids	bta01040	-	-	-1.59	-		-	-	0.09	-
Ovarian steroidogenesis	bta04913	-	-	-1.60	-		-	-	0.08	-
Valine, leucine and isoleucine degradation	bta00280	-	-	-1.64	-		-	-	0.07	-
β-alanine metabolism	bta00410	-	-	-1.73	-		-	-	0.04	-

Liver Abscess Induction Model
Study Number: GJC-LHB-3

Table 23: *Post hoc* gene-set enrichment analysis of select gene ontology pathways in control (CON), successful liver abscess induction protocol (LAIP-Y), or failed liver abscess induction protocol (LAIP-N).Proteins with Gene IDs were ranked by log_2 fold change and *P* value within pairwise comparison and ranks were used to compute normalized enrichment score.

Pathway Description	Pathway ID	Normalized Enrichment Score				*P*			
		LAIP-N vs. CON	LAIP-Y vs. CON	LAIP vs. CON	LAIP-Y vs. LAIP-N	CON vs. LAIP-N	CON vs. LAIP-Y	CON vs. LAIP	LAIP-N vs. LAIP-Y
Biological Process									
Nucleic acid metabolic process	GO:0090304	1.42	1.40	1.43	-	0.08	0.10	0.07	-
Small molecule metabolic process	GO:0044281	-1.48	-1.60	-1.67	-	0.01	<0.01	<0.01	-
Organic acid metabolic process	GO:0006082	-1.53	-1.49	-1.75	-	0.04	0.05	<0.01	-
Small molecule biosynthetic process	GO:0044283	-1.59	-1.61	-1.77	-	0.08	0.05	0.01	-
Mitochondrion organization	GO:0007005	-1.68	-1.93	-1.87	-	0.07	<0.01	<0.01	-
NADH dehydrogenase complex assembly	GO:0010257	-1.89	-2.03	-2.03	-	0.07	<0.01	<0.01	-
Mitochondrial respiratory chain complex I assembly	GO:0032981	-1.89	-2.03	-2.03	-	0.07	<0.01	<0.01	-
Generation of precursor metabolites and energy	GO:0006091	-1.77	-	-1.82	-	0.04	-	<0.01	-
Defense response to other organism	GO:0098542	-	1.78	1.68	-	-	<0.01	0.01	-
Response to biotic stimulus	GO:0009607	-	1.71	1.61	-	-	<0.01	0.02	-
Defense response	GO:0006952	-	1.69	1.61	-	-	<0.01	0.02	-
Biological process involved in interspecies interaction between organisms	GO:0044419	-	1.60	1.52	-	-	0.03	0.10	-
Alcohol biosynthetic process	GO:0046165	-	-1.77	-1.83	-	-	0.08	0.05	-
Oxidative phosphorylation	GO:0006119	-	-1.88	-1.89	-	-	0.02	0.03	-
Cellular respiration	GO:0045333	-	-1.93	-1.96	-	-	<0.01	<0.01	-
Alcohol metabolic process	GO:0006066	-	-1.99	-1.86	-	-	<0.01	0.02	-
Steroid metabolic process	GO:0008202	-	-2.10	-1.97	-	-	<0.01	<0.01	-
Aminoglycan metabolic process	GO:0006022	-	1.69	-	-	-	0.02	-	-
Glycosaminoglycan metabolic process	GO:0030203	-	1.69	-	-	-	0.02	-	-
Immune system process	GO:0002376	-	1.61	-	-	-	0.01	-	-
Response to external stimulus	GO:0009605	-	1.56	-	-	-	0.03	-	-
Immune response	GO:0006955	-	1.56	-	-	-	0.07	-	-
Response to chemical	GO:0042221	-	1.42	-	-	-	0.10	-	-
Gene expression	GO:0010467	-	1.34	-	-	-	0.10	-	-
Proton transmembrane transport	GO:1902600	-	-1.80	-	-	-	0.05	-	-
Carboxylic acid metabolic process	GO:0019752	-	-	-1.74	-	-	-	<0.01	-

Liver Abscess Induction Model
Study Number: GJC-LHB-3

Table 23: *Post hoc* gene-set enrichment analysis of select gene ontology pathways in control (CON), successful liver abscess induction protocol (LAIP-Y), or failed liver abscess induction protocol (LAIP-N).Proteins with Gene IDs were ranked by $\log_2$ fold change and *P* value within pairwise comparison and ranks were used to compute normalized enrichment score.

Pathway Description	Pathway ID	Normalized Enrichment Score				*P*			
		LAIP-N vs. CON	LAIP-Y vs. CON	LAIP vs. CON	LAIP-Y vs. LAIP-N	CON vs. LAIP-N	CON vs. LAIP-Y	CON vs. LAIP	LAIP-N vs. LAIP-Y
Steroid biosynthetic process	GO:0006694	-	-	-1.81	-	-	-	0.08	-
Mitochondrial respiratory chain complex assembly	GO:0033108	-	-	-2.02	-	-	-	<0.01	-
Molecular Function									
Oxidoreductase activity	GO:0016491	-1.93	-2.03	-2.10	-	<0.01	<0.01	<0.01	-
Transporter activity	GO:0005215	-1.74	-	-	-	0.06	-	-	-
Zinc ion binding	GO:0008270	-	1.79	1.66	-	-	<0.01	0.08	-
Molecular function regulator activity	GO:0098772	-	1.62	1.53	-	-	0.01	0.10	-
Nucleic acid binding	GO:0003676	-	1.62	1.50	-	-	<0.01	0.06	-
Transmembrane transporter activity	GO:0022857	-	-1.65	-1.74	-	-	0.06	0.10	-
Enzyme inhibitor activity	GO:0004857	-	1.77	-	-	-	0.01	-	-
Molecular function inhibitor activity	GO:0140678	-	1.62	-	-	-	0.07	-	-

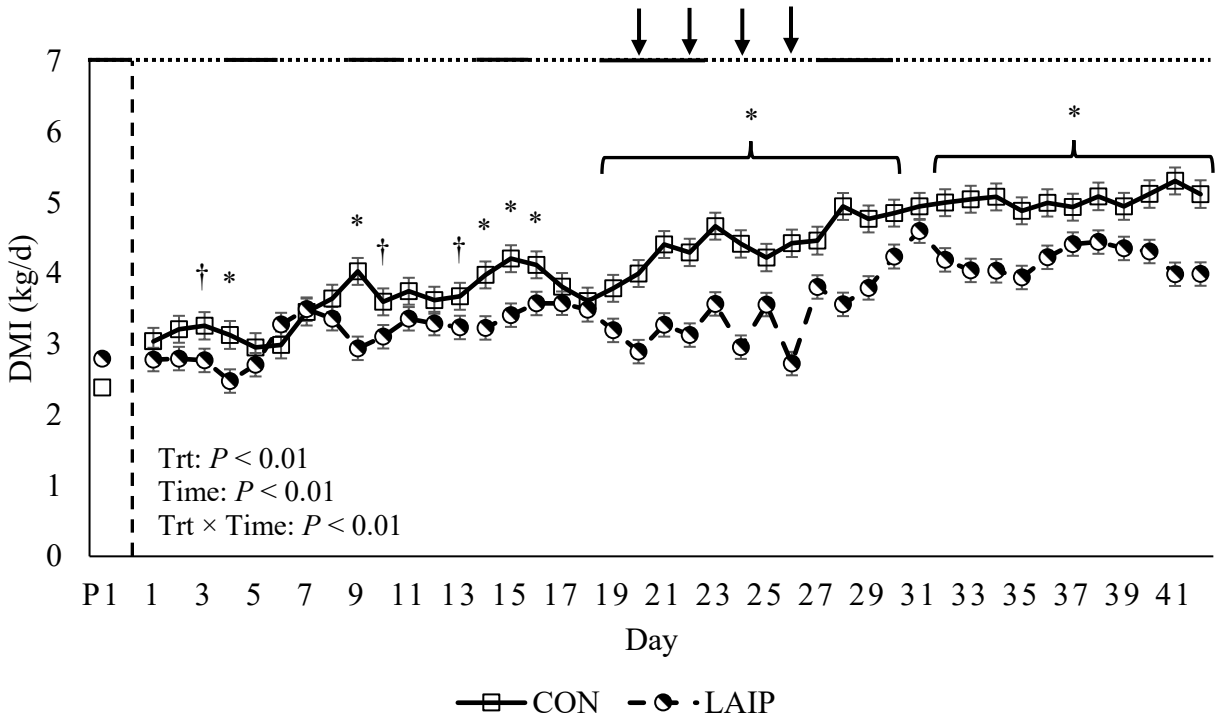

Figure 2. Effects of liver abscess induction protocol (LAIP) or control (CON) on dry matter intake during P2 Top axis depicts solid line, dashed line, and arrows for LS, HS, and feed restriction, respectively, in LAIP. * denotes $P < 0.05$, † denotes $0.05 < P \leq 0.10$.

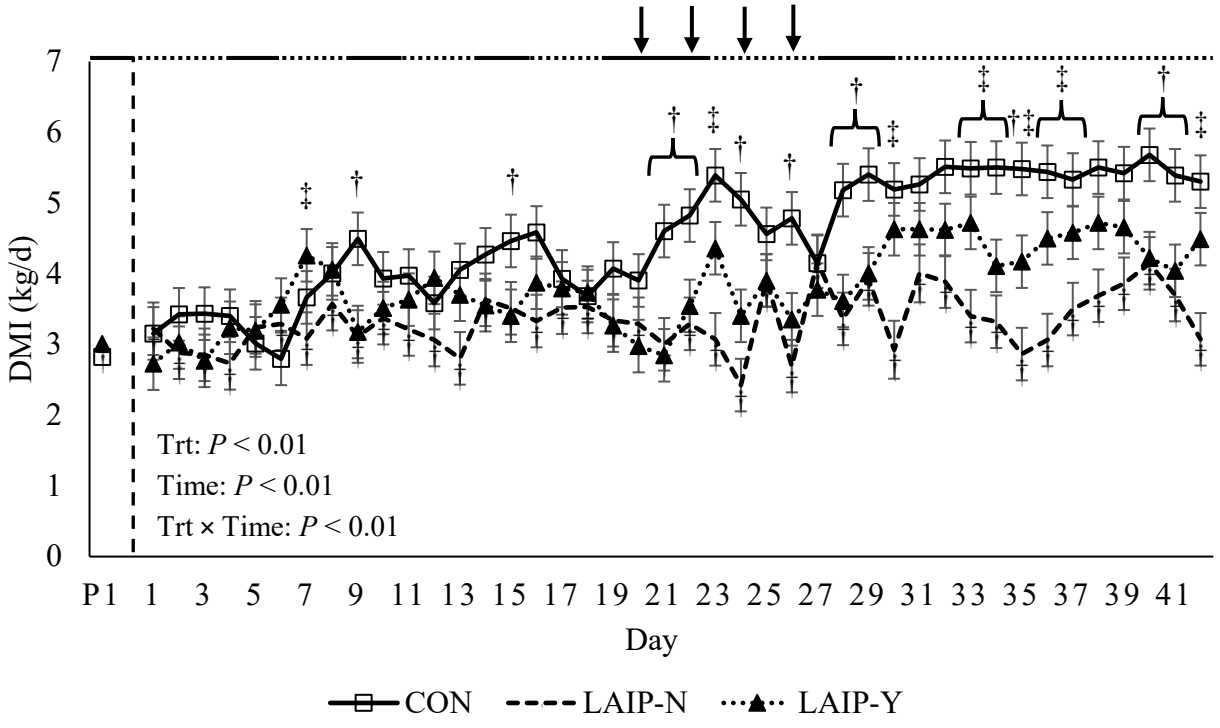

Figure 3. *Post hoc* comparison of the effects of successful liver abscess induction (LAIP-Y), failed liver abscess induction (LAIP-N), or control (CON) on dry matter intake during P2**.** Top axis depicts solid line, dashed line, and arrows for LS, HS, and feed restriction, respectively, in LAIP. † denotes pairwise differences between LAIP-Y and CON, . ‡ denotes pairwise differences between LAIP-Y and LAIP-N.

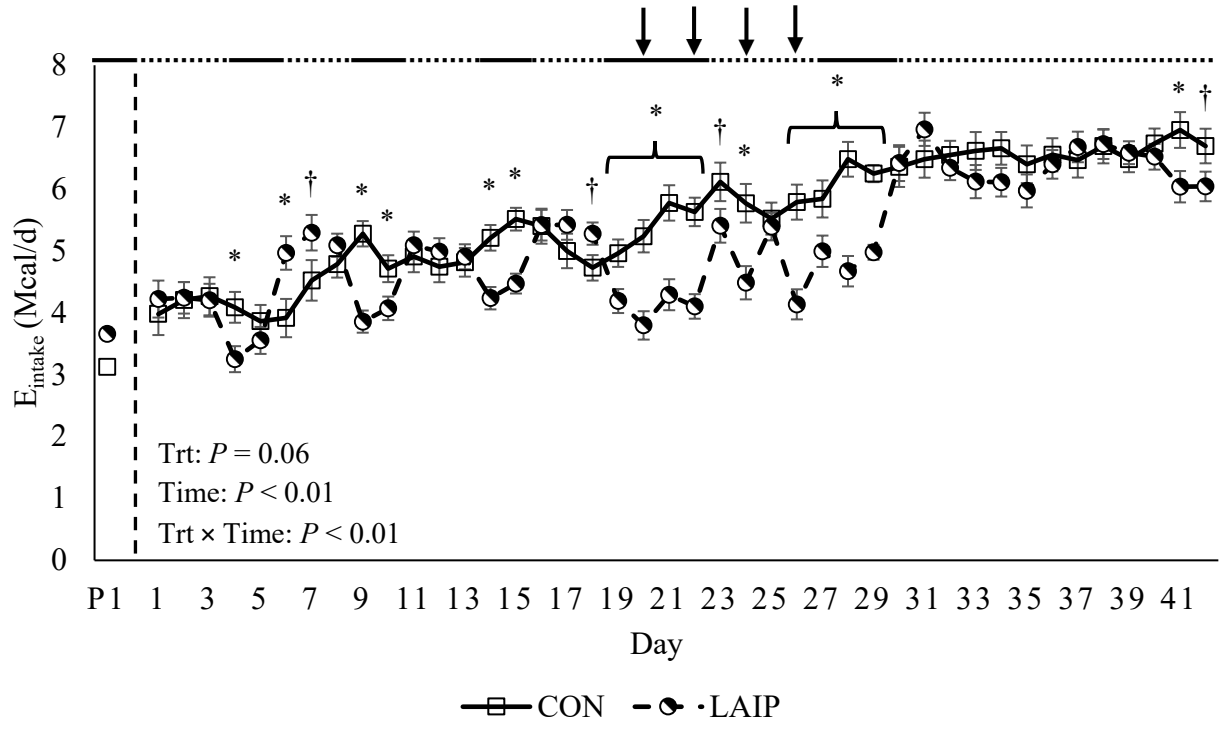

Figure 4. Effects of liver abscess induction protocol (LAIP) or control (CON) on dietary energy intake during P2. Top axis depicts solid line, dashed line, and arrows for LS, HS, and feed restriction, respectively, in LAIP. * denotes $P < 0.05$, † denotes $0.05 < P \leq 0.10$.

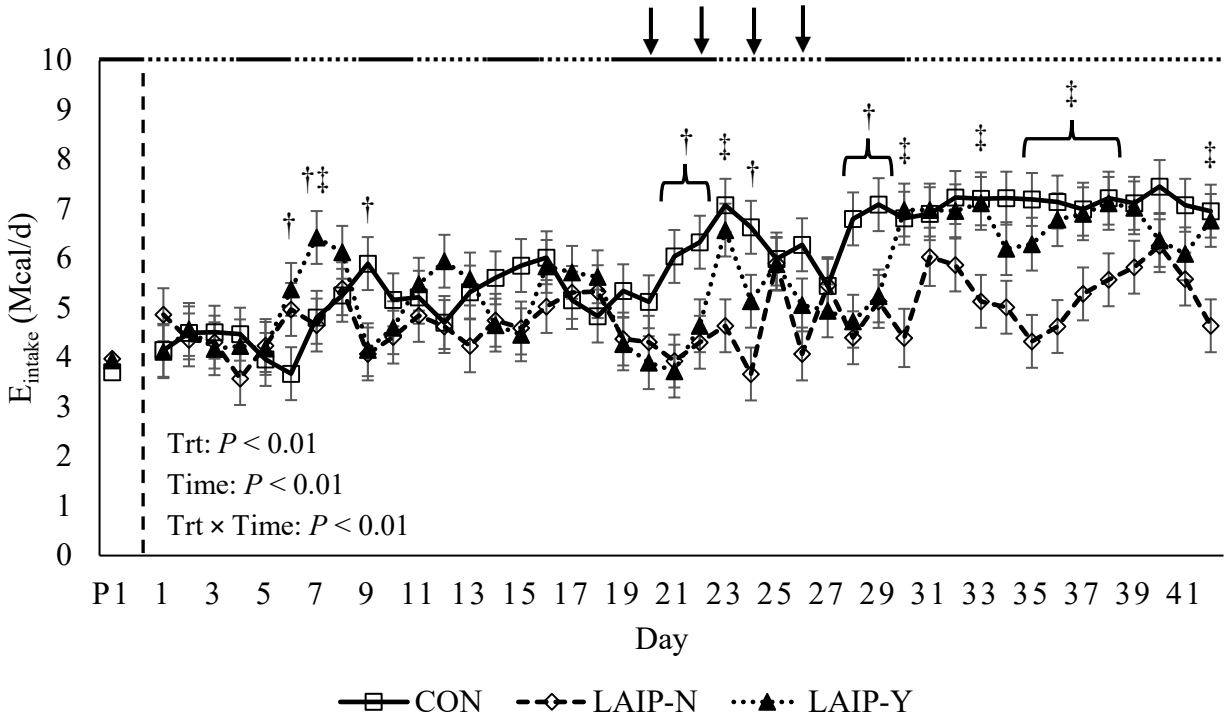

Figure 5. *Post hoc* comparison of the effects of successful liver abscess induction (LAIP-Y), failed liver abscess induction (LAIP-N), or control (CON) on dietary energy intake during P2. Top axis depicts solid line, dashed line, and arrows for LS, HS, and feed restriction, respectively, in LAIP. † denotes pairwise differences between LAIP-Y and CON. ‡ denotes pairwise differences between LAIP-Y and LAIP-N.

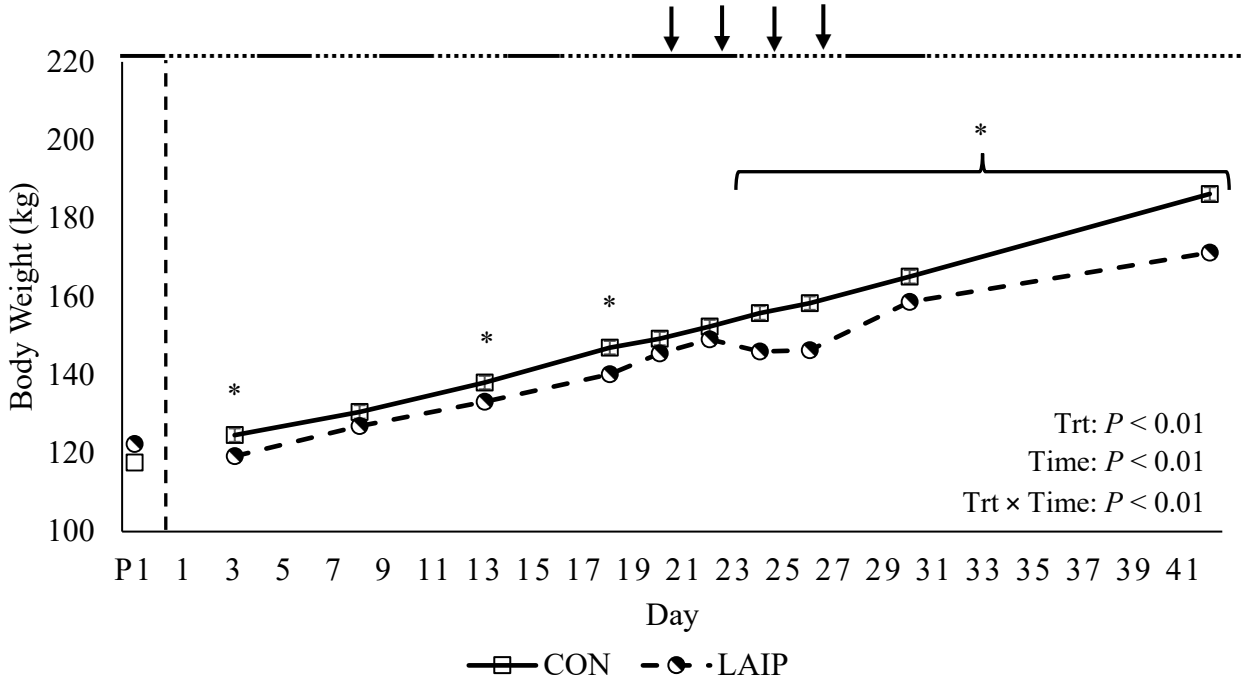

Figure 6. Effects of liver abscess induction protocol (LAIP) or control (CON) on body weight during P2. Top axis depicts solid line, dashed line, and arrows for LS, HS, and feed restriction, respectively, in LAIP. * denotes $P < 0.05$.

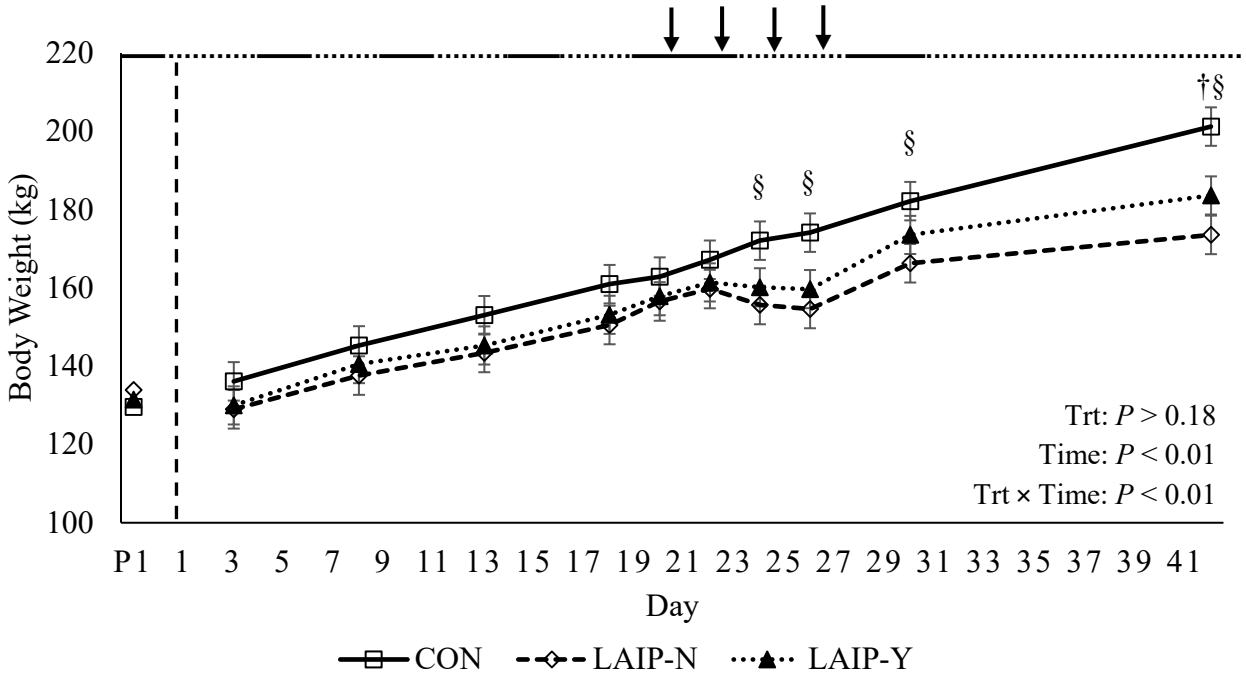

Figure 7. *Post hoc* comparison of the effects of successful liver abscess induction (LAIP-Y), failed liver abscess induction (LAIP-N), or control (CON) on body weight during P2. Top axis depicts solid line, dashed line, and arrows for LS, HS, and FR, respectively. † denotes pairwise differences between LAIP-Y and CON. § denotes pairwise differences between LAIP-N and CON.

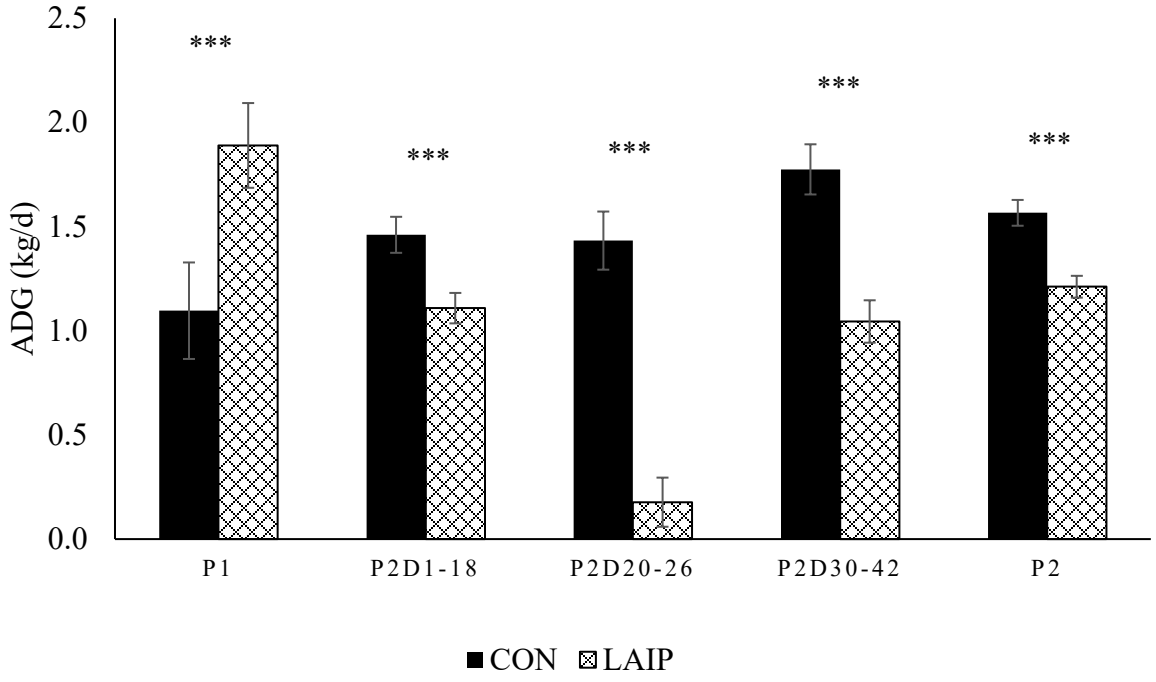

Figure 8. Effects of liver abscess induction protocol (LAIP) or control (CON) on average daily gain during P2. *** denotes $P < 0.05$.

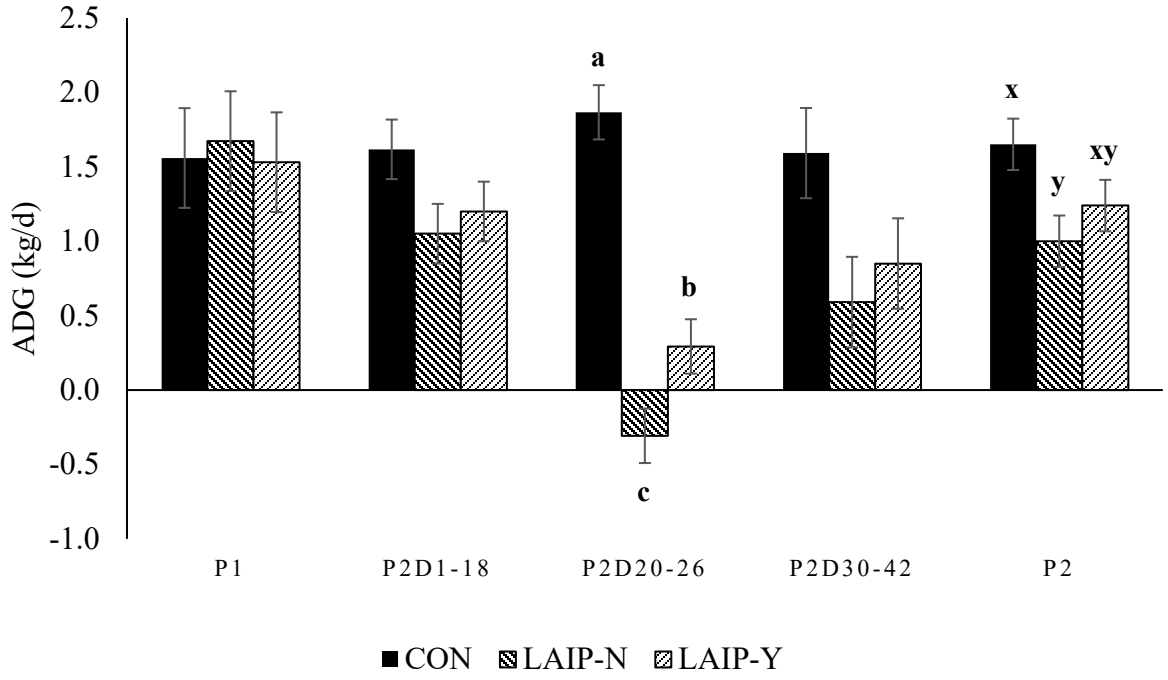

Figure 9. *Post hoc* comparison of the effects of successful liver abscess induction (LAIP-Y), failed liver abscess induction (LAIP-N), or control (CON) on average daily gain during P2. A, b, c denotes $P < 0.05$, x, y, z denotes $0.05 < P \leq 0.10$.

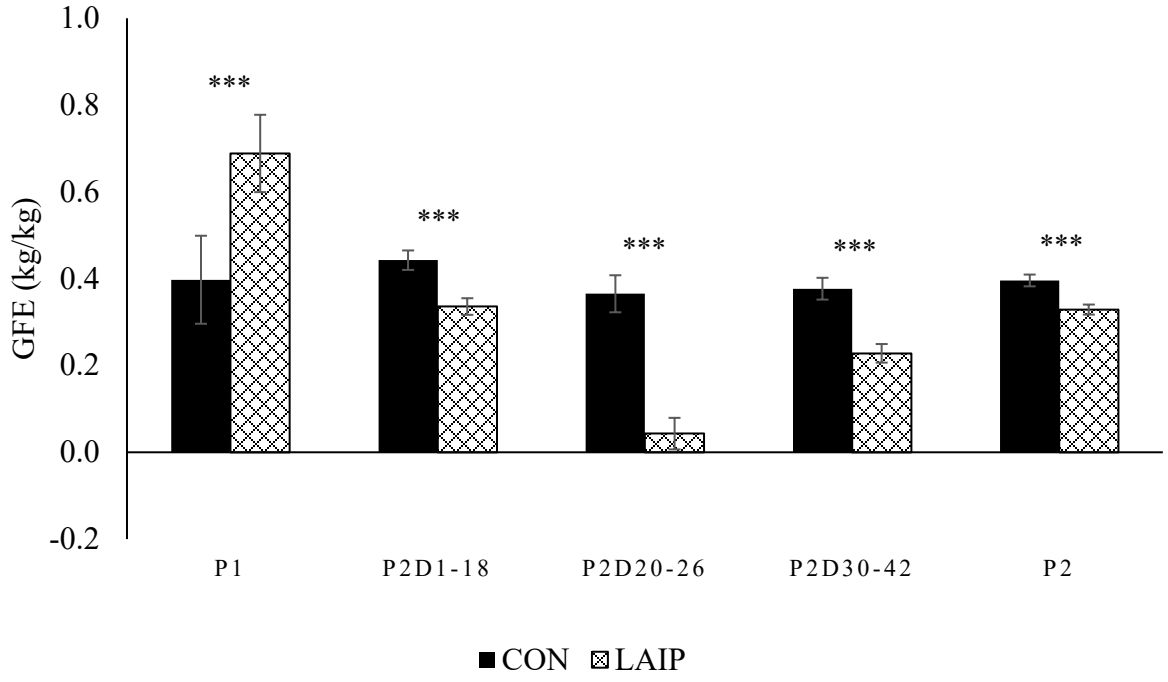

Figure 10. Effects of liver abscess induction protocol (LAIP) or control (CON) on gross feed efficiency during P2. *** denotes $P < 0.05$.

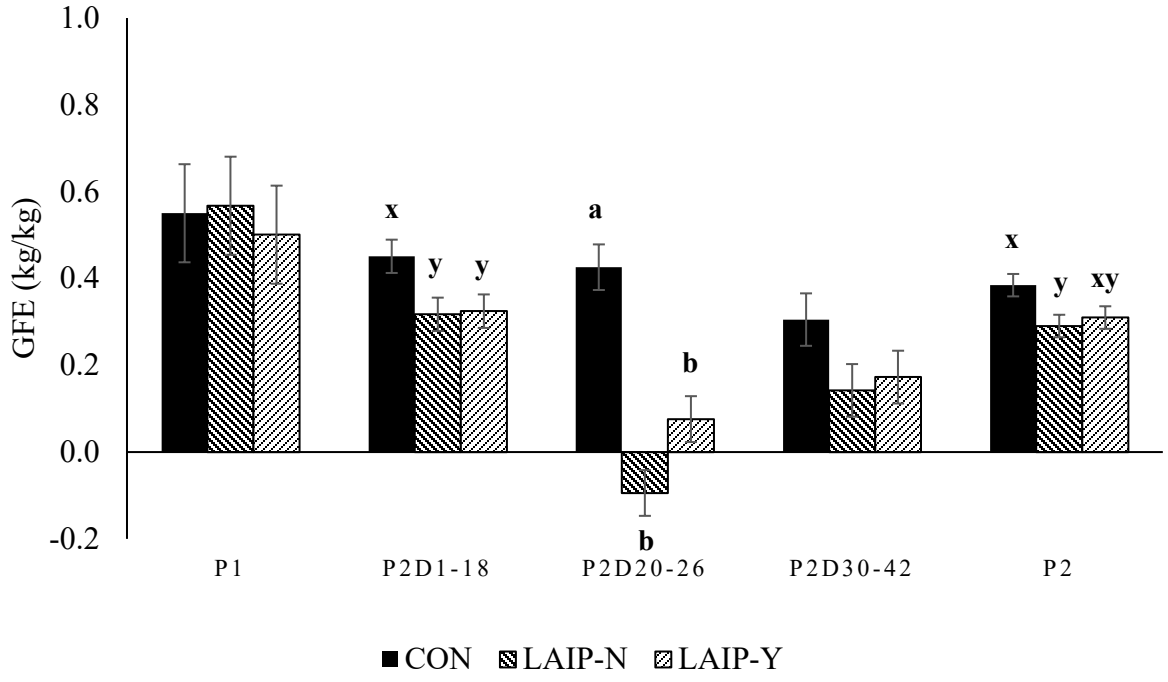

Figure 11. *Post hoc* comparison of the effects of successful liver abscess induction (LAIP-Y), failed liver abscess induction (LAIP-N), or control (CON) on gross feed efficiency during P2. a, b, c denotes $P < 0.05$, x, y, z denotes P $0.05 < P \leq 0.10$.

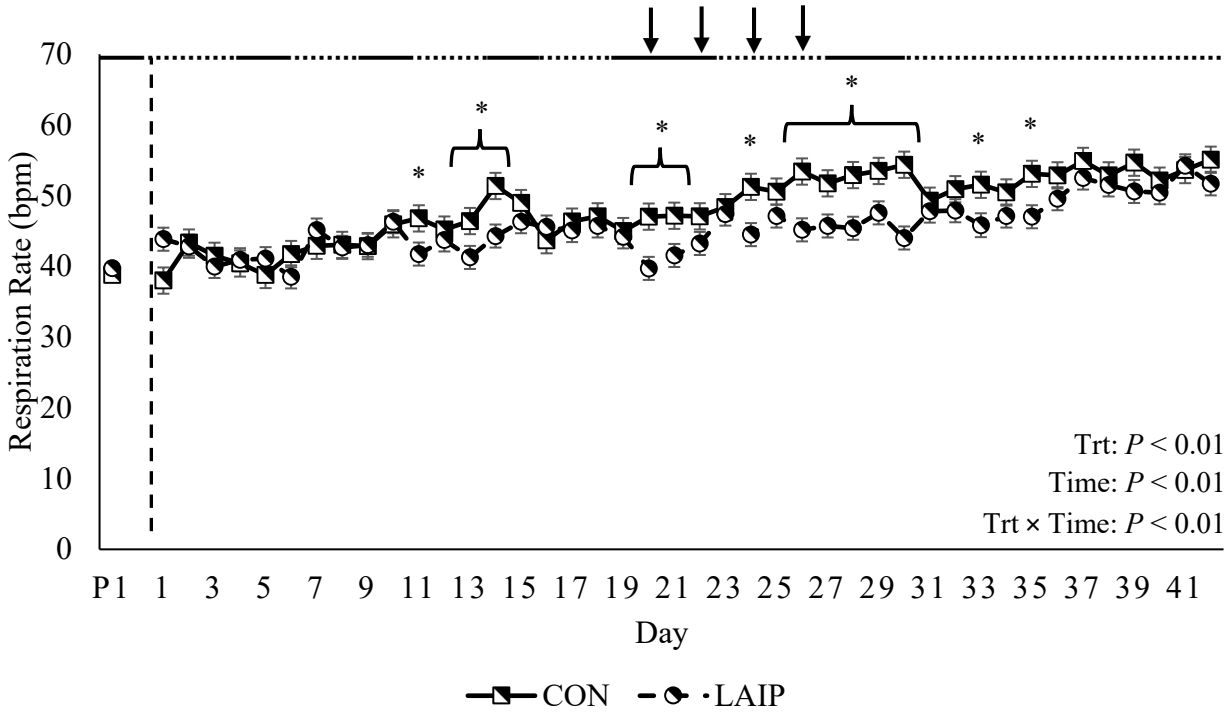

Figure 12. Effects of liver abscess induction protocol (LAIP) or control (CON) on respiration rate during P2. Top axis depicts solid line, dashed line, and arrows for LS, HS, and feed restriction, respectively, in LAIP. * denotes $P < 0.05$.

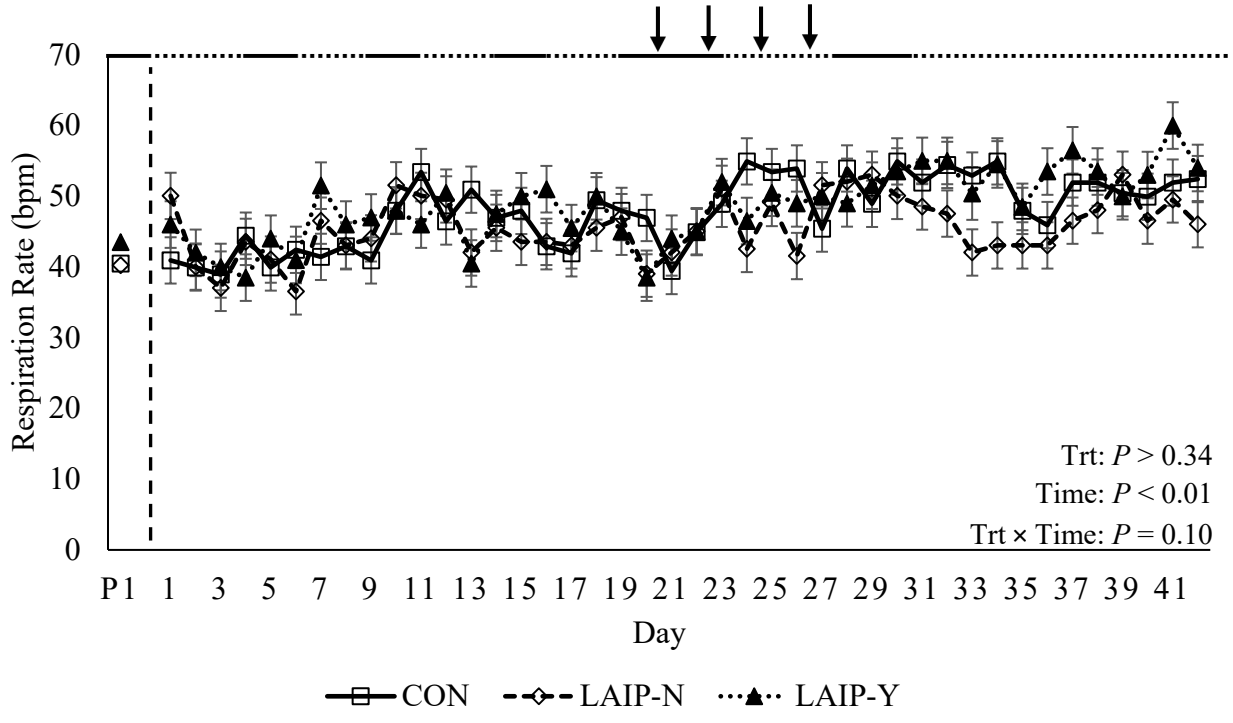

Figure 13. *Post hoc* comparison of the effects of successful liver abscess induction (LAIP-Y), failed liver abscess induction (LAIP-N), or control (CON) on respiration rate during P2. Top axis depicts solid line, dashed line, and arrows for LS, HS, and feed restriction, respectively, in LAIP.

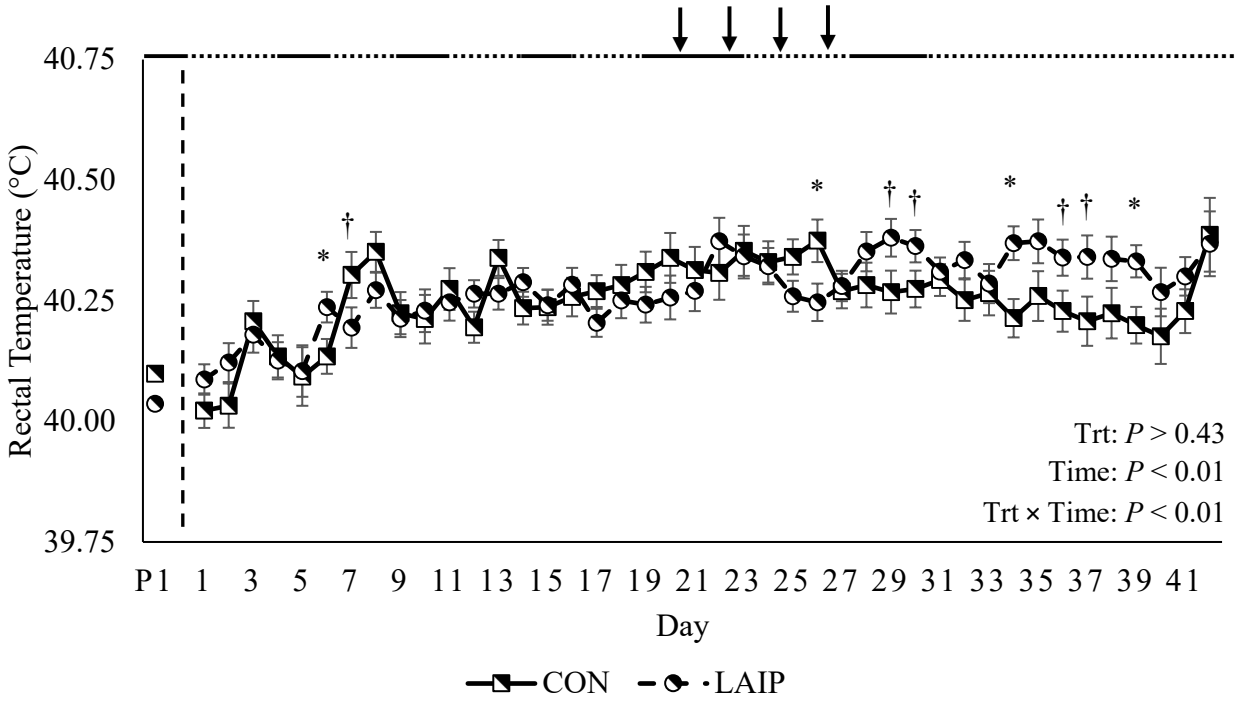

Figure 14. Effects of liver abscess induction protocol (LAIP) or control (CON) on rectal temperature during P2. Top axis depicts solid line, dashed line, and arrows for LS, HS, and feed restriction, respectively, in LAIP. * denotes $P < 0.05$, † denotes $0.05 < P \leq 0.10$.

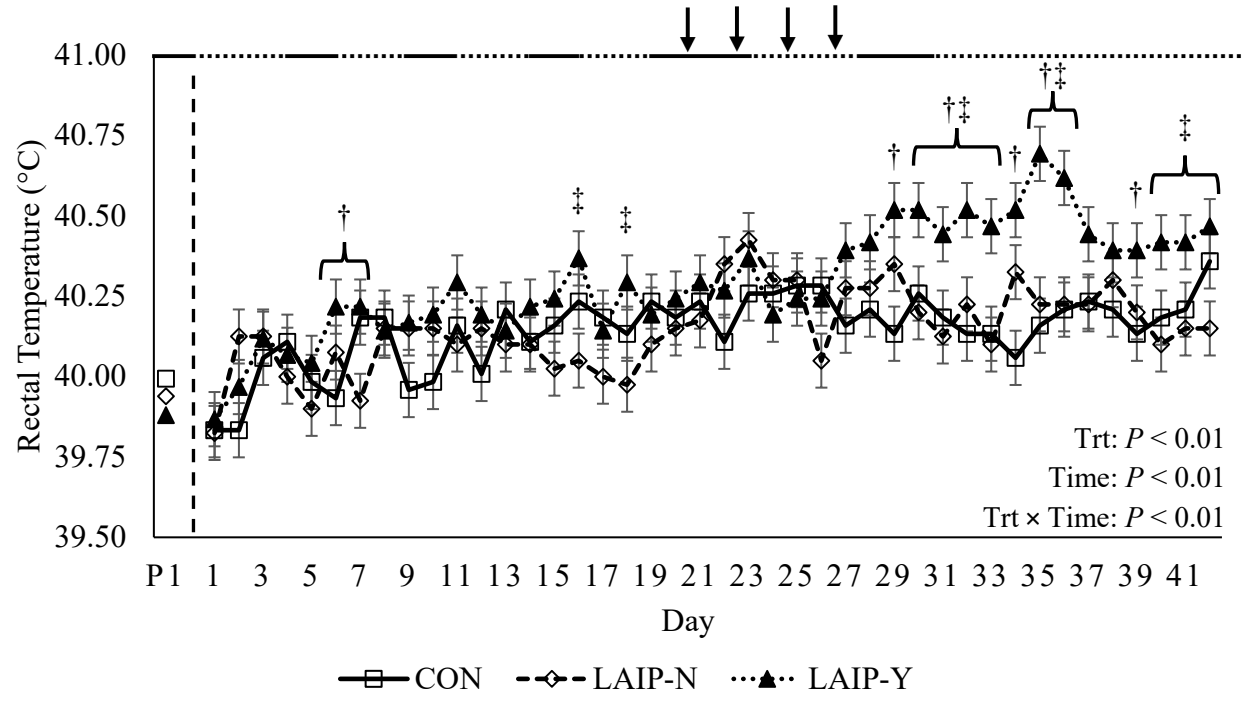

Figure 15. *Post hoc* comparison of the effects of successful liver abscess induction (LAIP-Y), failed liver abscess induction (LAIP-N), or control (CON) on rectal temperature during P2. Top axis depicts solid line, dashed line, and arrows for LS, HS, and feed restriction, respectively, in LAIP. † denotes pairwise differences between LAIP-Y and CON.‡ denotes pairwise differences between LAIP-Y and LAIP-N.

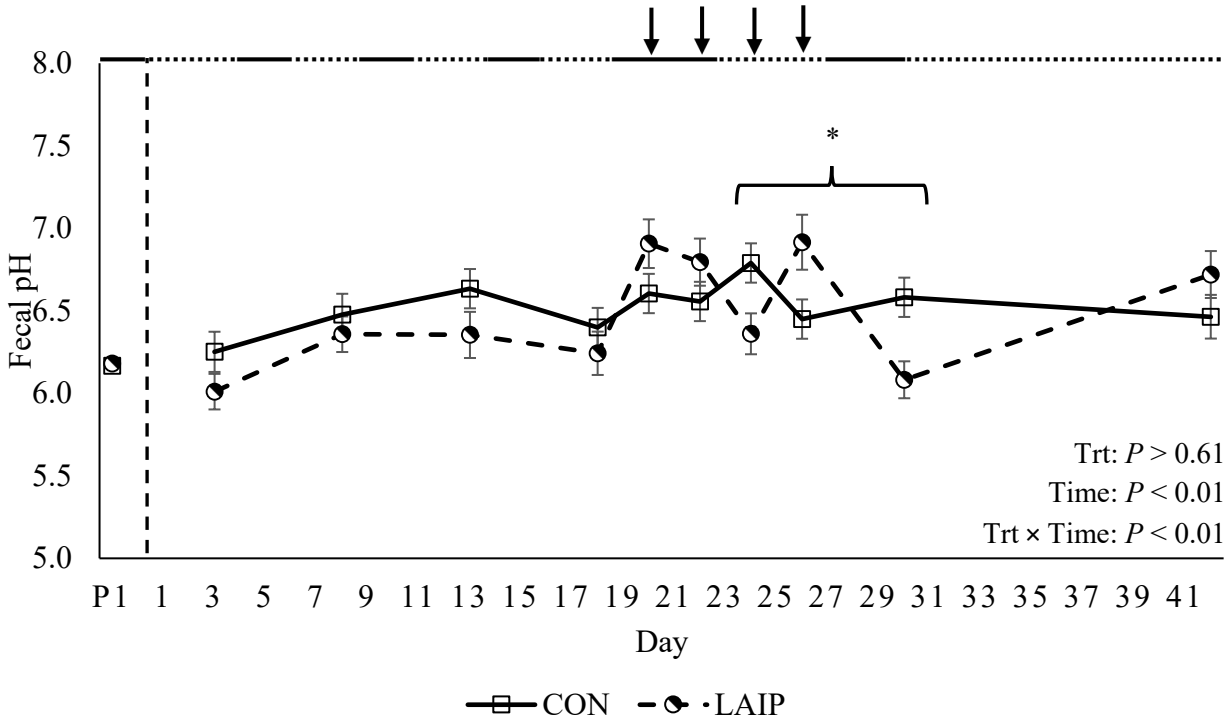

Figure 16. Effects of liver abscess induction protocol (LAIP) or control (CON) on fecal pH during P2. Top axis depicts solid line, dashed line, and arrows for LS, HS, and feed restriction, respectively, in LAIP. * denotes $P < 0.05$.

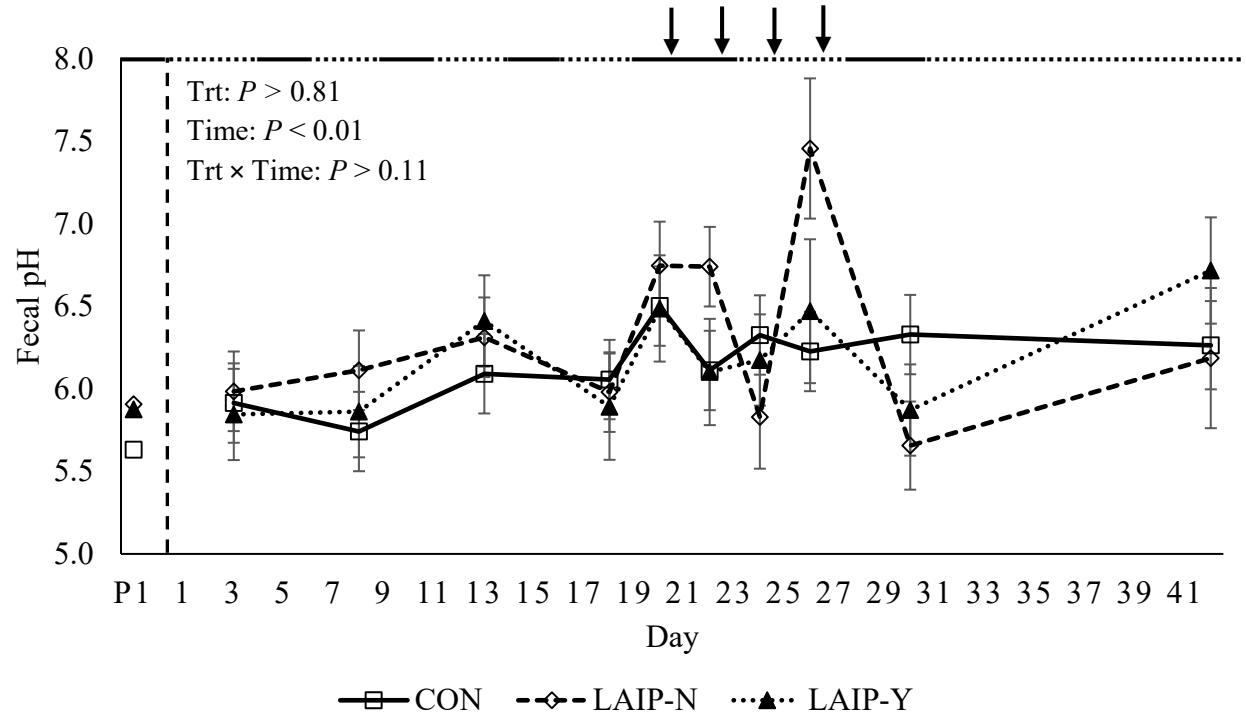

Figure 17. *Post hoc* comparison of the effects of successful liver abscess induction (LAIP-Y), failed liver abscess induction (LAIP-N), or control (CON) on fecal pH during P2. Top axis depicts solid line, dashed line, and arrows for LS, HS, and feed restriction, respectively, in LAIP.

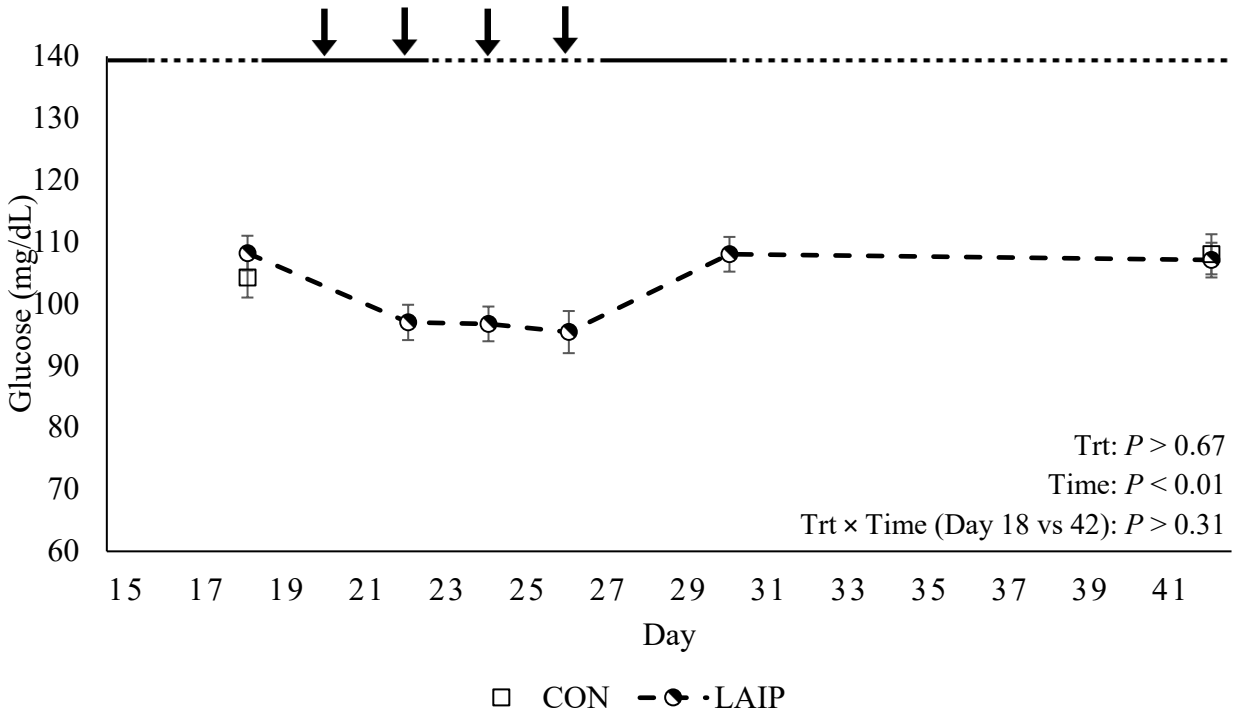

Figure 18. Effects of liver abscess induction protocol (LAIP) or control (CON) on glucose during P2. Top axis depicts solid line, dashed line, and arrows for LS, HS, and feed restriction, respectively, in LAIP.

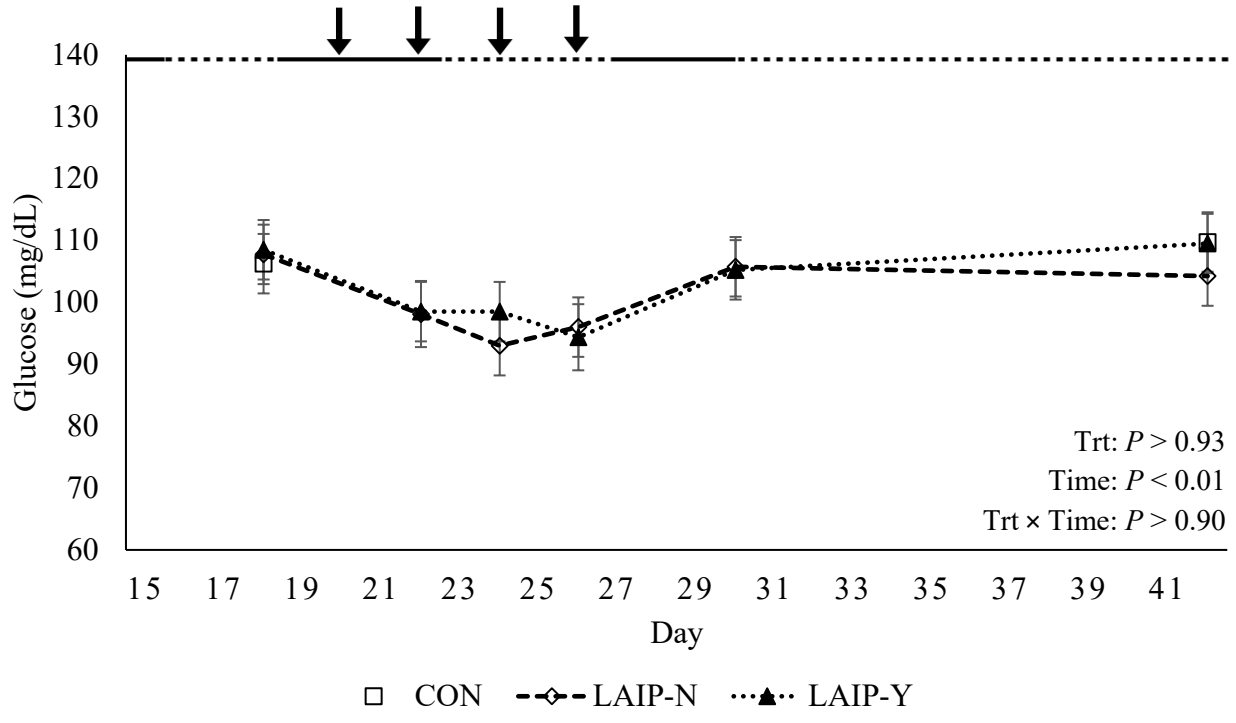

Figure 19. *Post hoc* comparison of the effects of successful liver abscess induction (LAIP-Y), failed liver abscess induction (LAIP-N), or control (CON) on glucose during P2. Top axis depicts solid line, dashed line, and arrows for LS, HS, and feed restriction, respectively, in LAIP.

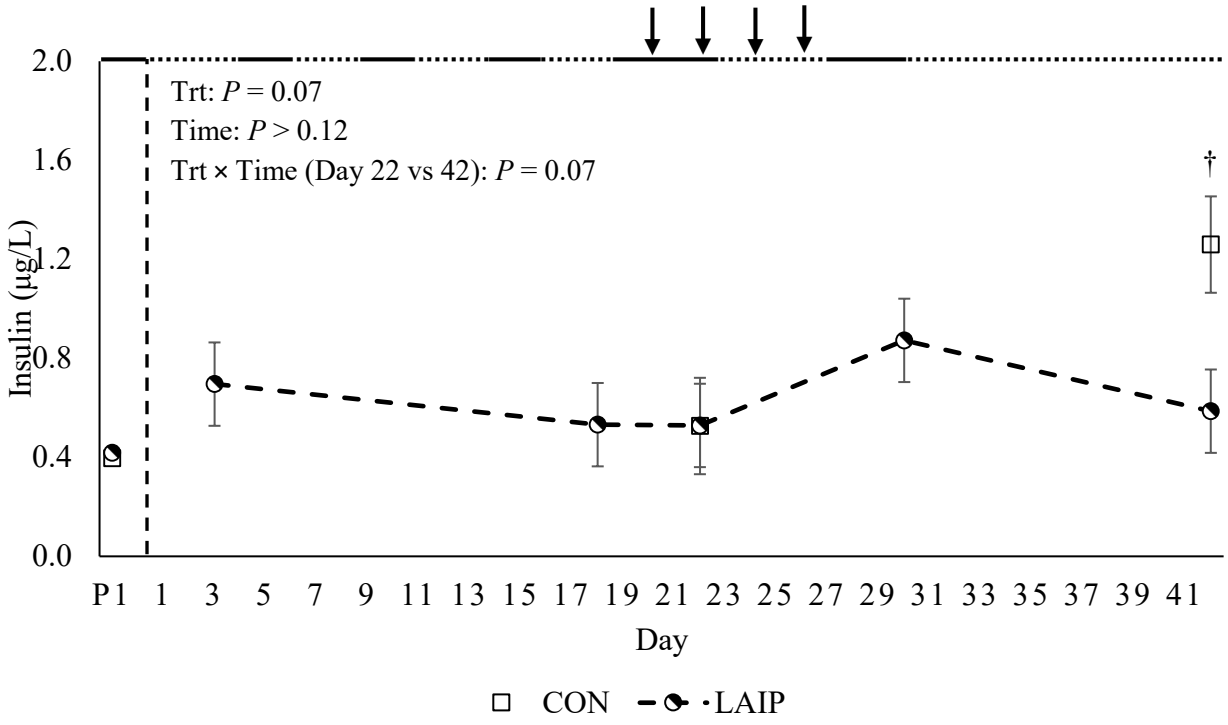

Figure 20. Effects of liver abscess induction protocol (LAIP) or control (CON) on insulin during P2. Top axis depicts solid line, dashed line, and arrows for LS, HS, and feed restriction, respectively, in LAIP. † denotes $0.05 < P \leq 0.10$.

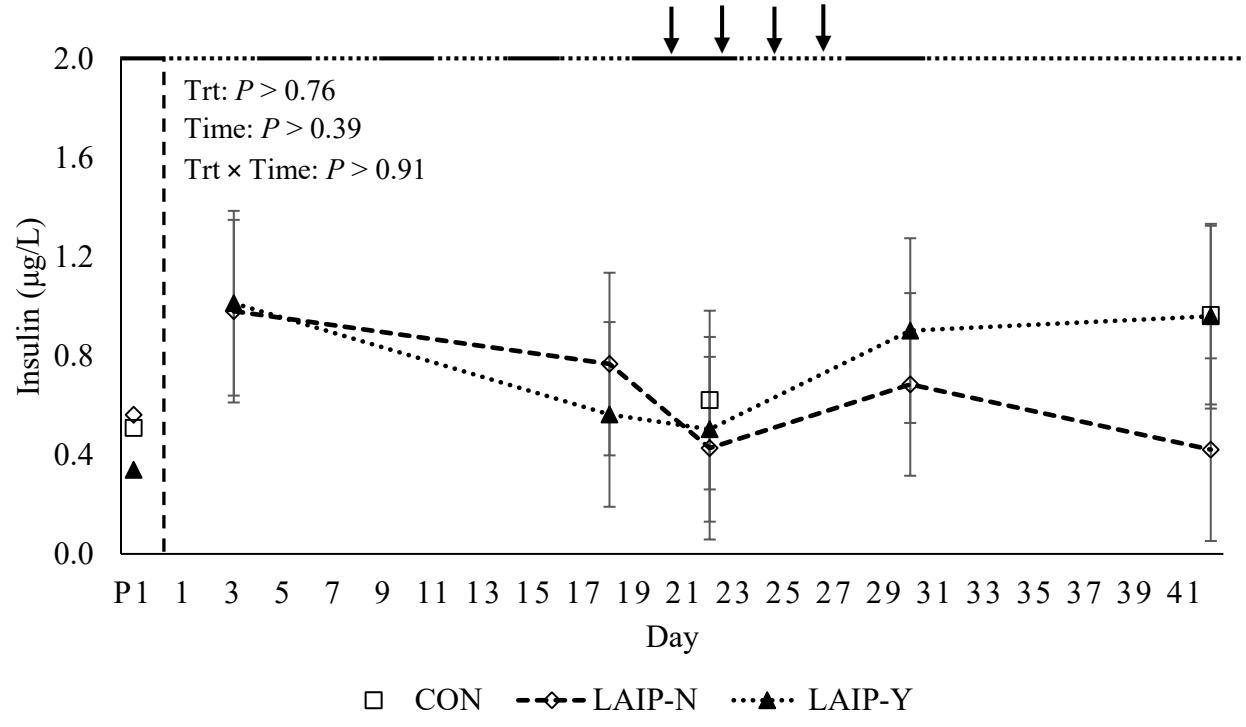

Figure 21. *Post hoc* comparison of the effects of successful liver abscess induction (LAIP-Y), failed liver abscess induction (LAIP-N), or control (CON) on insulin during P2. Top axis depicts solid line, dashed line, and arrows for LS, HS, and feed restriction, respectively, in LAIP.

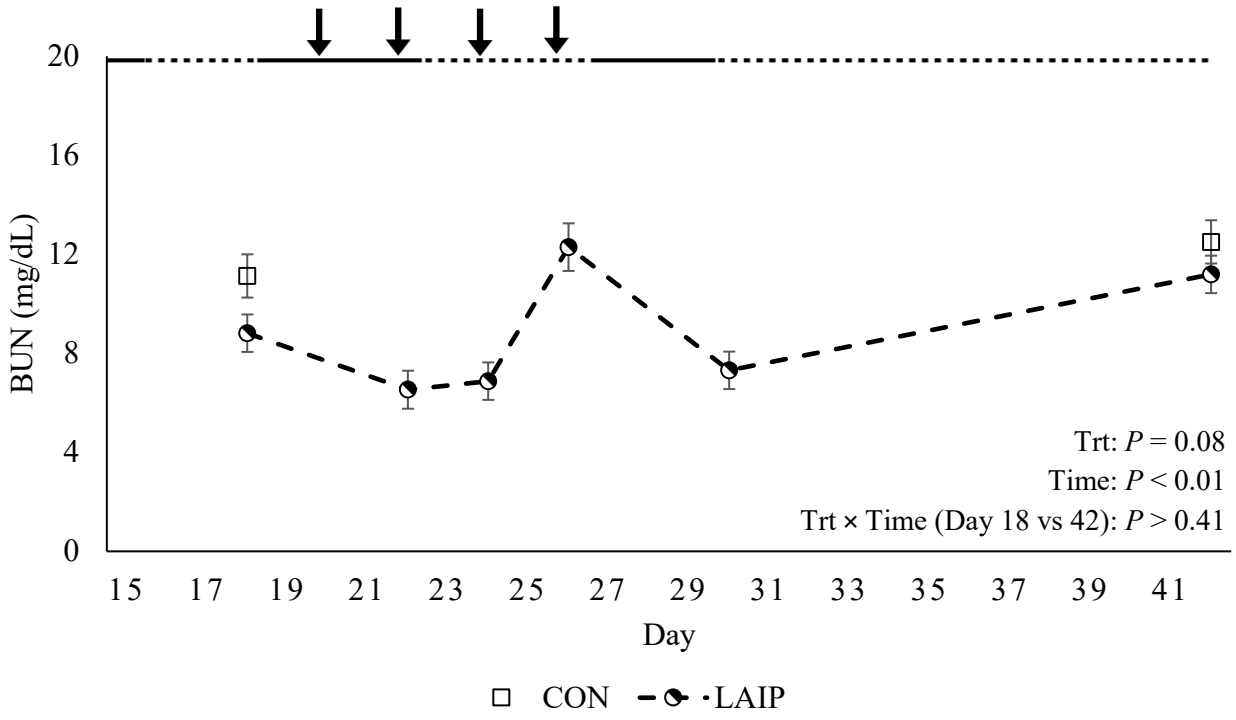

Figure 22. Effects of liver abscess induction protocol (LAIP) or control (CON) on blood urea nitrogen during P2. Top axis depicts solid line, dashed line, and arrows for LS, HS, and feed restriction, respectively, in LAIP.

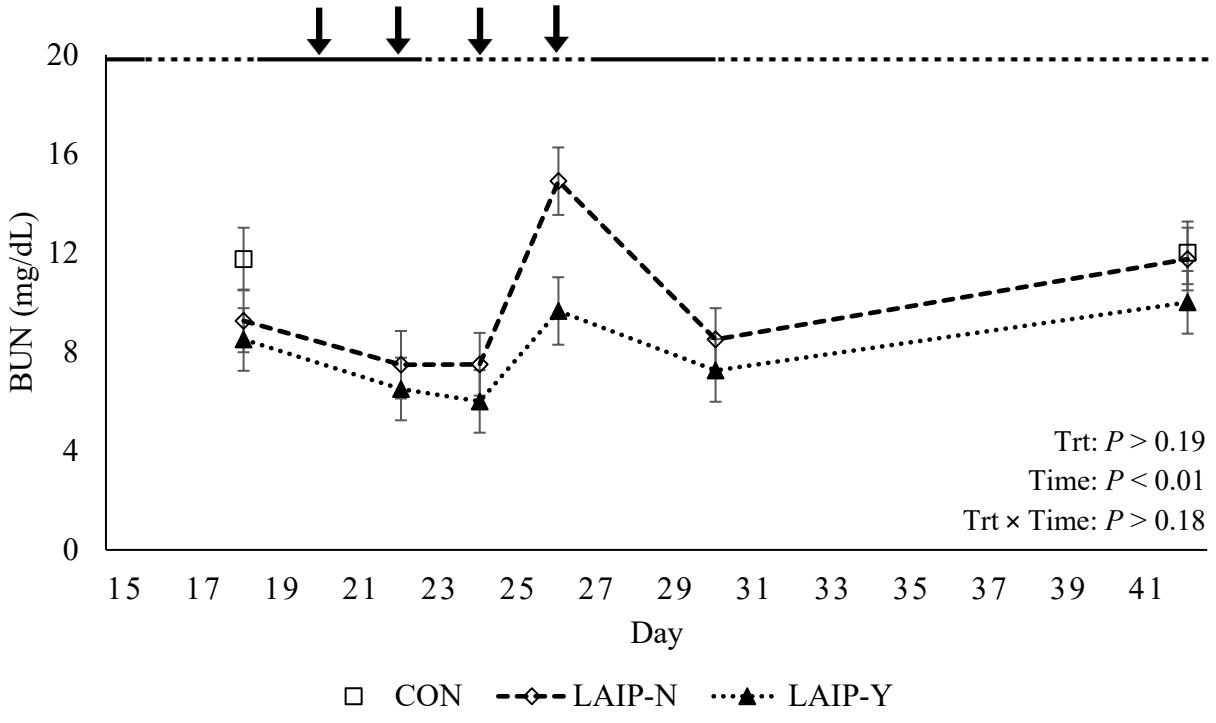

Figure 23. *Post hoc* comparison of the effects of successful liver abscess induction (LAIP-Y), failed liver abscess induction (LAIP-N), or control (CON) on blood urea nitrogen during P2. Top axis depicts solid line, dashed line, and arrows for LS, HS, and feed restriction, respectively, in LAIP.

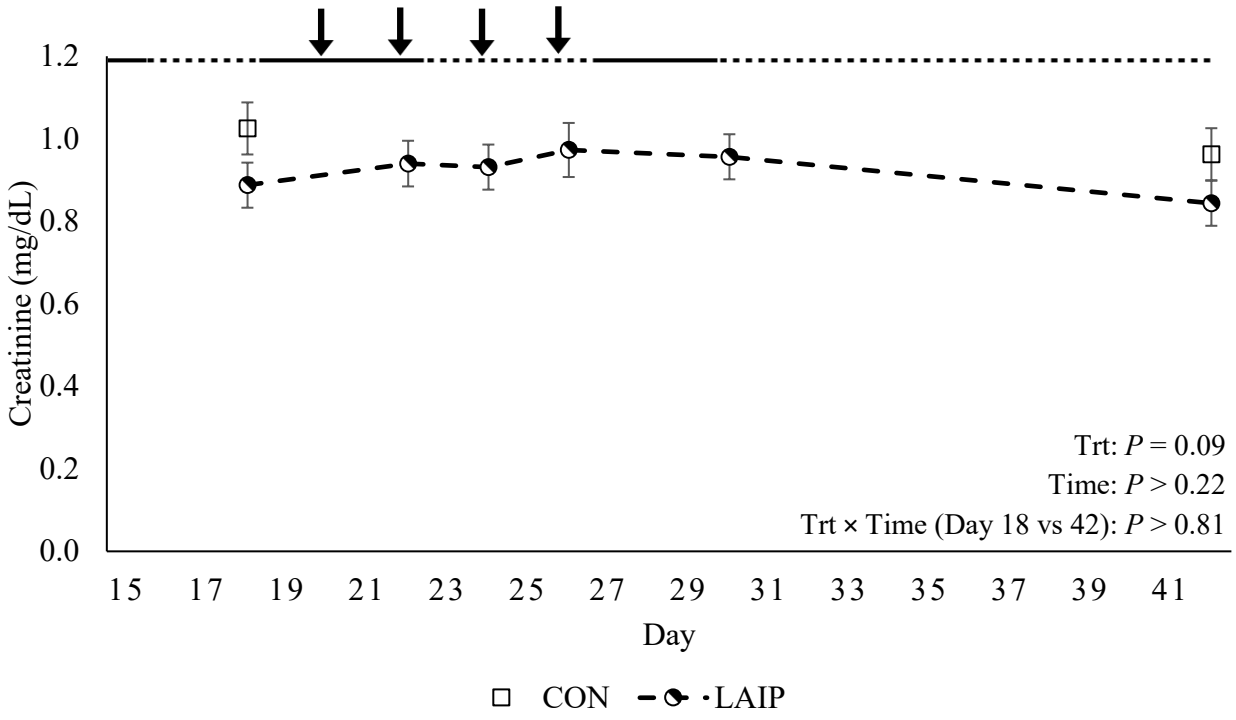

Figure 24. Effects of liver abscess induction protocol (LAIP) or control (CON) on creatinine during P2. Top axis depicts solid line, dashed line, and arrows for LS, HS, and feed restriction, respectively, in LAIP.

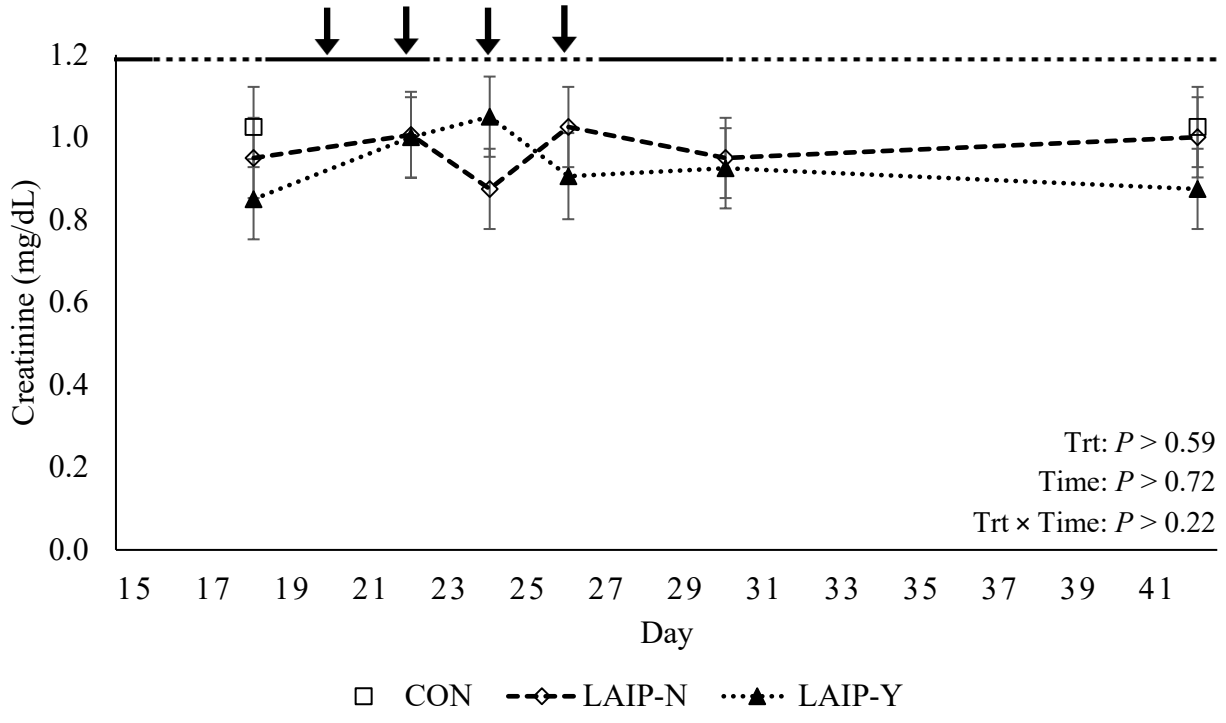

Figure 25. *Post hoc* comparison of the effects of successful liver abscess induction (LAIP-Y), failed liver abscess induction (LAIP-N), or control (CON) on creatinine during P2. Top axis depicts solid line, dashed line, and arrows for LS, HS, and feed restriction, respectively, in LAIP.

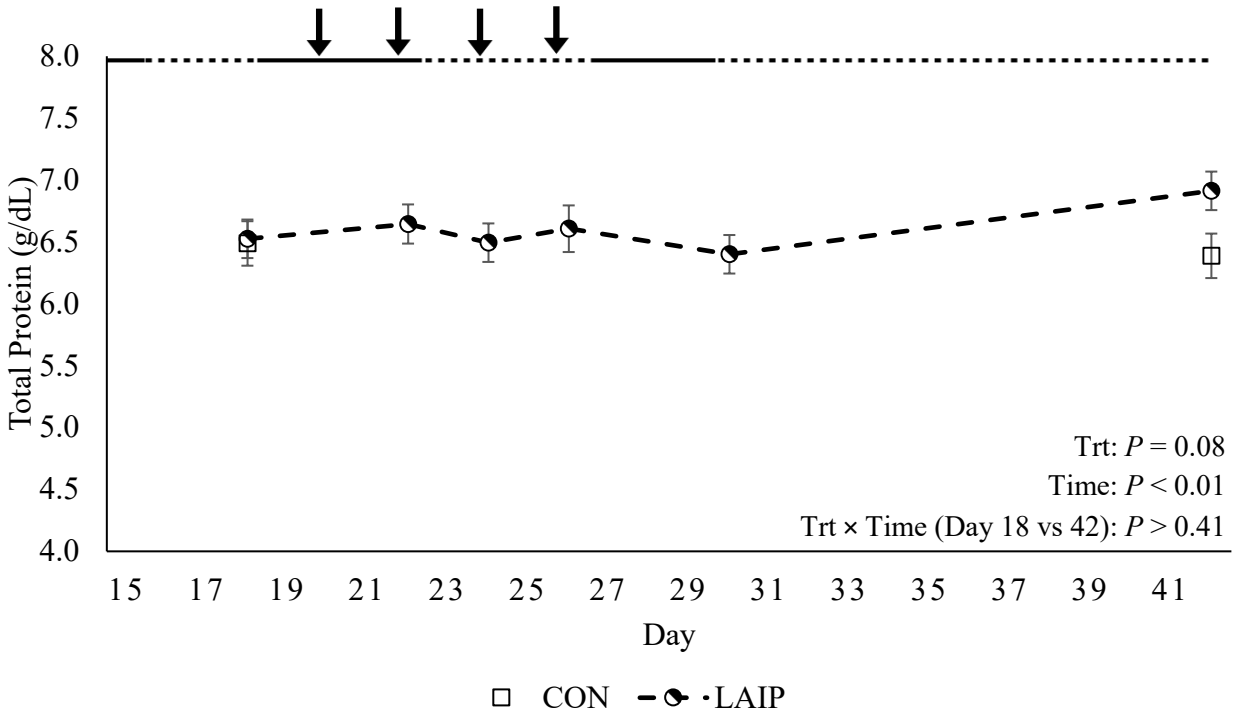

Figure 26. Effects of liver abscess induction protocol (LAIP) or control (CON) on total protein during P2. Top axis depicts solid line, dashed line, and arrows for LS, HS, and feed restriction, respectively, in LAIP.

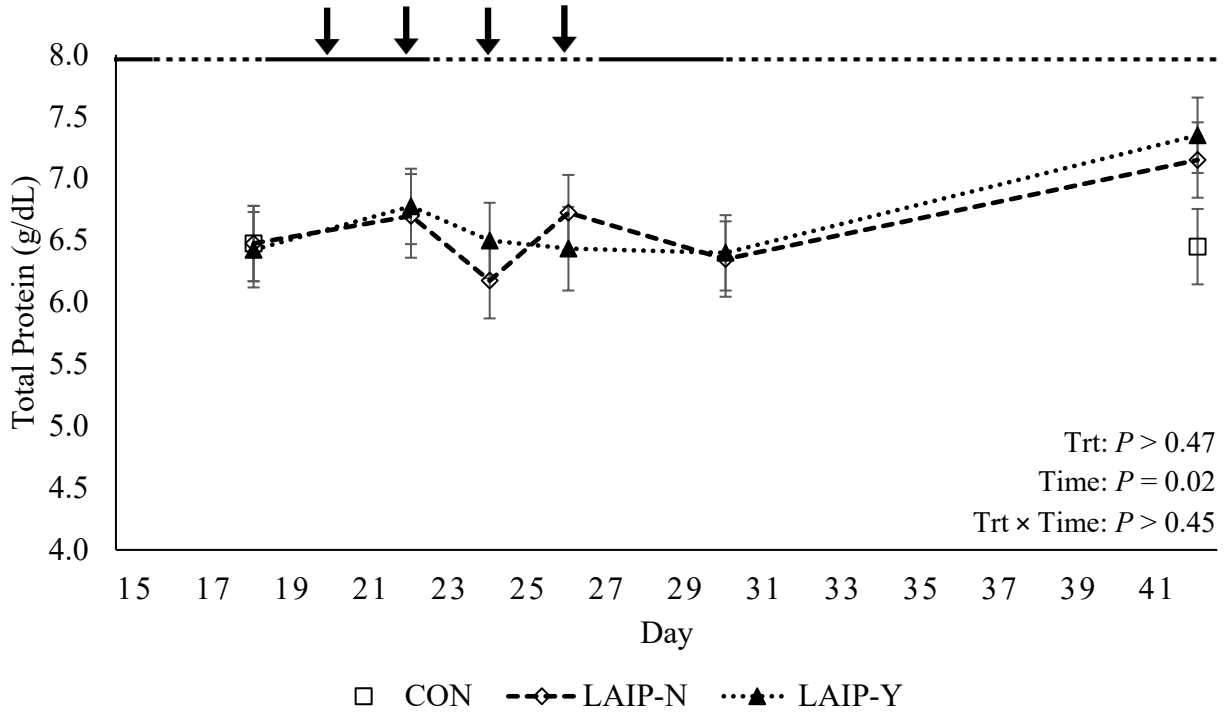

Figure 27. *Post hoc* comparison of the effects of successful liver abscess induction (LAIP-Y), failed liver abscess induction (LAIP-N), or control (CON) on total protein during P2. Top axis depicts solid line, dashed line, and arrows for LS, HS, and feed restriction, respectively, in LAIP.

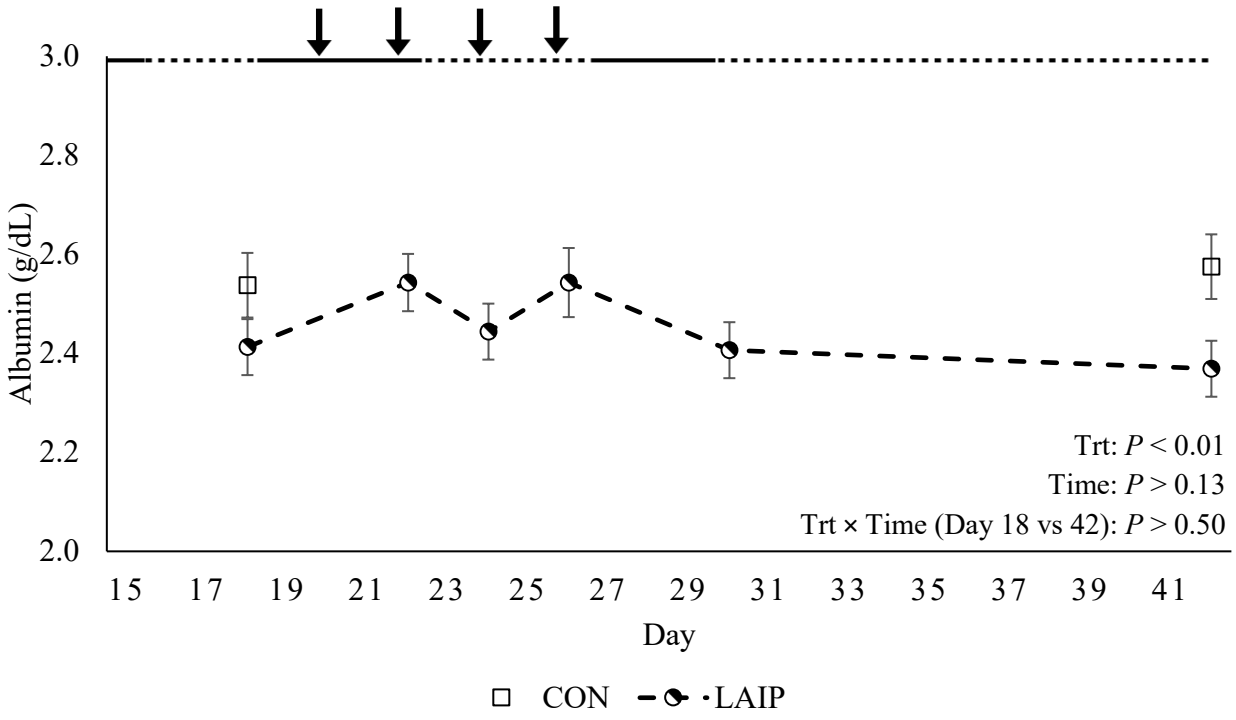

Figure 28. Effects of liver abscess induction protocol (LAIP) or control (CON) on albumin during P2. Top axis depicts solid line, dashed line, and arrows for LS, HS, and feed restriction, respectively, in LAIP.

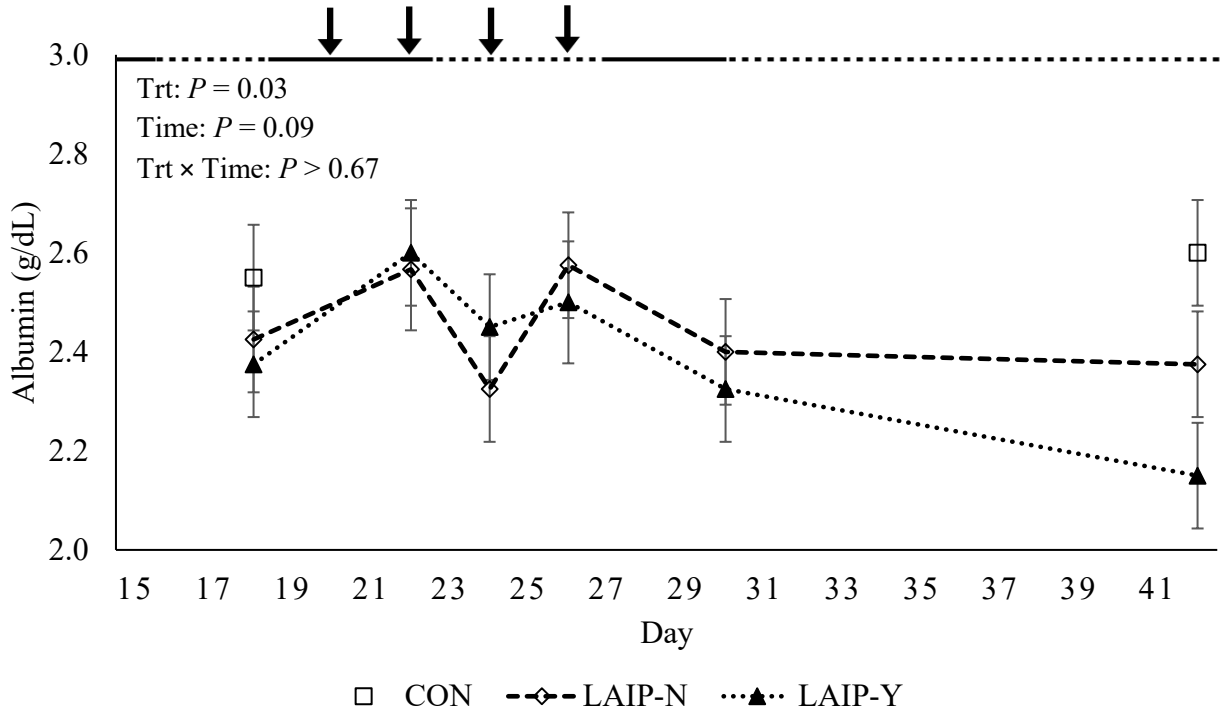

Figure 29. *Post hoc* comparison of the effects of successful liver abscess induction (LAIP-Y), failed liver abscess induction (LAIP-N), or control (CON) on albumin during P2. Top axis depicts solid line, dashed line, and arrows for LS, HS, and feed restriction, respectively, in LAIP.

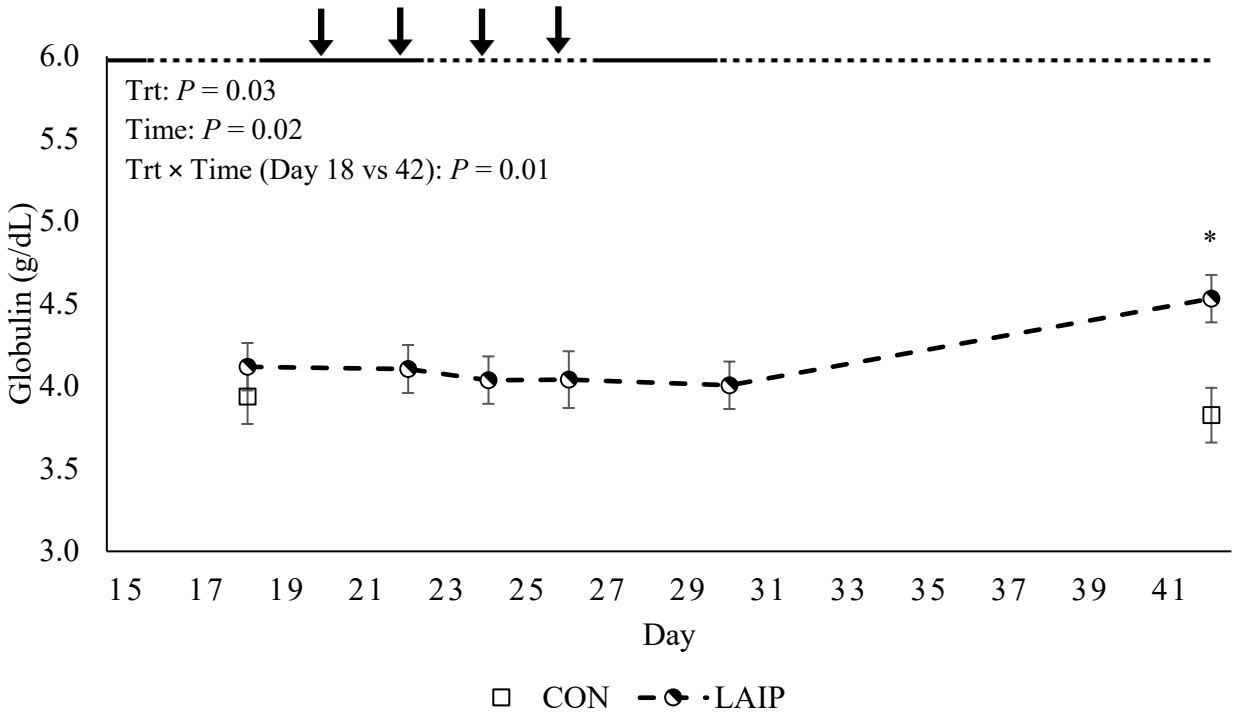

Figure 30. Effects of liver abscess induction protocol (LAIP) or control (CON) on globulin during P2. Top axis depicts solid line, dashed line, and arrows for LS, HS, and feed restriction, respectively, in LAIP. * denotes $P < 0.05$.

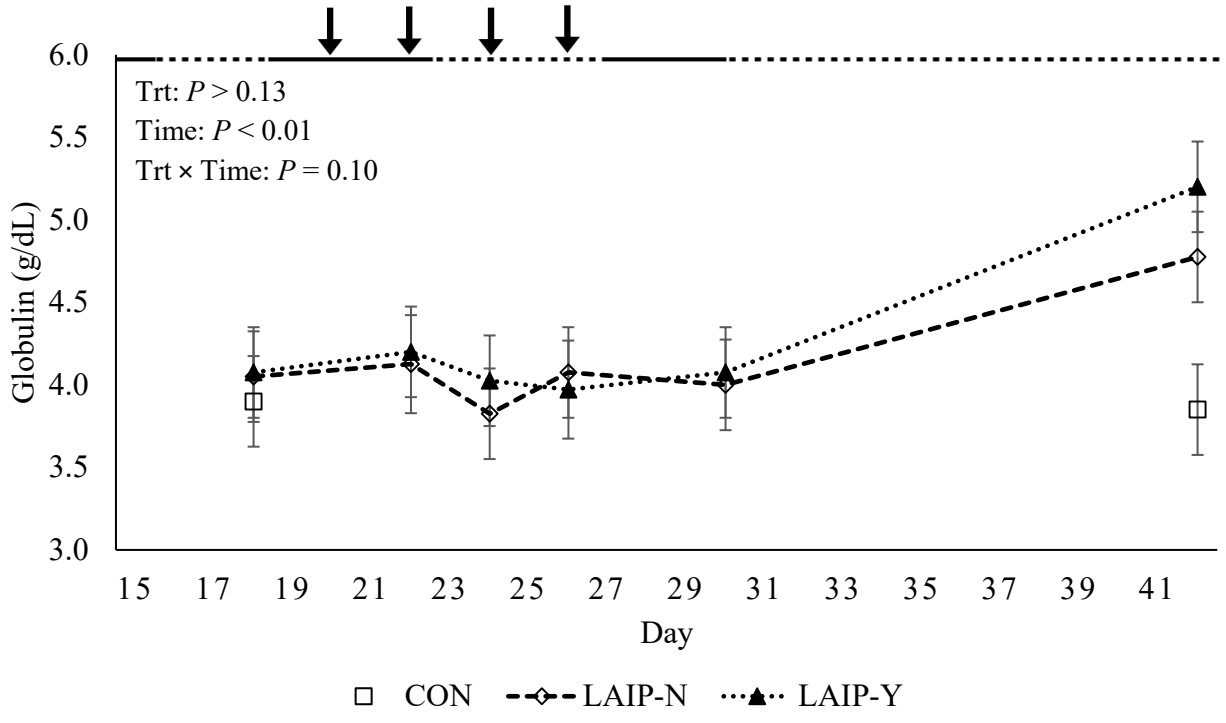

Figure 31. *Post hoc* comparison of the effects of successful liver abscess induction (LAIP-Y), failed liver abscess induction (LAIP-N), or control (CON) on globulin during P2. Top axis depicts solid line, dashed line, and arrows for LS, HS, and feed restriction, respectively, in LAIP.

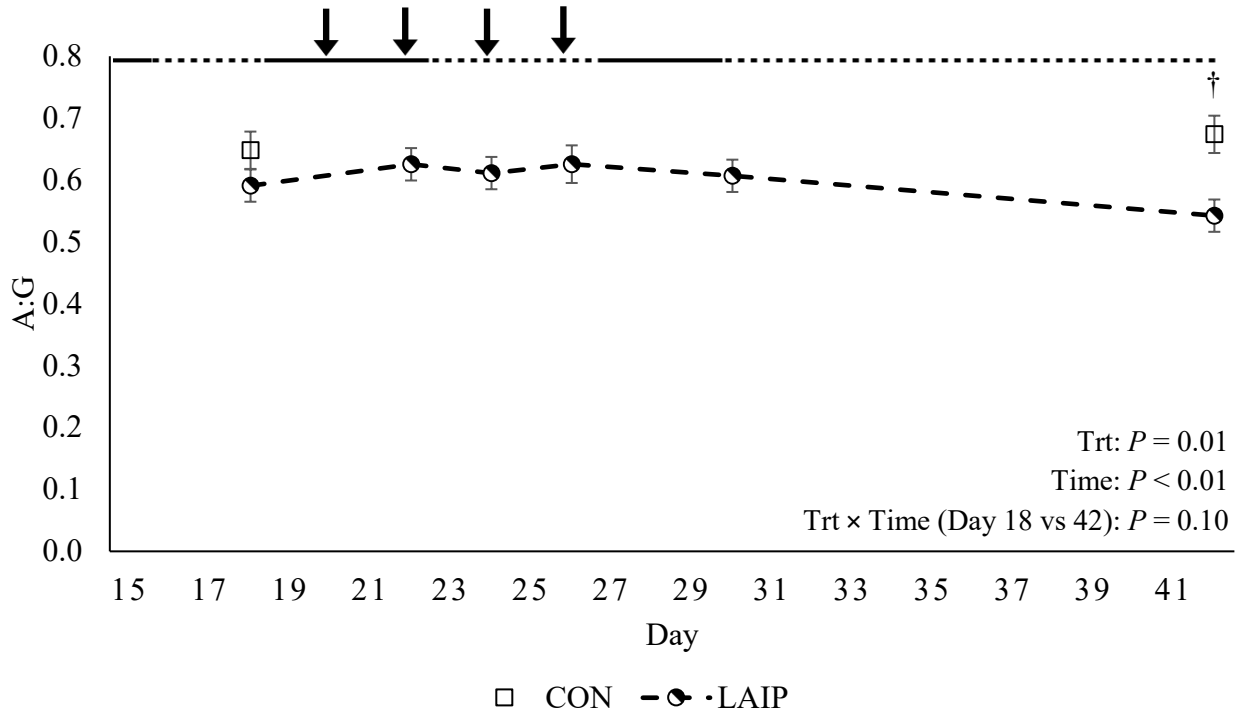

Figure 32. Effects of liver abscess induction protocol (LAIP) or control (CON) on albumin-to-globulin ratio during P2. Top axis depicts solid line, dashed line, and arrows for LS, HS, and feed restriction, respectively, in LAIP.

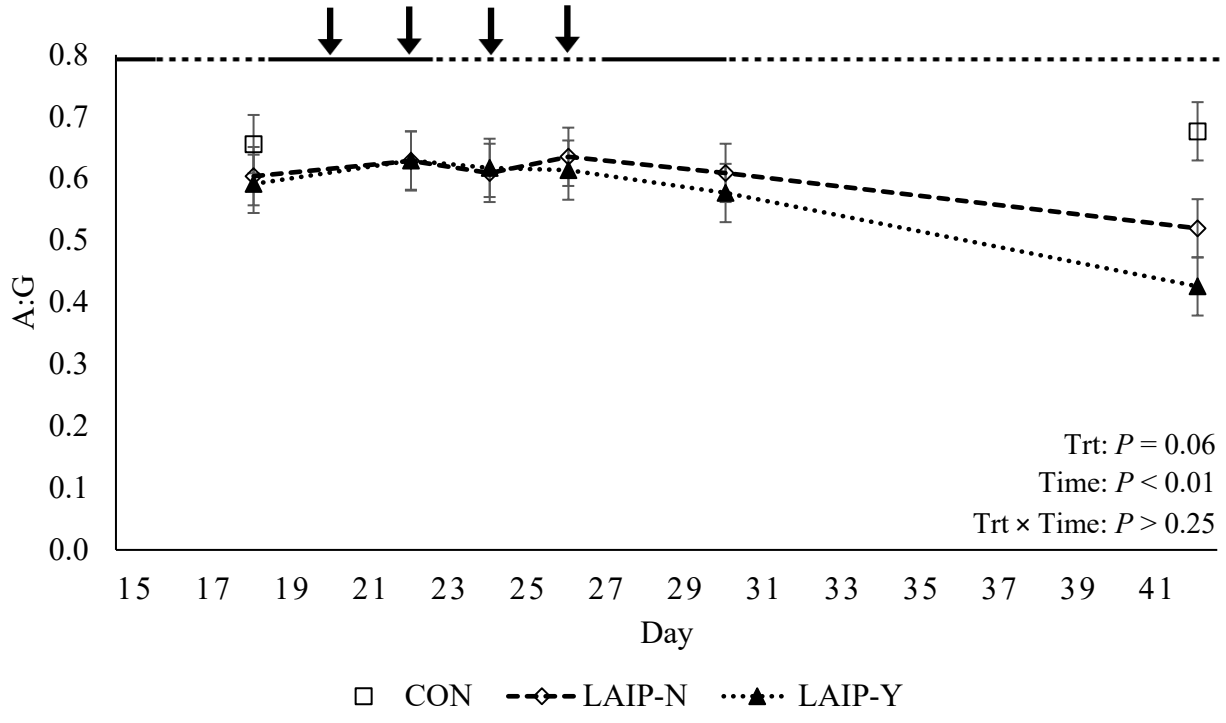

Figure 33. *Post hoc* comparison of the effects of successful liver abscess induction (LAIP-Y), failed liver abscess induction (LAIP-N), or control (CON) on albumin-to-globulin ratio during P2. Top axis depicts solid line, dashed line, and arrows for LS, HS, and feed restriction, respectively, in LAIP.

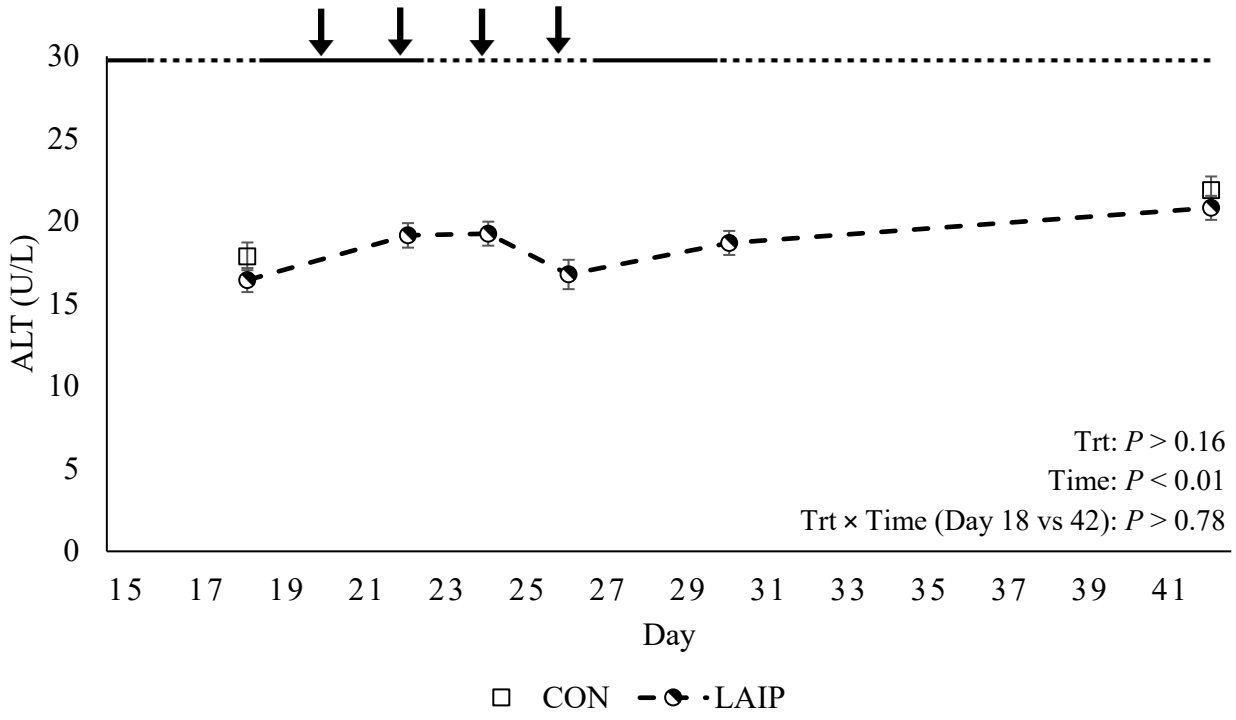

Figure 34. Effects of liver abscess induction protocol (LAIP) or control (CON) on alanine transaminase ratio during P2. Top axis depicts solid line, dashed line, and arrows for LS, HS, and feed restriction, respectively, in LAIP.

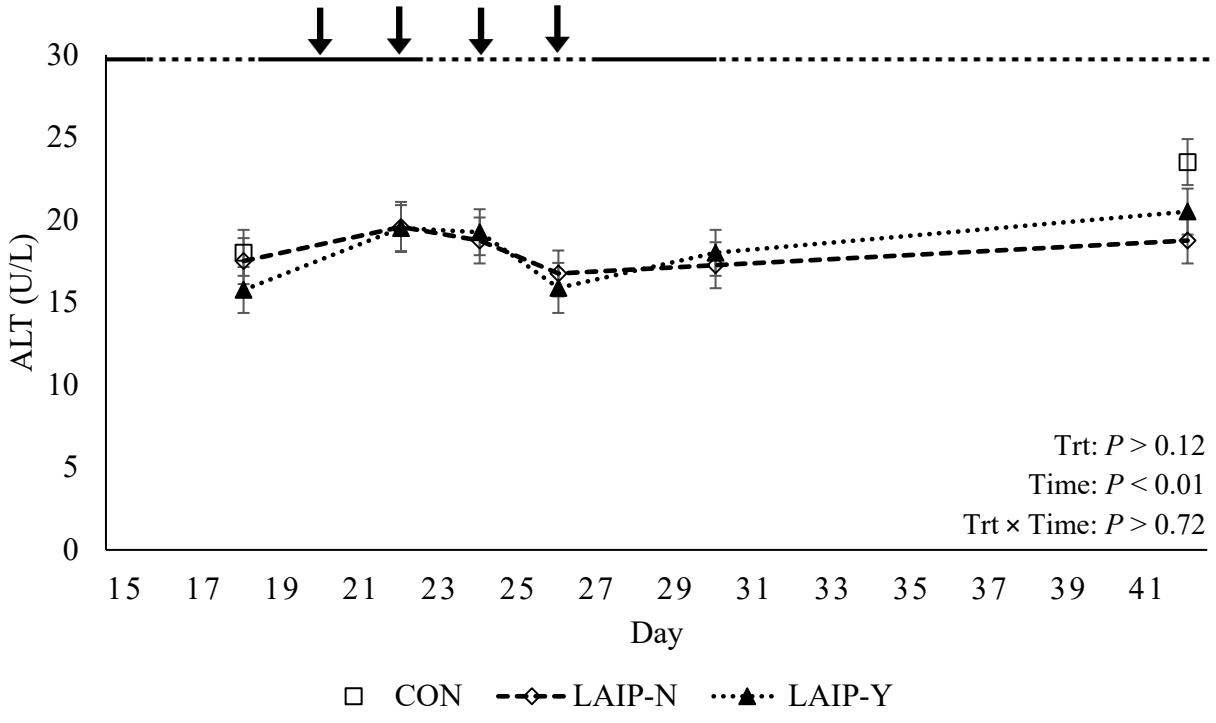

Figure 35. *Post hoc* comparison of the effects of successful liver abscess induction (LAIP-Y), failed liver abscess induction (LAIP-N), or control (CON) on alanine transaminase ratio during P2. Top axis depicts solid line, dashed line, and arrows for LS, HS, and feed restriction, respectively, in LAIP.

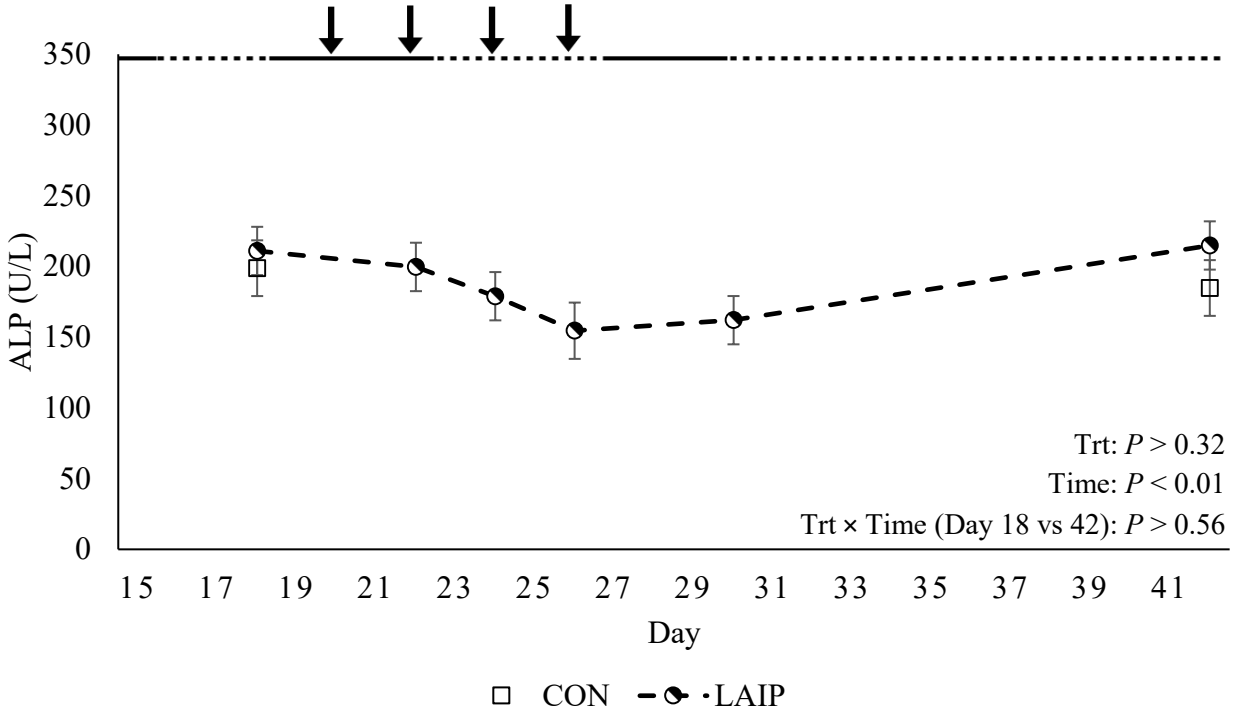

Figure 36. Effects of liver abscess induction protocol (LAIP) or control (CON) on alkaline phosphatase during P2. Top axis depicts solid line, dashed line, and arrows for LS, HS, and feed restriction, respectively, in LAIP.

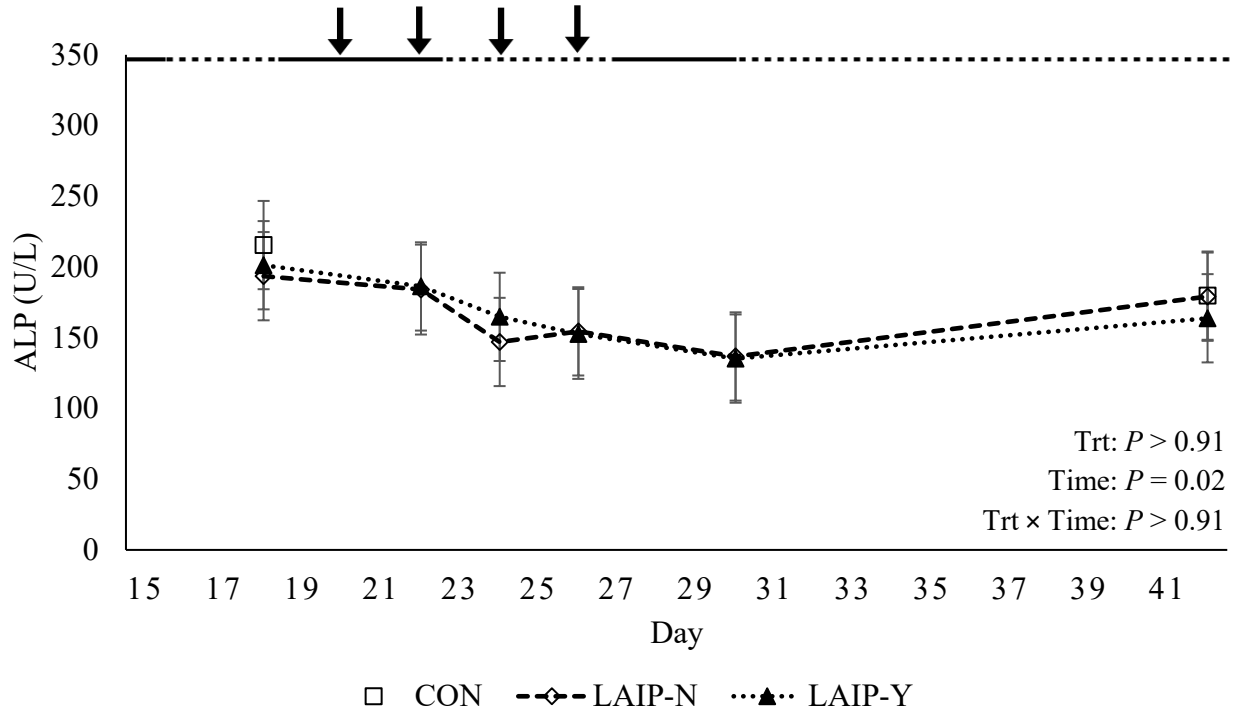

Figure 37. *Post hoc* comparison of the effects of successful liver abscess induction (LAIP-Y), failed liver abscess induction (LAIP-N), or control (CON) on alkaline phosphatase during P2. Top axis depicts solid line, dashed line, and arrows for LS, HS, and feed restriction, respectively, in LAIP.

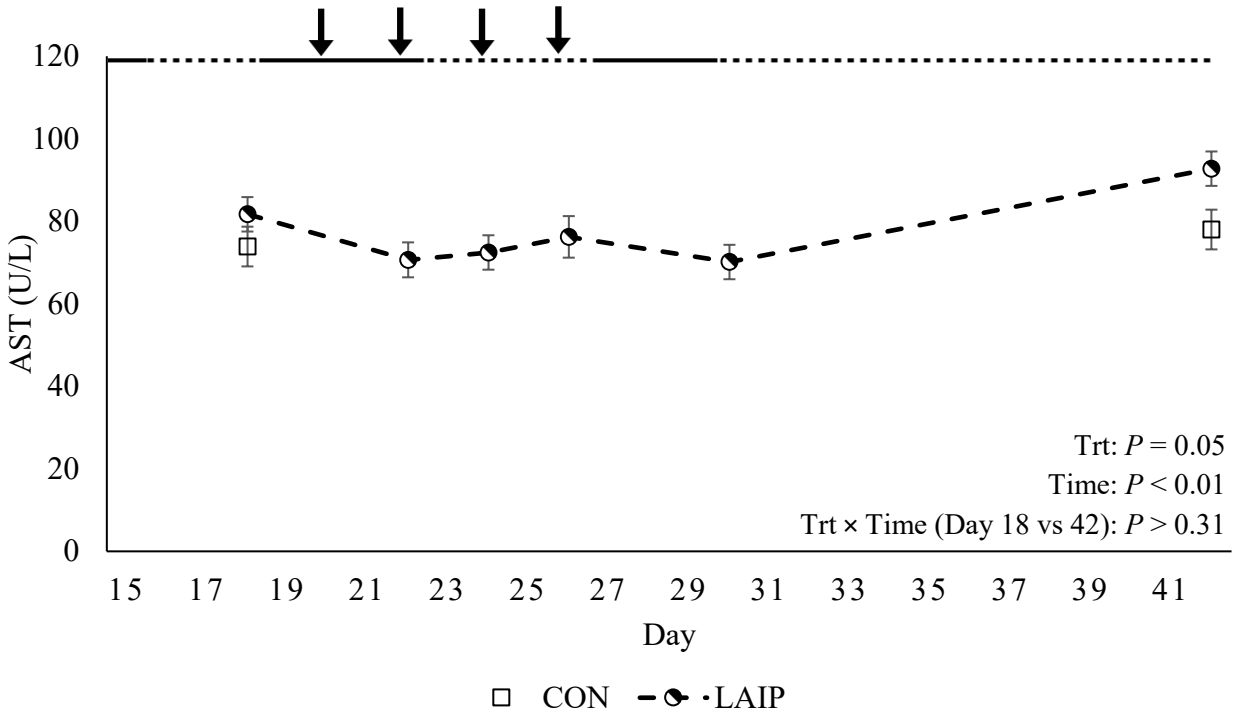

Figure 38. Effects of liver abscess induction protocol (LAIP) or control (CON) on aspartate aminotransferase during P2. Top axis depicts solid line, dashed line, and arrows for LS, HS, and feed restriction, respectively, in LAIP.

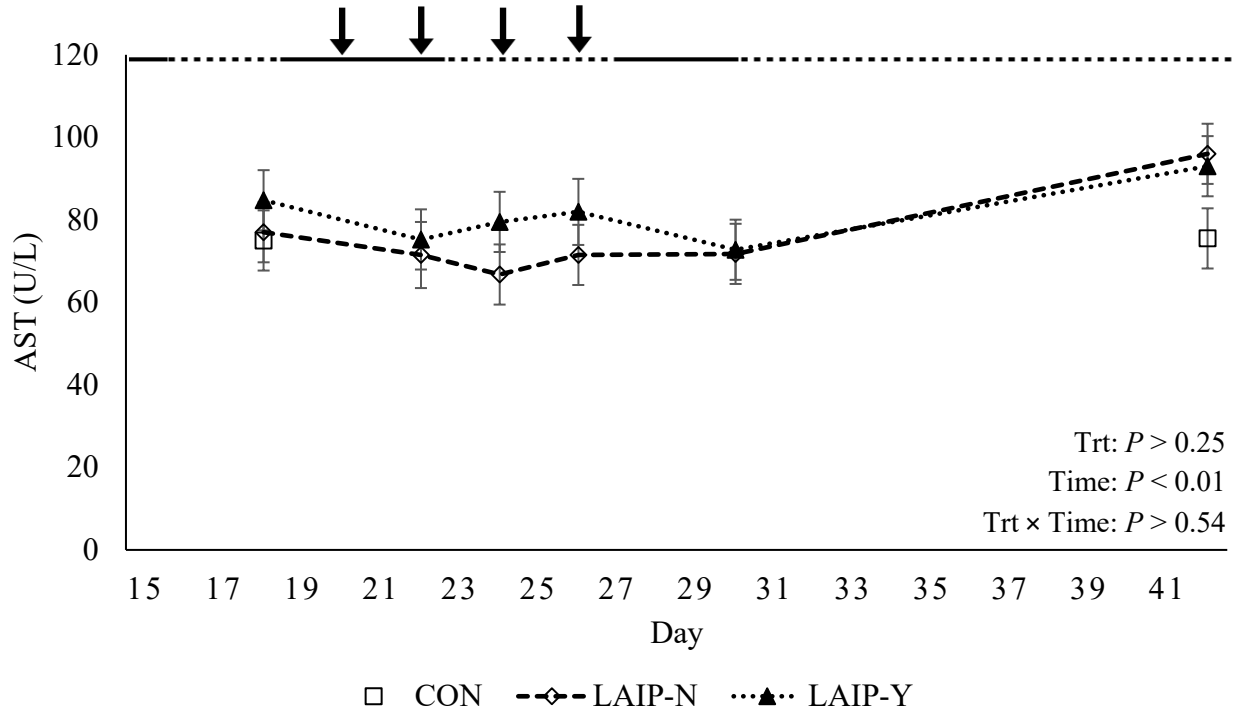

Figure 39. *Post hoc* comparison of the effects of successful liver abscess induction (LAIP-Y), failed liver abscess induction (LAIP-N), or control (CON) on aspartate aminotransferase during P2. Top axis depicts solid line, dashed line, and arrows for LS, HS, and feed restriction, respectively, in LAIP.

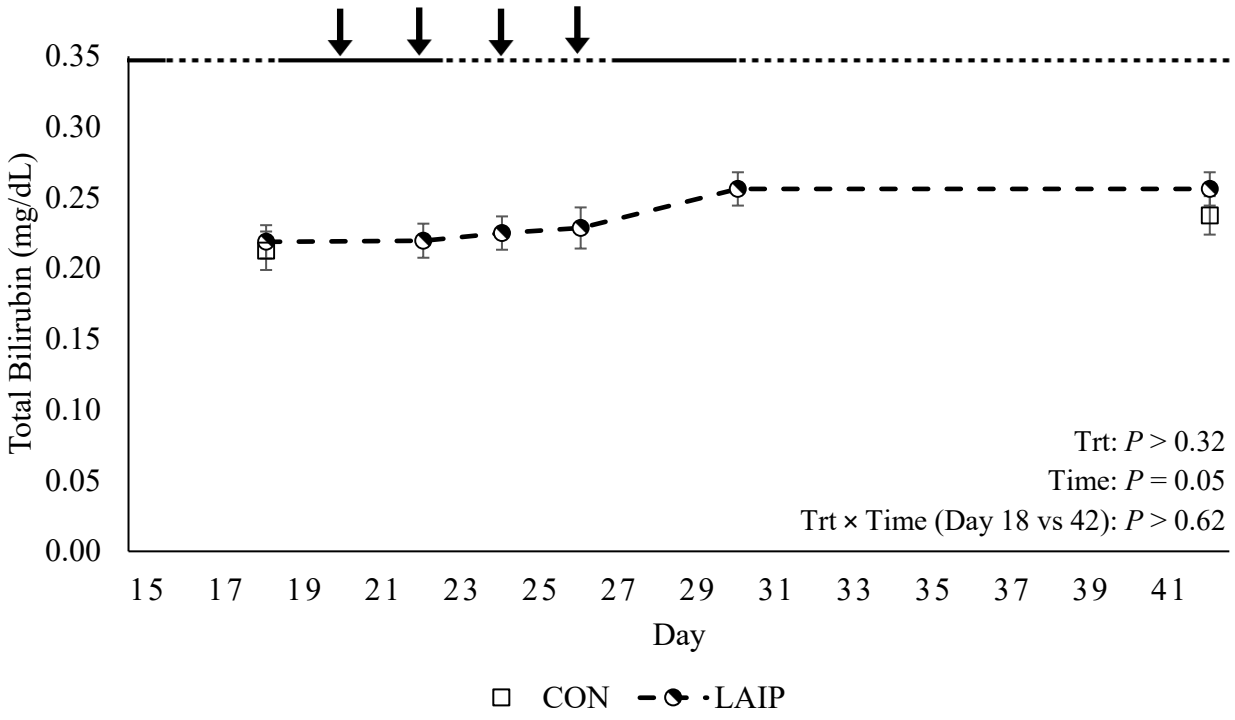

Figure 40. Effects of liver abscess induction protocol (LAIP) or control (CON) on total bilirubin during P2. Top axis depicts solid line, dashed line, and arrows for LS, HS, and feed restriction, respectively, in LAIP.

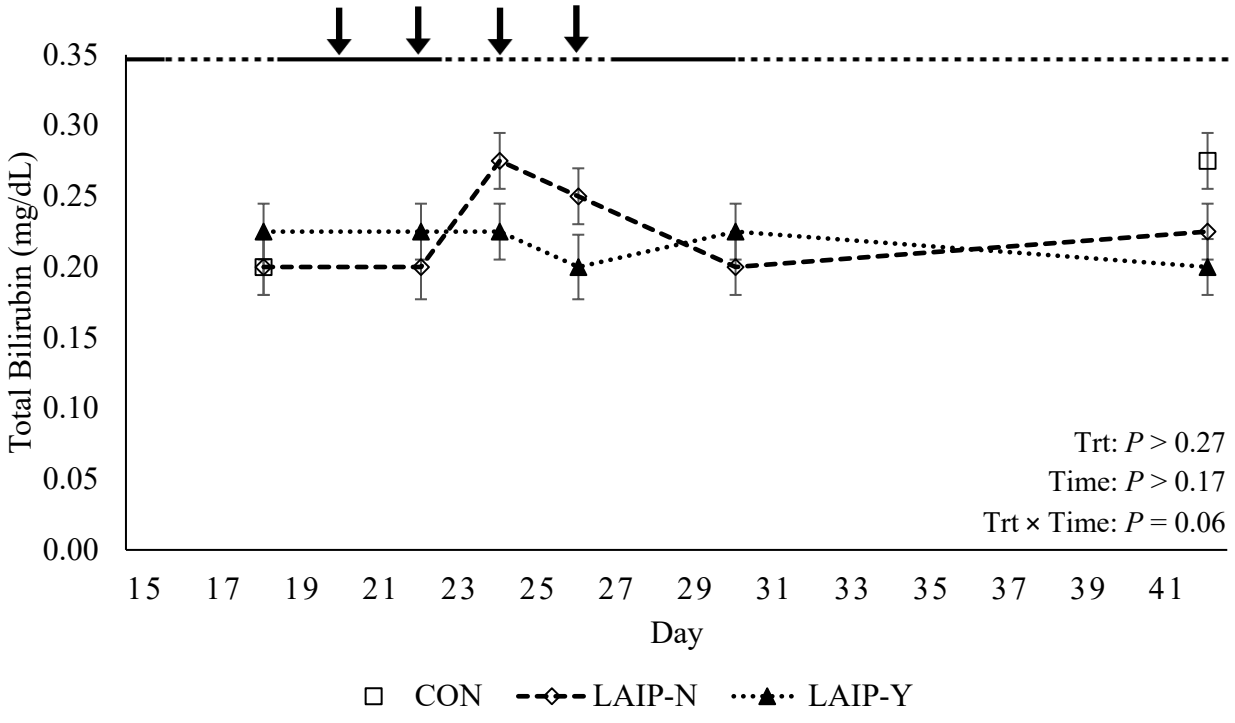

Figure 41. *Post hoc* comparison of the effects of successful liver abscess induction (LAIP-Y), failed liver abscess induction (LAIP-N), or control (CON) on total bilirubin during P2. Top axis depicts solid line, dashed line, and arrows for LS, HS, and feed restriction, respectively, in LAIP.

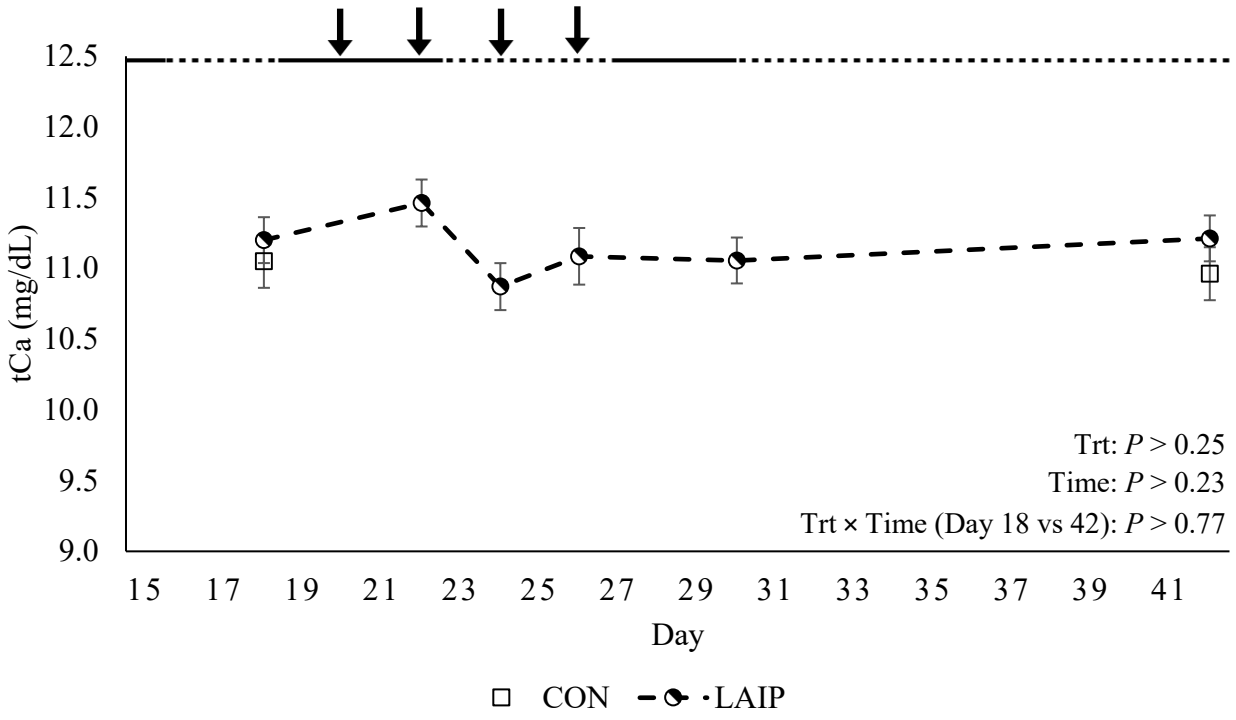

Figure 42. Effects of liver abscess induction protocol (LAIP) or control (CON) on total calcium during P2. Top axis depicts solid line, dashed line, and arrows for LS, HS, and feed restriction, respectively, in LAIP.

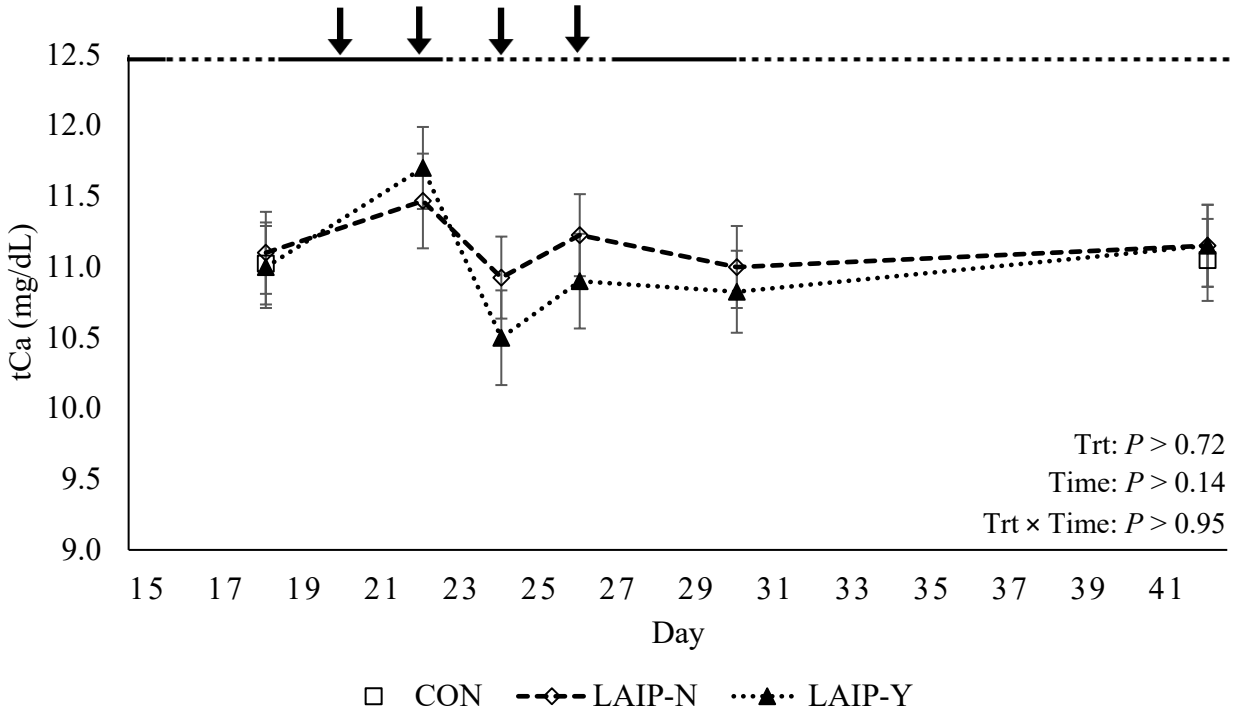

Figure 43. *Post hoc* comparison of the effects of successful liver abscess induction (LAIP-Y), failed liver abscess induction (LAIP-N), or control (CON) on total calcium during P2. Top axis depicts solid line, dashed line, and arrows for LS, HS, and feed restriction, respectively, in LAIP.

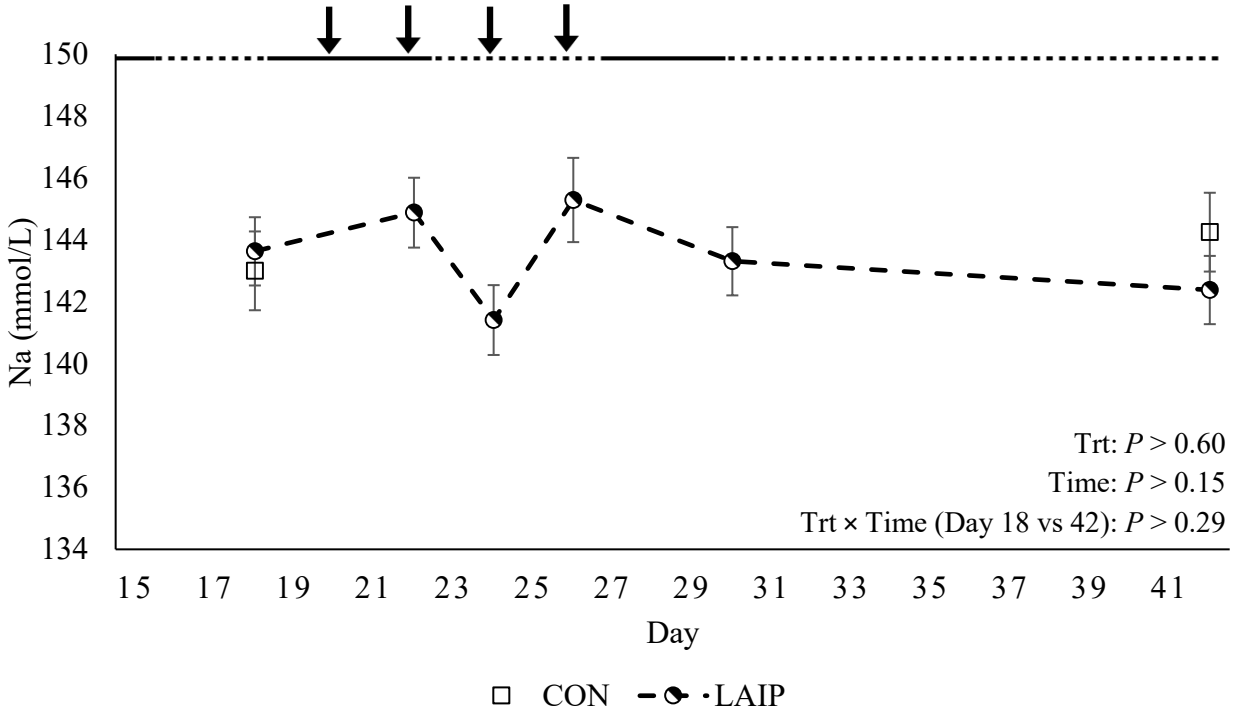

Figure 44. Effects of liver abscess induction protocol (LAIP) or control (CON) on sodium during P2. Top axis depicts solid line, dashed line, and arrows for LS, HS, and feed restriction, respectively, in LAIP.

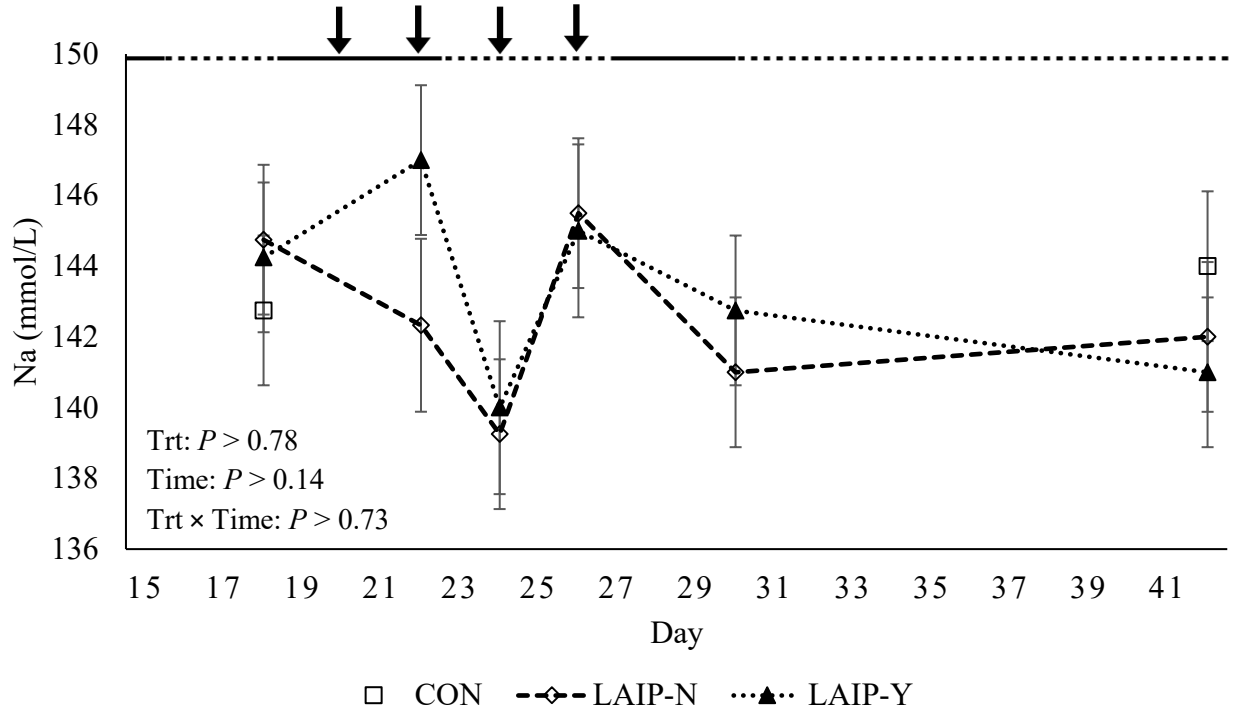

Figure 45. *Post hoc* comparison of the effects of successful liver abscess induction (LAIP-Y), failed liver abscess induction (LAIP-N), or control (CON) on sodium during P2. Top axis depicts solid line, dashed line, and arrows for LS, HS, and feed restriction, respectively, in LAIP.

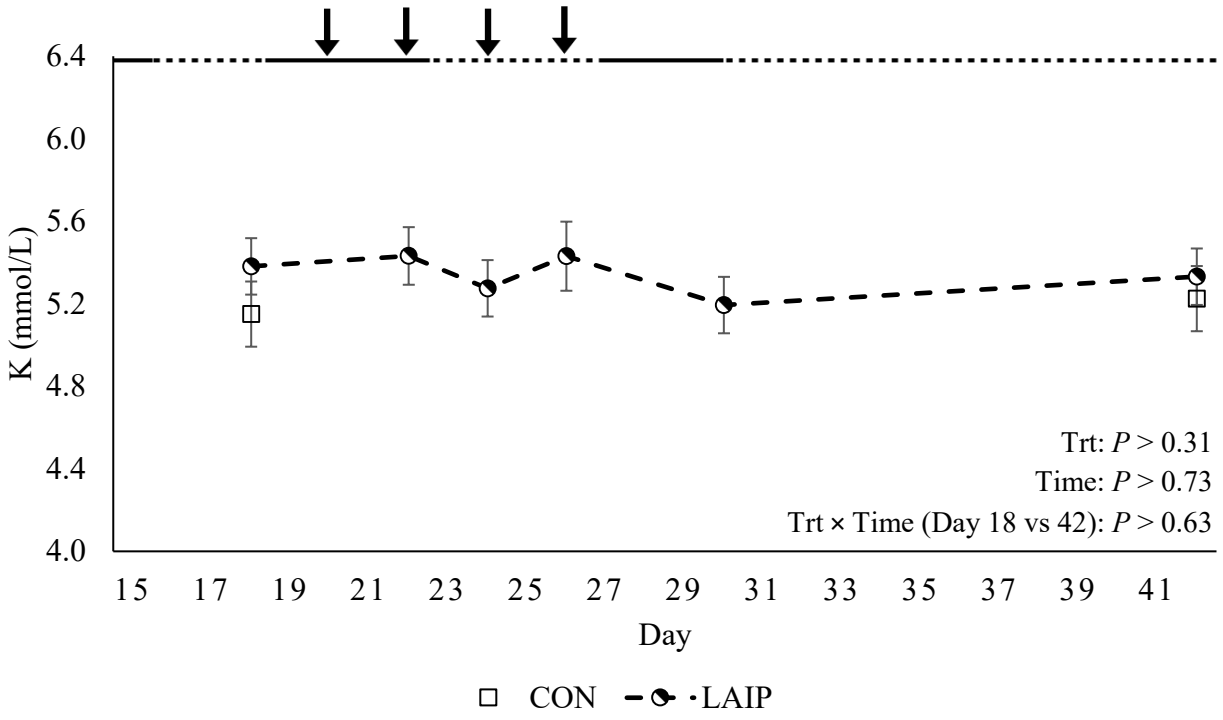

Figure 46. Effects of liver abscess induction protocol (LAIP) or control (CON) on potassium during P2. Top axis depicts solid line, dashed line, and arrows for LS, HS, and feed restriction, respectively, in LAIP.

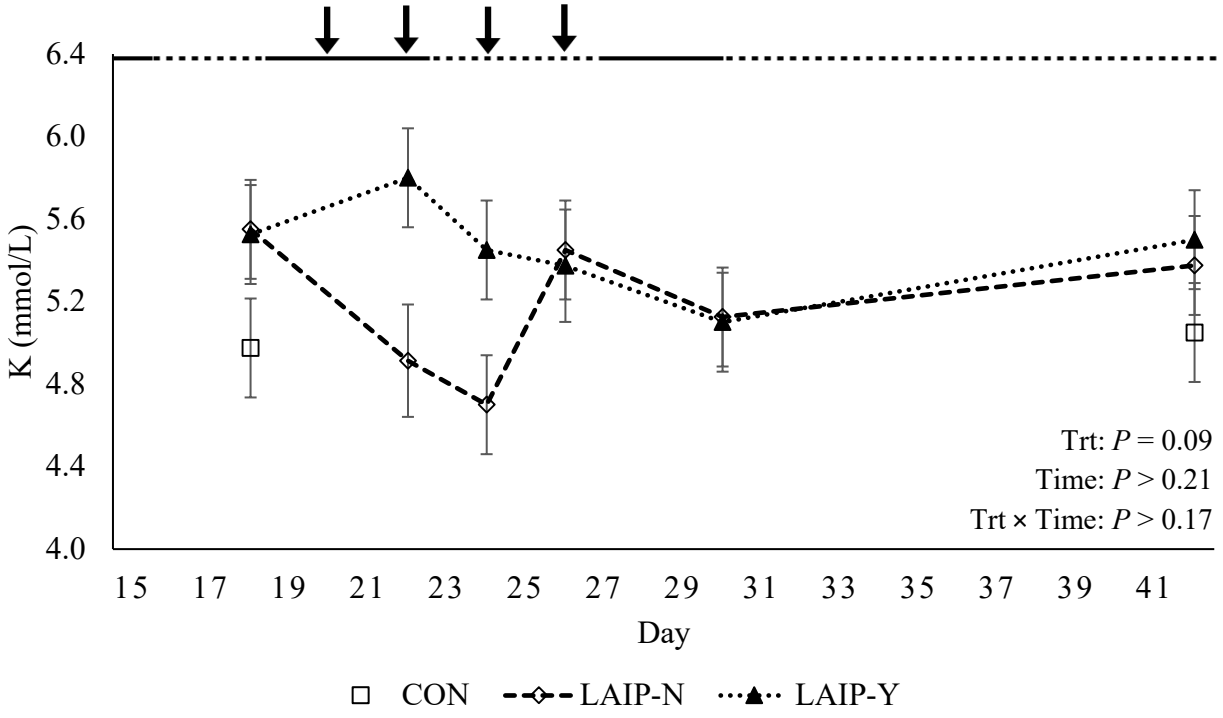

Figure 47. *Post hoc* comparison of the effects of successful liver abscess induction (LAIP-Y), failed liver abscess induction (LAIP-N), or control (CON) on potassium during P2. Top axis depicts solid line, dashed line, and arrows for LS, HS, and feed restriction, respectively, in LAIP.

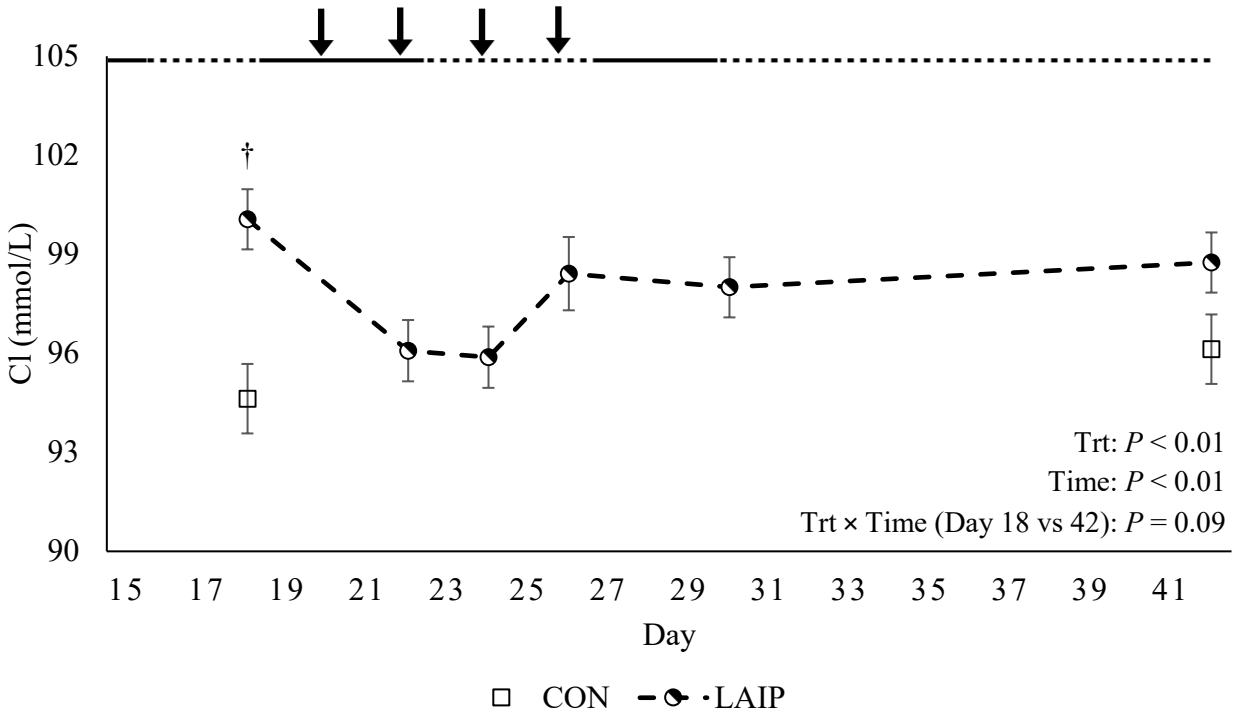

Figure 48. Effects of liver abscess induction protocol (LAIP) or control (CON) on chloride during P2. Top axis depicts solid line, dashed line, and arrows for LS, HS, and feed restriction, respectively, in LAIP. † denotes $0.05 < P \leq 0.10$.

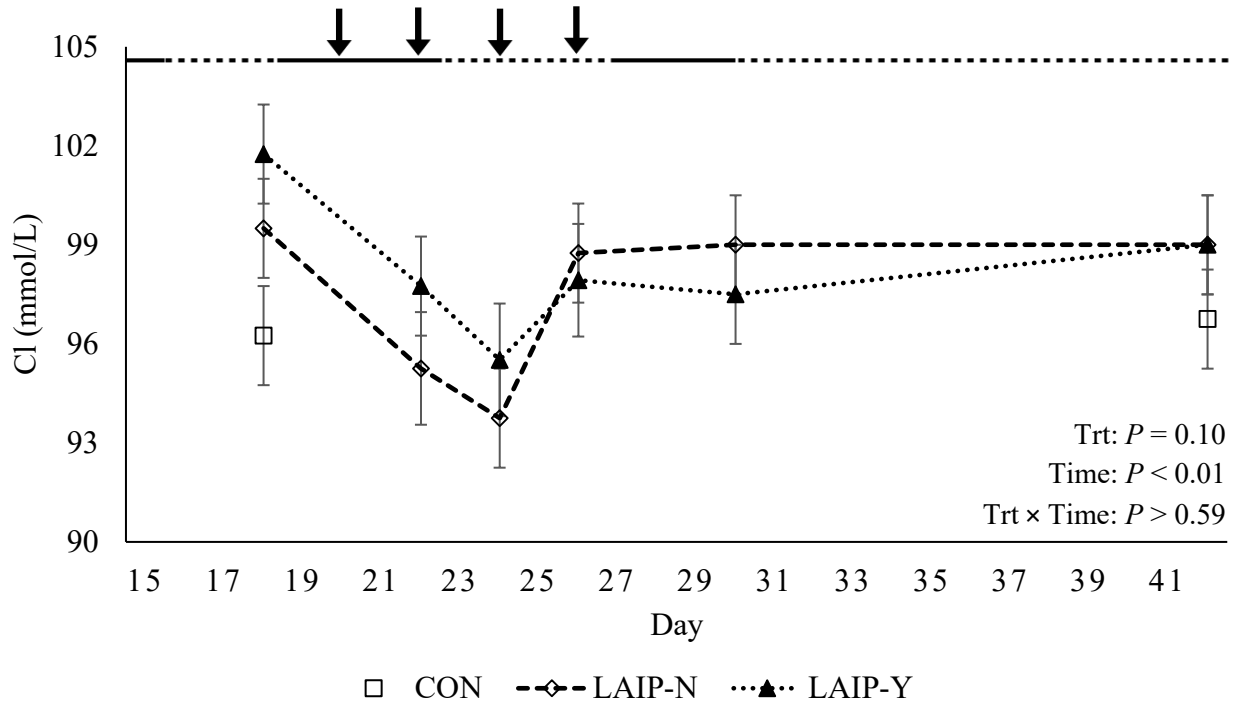

Figure 49. *Post hoc* comparison of the effects of successful liver abscess induction (LAIP-Y), failed liver abscess induction (LAIP-N), or control (CON) on chloride during P2. Top axis depicts solid line, dashed line, and arrows for LS, HS, and feed restriction, respectively, in LAIP.

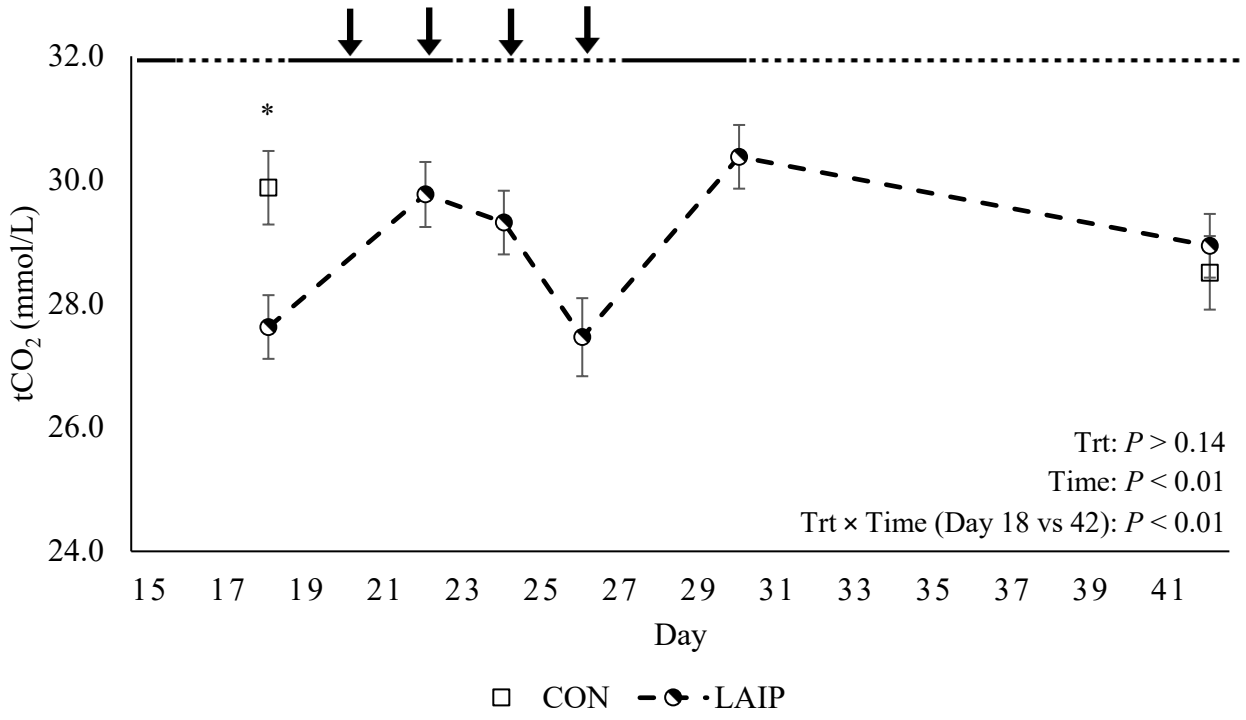

Figure 50. Effects of liver abscess induction protocol (LAIP) or control (CON) on total CO_2 during P2. Top axis depicts solid line, dashed line, and arrows for LS, HS, and feed restriction, respectively, in LAIP. * denotes $P < 0.05$.

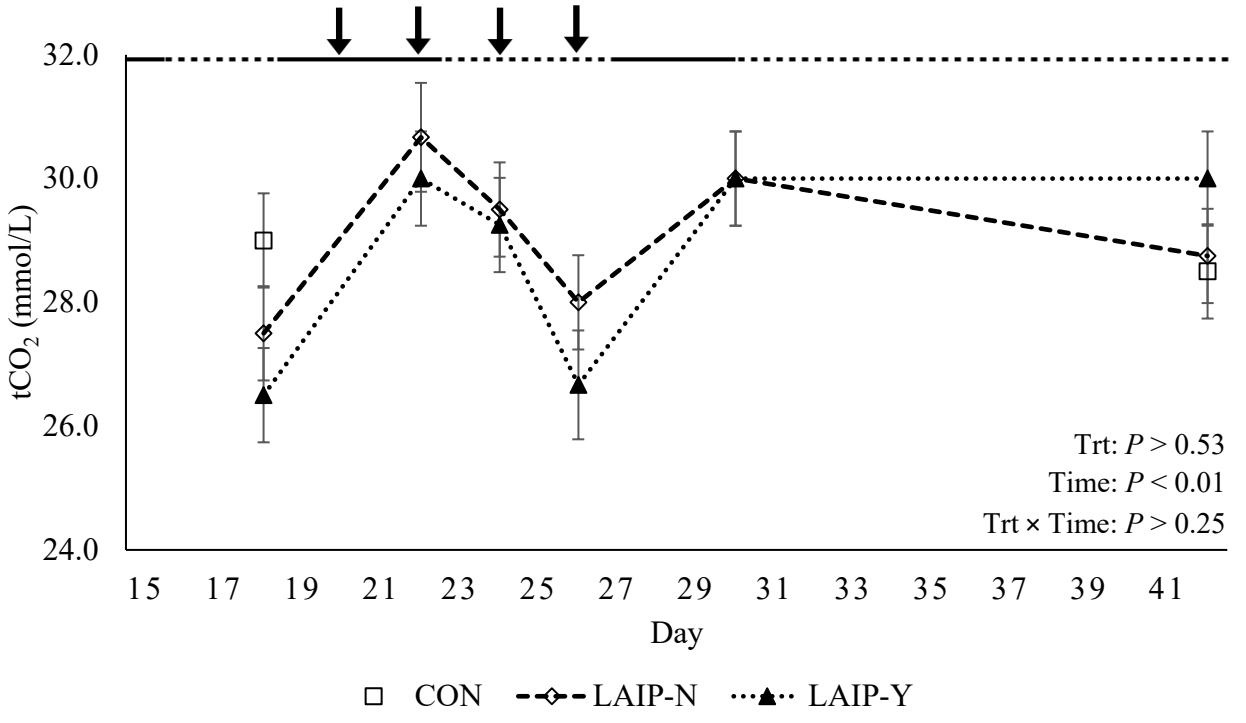

Figure 51. *Post hoc* comparison of the effects of successful liver abscess induction (LAIP-Y), failed liver abscess induction (LAIP-N), or control (CON) on total CO_2 during P2. Top axis depicts solid line, dashed line, and arrows for LS, HS, and feed restriction, respectively, in LAIP.

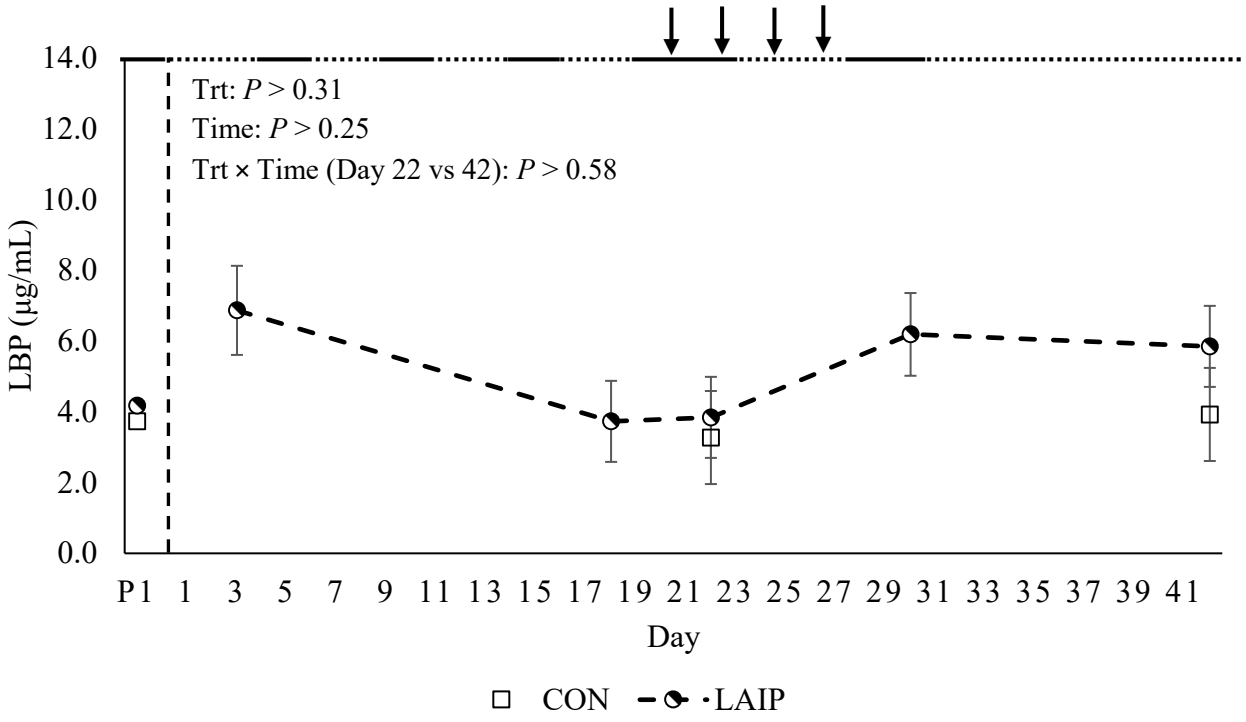

Figure 52. Effects of liver abscess induction protocol (LAIP) or control (CON) on lipopolysaccharide binding protein during P2. Top axis depicts solid line, dashed line, and arrows for LS, HS, and feed restriction, respectively, in LAIP.

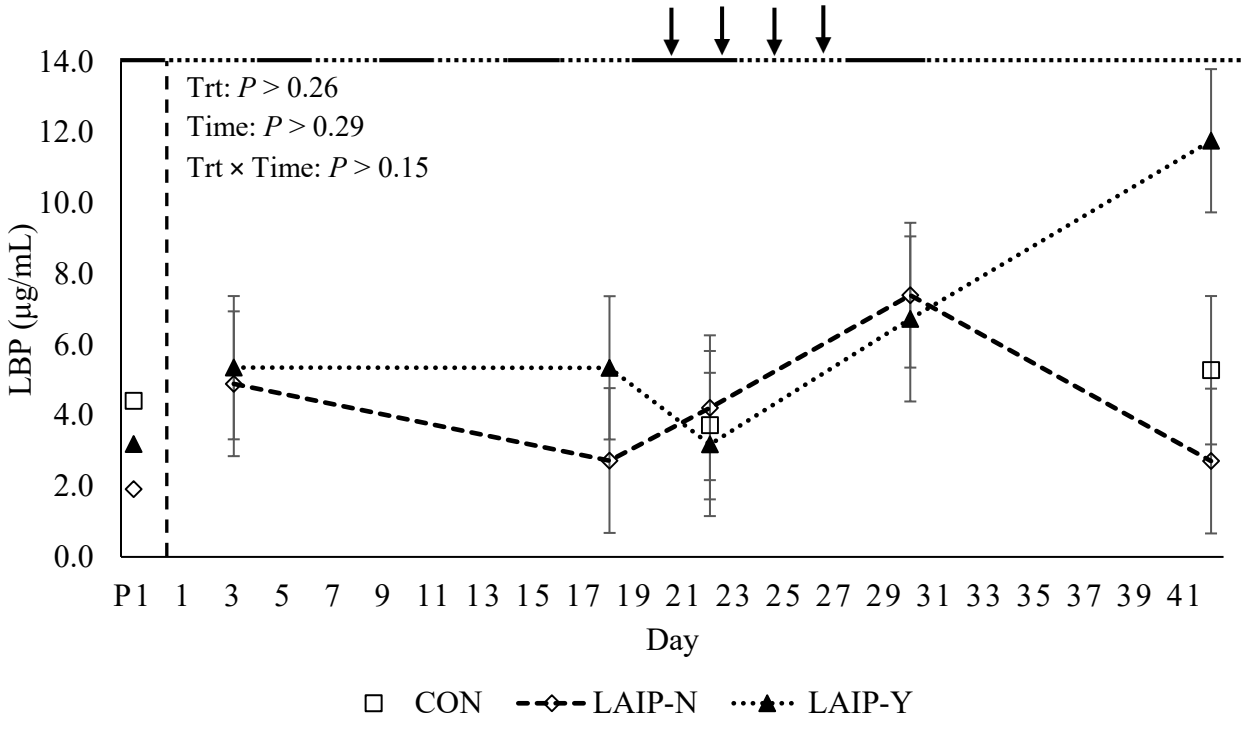

Figure 53. *Post hoc* comparison of the effects of successful liver abscess induction (LAIP-Y), failed liver abscess induction (LAIP-N), or control (CON) on lipopolysaccharide binding protein during P2. Top axis depicts solid line, dashed line, and arrows for LS, HS, and feed restriction, respectively, in LAIP.

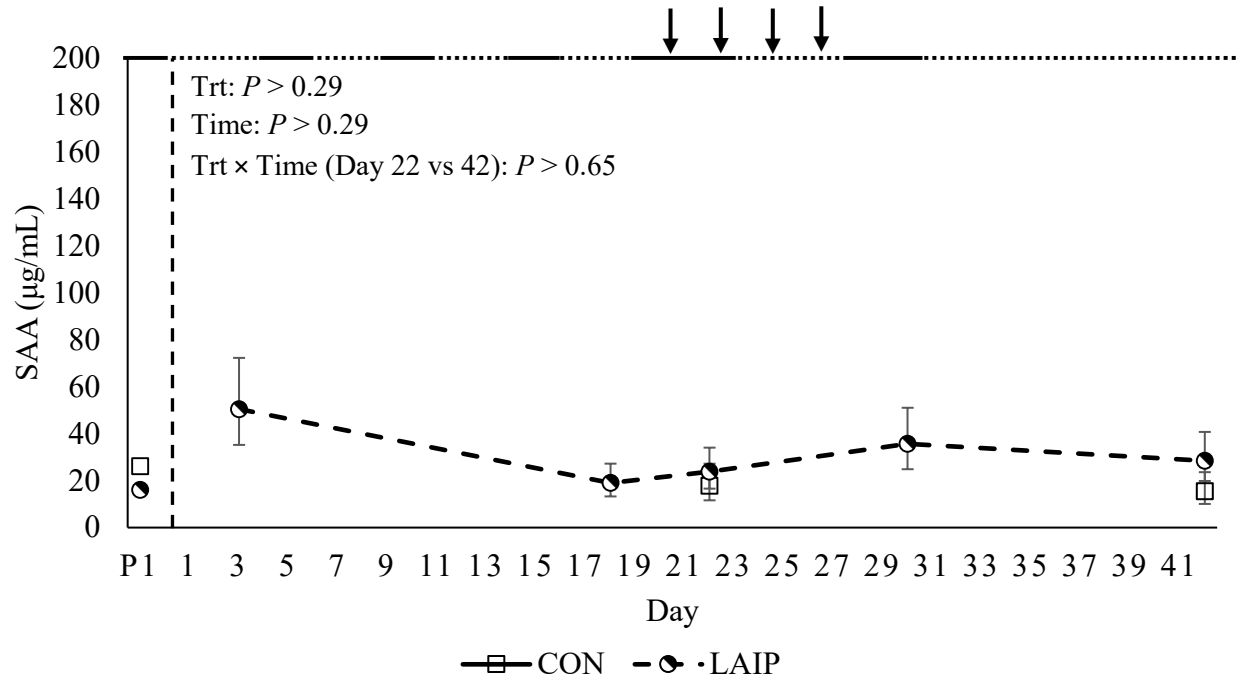

Figure 54. Effects of liver abscess induction protocol (LAIP) or control (CON) on serum amyloid A during P2. Top axis depicts solid line, dashed line, and arrows for LS, HS, and feed restriction, respectively, in LAIP. Values were log-transformed for statistical analysis and back transformed for interpretation.

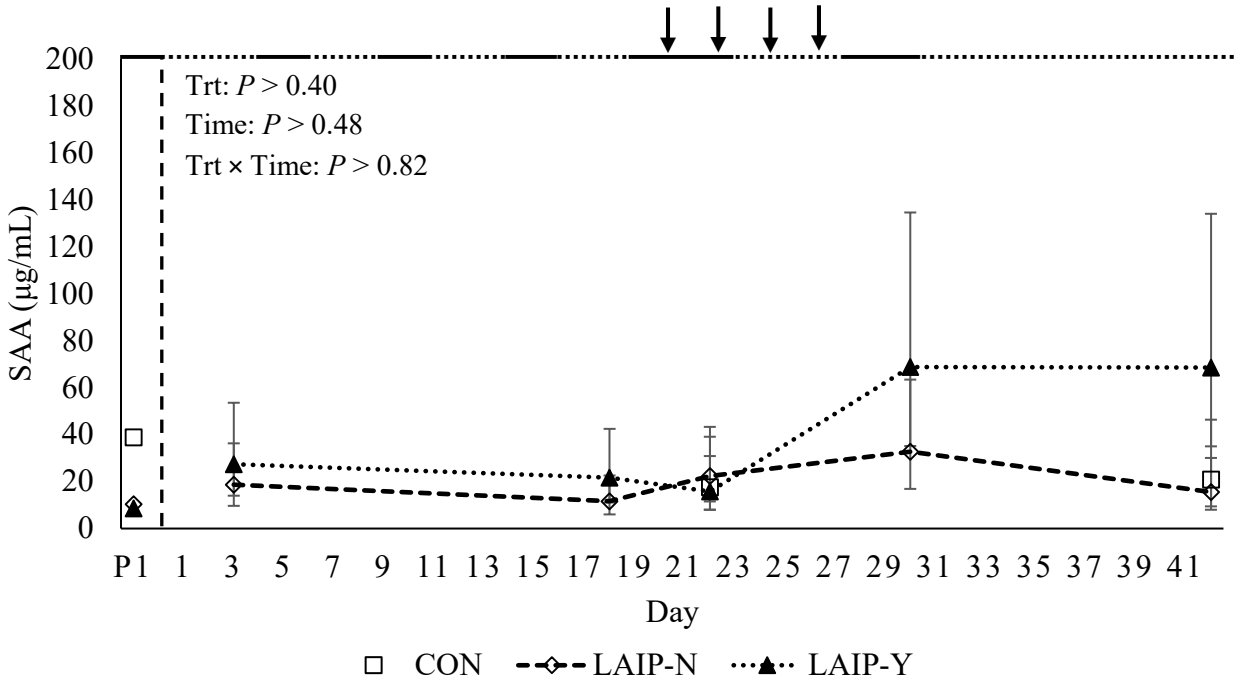

Figure 55. *Post hoc* comparison of the effects of successful liver abscess induction (LAIP-Y), failed liver abscess induction (LAIP-N), or control (CON) on serum amyloid A during P2. Top axis depicts solid line, dashed line, and arrows for LS, HS, and feed restriction, respectively, in LAIP. Values were log-transformed for statistical analysis and back transformed for interpretation.

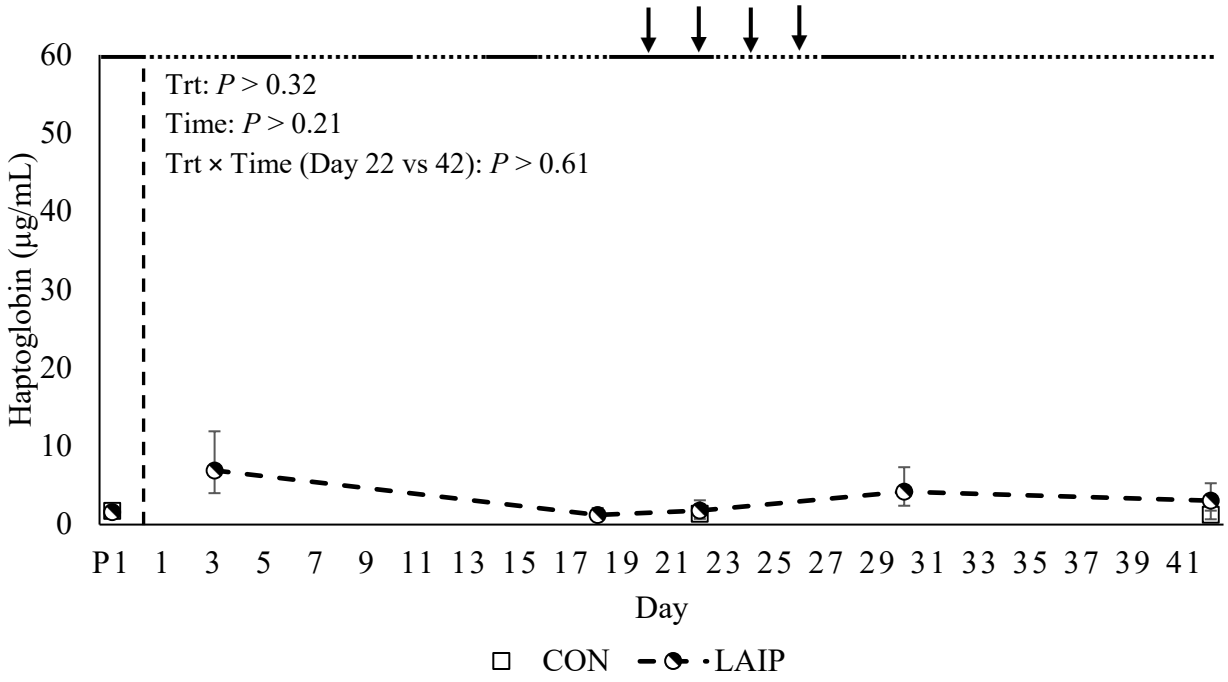

Figure 56. Effects of liver abscess induction protocol (LAIP) or control (CON) on haptoglobin during P2. Top axis depicts solid line, dashed line, and arrows for LS, HS, and feed restriction, respectively, in LAIP. Values were log-transformed for statistical analysis and back transformed for interpretation.

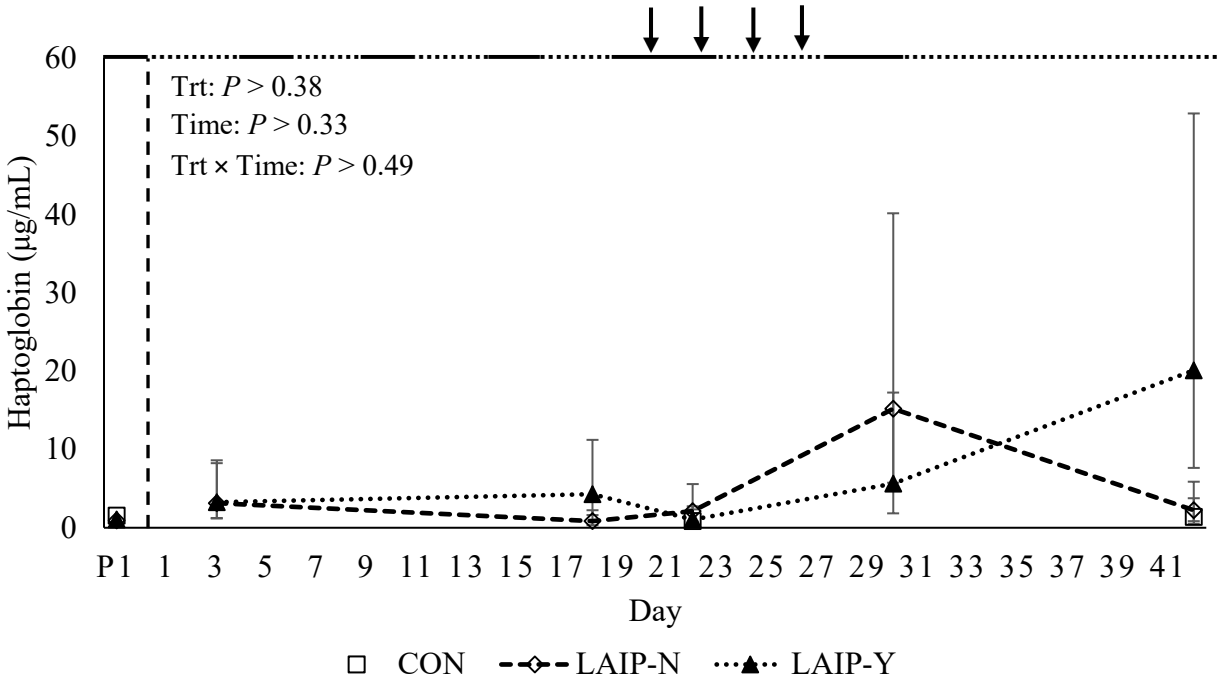

Figure 57. *Post hoc* comparison of the effects of successful liver abscess induction (LAIP-Y), failed liver abscess induction (LAIP-N), or control (CON) on haptoglobin during P2. Top axis depicts solid line, dashed line, and arrows for LS, HS, and feed restriction, respectively, in LAIP. Values were log-transformed for statistical analysis and back transformed for interpretation.

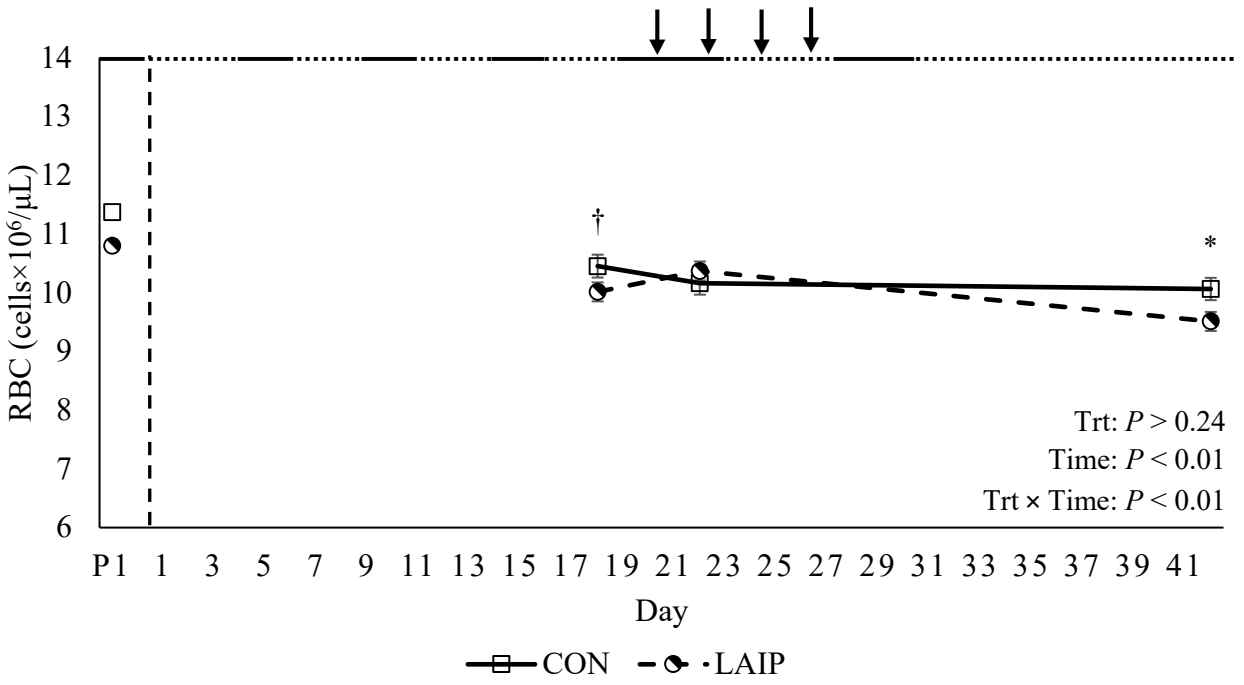

Figure 58. Effects of liver abscess induction protocol (LAIP) or control (CON) on red blood cells during P2. Top axis depicts solid line, dashed line, and arrows for LS, HS, and feed restriction, respectively, in LAIP. * denotes $P < 0.05$, † denotes $0.05 < P \leq 0.10$.

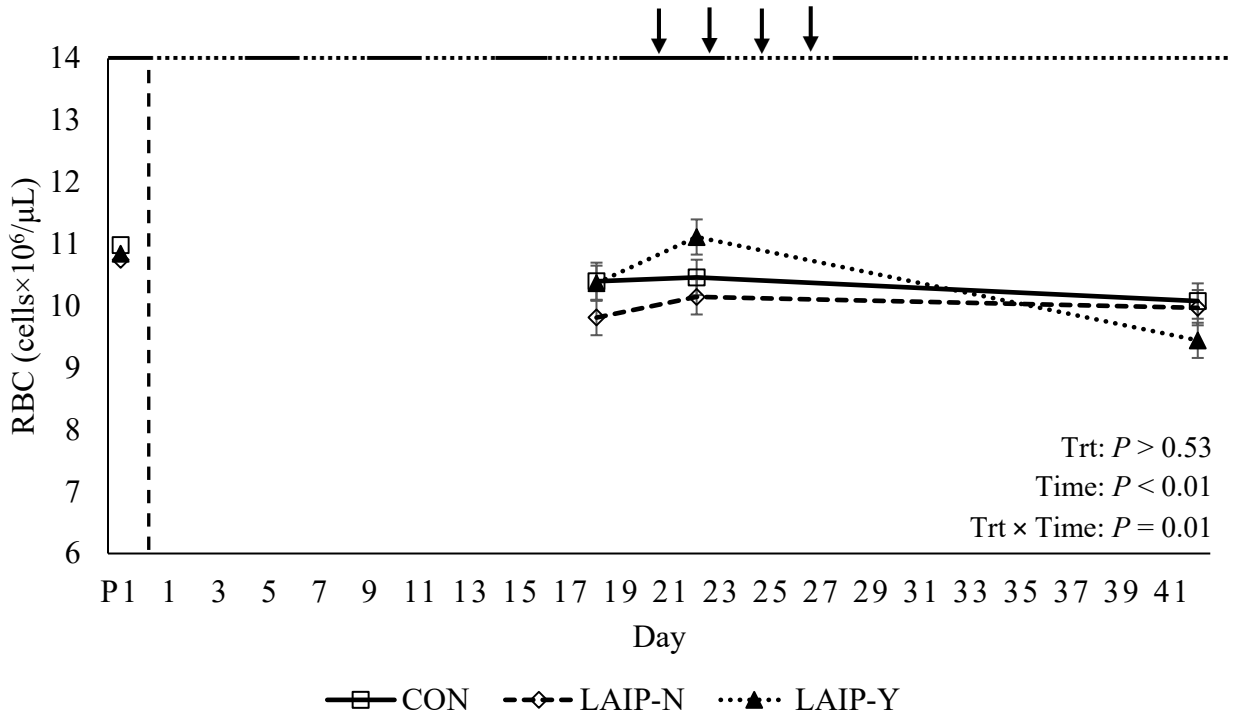

Figure 59. *Post hoc* comparison of the effects of successful liver abscess induction (LAIP-Y), failed liver abscess induction (LAIP-N), or control (CON) on red blood cells during P2. Top axis depicts solid line, dashed line, and arrows for LS, HS, and feed restriction, respectively, in LAIP.

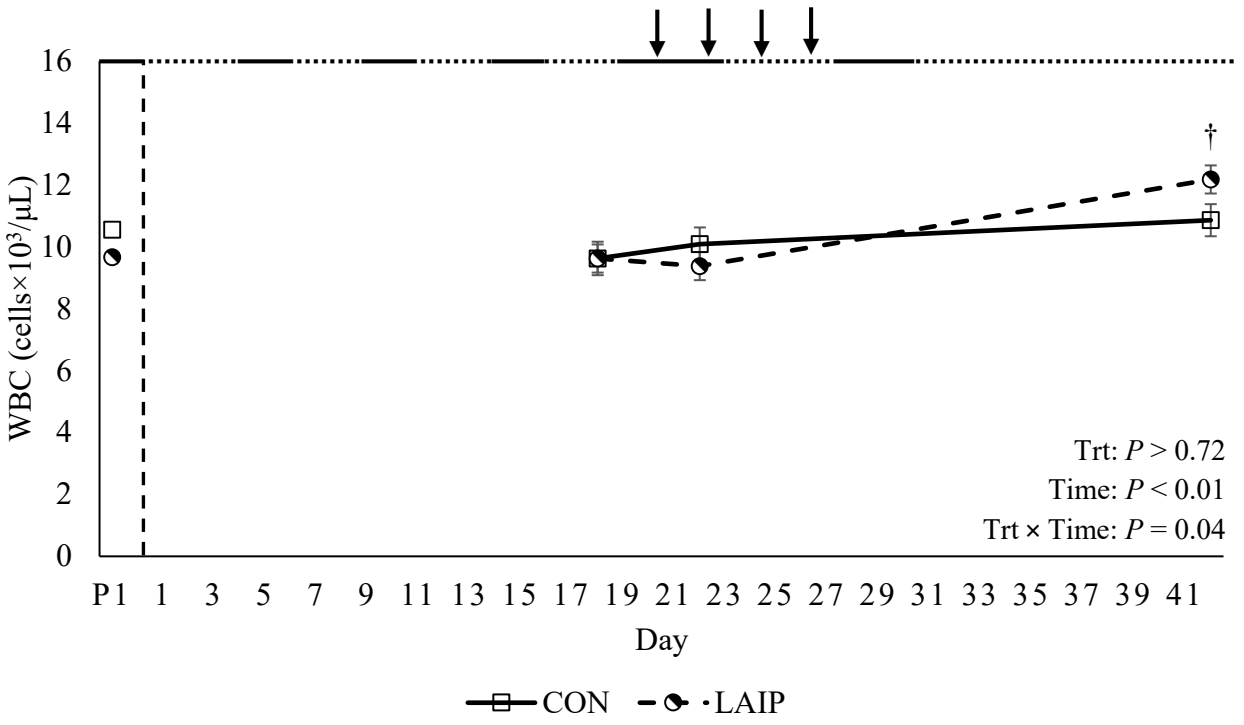

Figure 60. Effects of liver abscess induction protocol (LAIP) or control (CON) on white blood cells during P2. Top axis depicts solid line, dashed line, and arrows for LS, HS, and feed restriction, respectively, in LAIP. † denotes $0.05 < P \leq 0.10$.

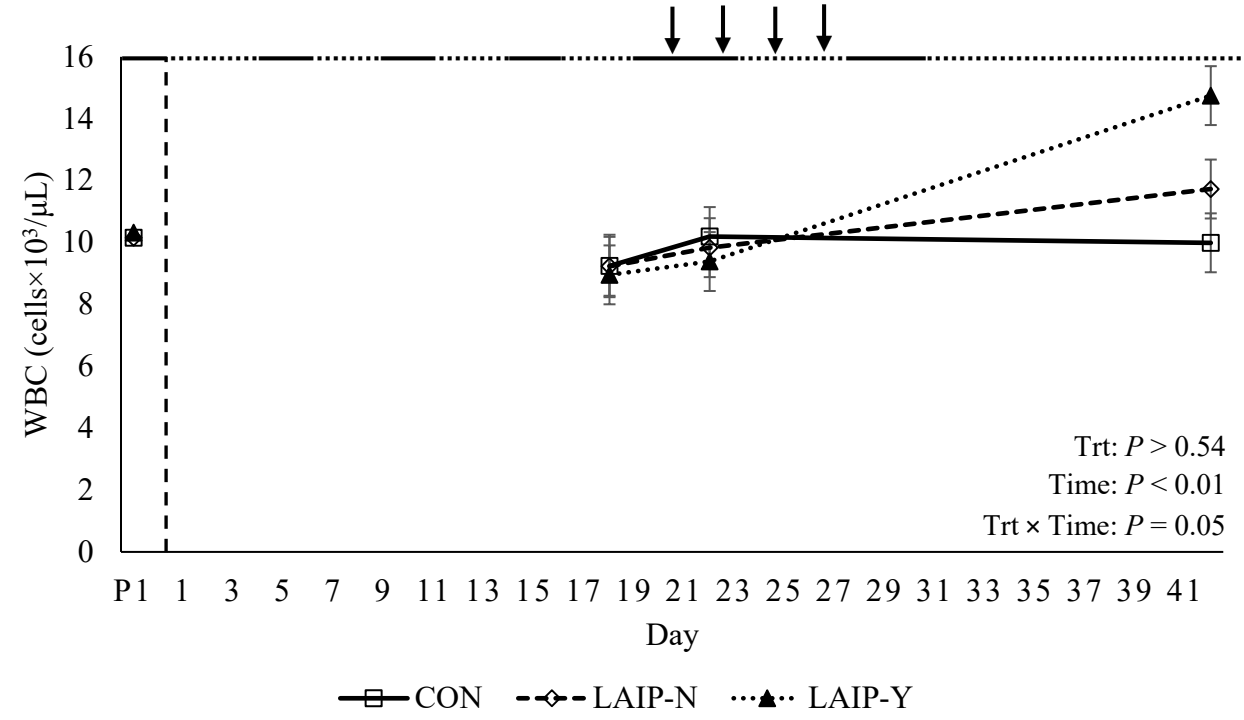

Figure 61. *Post hoc* comparison of the effects of successful liver abscess induction (LAIP-Y), failed liver abscess induction (LAIP-N), or control (CON) on white blood cells during P2. Top axis depicts solid line, dashed line, and arrows for LS, HS, and feed restriction, respectively, in LAIP.

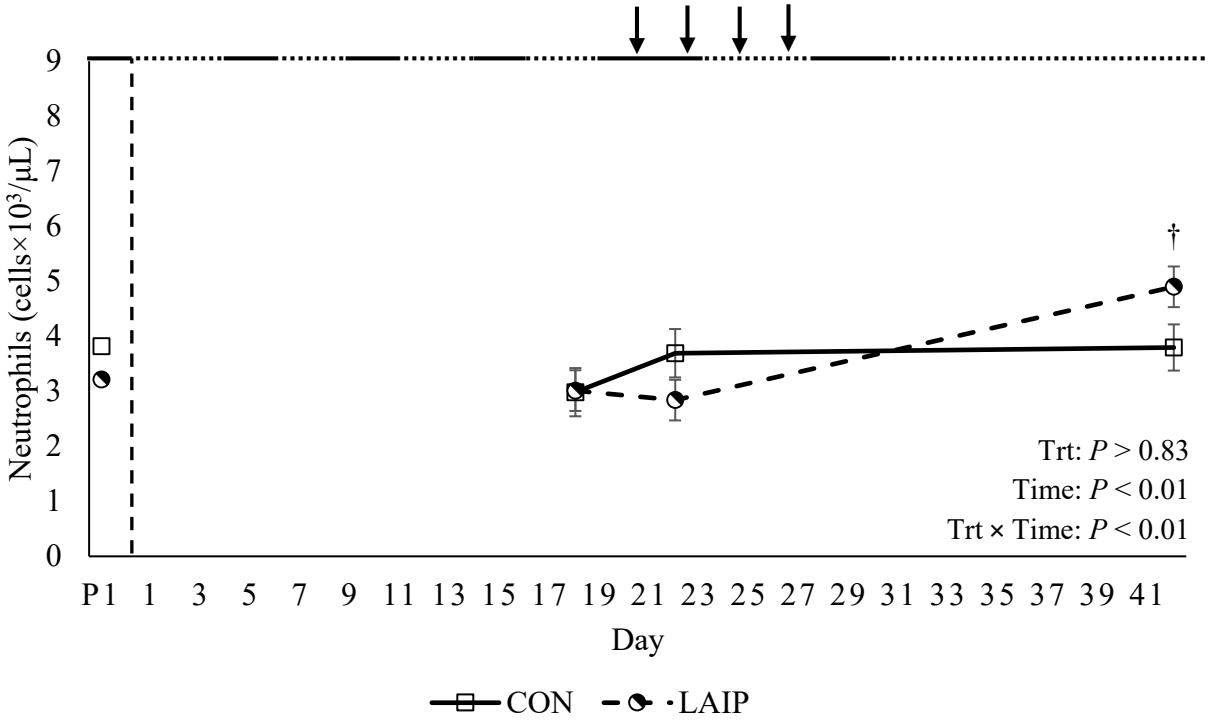

Figure 62. Effects of liver abscess induction protocol (LAIP) or control (CON) on neutrophils during P2. Top axis depicts solid line, dashed line, and arrows for LS, HS, and feed restriction, respectively, in LAIP. † denotes $0.05 < P \leq 0.10$.

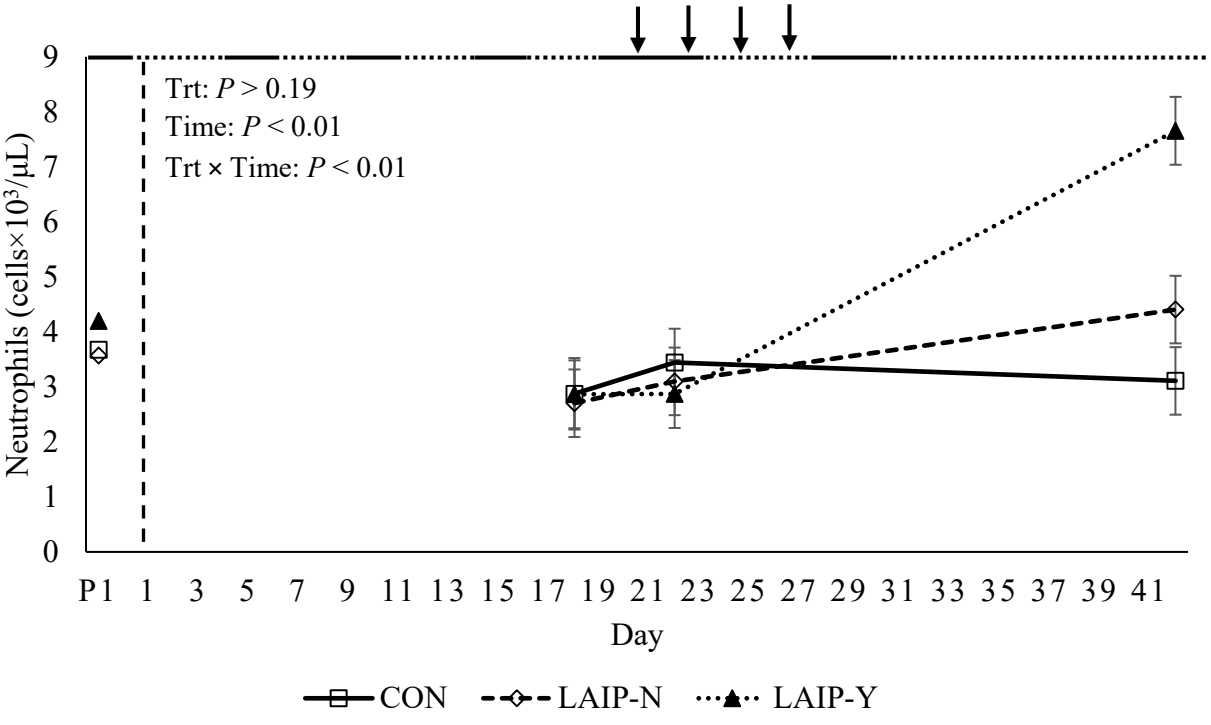

Figure 63. *Post hoc* comparison of the effects of successful liver abscess induction (LAIP-Y), failed liver abscess induction (LAIP-N), or control (CON) on neutrophils during P2. Top axis depicts solid line, dashed line, and arrows for LS, HS, and feed restriction, respectively, in LAIP.

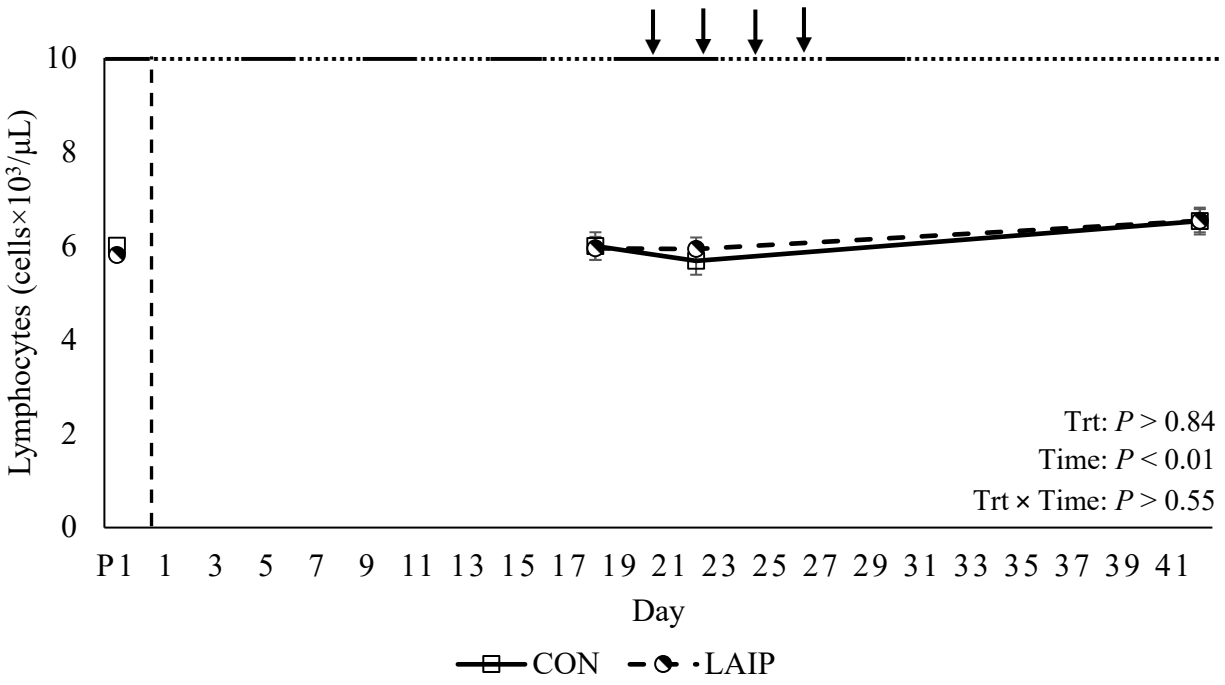

Figure 64. Effects of liver abscess induction protocol (LAIP) or control (CON) on lymphocytes during P2. Top axis depicts solid line, dashed line, and arrows for LS, HS, and feed restriction, respectively, in LAIP.

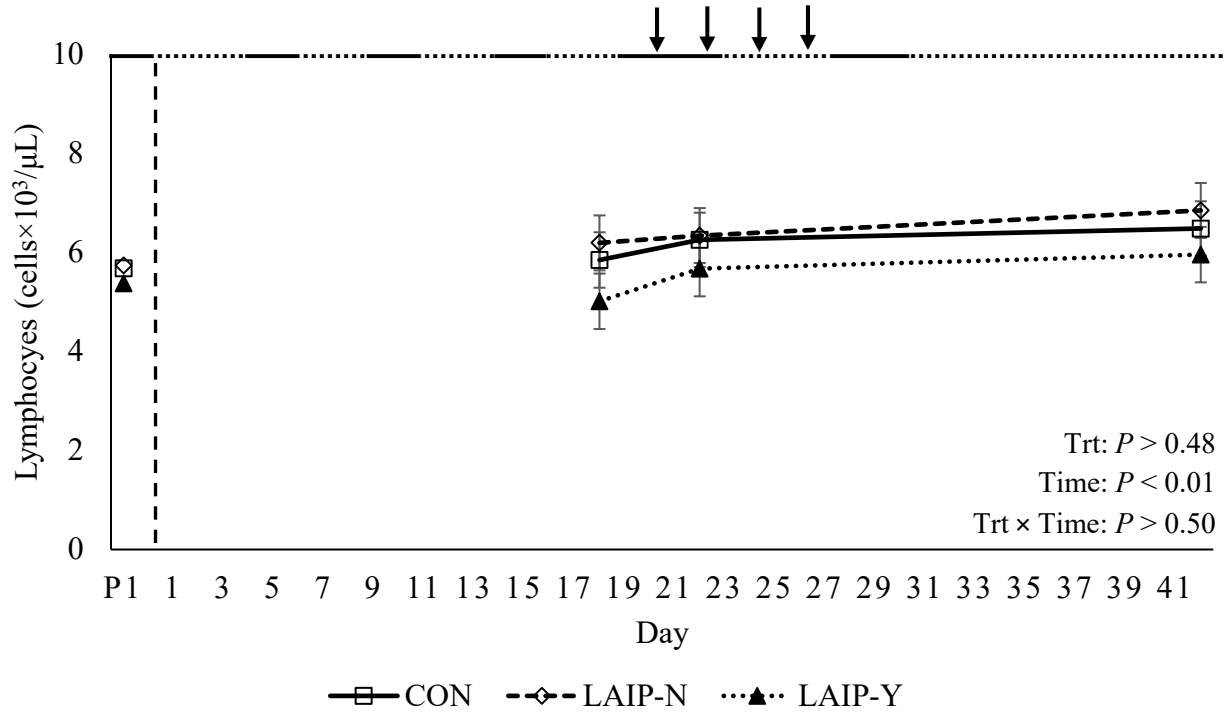

Figure 65. *Post hoc* comparison of the effects of successful liver abscess induction (LAIP-Y), failed liver abscess induction (LAIP-N), or control (CON) on lymphocytes during P2. Top axis depicts solid line, dashed line, and arrows for LS, HS, and feed restriction, respectively, in LAIP.

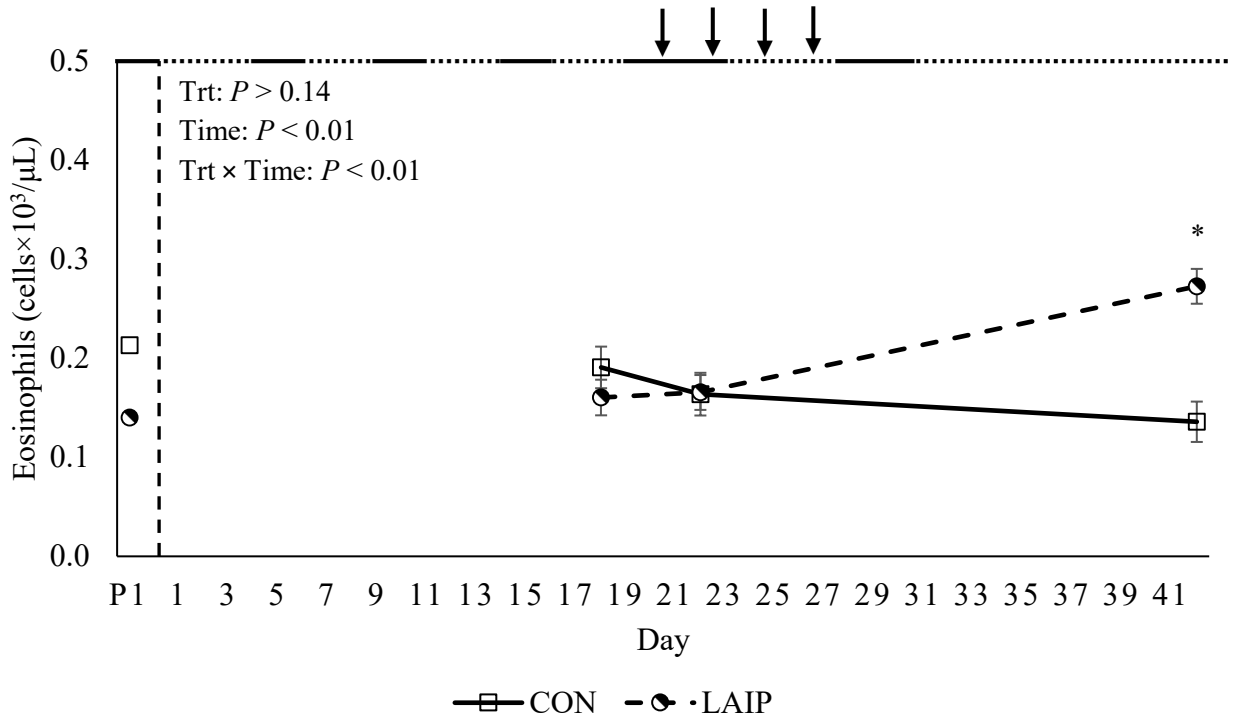

Figure 66. Effects of liver abscess induction protocol (LAIP) or control (CON) on eosinophils during P2. Top axis depicts solid line, dashed line, and arrows for LS, HS, and feed restriction, respectively, in LAIP. * denotes $P < 0.05$.

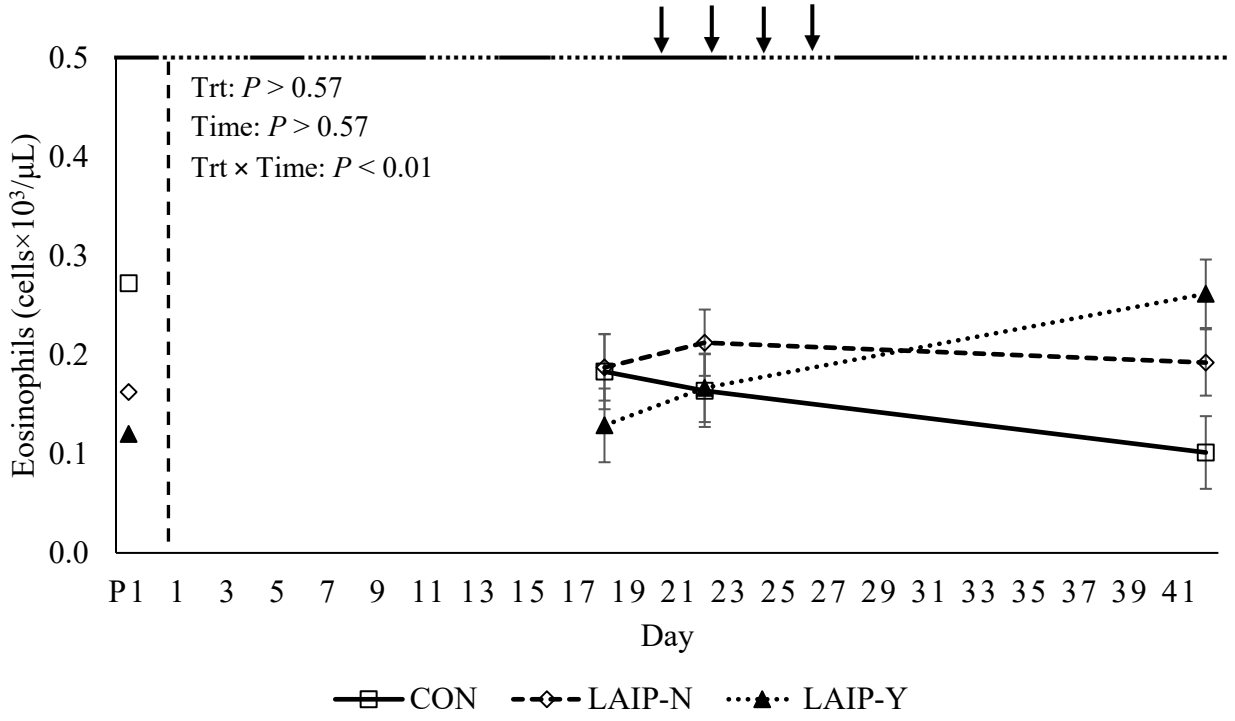

Figure 67. *Post hoc* comparison of the effects of successful liver abscess induction (LAIP-Y), failed liver abscess induction (LAIP-N), or control (CON) on eosinophils during P2. Top axis depicts solid line, dashed line, and arrows for LS, HS, and feed restriction, respectively, in LAIP.

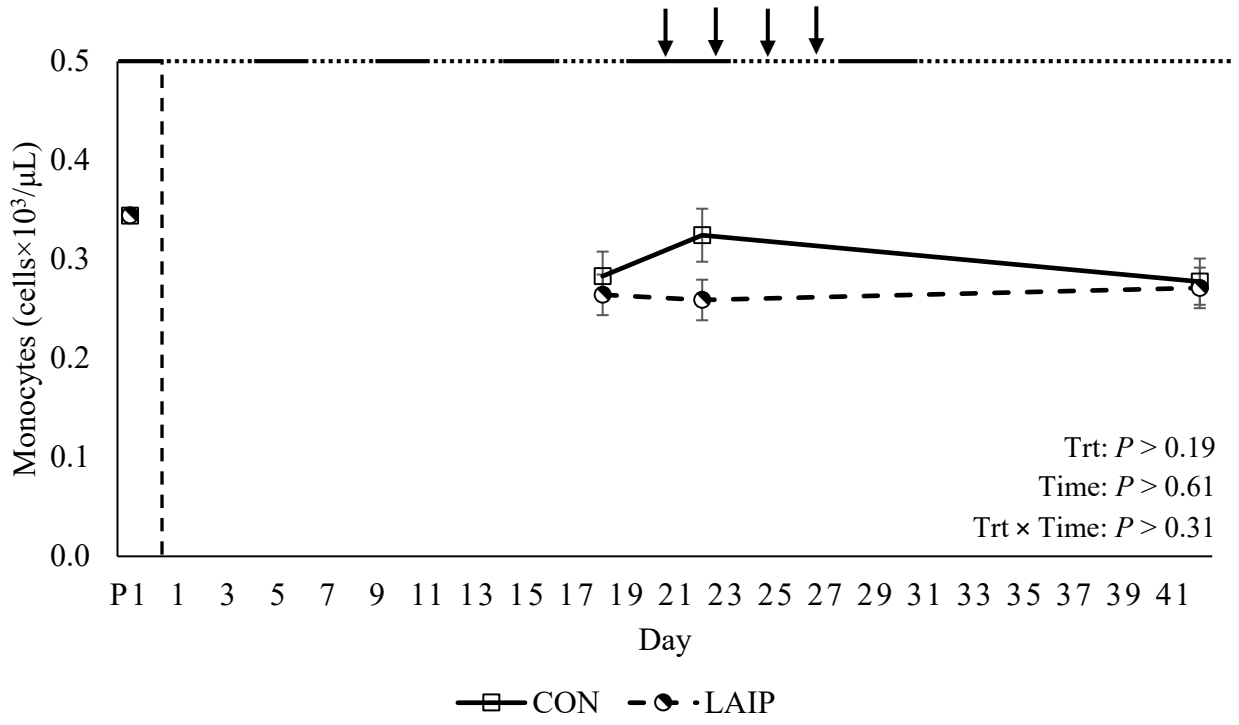

Figure 68. Effects of liver abscess induction protocol (LAIP) or control (CON) on monocytes during P2. Top axis depicts solid line, dashed line, and arrows for LS, HS, and feed restriction, respectively, in LAIP.

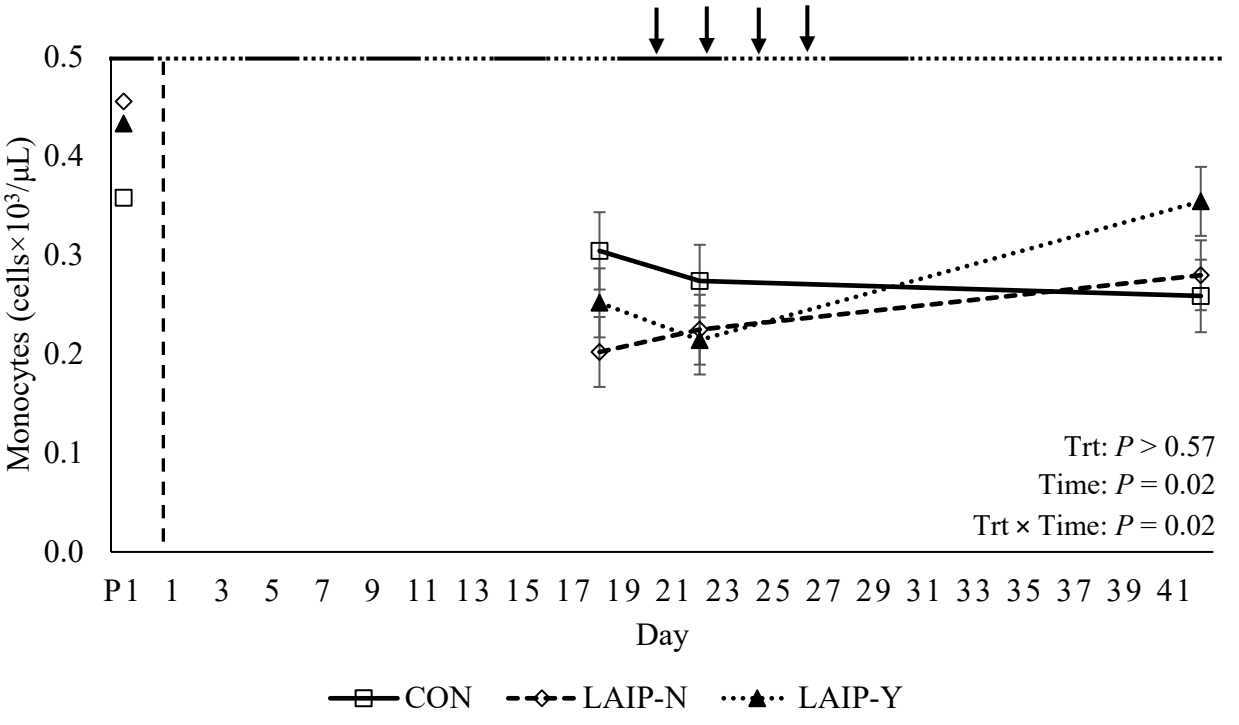

Figure 69. *Post hoc* comparison of the effects of successful liver abscess induction (LAIP-Y), failed liver abscess induction (LAIP-N), or control (CON) on monocytes during P2. Top axis depicts solid line, dashed line, and arrows for LS, HS, and feed restriction, respectively, in LAIP.

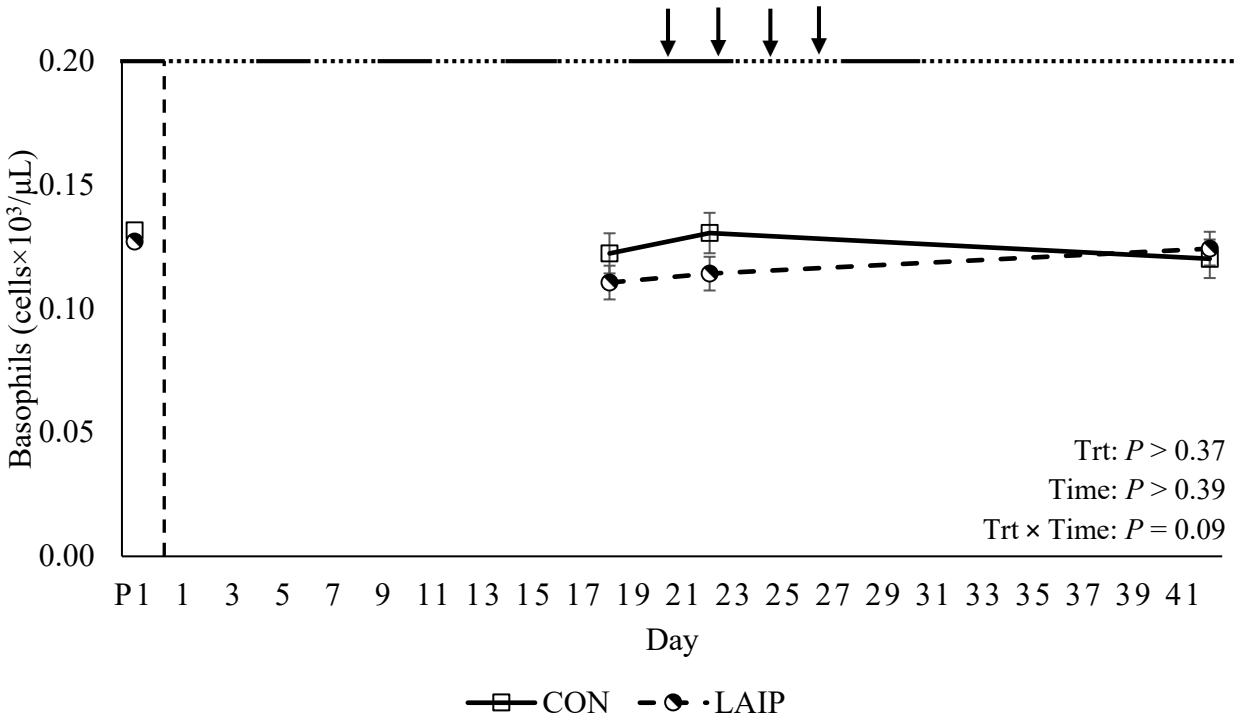

Figure 70. Effects of liver abscess induction protocol (LAIP) or control (CON) on basophils during P2. Top axis depicts solid line, dashed line, and arrows for LS, HS, and feed restriction, respectively, in LAIP.

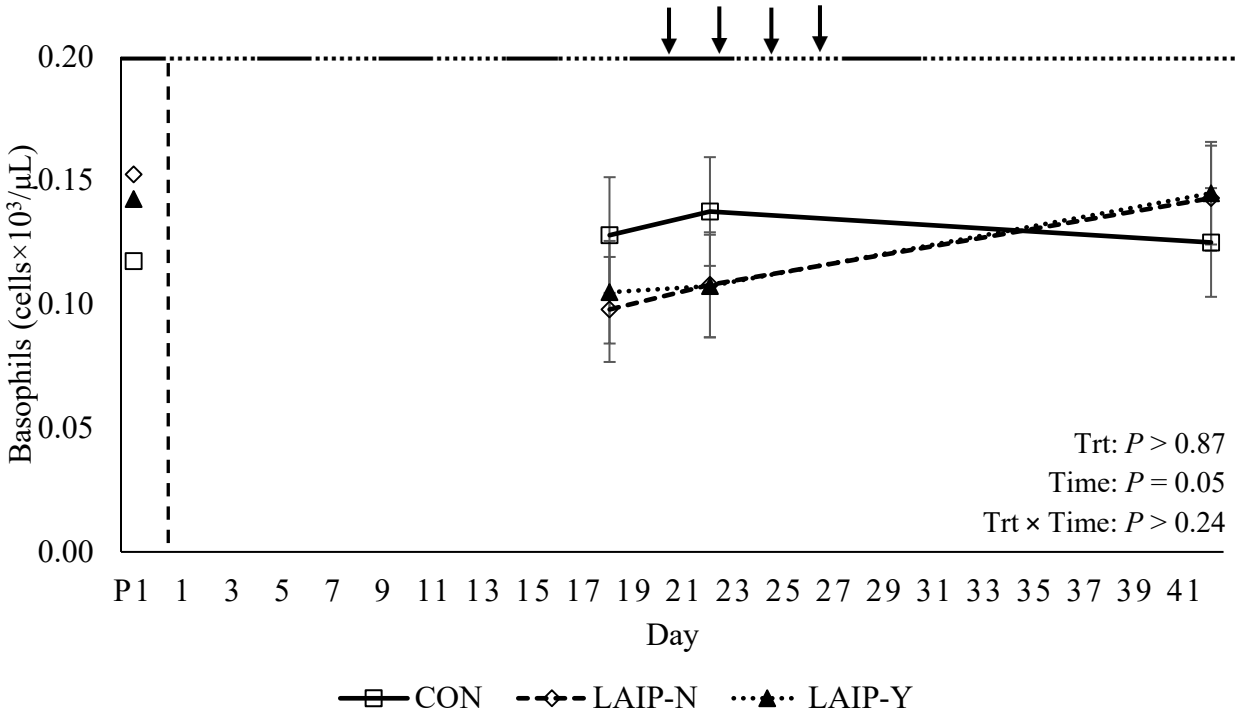

Figure 71. *Post hoc* comparison of the effects of successful liver abscess induction (LAIP-Y), failed liver abscess induction (LAIP-N), or control (CON) on basophils during P2. Top axis depicts solid line, dashed line, and arrows for LS, HS, and feed restriction, respectively, in LAIP.

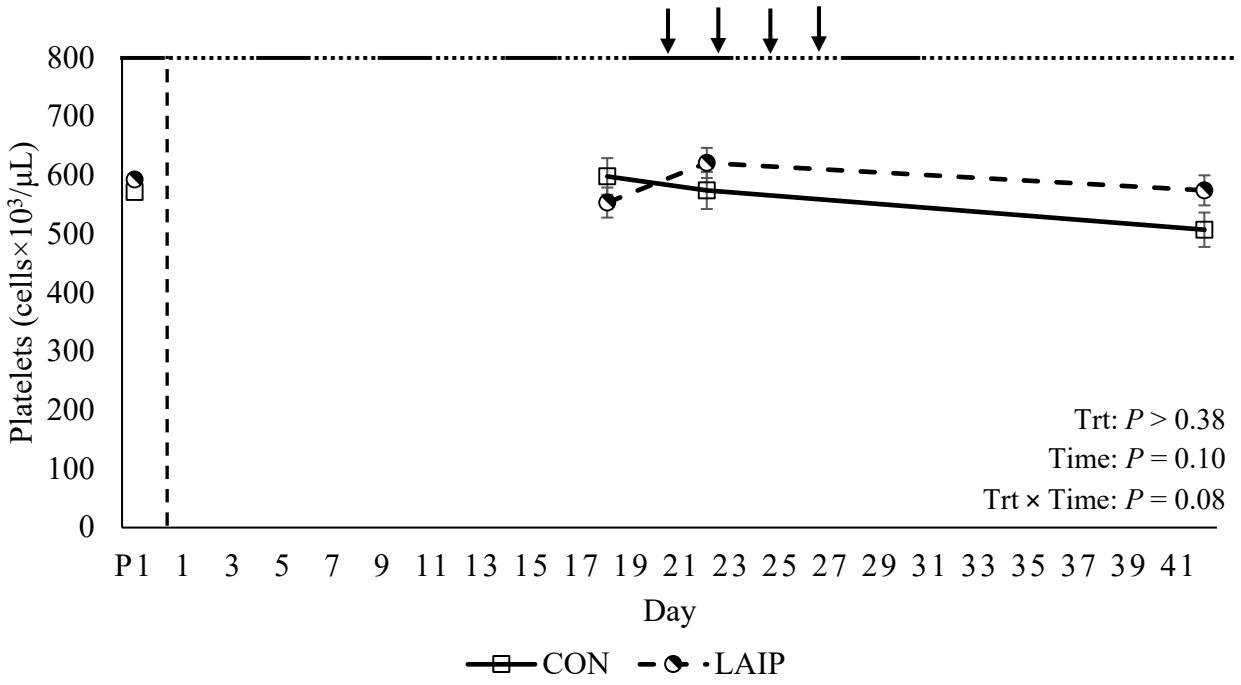

Figure 72. Effects of liver abscess induction protocol (LAIP) or control (CON) on platelets during P2. Top axis depicts solid line, dashed line, and arrows for LS, HS, and feed restriction, respectively, in LAIP.

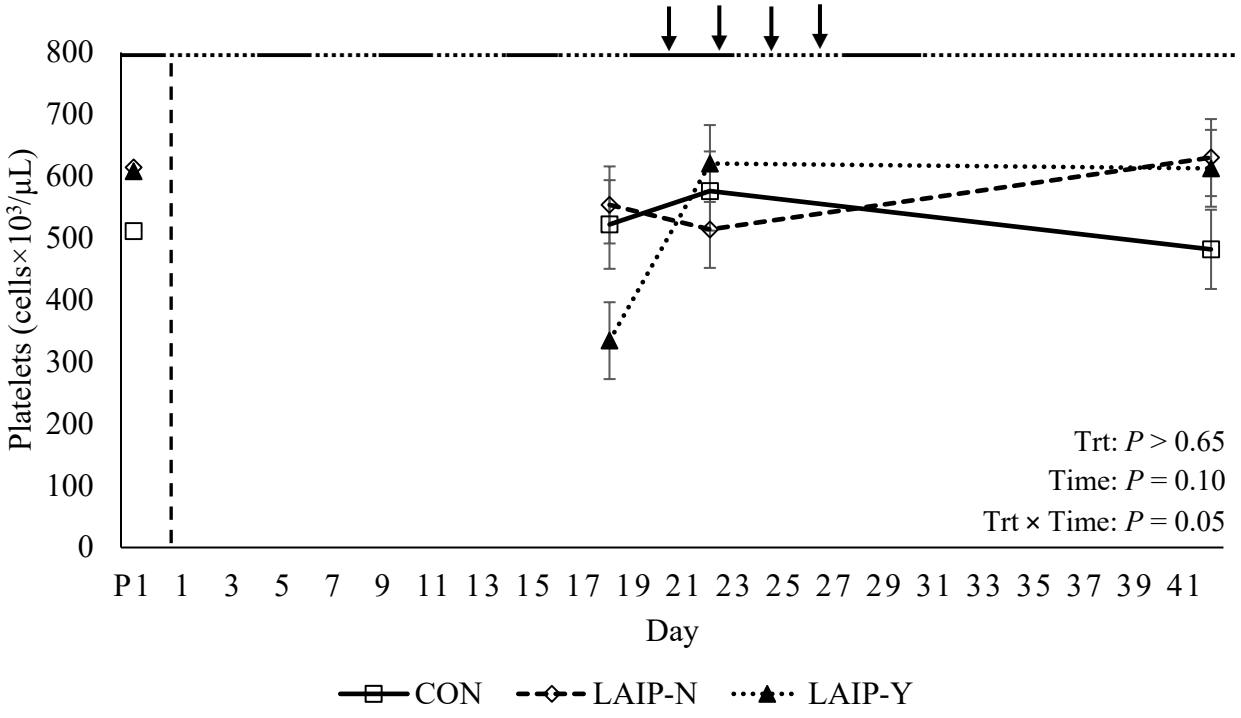

Figure 73. *Post hoc* comparison of the effects of successful liver abscess induction (LAIP-Y), failed liver abscess induction (LAIP-N), or control (CON) on platelets during P2. Top axis depicts solid line, dashed line, and arrows for LS, HS, and feed restriction, respectively, in LAIP.

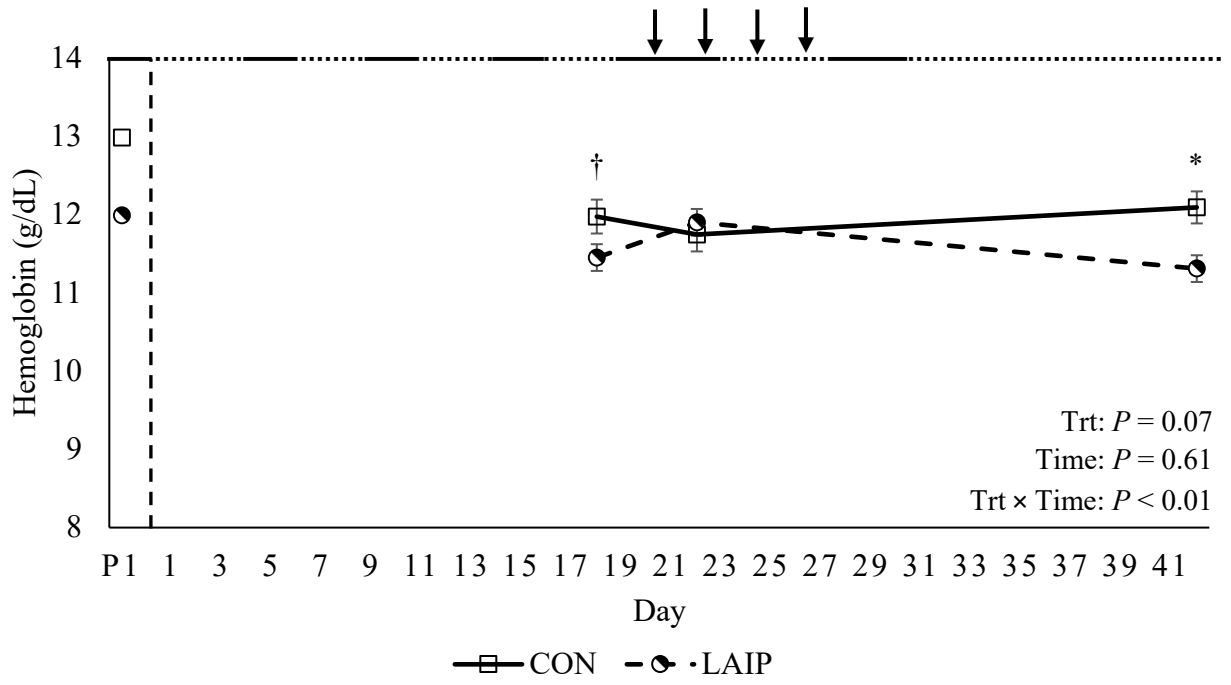

Figure 74. Effects of liver abscess induction protocol (LAIP) or control (CON) on hemoglobin during P2. Top axis depicts solid line, dashed line, and arrows for LS, HS, and feed restriction, respectively, in LAIP. * denotes $P < 0.05$, † denotes $0.05 < P \leq 0.10$.

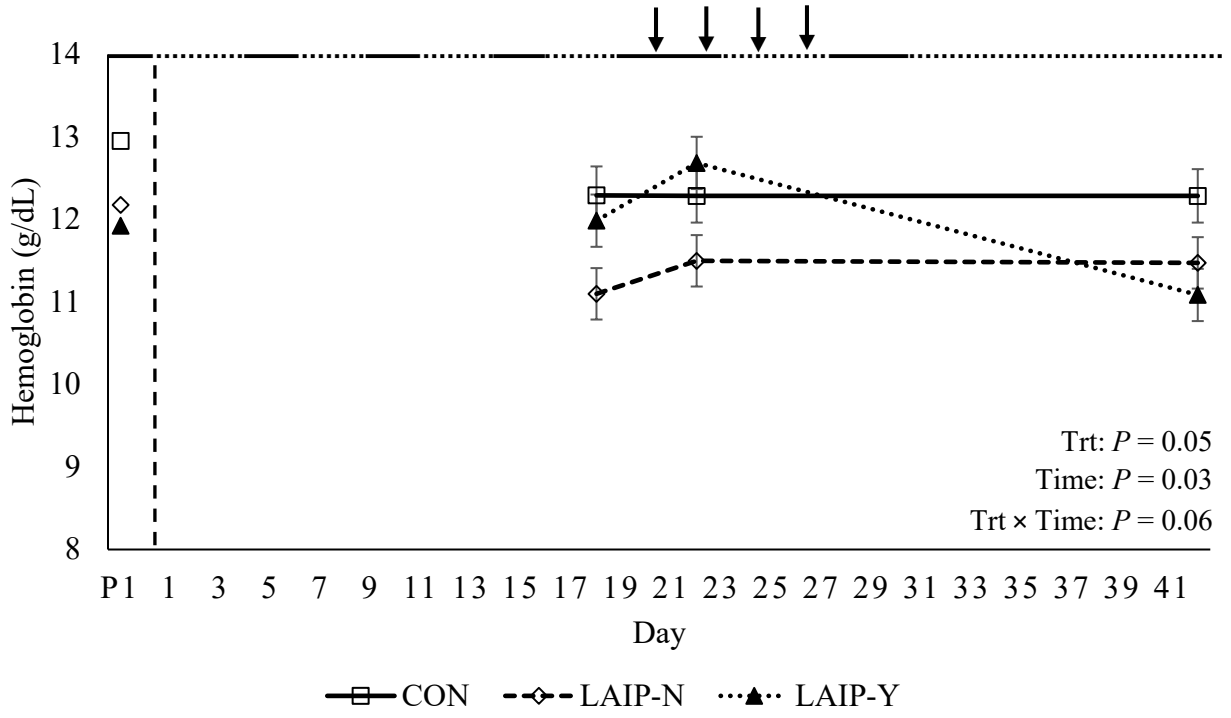

Figure 75. *Post hoc* comparison of the effects of successful liver abscess induction (LAIP-Y), failed liver abscess induction (LAIP-N), or control (CON) on hemoglobin during P2. Top axis depicts solid line, dashed line, and arrows for LS, HS, and feed restriction, respectively, in LAIP.

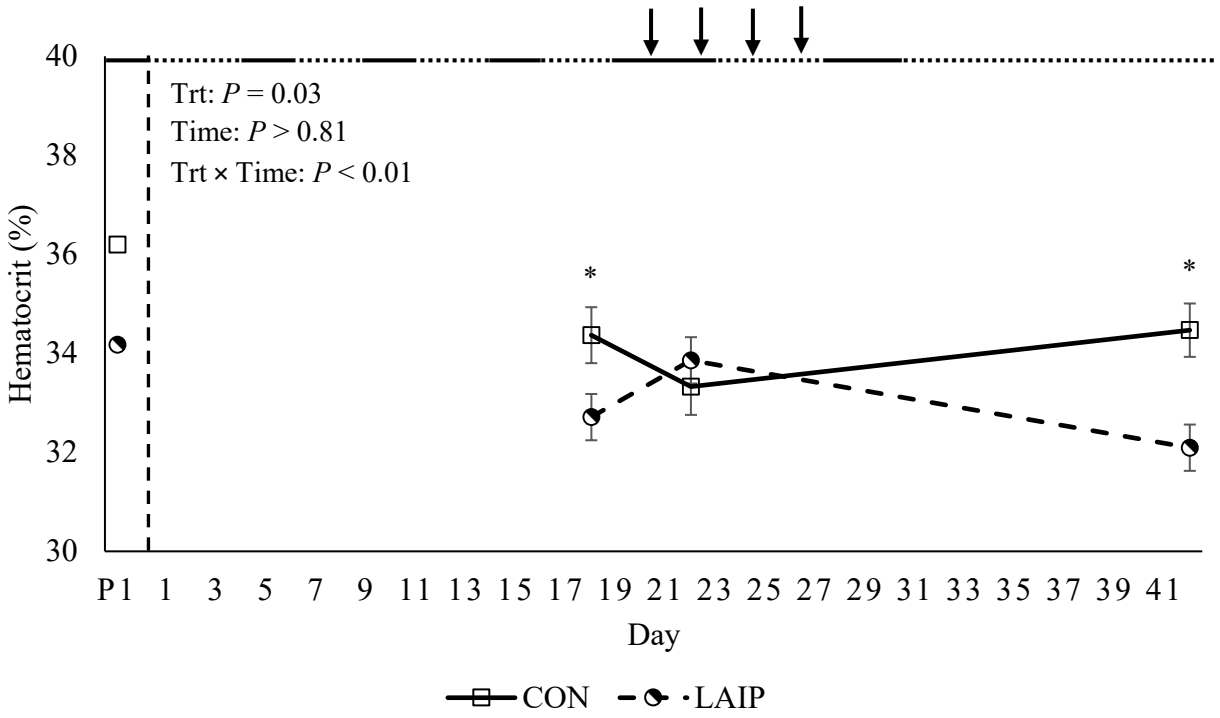

Figure 76. Effects of liver abscess induction protocol (LAIP) or control (CON) on hematocrit during P2. Top axis depicts solid line, dashed line, and arrows for LS, HS, and feed restriction, respectively, in LAIP. * denotes $P < 0.05$.

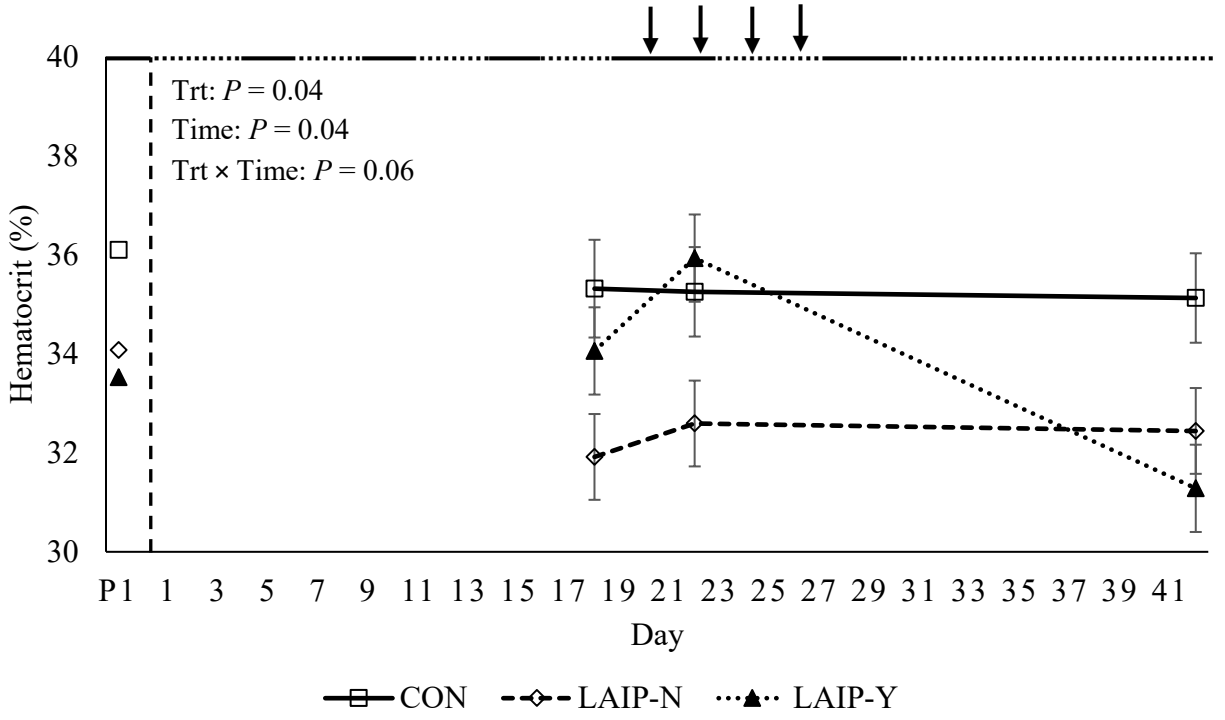

Figure 77. *Post hoc* comparison of the effects of successful liver abscess induction (LAIP-Y), failed liver abscess induction (LAIP-N), or control (CON) on hematocrit during P2. Top axis depicts solid line, dashed line, and arrows for LS, HS, and feed restriction, respectively, in LAIP.

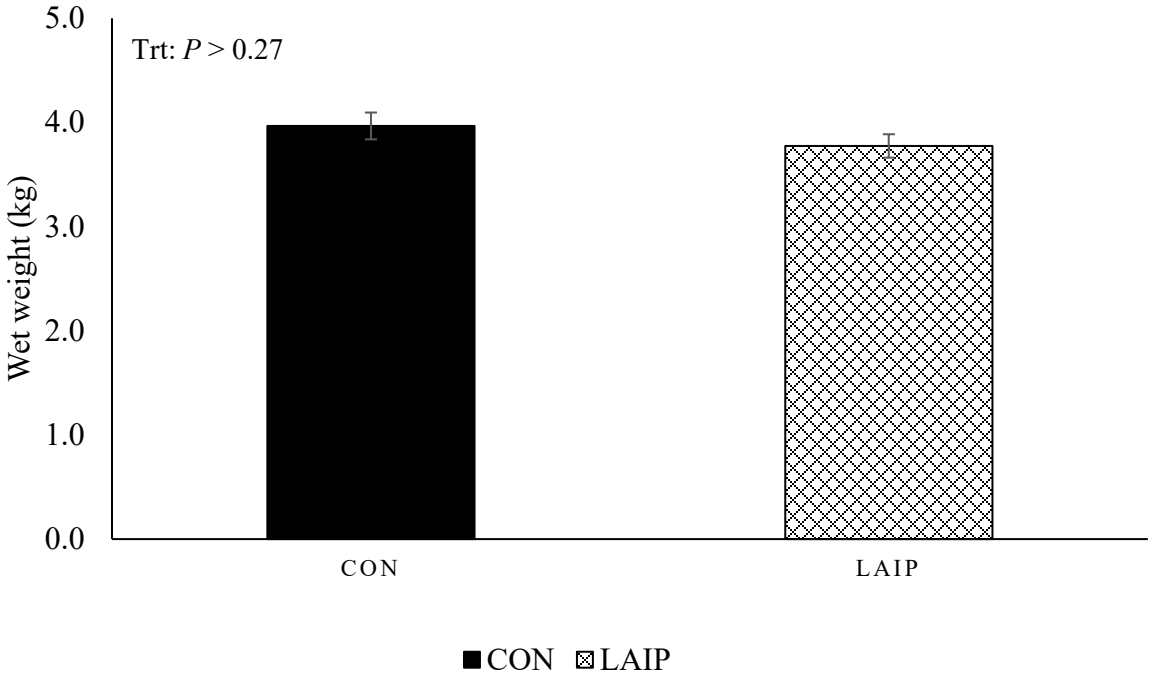

Figure 78. Effects of liver abscess induction protocol (LAIP) or control (CON) on wet liver weight at euthanasia.

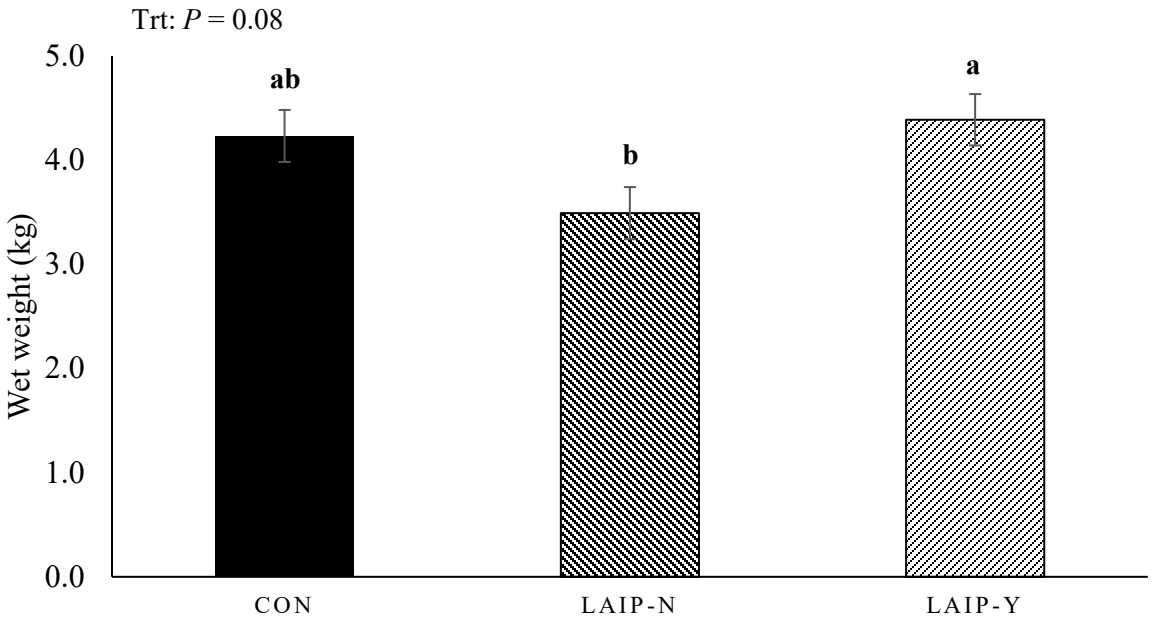

Figure 79. *Post hoc* comparison of the effects of successful liver abscess induction (LAIP-Y), failed liver abscess induction (LAIP-N), or control (CON) on wet liver weight at euthanasia. a, b, c denotes $P < 0.05$.

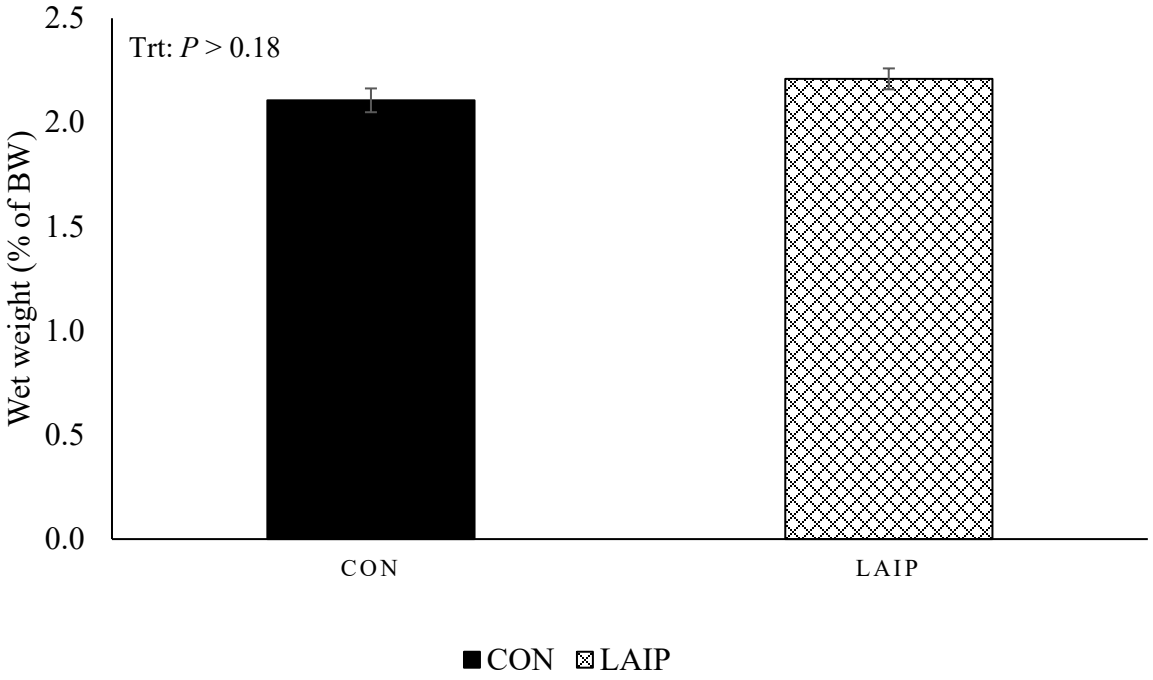

Figure 80. Effects of liver abscess induction protocol (LAIP) or control (CON) on wet liver weight as a percentage of body weight at euthanasia.

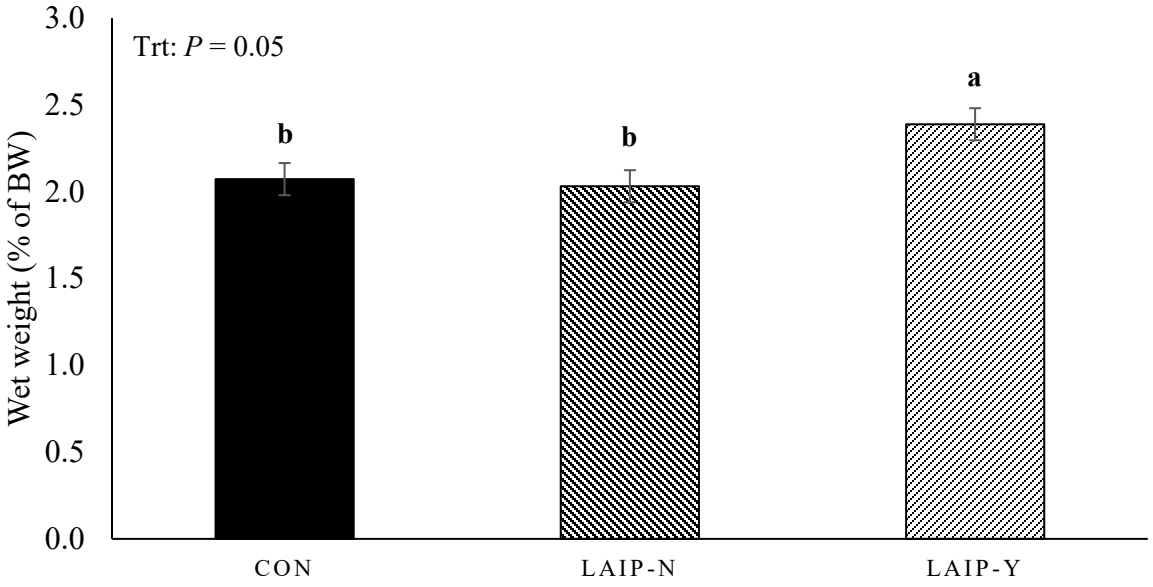

Figure 81. *Post hoc* comparison of the effects of successful liver abscess induction (LAIP-Y), failed liver abscess induction (LAIP-N), or control (CON) on wet liver weight as a percentage of body weight at euthanasia. a, b, c denotes $P < 0.05$.

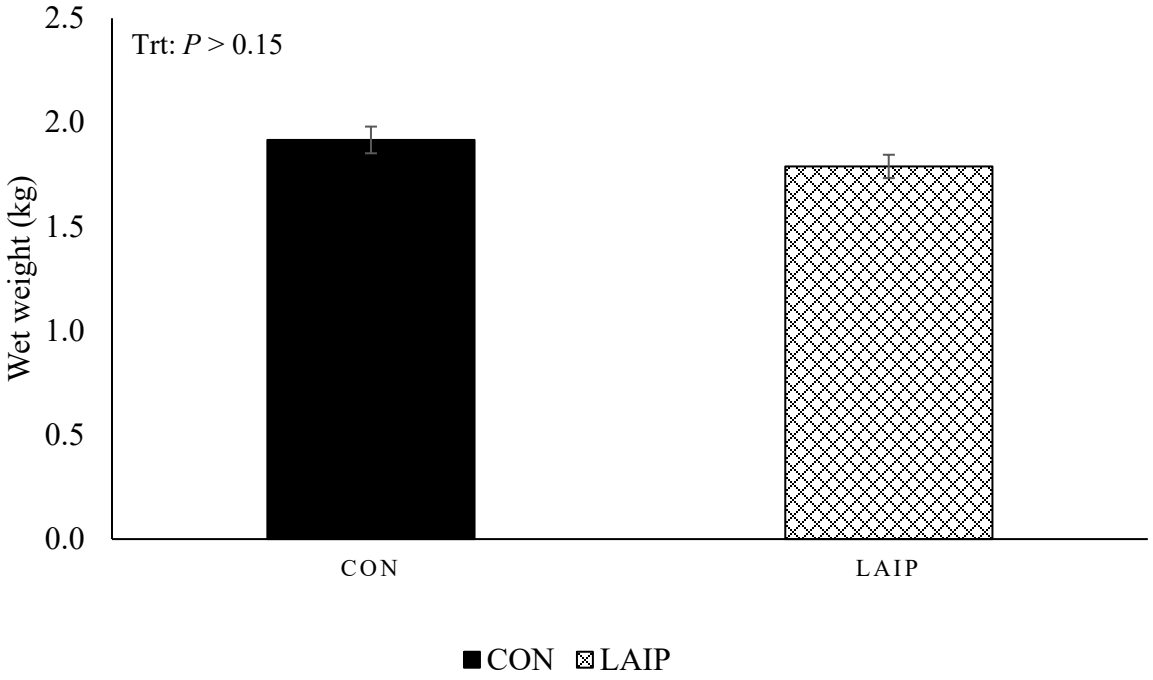

Figure 82. Effects of liver abscess induction protocol (LAIP) or control (CON) on wet lung weight at euthanasia.

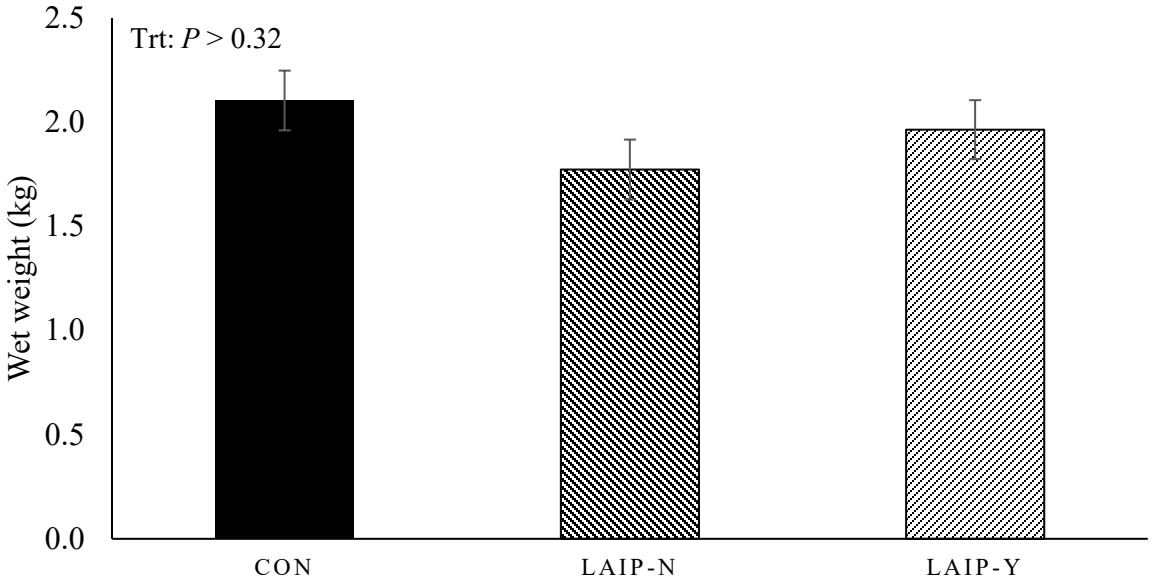

Figure 83. *Post hoc* comparison of the effects of successful liver abscess induction (LAIP-Y), failed liver abscess induction (LAIP-N), or control (CON) on wet lung weight at euthanasia.

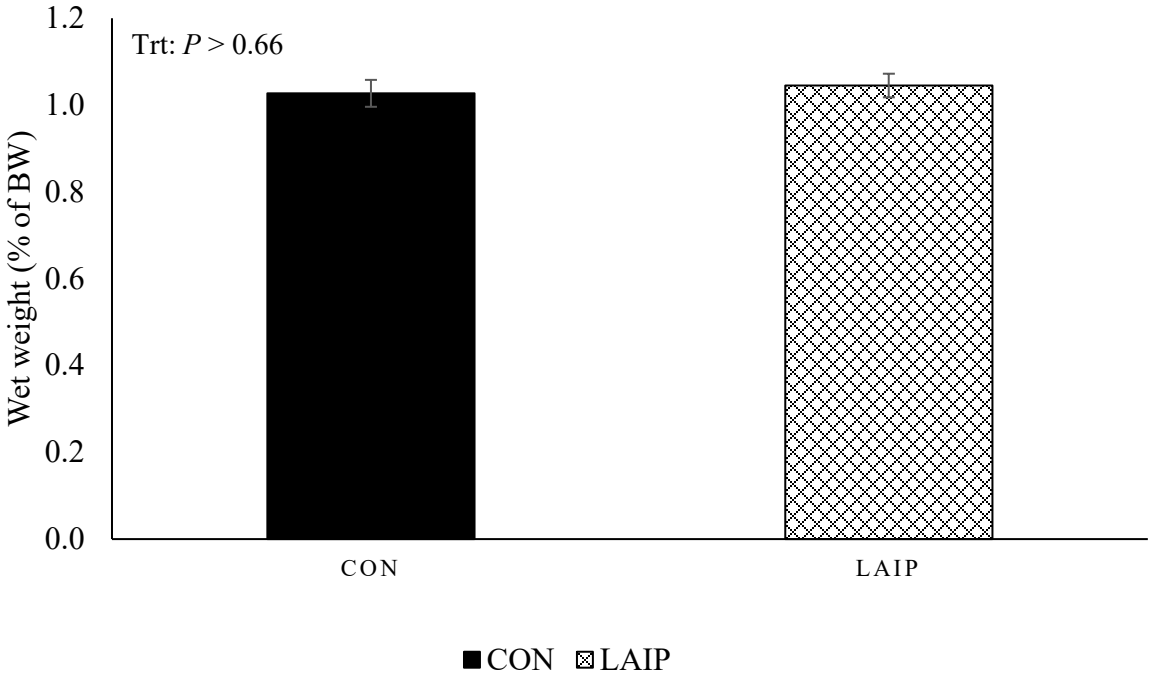

Figure 84. Effects of liver abscess induction protocol (LAIP) or control (CON) on wet lung weight as a percentage of body weight at euthanasia.

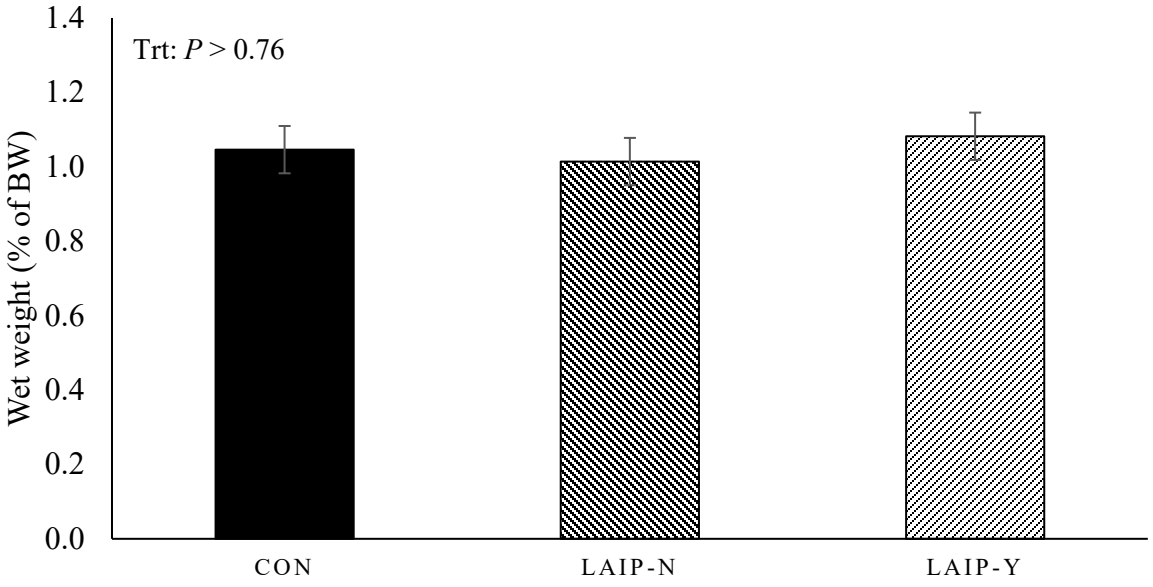

Figure 85. *Post hoc* comparison of the effects of successful liver abscess induction (LAIP-Y), failed liver abscess induction (LAIP-N), or control (CON) on wet lung weight as a percentage of body weight at euthanasia.

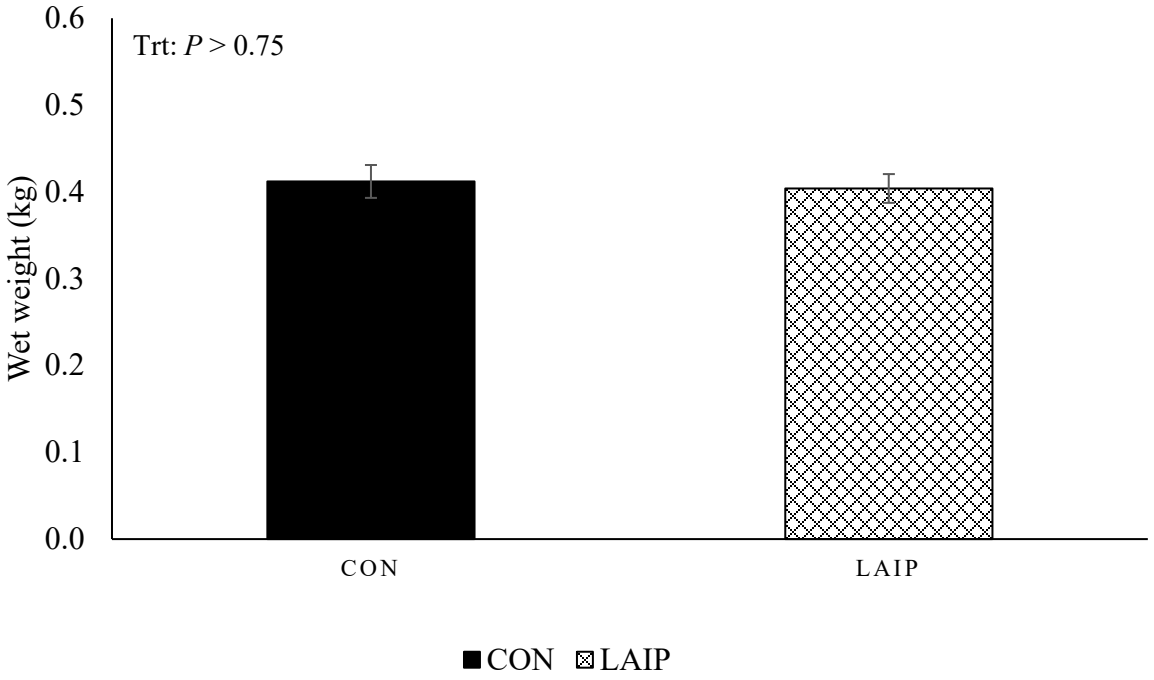

Figure 86. Effects of liver abscess induction protocol (LAIP) or control (CON) on wet spleen weight at euthanasia.

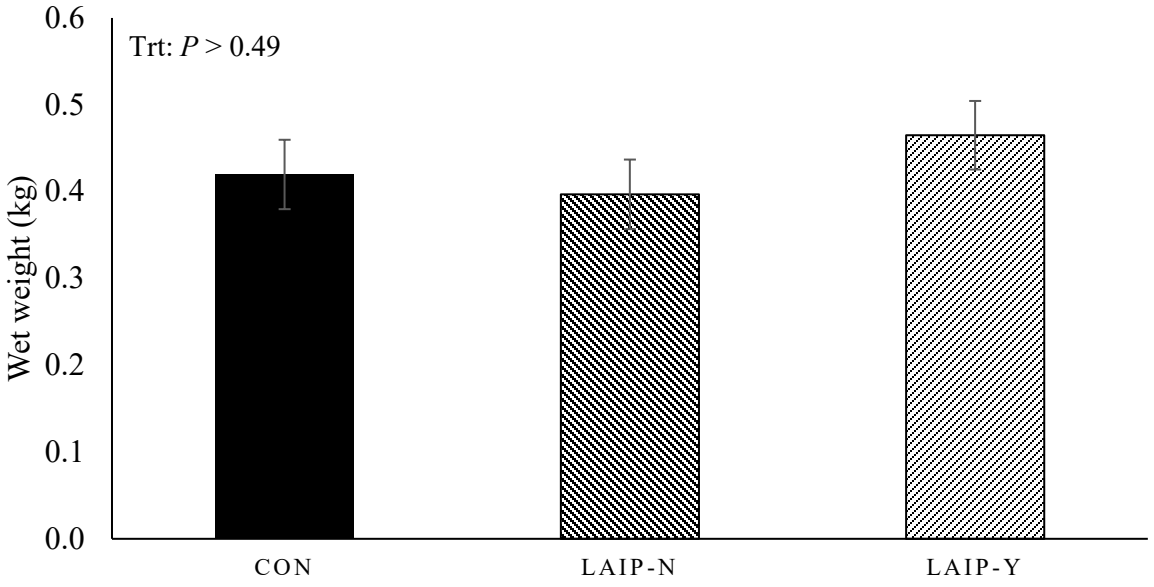

Figure 87. *Post hoc* comparison of the effects of successful liver abscess induction (LAIP-Y), failed liver abscess induction (LAIP-N), or control (CON) on wet spleen weight at euthanasia.

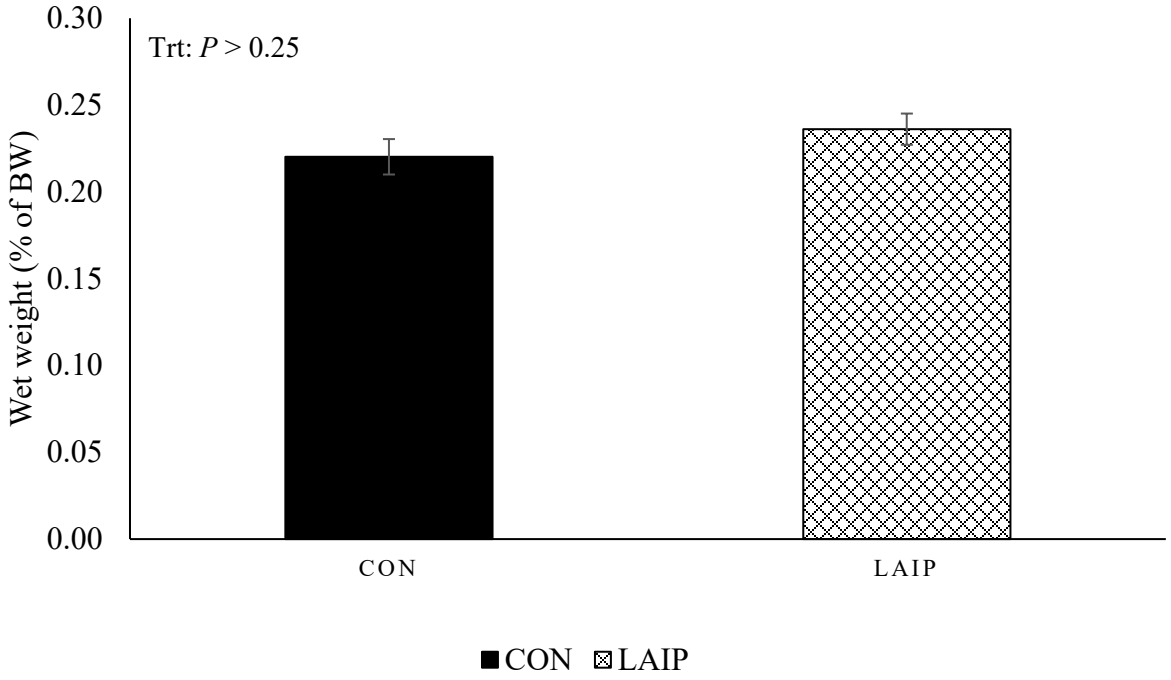

Figure 88. Effects of liver abscess induction protocol (LAIP) or control (CON) on wet spleen weight as a percentage of body weight at euthanasia.

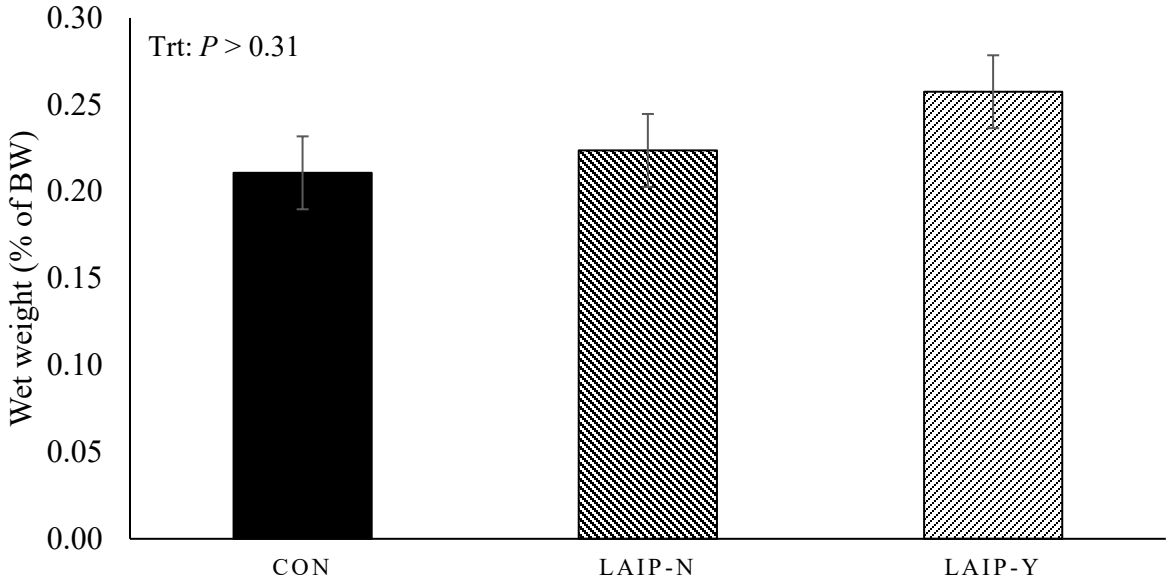

Figure 89. *Post hoc* comparison of the effects of successful liver abscess induction (LAIP-Y), failed liver abscess induction (LAIP-N), or control (CON) on wet spleen weight as a percentage of body weight at euthanasia.

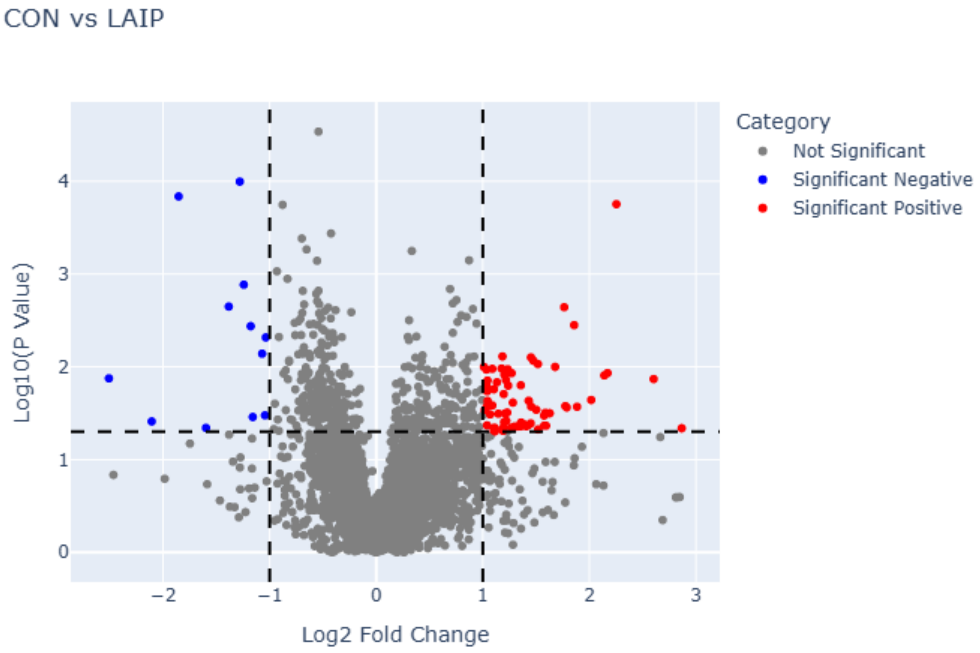

Figure 90. *Post hoc* volcano-plot analysis of liver abscess induction protocol (LAIP) or control (CON) on different expressed liver proteins. The horizontal dashed line indicates $P = 0.05$, with dots above the line indicating proteins that differ ($P < 0.05$) between treatments.

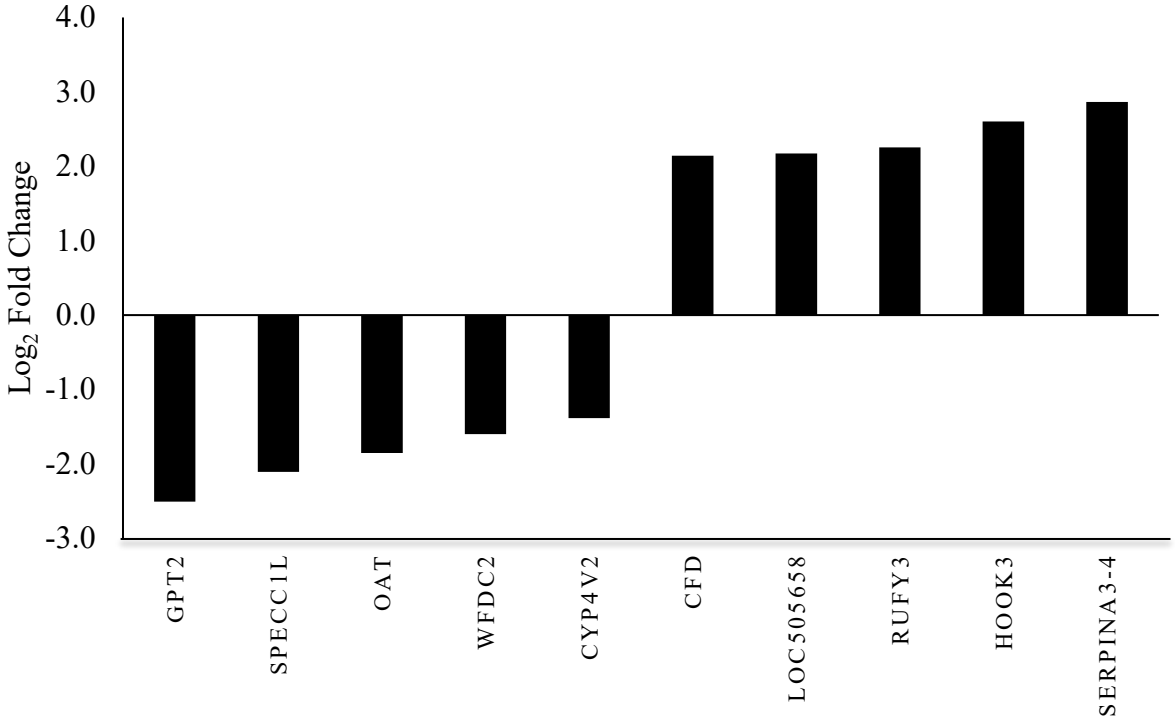

Figure 91. *Post hoc* analysis of liver abscess induction protocol (LAIP) or control (CON) on the ten most differentially enriched liver proteins.

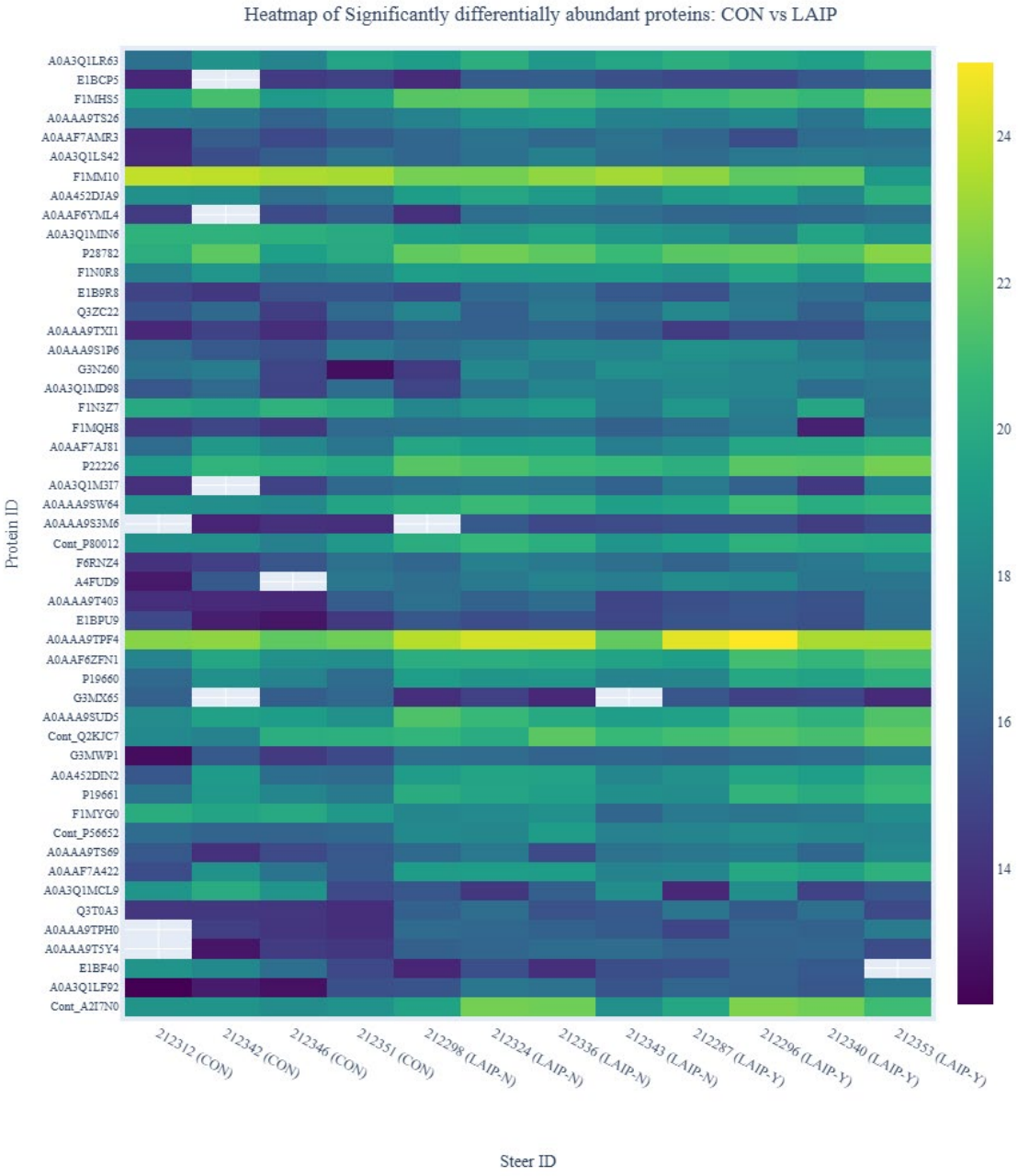

Figure 92. *Post hoc* heat map of liver abscess induction protocol (LAIP) or control (CON) on significantly different expressed liver proteins. Map capped at 50 differentially expressed proteins.

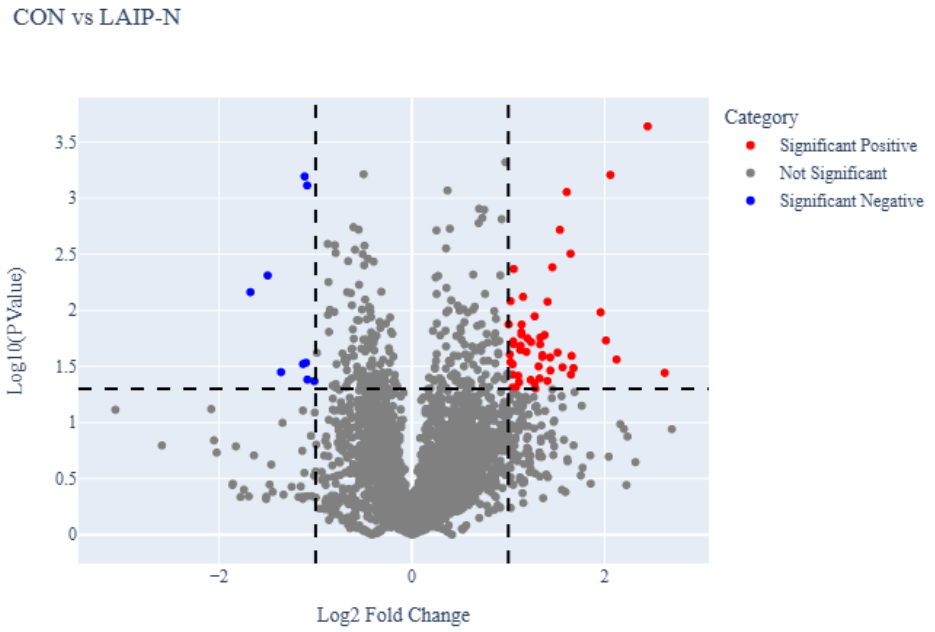

Figure 93. *Post hoc* volcano-plot analysis of failed liver induction (LAIP-N) or control (CON) on different expressed liver proteins. The horizontal dashed line indicates P = 0.05, with dots above the line indicating proteins that differ (P < 0.05) between treatments.

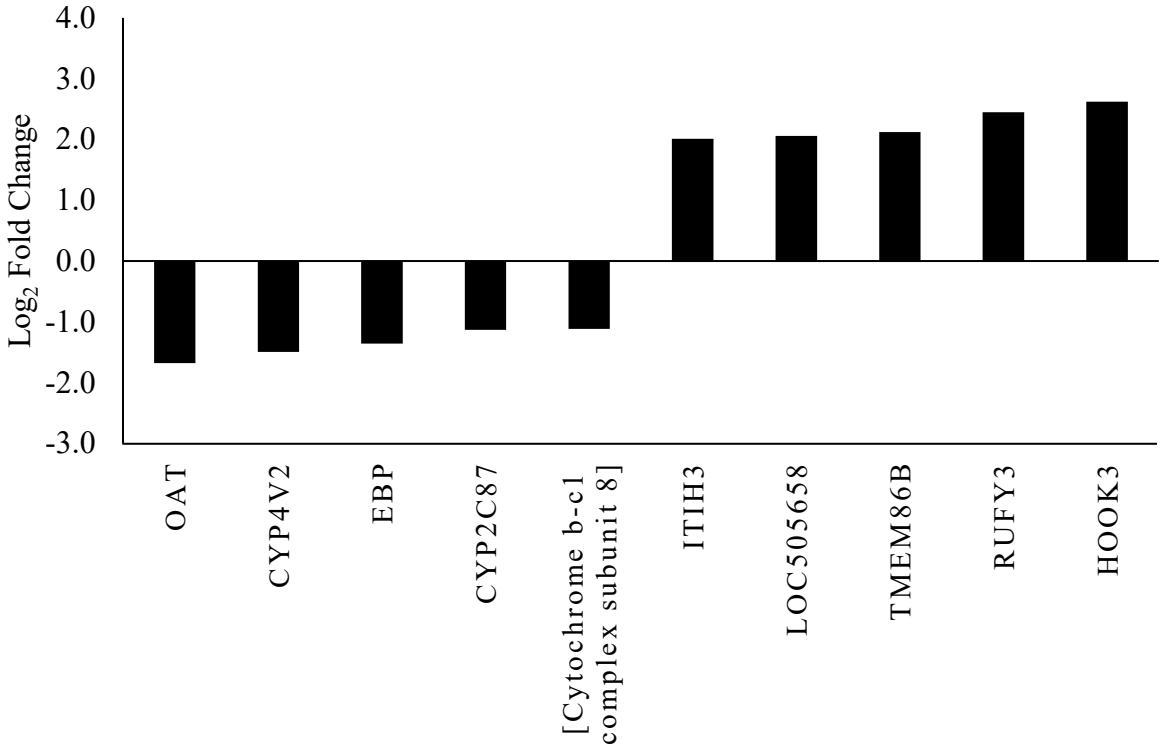

Figure 94. *Post hoc* analysis of failed liver abscess induction (LAIP-N) or control (CON) on the ten most differentially enriched liver proteins. Brackets delineate proteins with uncharacterized gene nomenclature.

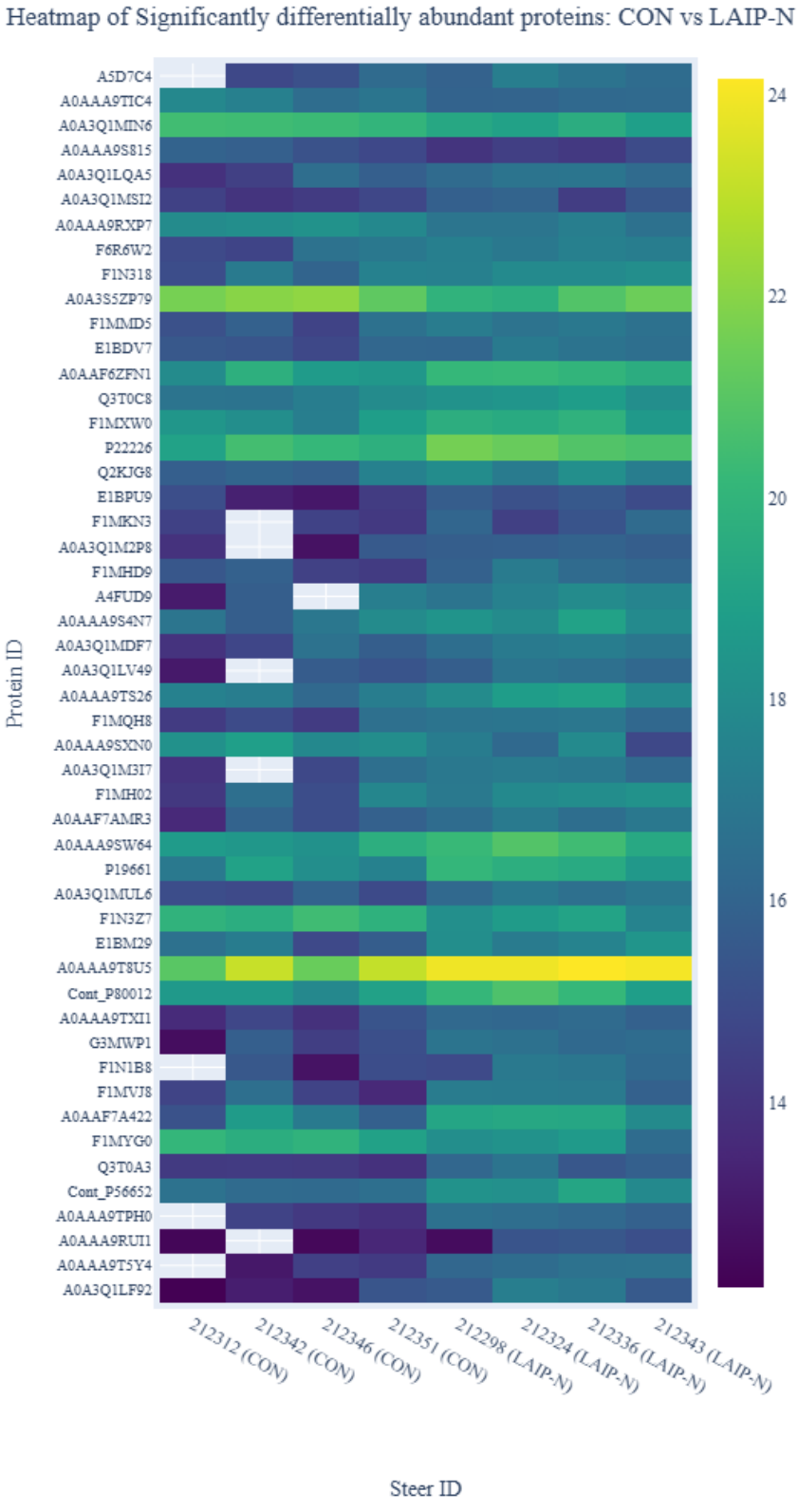

Figure 95. *Post hoc* heat map of failed liver abscess induction (LAIP-N) or control (CON) on significantly different expressed liver proteins. Map capped at 50 differentially expressed proteins.

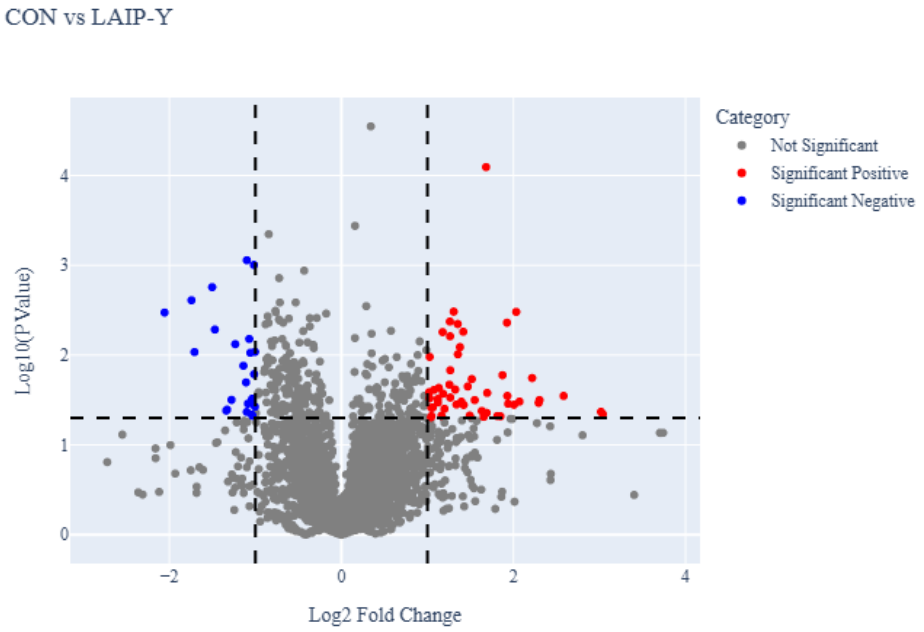

Figure 96. *Post hoc* volcano-plot analysis of successful liver abscess induction (LAIP-Y) or control (CON) on different expressed liver proteins. The horizontal dashed line indicates $P = 0.05$, with dots above the line indicating proteins that differ ($P < 0.05$) between treatments.

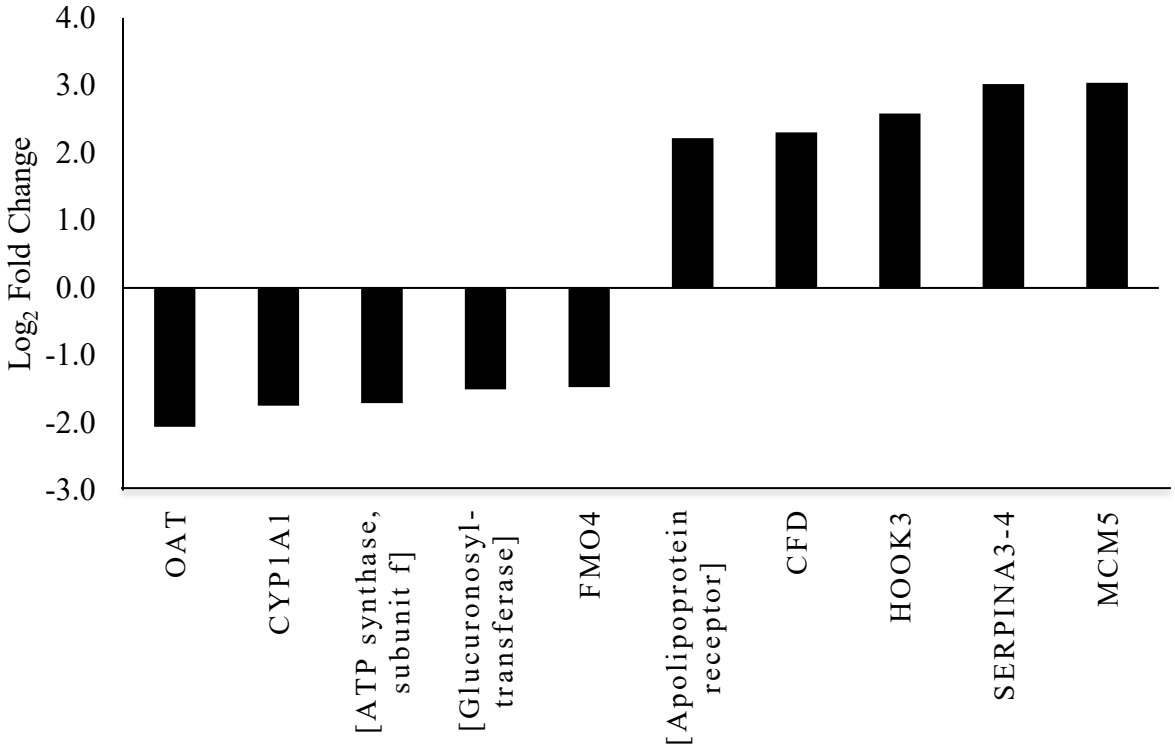

Figure 97. *Post hoc* analysis of successful liver abscess induction (LAIP-Y) or control (CON) on the ten most differentially enriched liver proteins. Brackets delineate proteins with uncharacterized gene nomenclature and uncharacterized proteins omitted from analysis.

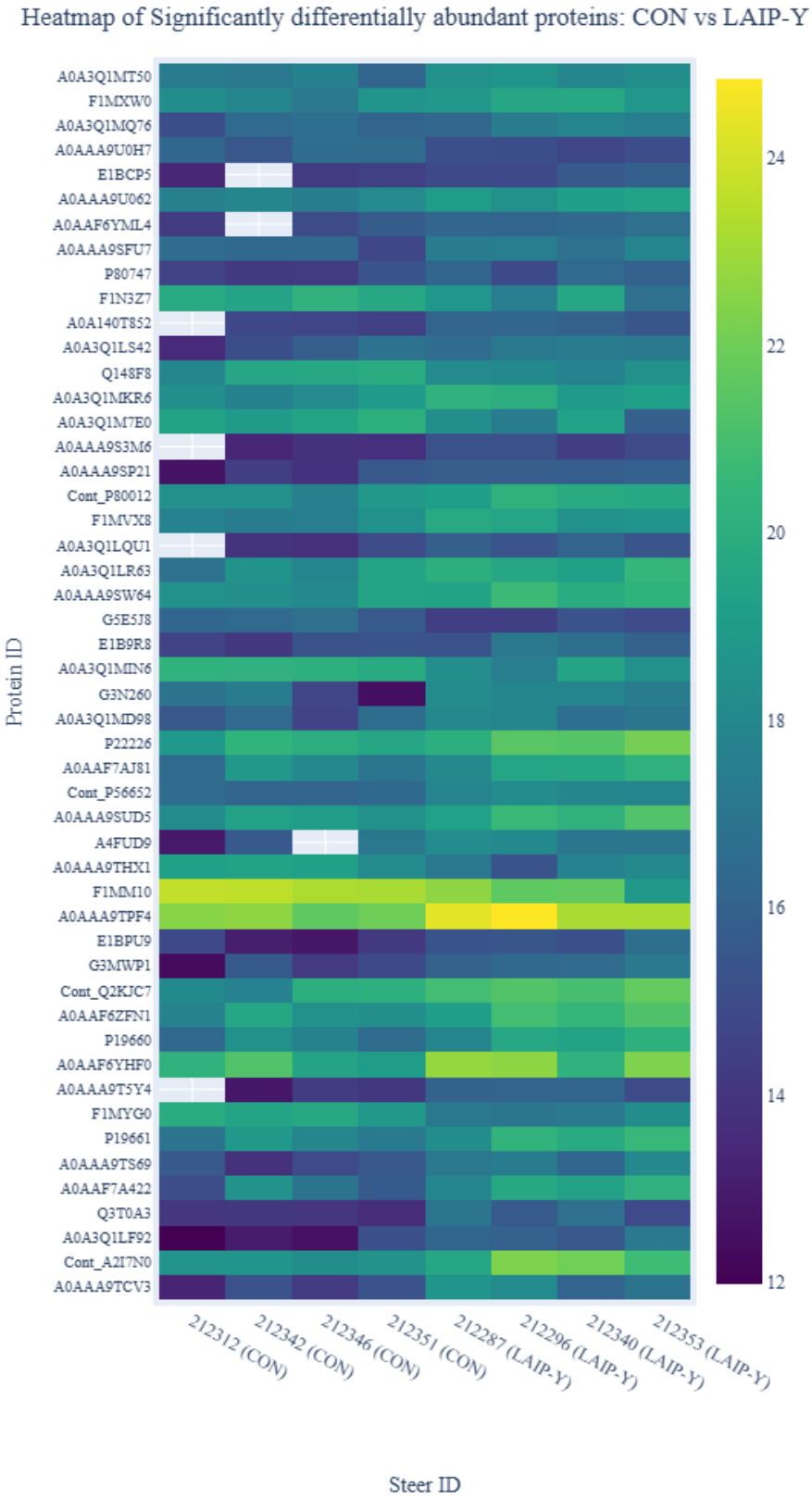

Figure 98. *Post hoc* heat map of successful liver abscess induction (LAIP-Y) or control (CON) on significantly different expressed liver proteins. Map capped at 50 differentially expressed proteins.

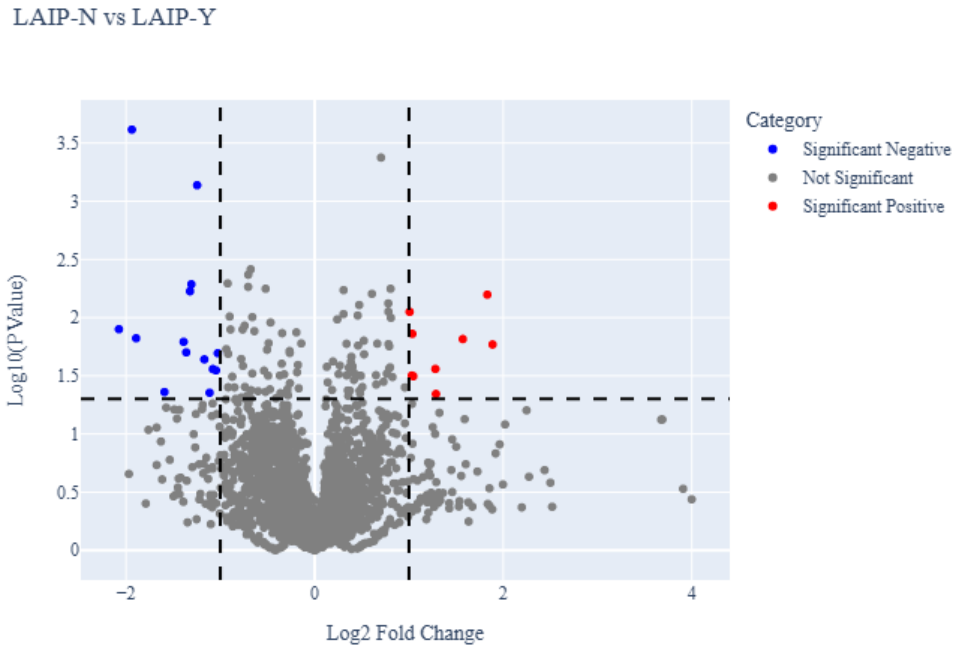

Figure 99. *Post hoc* volcano-plot analysis of failed liver abscess induction (LAIP-N) or successful liver abscess (LAIP-Y) on different expressed liver proteins. The horizontal dashed line indicates $P = 0.05$, with dots above the line indicating proteins that differ ($P < 0.05$) between treatments.

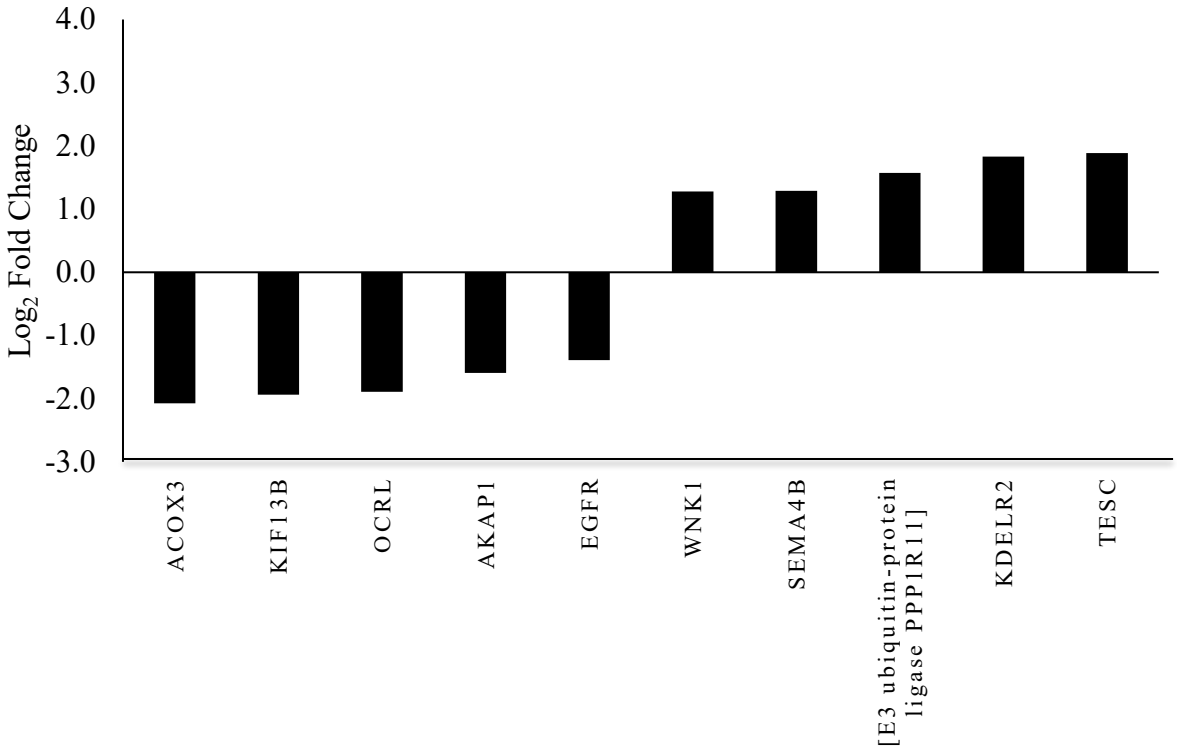

Figure 100. *Post hoc* analysis of failed liver abscess induction (LAIP-N) or successful liver abscess induction (LAIP-Y) on the ten most differentially enriched liver proteins. Brackets delineate proteins with uncharacterized gene nomenclature.

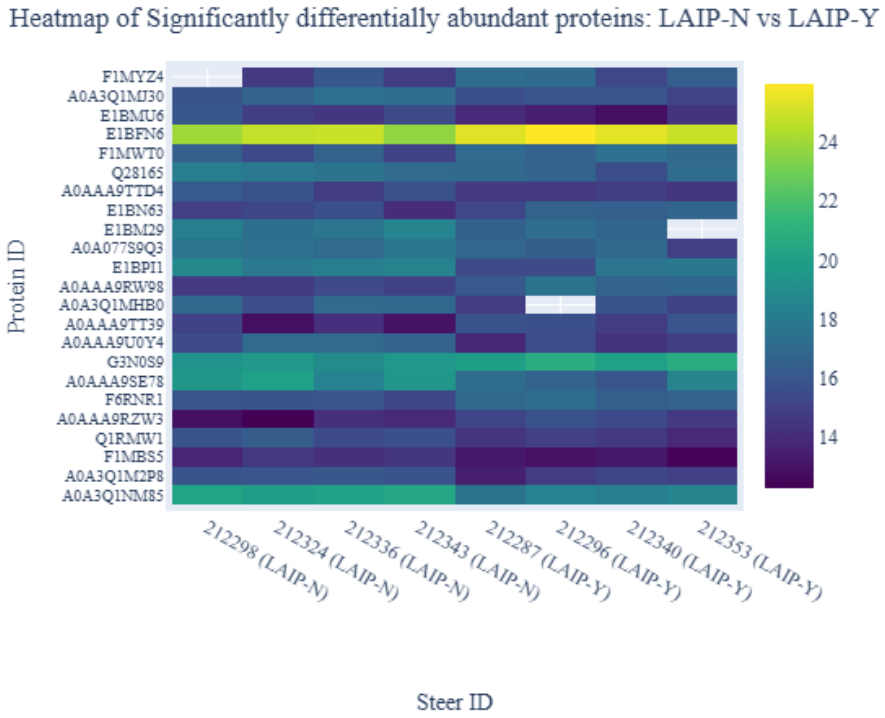

Figure 101. *Post hoc* heat map of failed liver abscess induction (LAIP-N) or successful liver abscess induction (LAIP-Y) on significantly different expressed liver proteins.

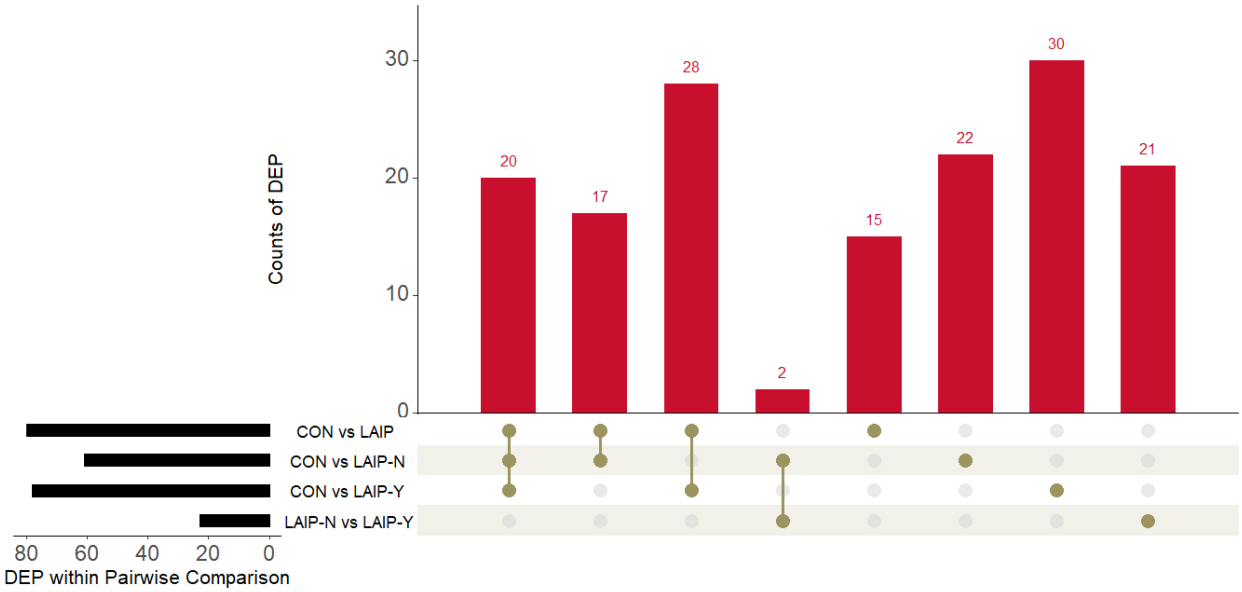

Figure 102. Upset plot of differentially expressed proteins (DEP) between control (CON), liver abscess induction protocol (LAIP), failed liver abscess induction (LAIP-N), and successful liver abscess induction (LAIP-Y). Horizontal bar chart represents count of DEPs within each comparison. Vertical bars represent DEPs shared between multiple comparisons.

Liver Abscess Induction Model
Study Number: GJC-LHB-3

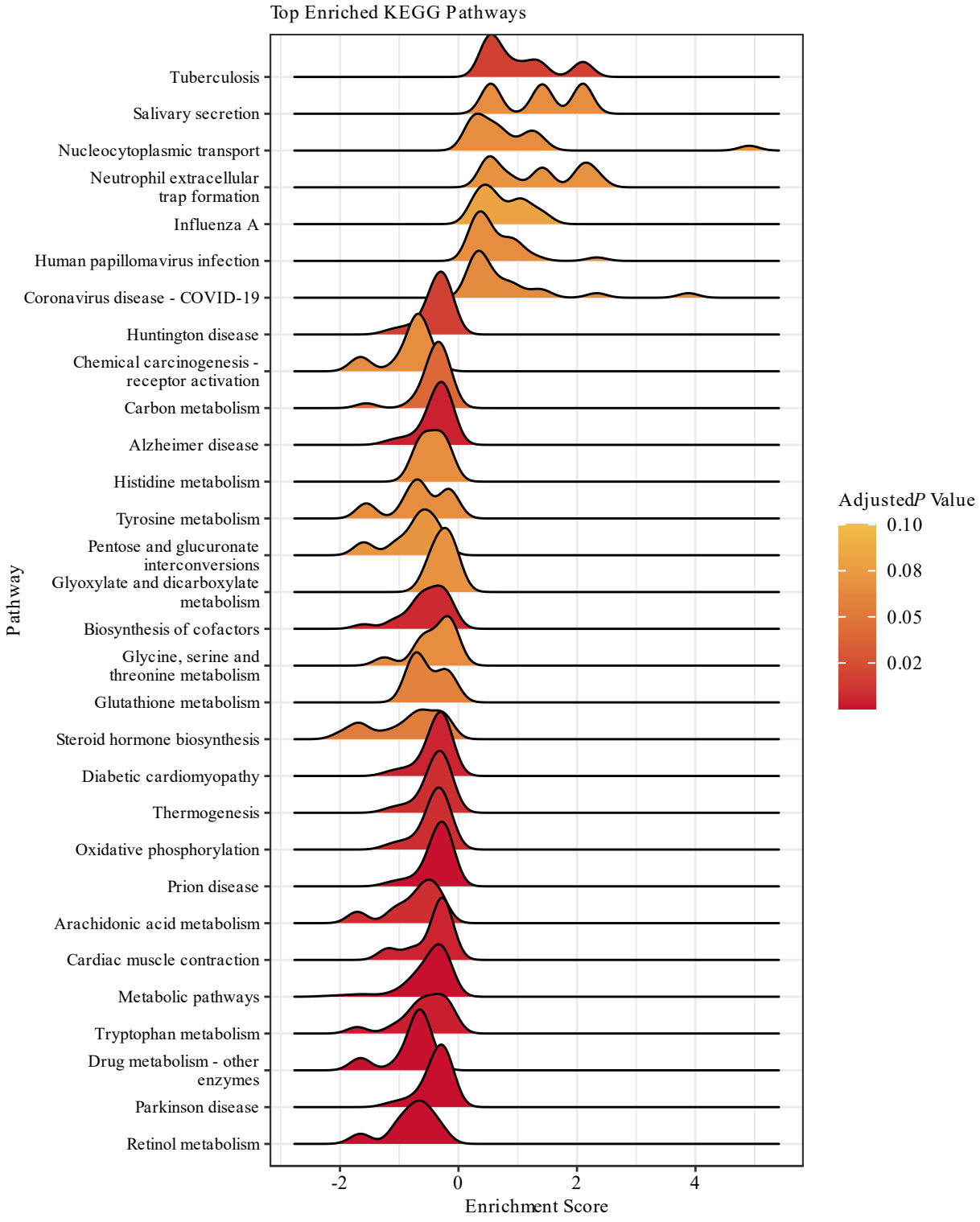

Figure 103. *Post hoc* ridge plot of enriched KEGG pathways in failed liver abscess induction (LAIP-N) relative to control (CON). Results were truncated at 30 most enriched pathways and results limited to ≥4 proteins in core enrichment.

Liver Abscess Induction Model
Study Number: GJC-LHB-3

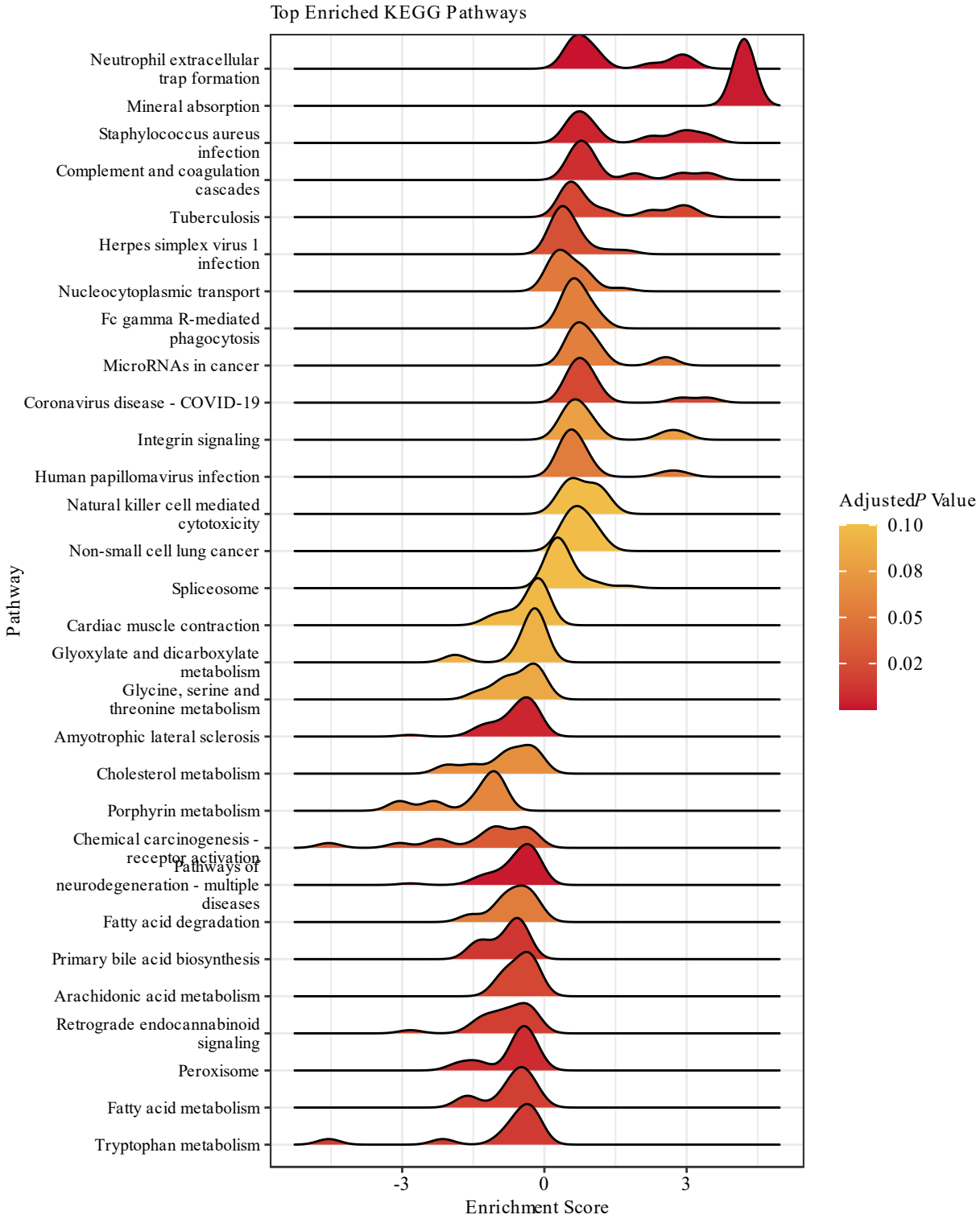

Figure 104. *Post hoc* ridge plot of enriched KEGG pathways in successful liver abscess induction (LAIP-Y) relative to control (CON). Results were truncated at 30 most enriched pathways and results limited to ≥4 proteins in core enrichment.

Liver Abscess Induction Model
Study Number: GJC-LHB-3

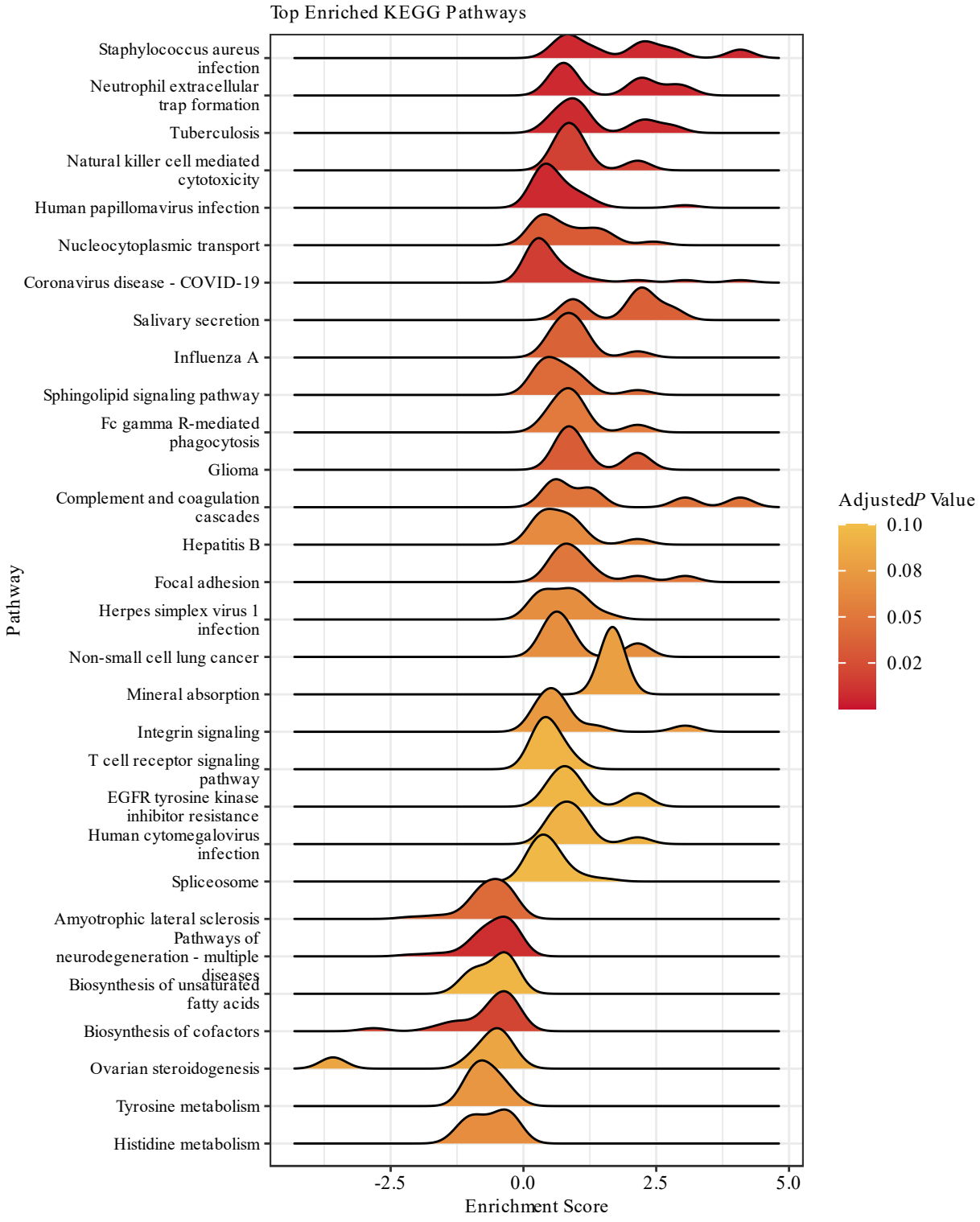

Figure 105. *Post hoc* ridge plot of enriched KEGG pathways in liver abscess induction protocol (LAIP) relative to control (CON). Results were truncated at 30 most enriched pathways and results limited to ≥4 proteins in core enrichment.

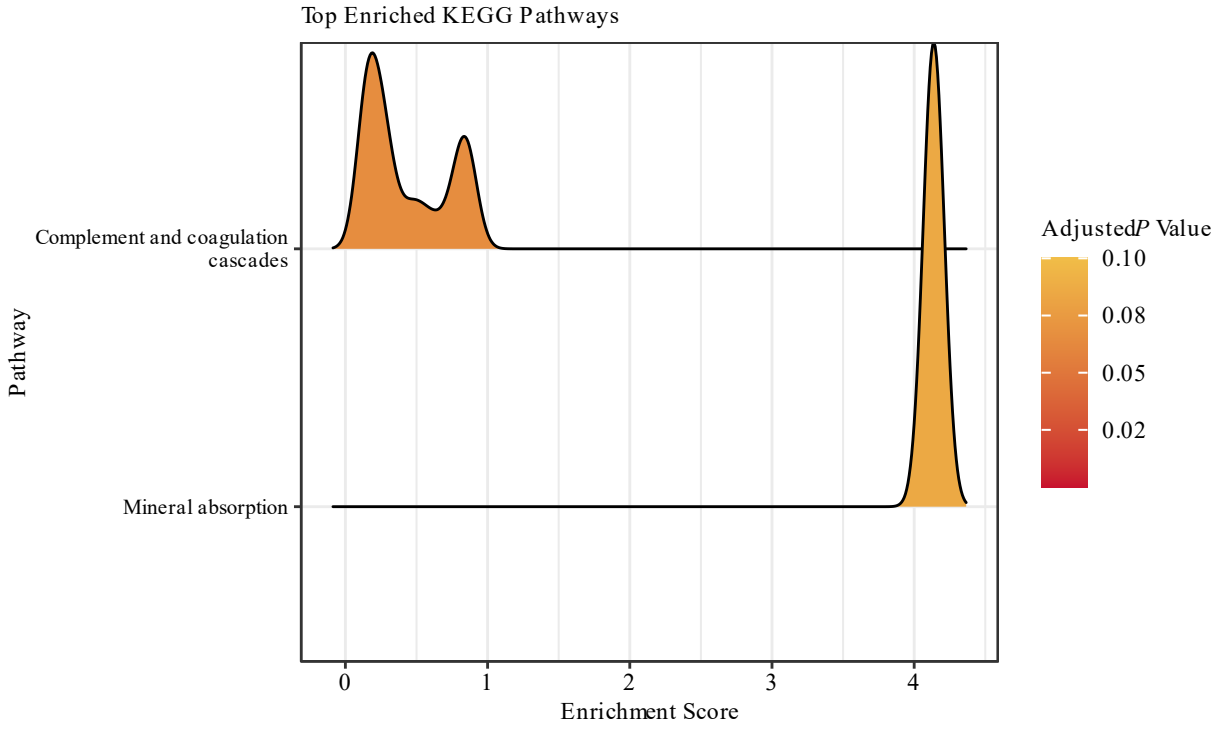

Figure 106. *Post hoc* ridge plot of enriched KEGG pathways in successful liver abscess induction (LAIP-Y) relative to failed liver abscess induction (LAIP-N). Results limited to ≥4 proteins in core enrichment.

Figure 107. *Post hoc* analysis of proteins involved in mineral absorption in successful liver abscess (LAIP-Y) relative to control (CON).

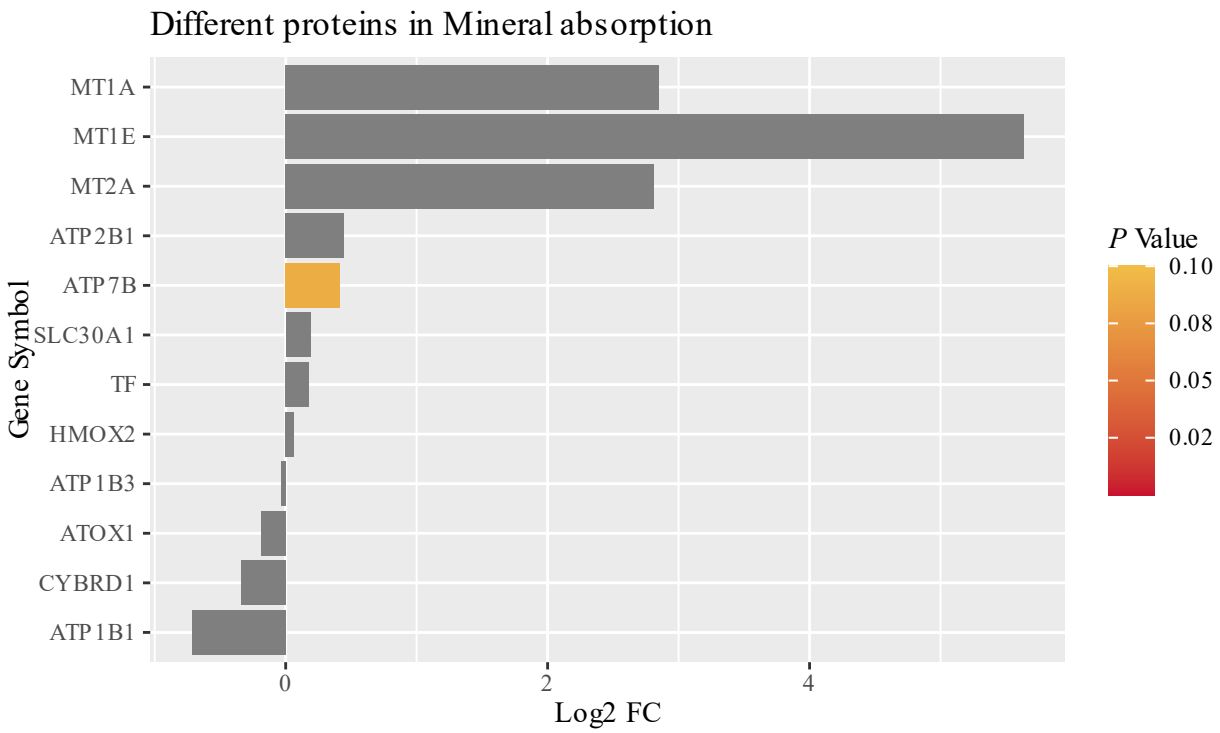

Figure 108. *Post hoc* analysis of proteins involved in mineral absorption in liver abscess induction protocol (LAIP) relative to control (CON).

Figure 109. *Post hoc* analysis of proteins involved in mineral absorption in successful liver abscess (LAIP-Y) relative to failed liver abscess (LAIP-N).

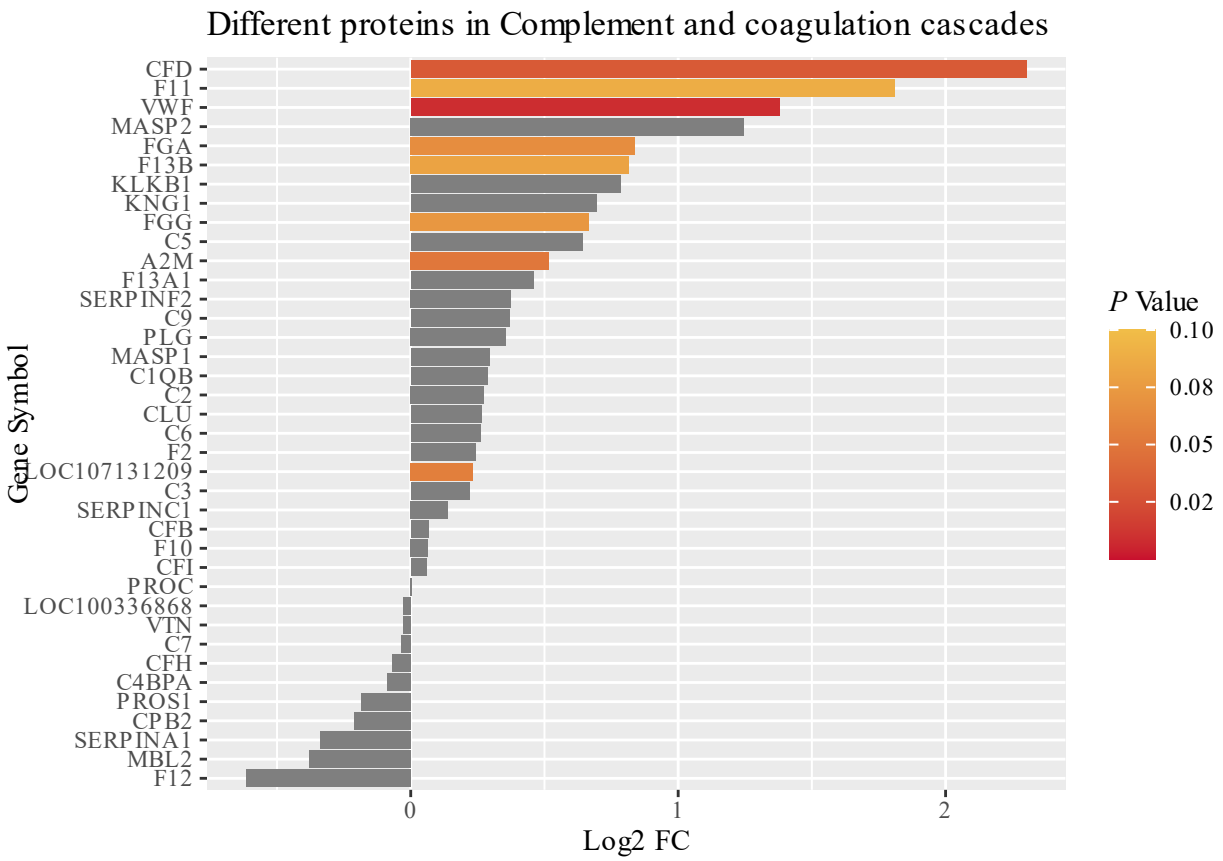

Figure 110. *Post hoc* analysis of proteins involved in complement and coagulation cascades in successful liver abscess (LAIP-Y) relative to control (CON).

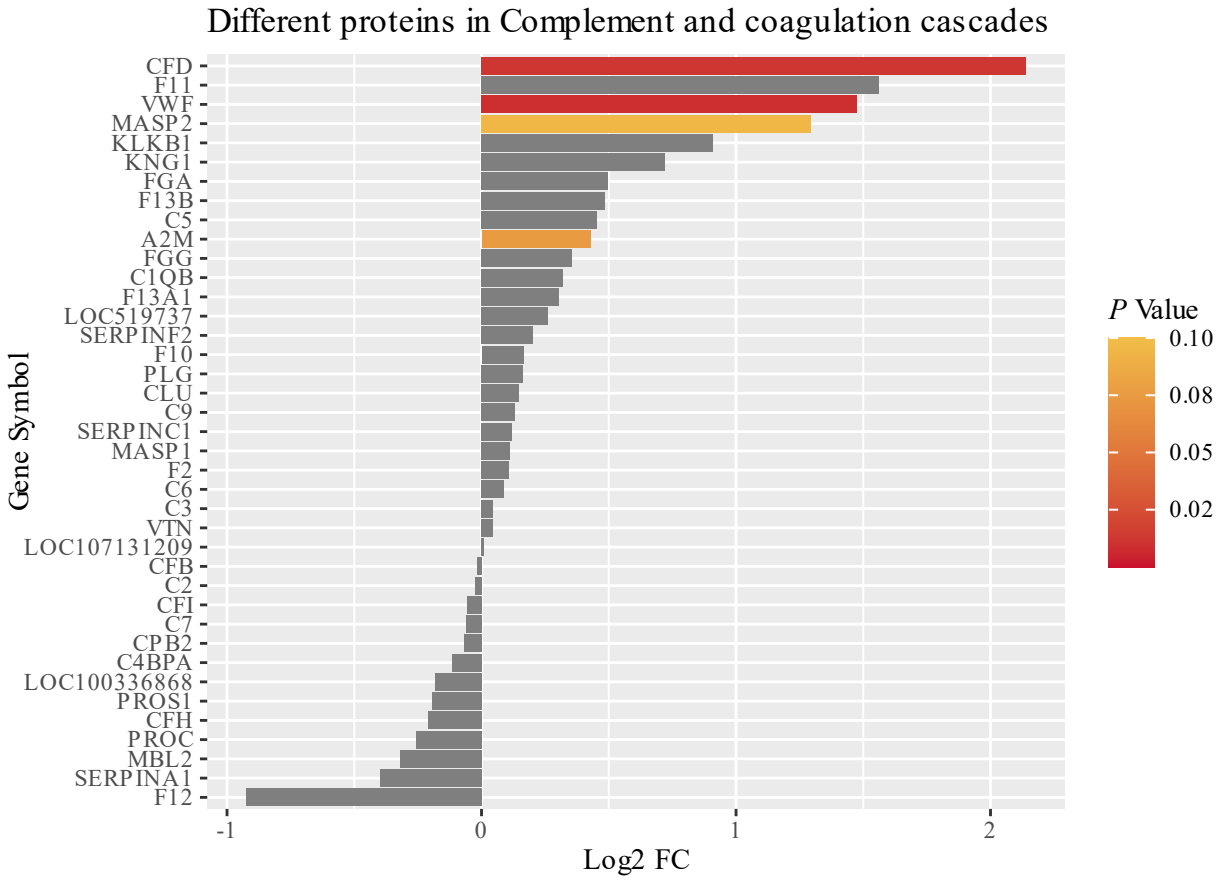

Figure 111. *Post hoc* analysis of proteins involved in complement and coagulation cascades in liver abscess induction protocol (LAIP) relative to control (CON).

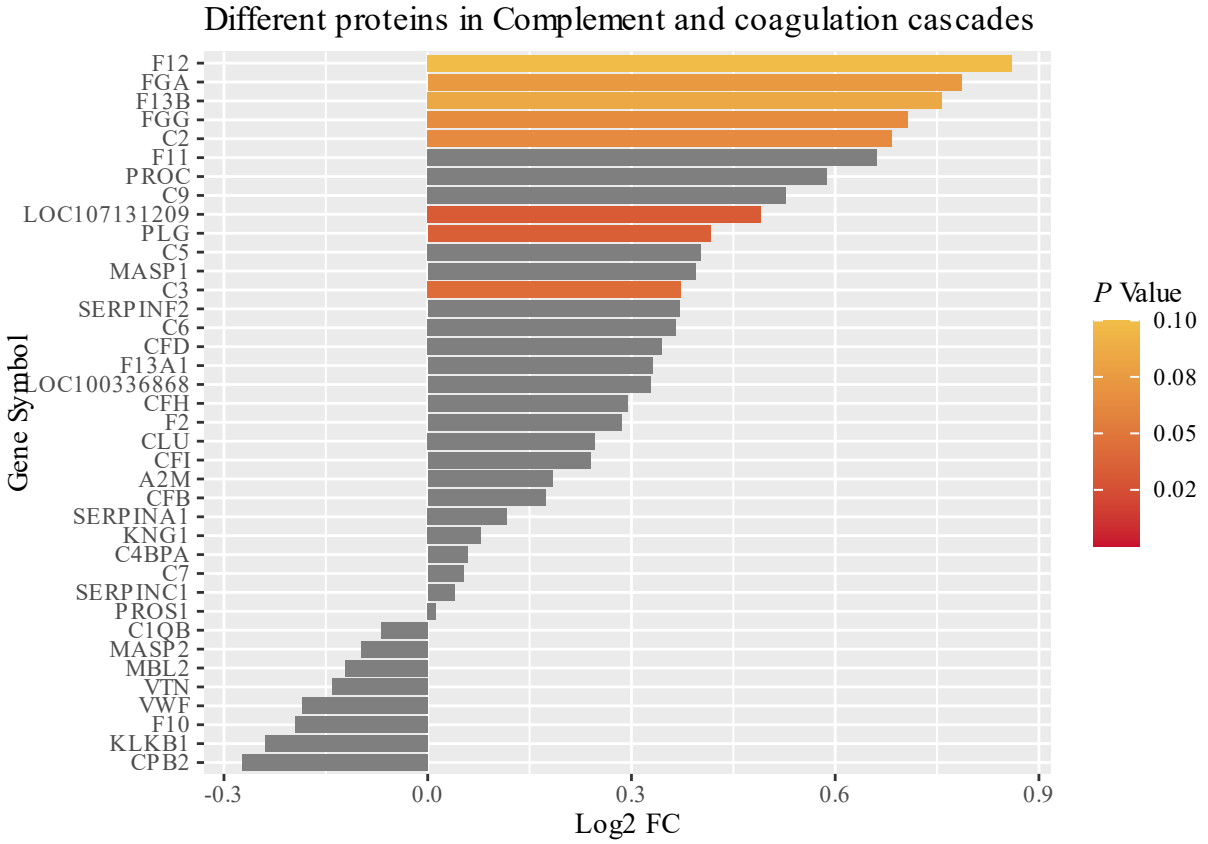

Figure 112. *Post hoc* analysis of proteins involved in complement and coagulation cascades in successful liver abscess (LAIP-Y) relative to failed liver abscess (LAIP-N).

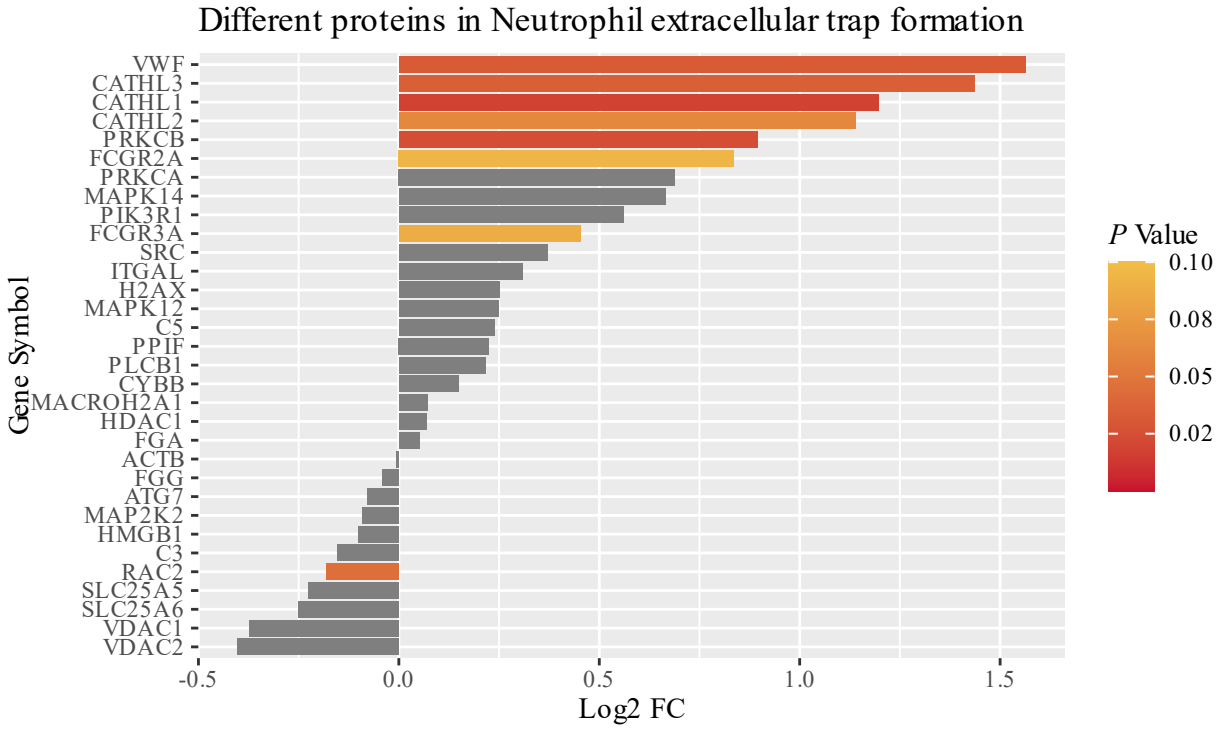

Figure 113. *Post hoc* analysis of proteins involved in neutrophil extracellular trap formation in failed liver abscess (LAIP-N) relative to control (CON).

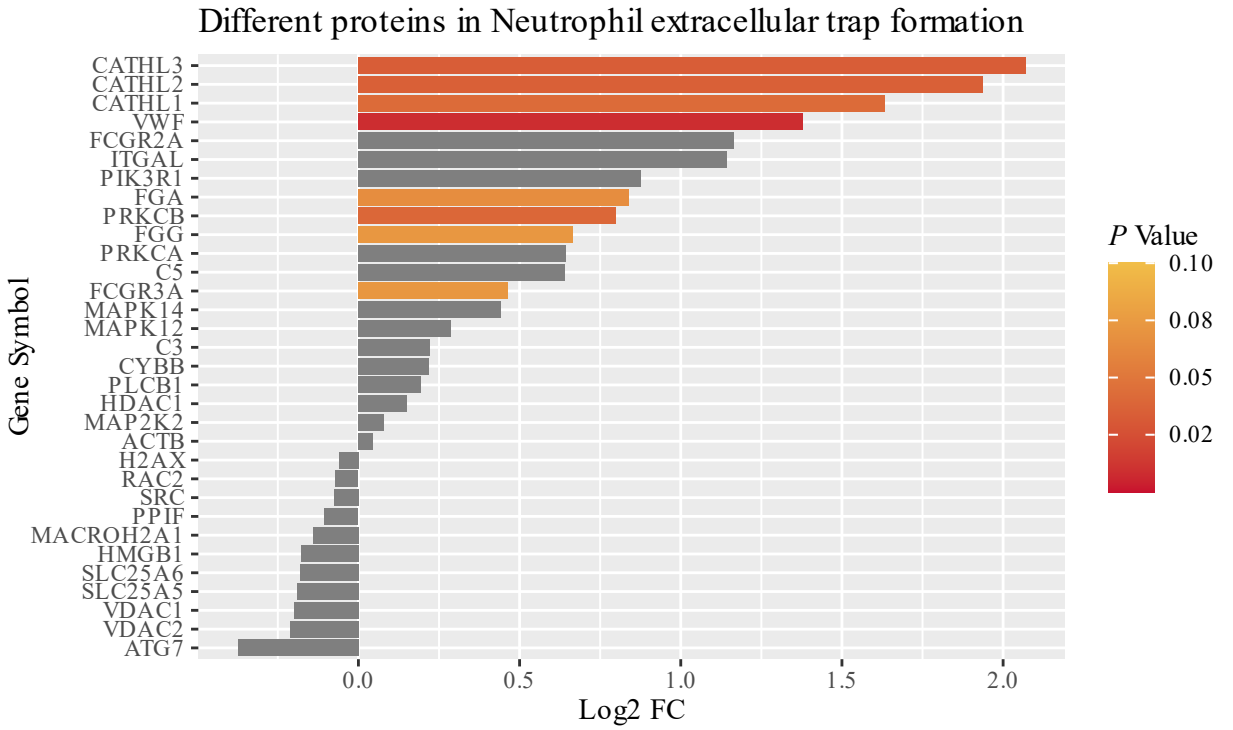

Figure 114. *Post hoc* analysis of proteins involved in neutrophil extracellular trap formation in successful liver abscess induction (LAIP-Y) relative to control (CON).

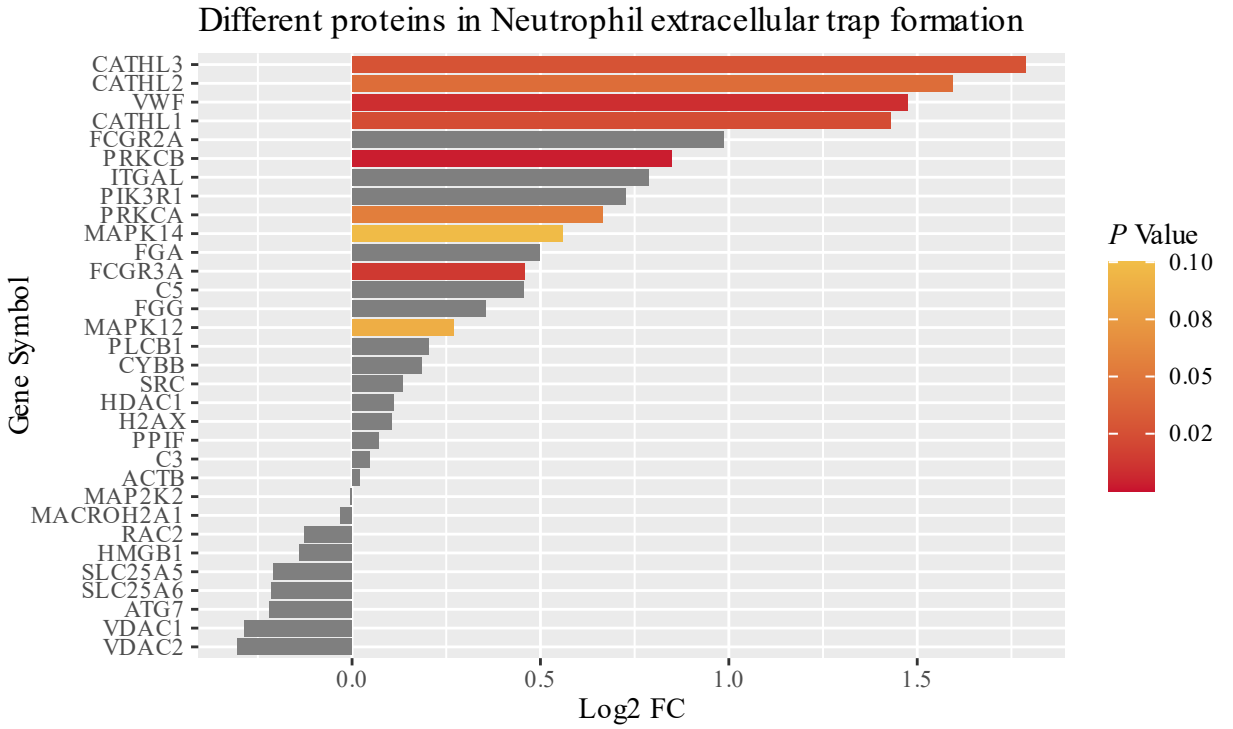

Figure 115. *Post hoc* analysis of proteins involved in neutrophil extracellular trap formation in liver abscess induction protocol (LAIP) relative to control (CON).

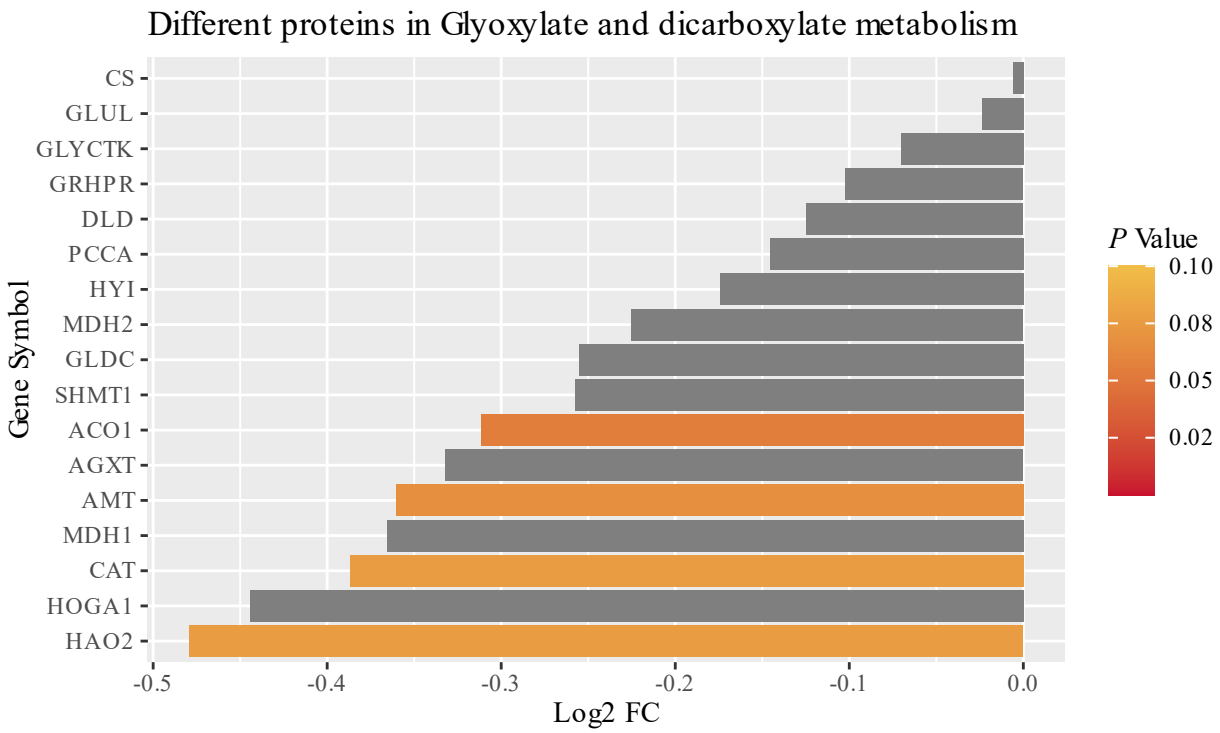

Figure 116. *Post hoc* analysis of proteins involved in glyoxylate and dicarboxylate metabolism in failed liver abscess (LAIP-N) relative to control (CON).

117

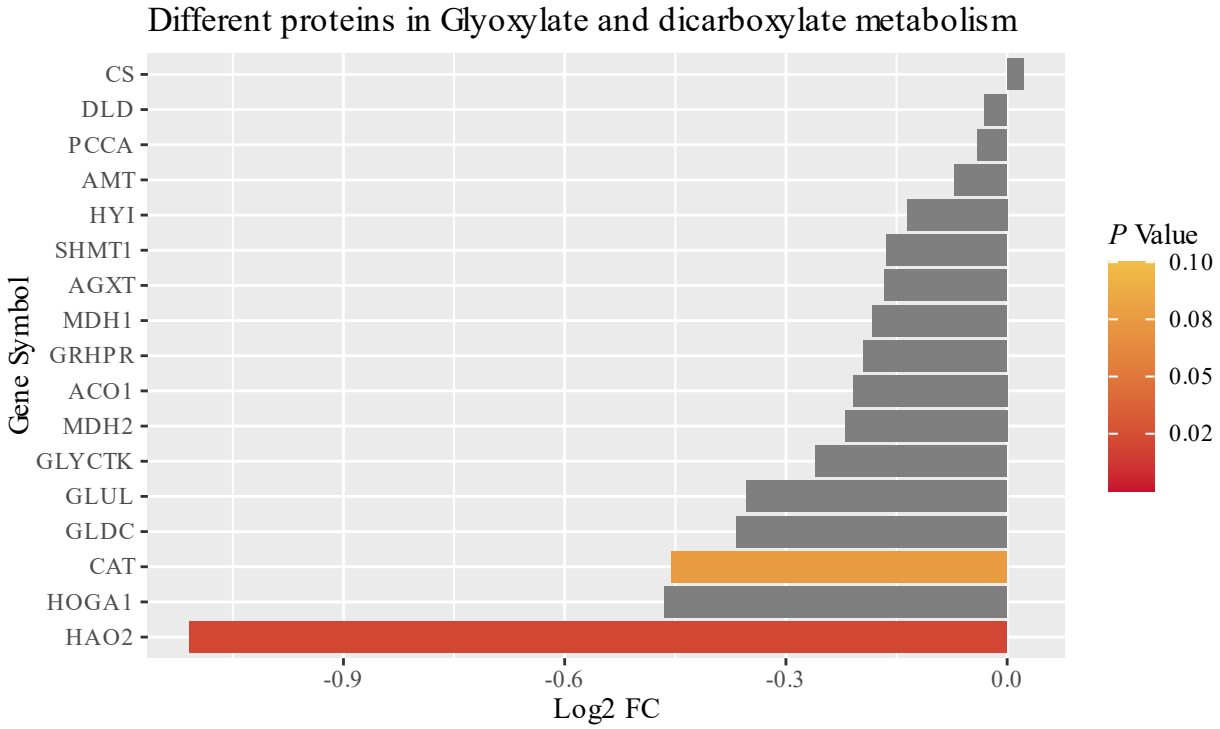

Figure 117. *Post hoc* analysis of proteins involved in glyoxylate and dicarboxylate metabolism in successful liver abscess induction (LAIP-Y) relative to control (CON).

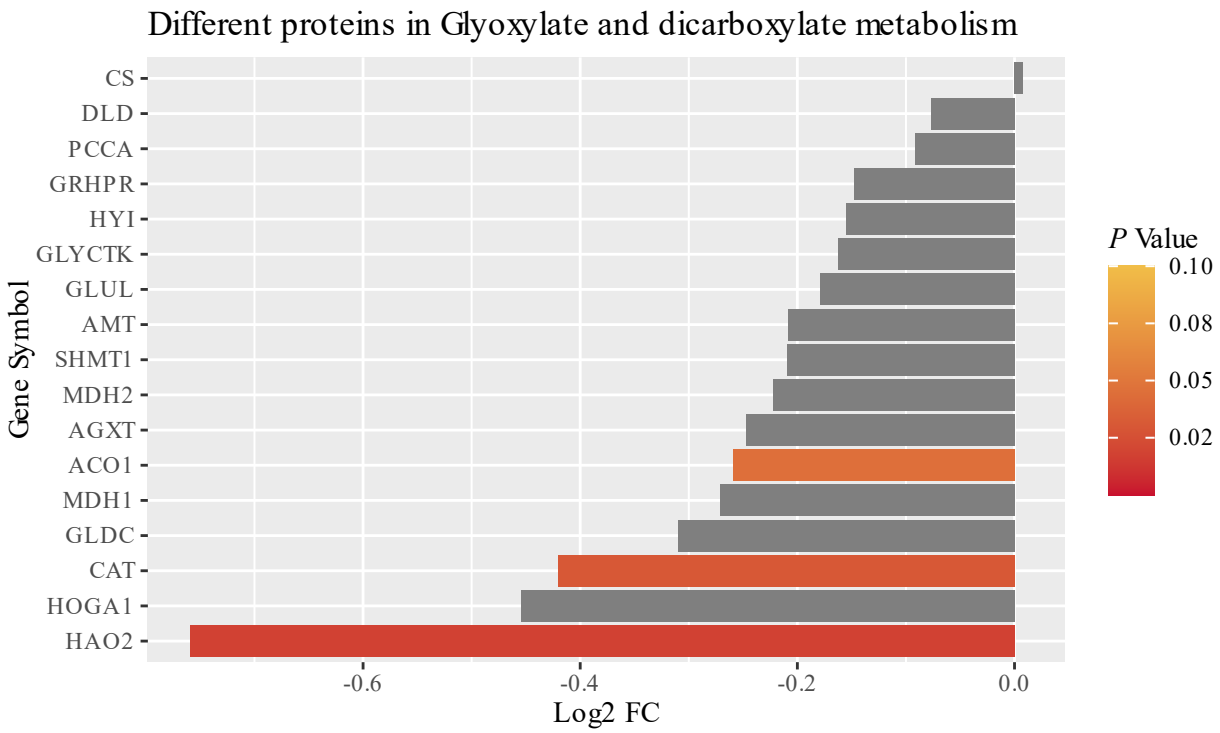

Figure 118. *Post hoc* analysis of proteins involved in glyoxylate and dicarboxylate metabolism in liver abscess induction protocol (LAIP) relative to control (CON).

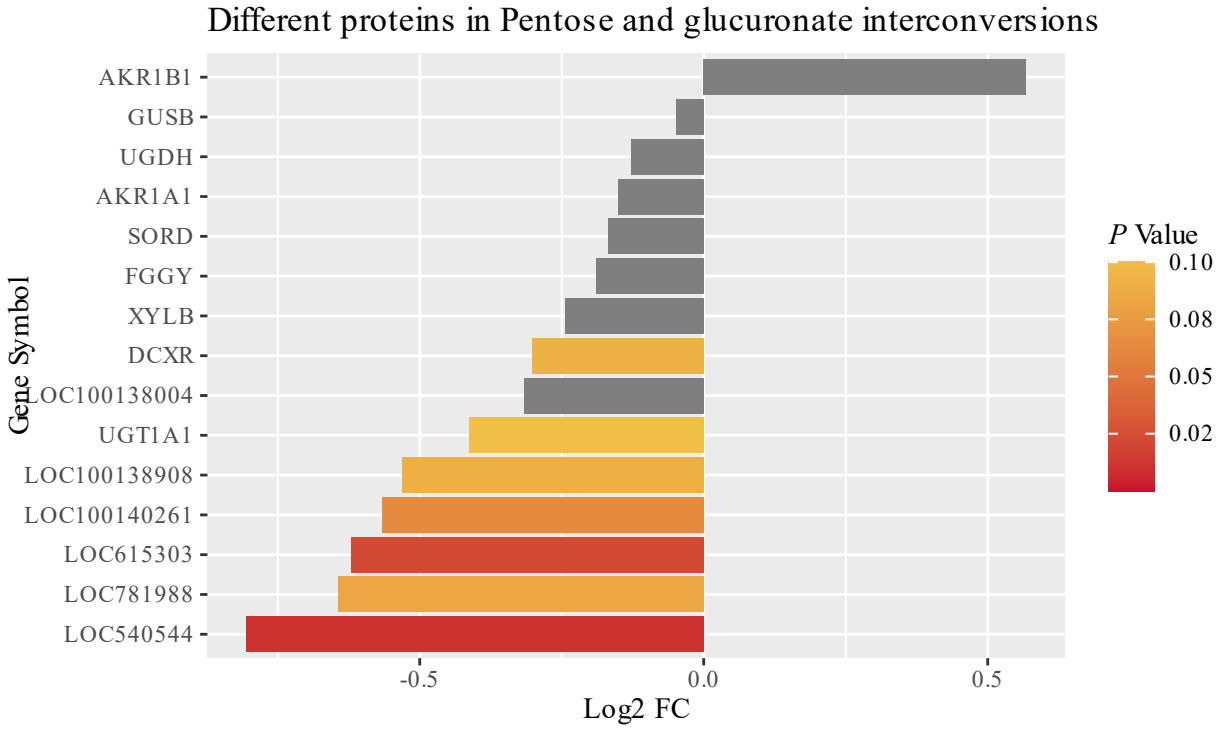

Figure 119. *Post hoc* analysis of proteins involved in pentose and glucuronate interconversions in failed liver abscess (LAIP-N) relative to control (CON).

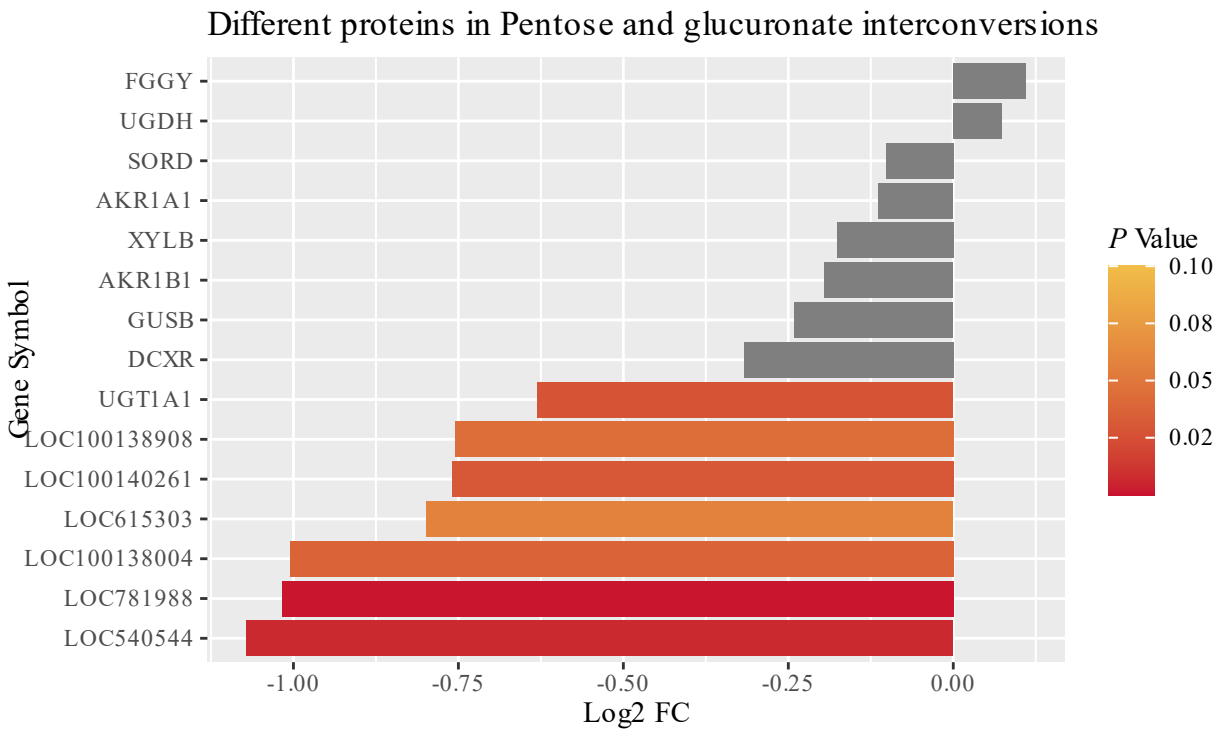

Figure 120. *Post hoc* analysis of proteins involved in pentose and glucuronate interconversions in successful liver abscess induction (LAIP-Y) relative to control (CON).

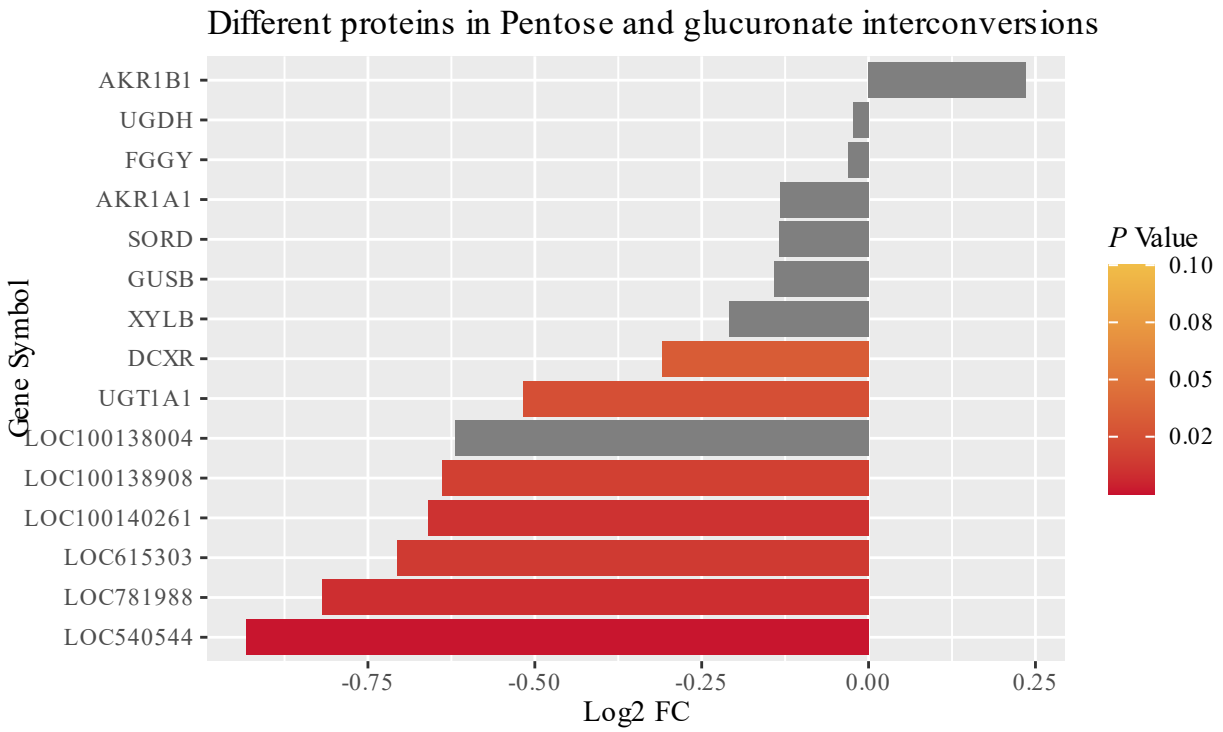

Figure 121. *Post hoc* analysis of proteins involved in pentose and glucuronate interconversions in liver abscess induction protocol (LAIP) relative to control (CON).

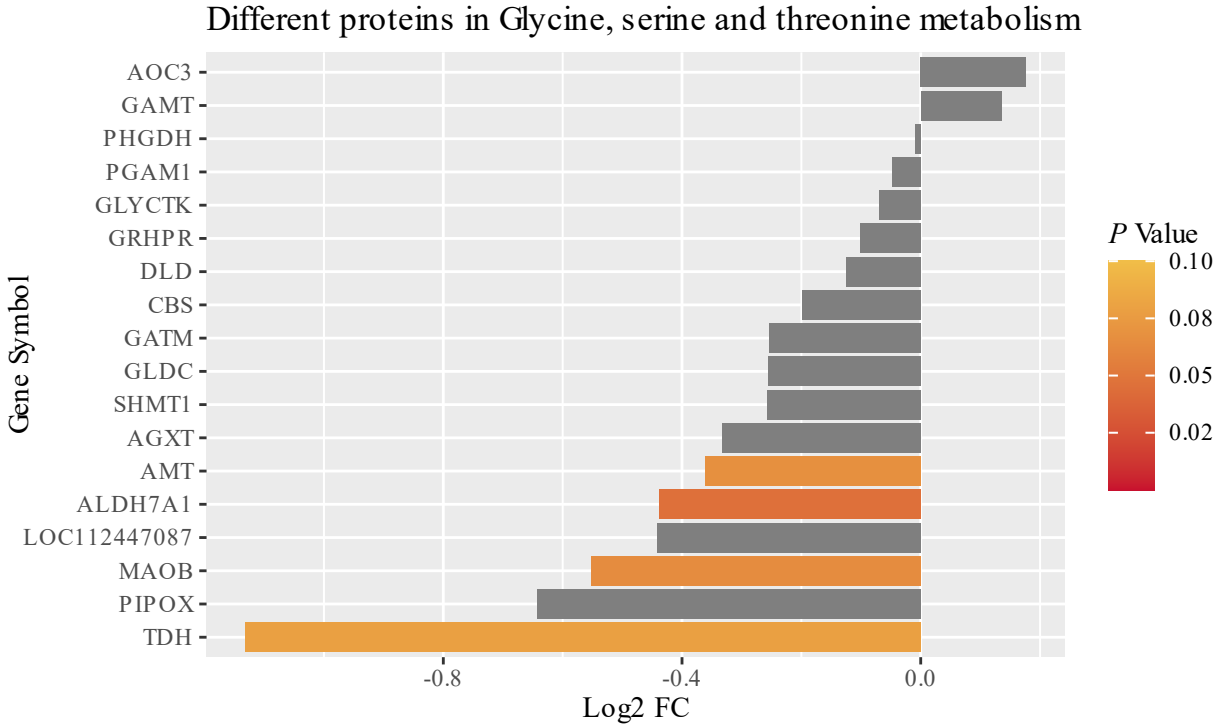

Figure 122. *Post hoc* analysis of proteins involved in glycine, serine, and threonine metabolism in failed liver abscess (LAIP-N) relative to control (CON).

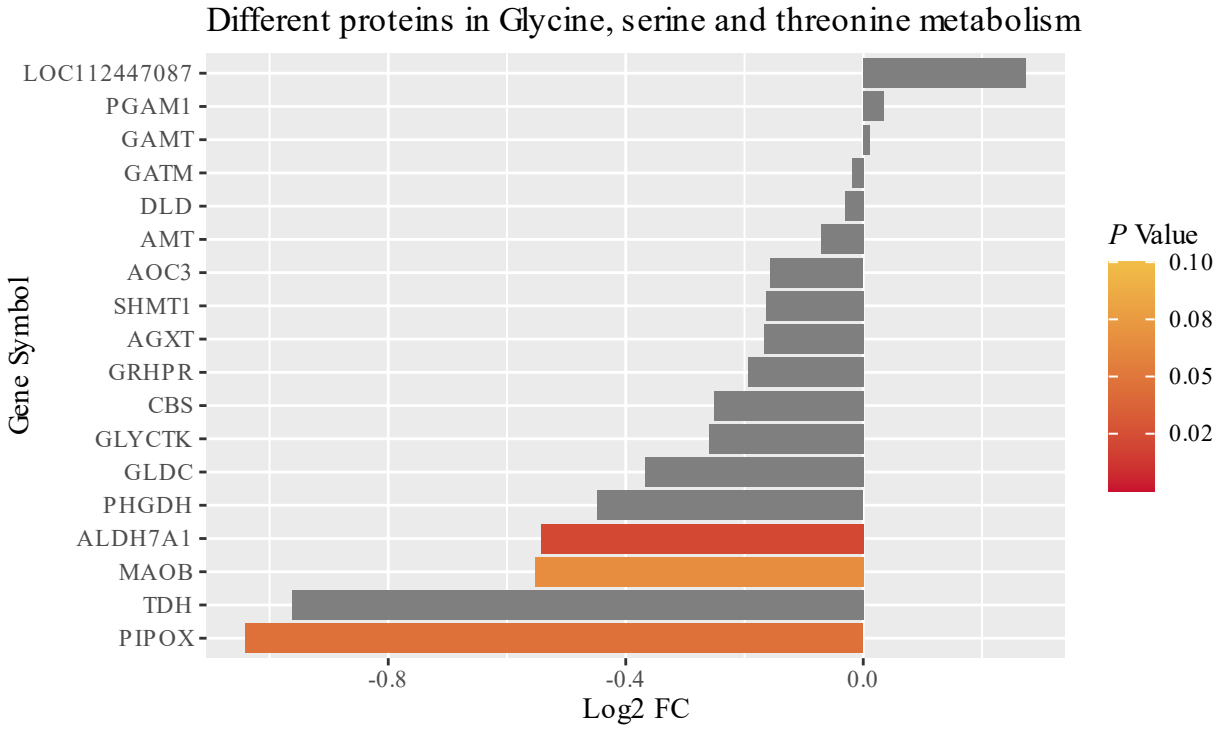

Figure 123. *Post hoc* analysis of proteins involved in glycine, serine, and threonine metabolism in successful liver abscess induction (LAIP-Y) relative to control (CON).

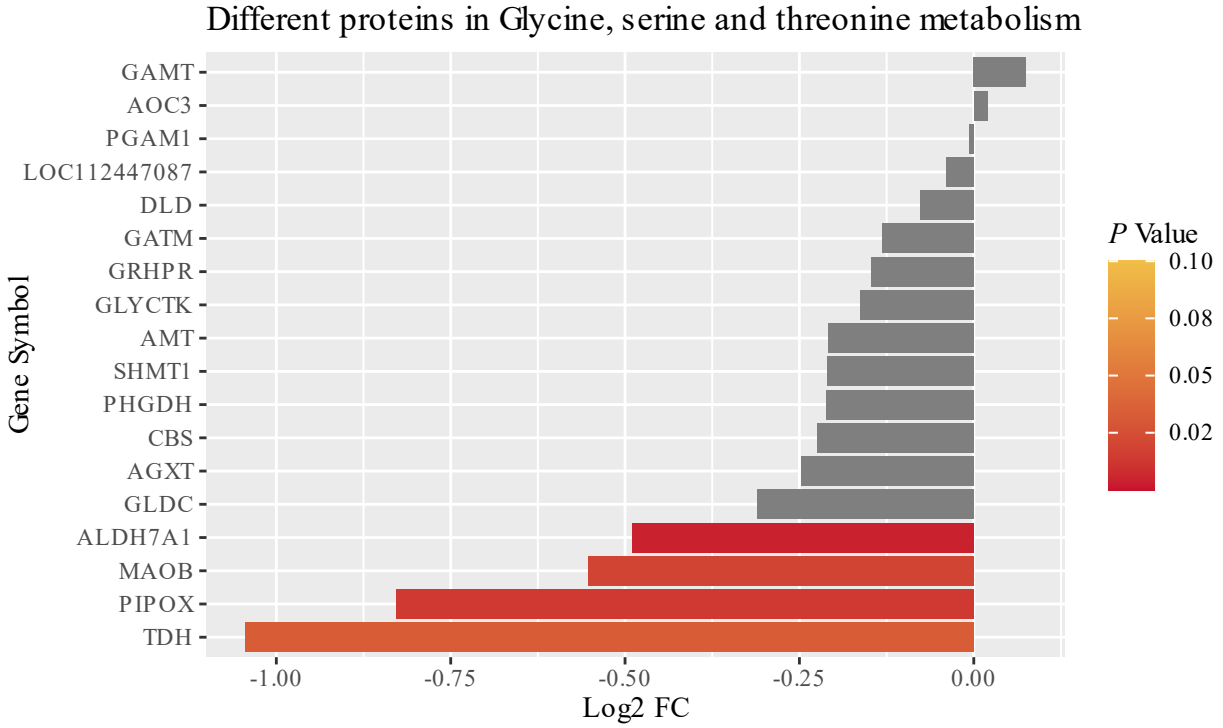

Figure 124. *Post hoc* analysis of proteins involved in glycine, serine, and threonine metabolism in liver abscess induction protocol (LAIP) relative to control (CON).

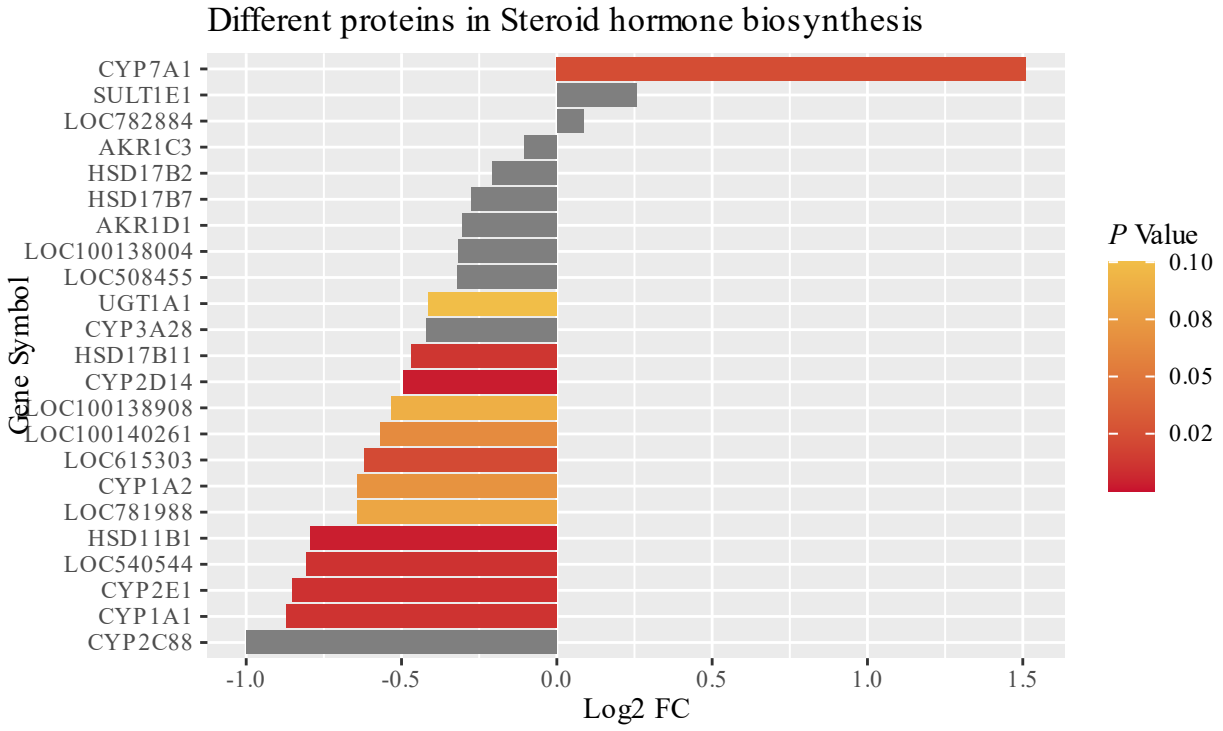

Figure 125. *Post hoc* analysis of proteins involved in steroid hormone biosynthesis in failed liver abscess (LAIP-N) relative to control (CON).

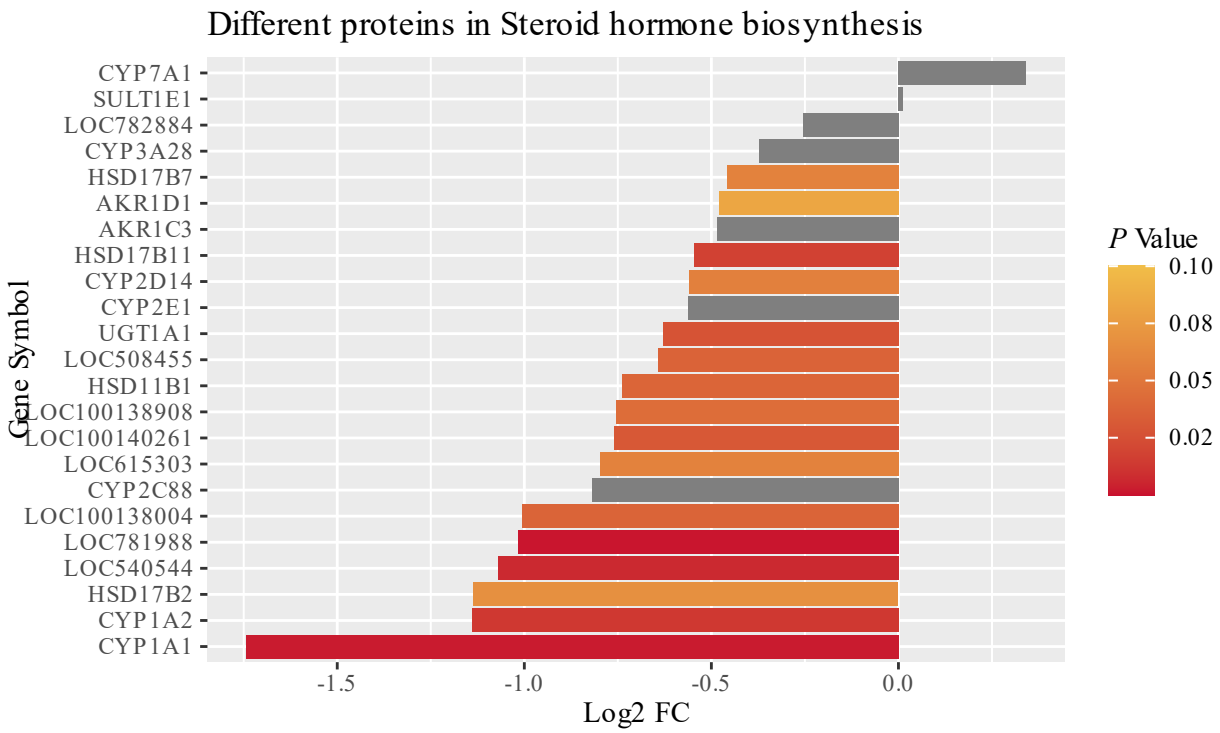

Figure 126. *Post hoc* analysis of proteins involved in steroid hormone biosynthesis in successful liver abscess induction (LAIP-Y) relative to control (CON).

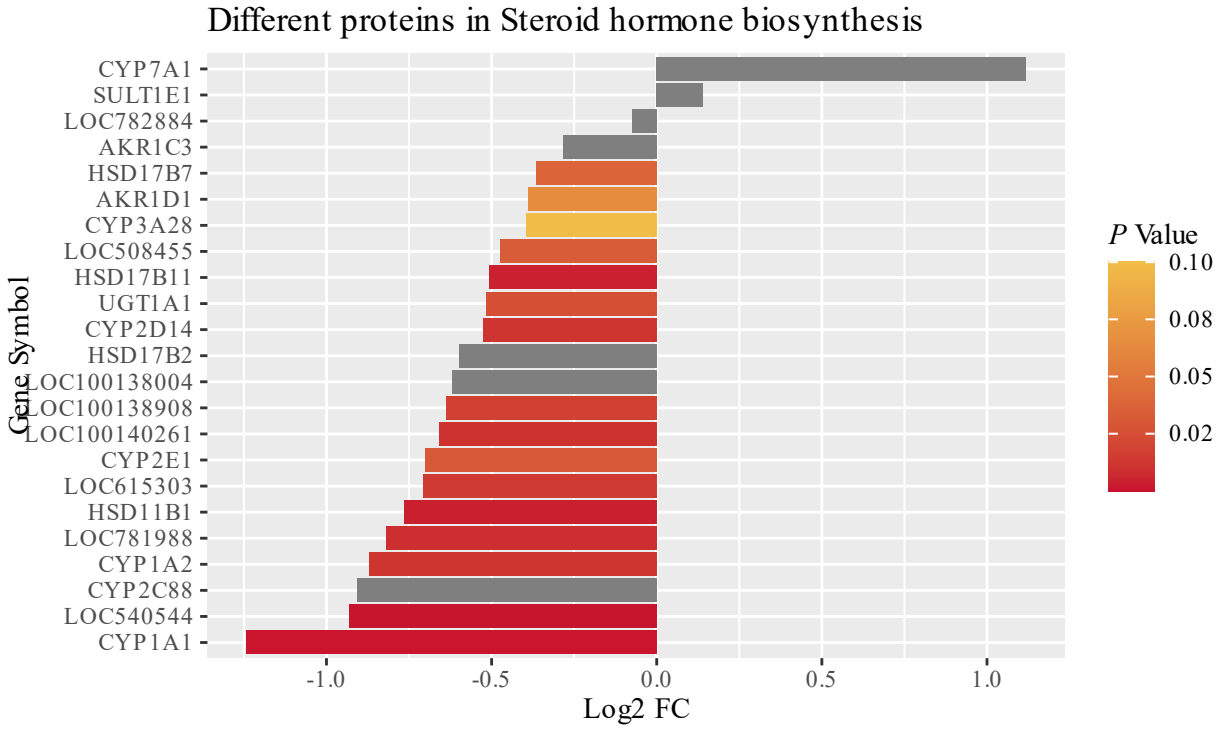

Figure 127. *Post hoc* analysis of proteins involved in steroid hormone biosynthesis in liver abscess induction protocol (LAIP) relative to control (CON).

Liver Abscess Induction Model
Study Number: GJC-LHB-3

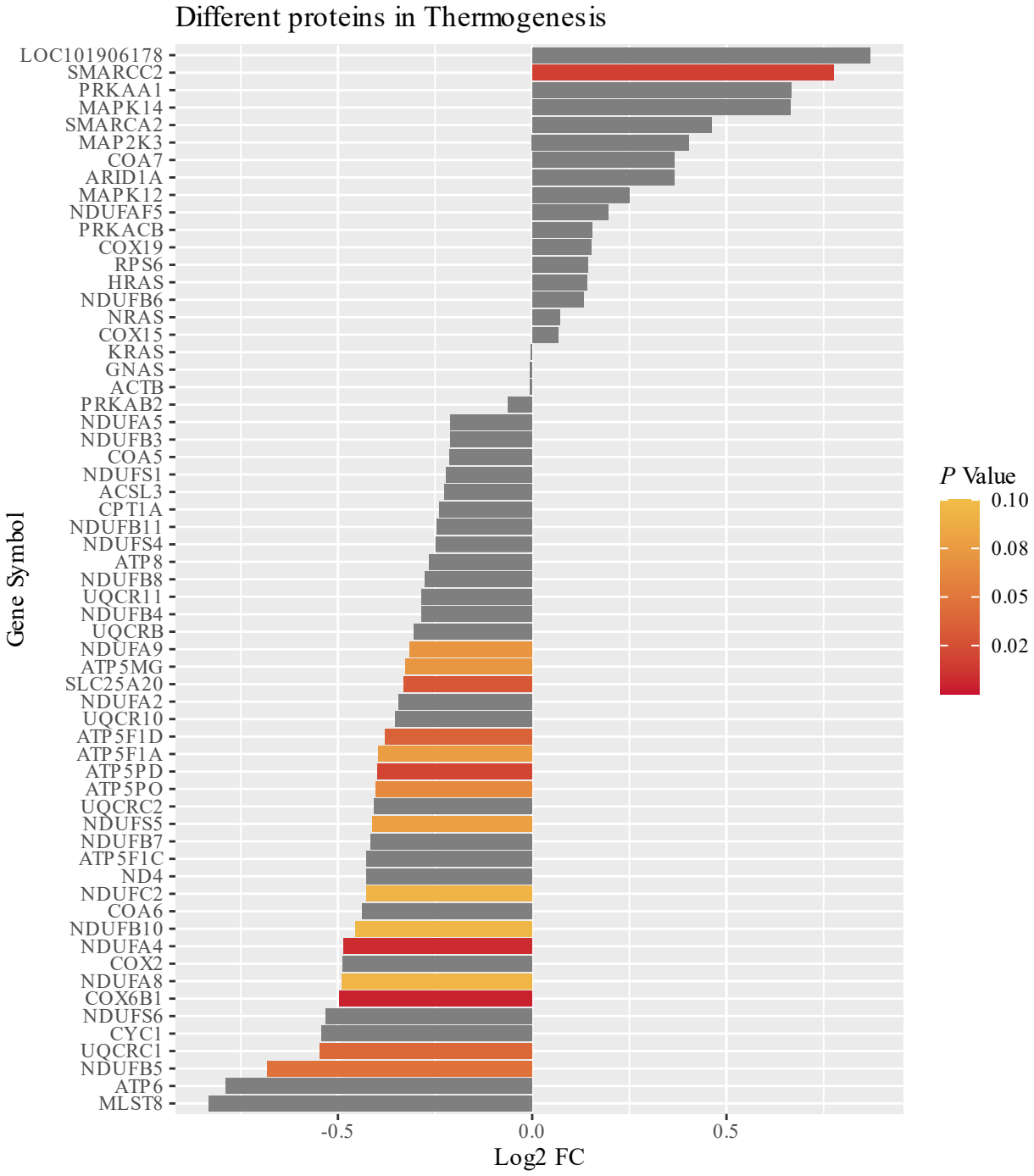

Figure 128. *Post hoc* analysis of proteins involved in thermogenesis in failed liver abscess (LAIP-N) relative to control (CON).

Liver Abscess Induction Model
Study Number: GJC-LHB-3

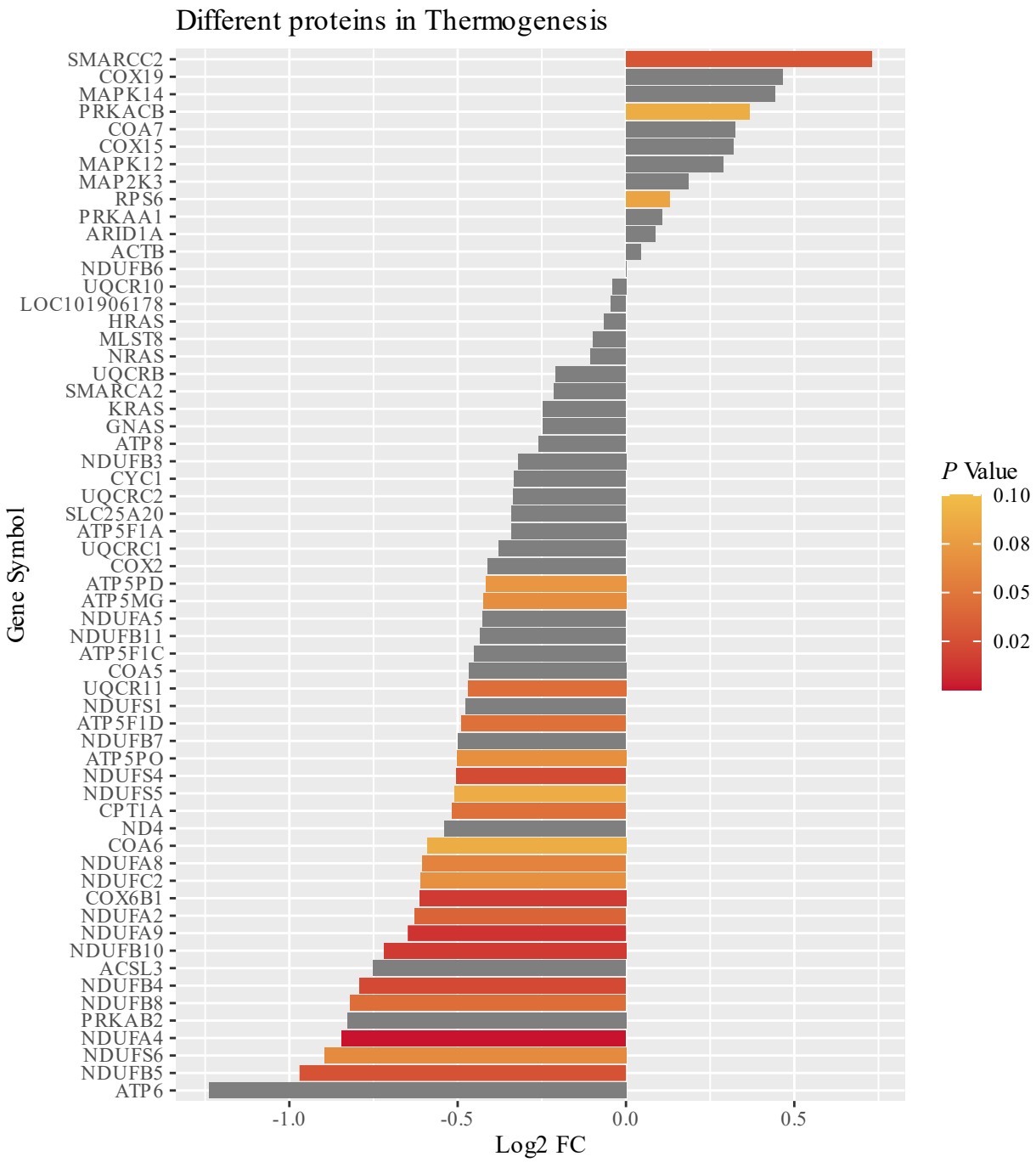

Figure 129. *Post hoc* analysis of proteins involved in thermogenesis in successful liver abscess induction (LAIP-Y) relative to control (CON).

Liver Abscess Induction Model
Study Number: GJC-LHB-3

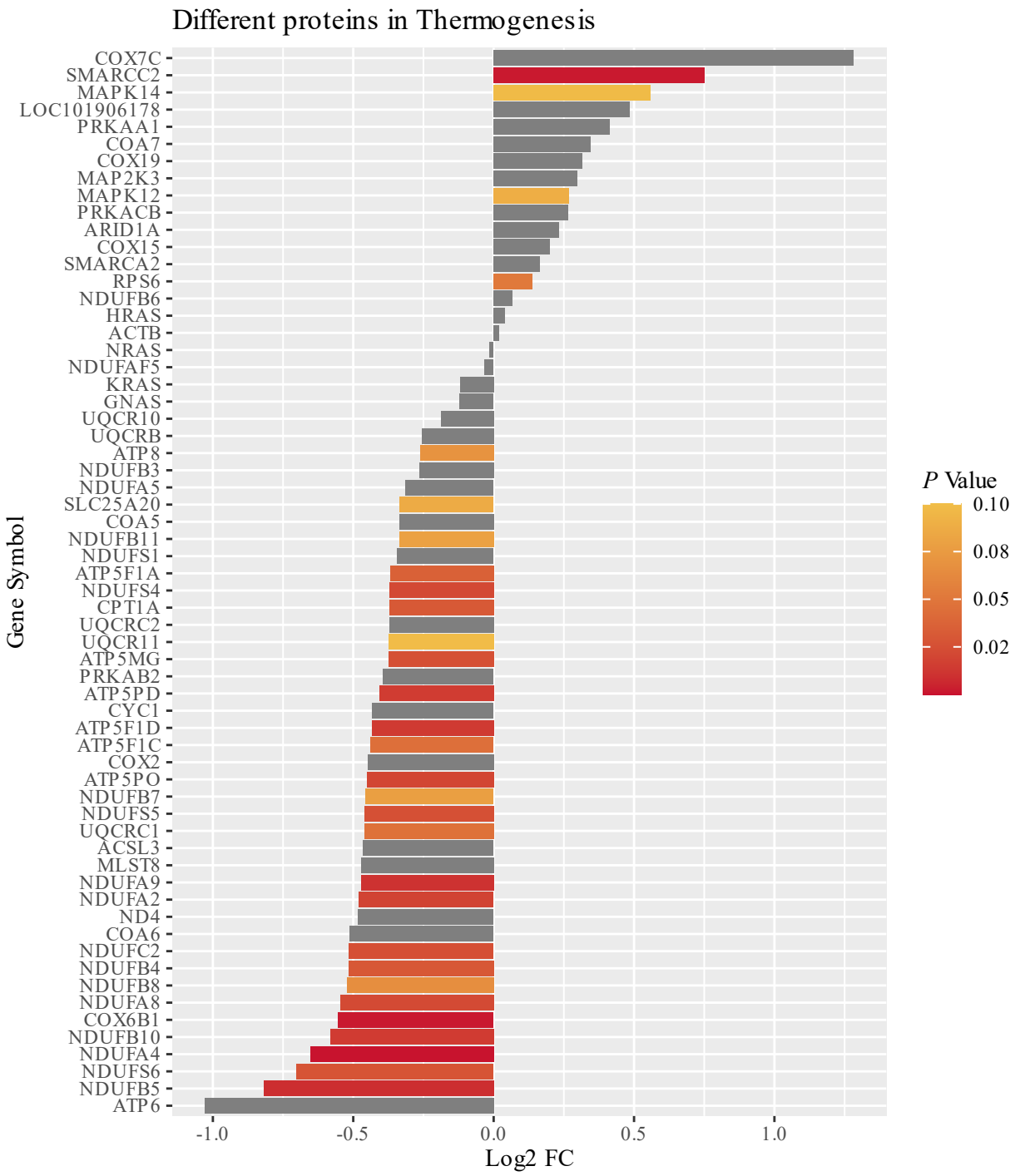

Figure 130. *Post hoc* analysis of proteins involved in thermogenesis in liver abscess induction protocol (LAIP) relative to control (CON).

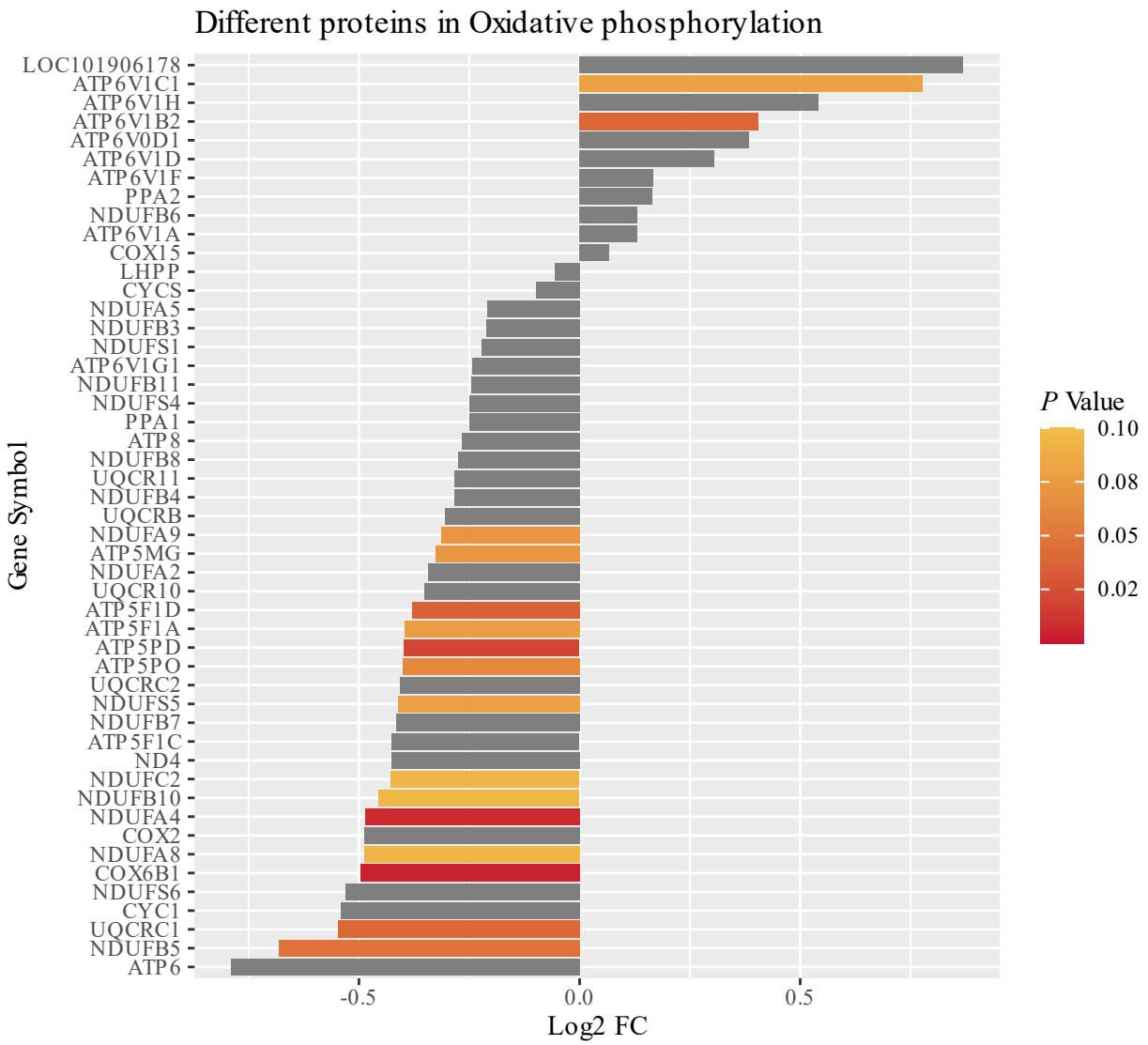

Figure 131. *Post hoc* analysis of proteins involved in oxidative phosphorylation in failed liver abscess (LAIP-N) relative to control (CON).

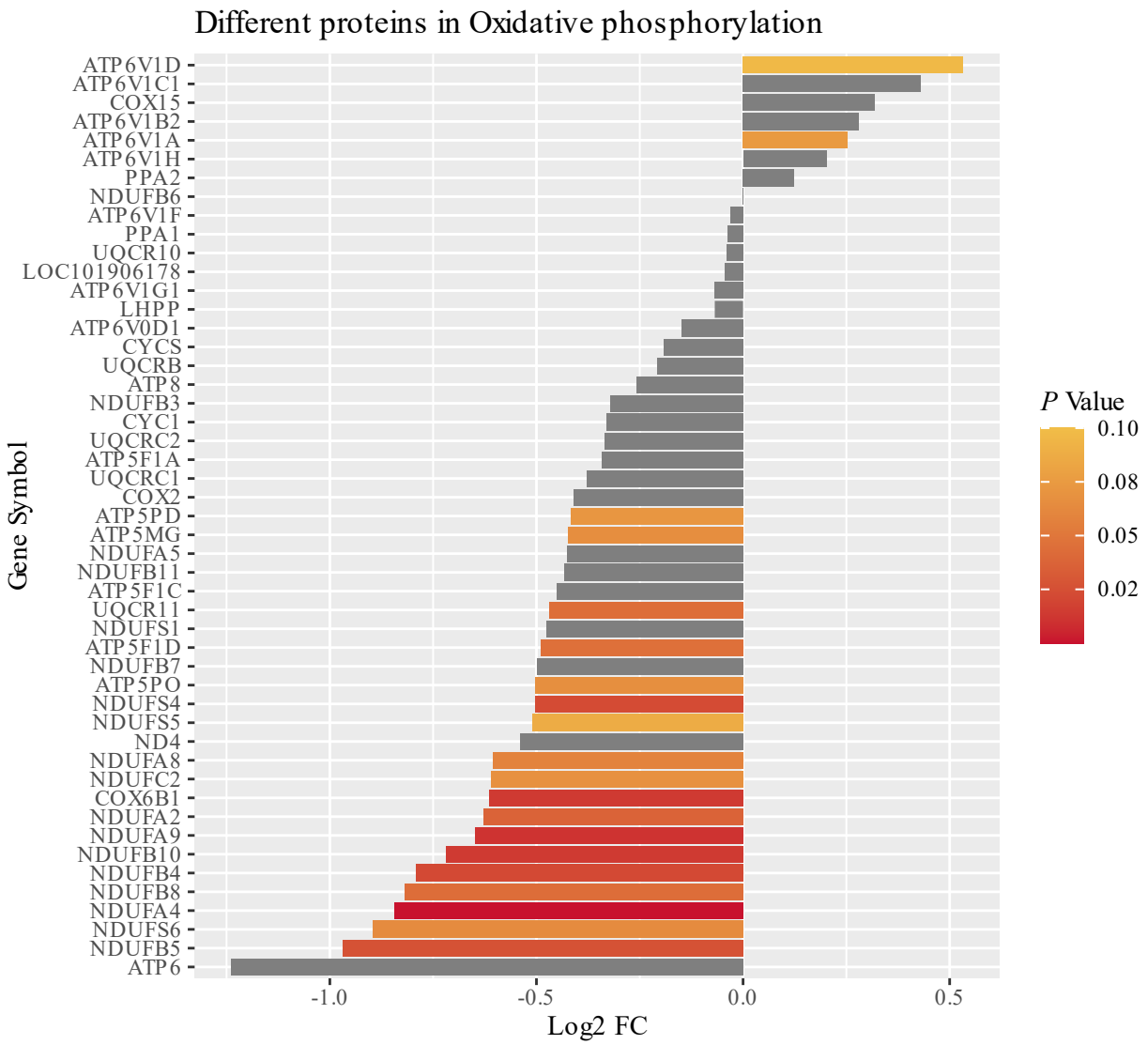

Figure 132. *Post hoc* analysis of proteins involved in oxidative phosphorylation in successful liver abscess induction (LAIP-Y) relative to control (CON).

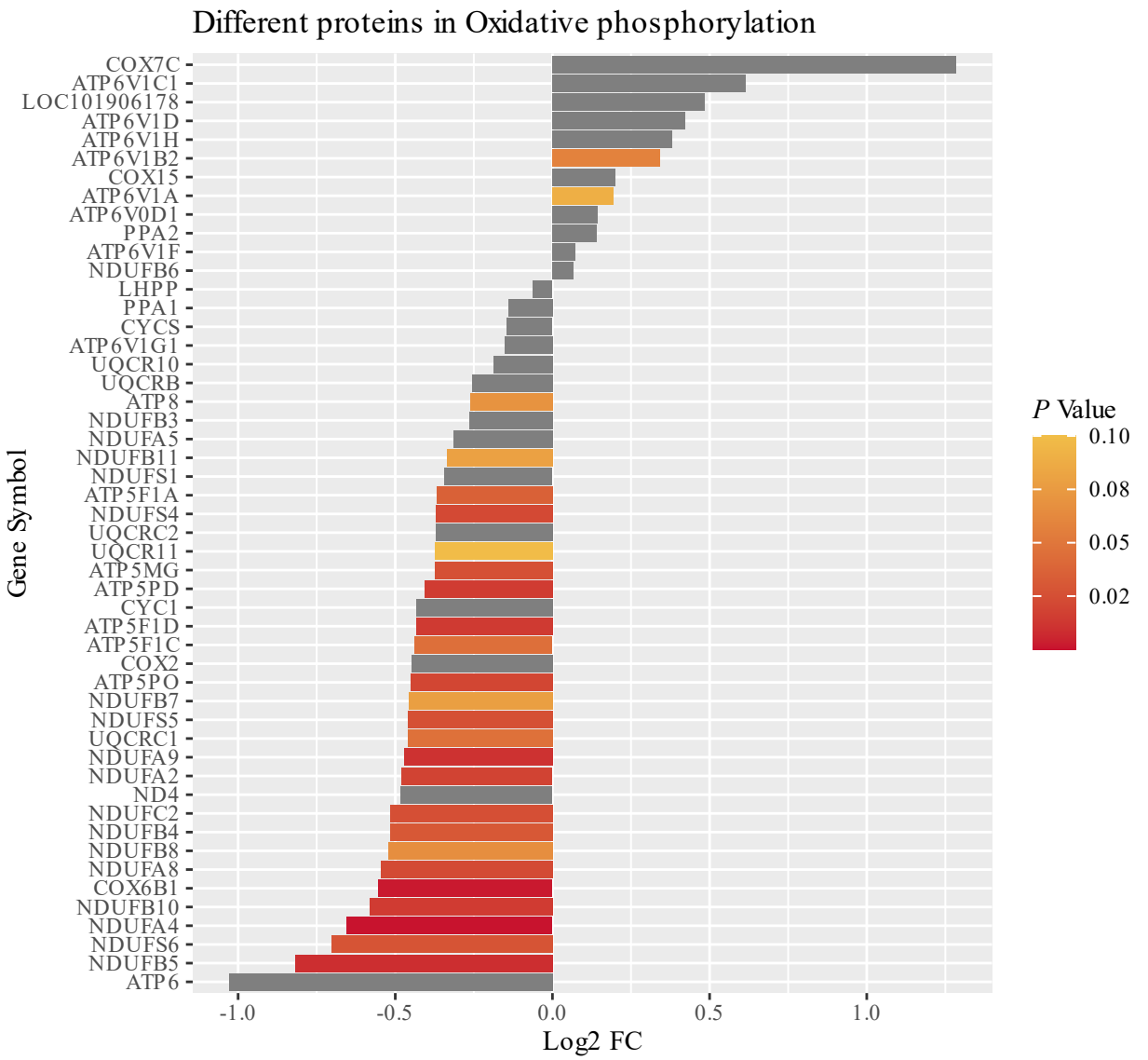

Figure 133. *Post hoc* analysis of proteins involved in oxidative phosphorylation in liver abscess induction protocol (LAIP) relative to control (CON).

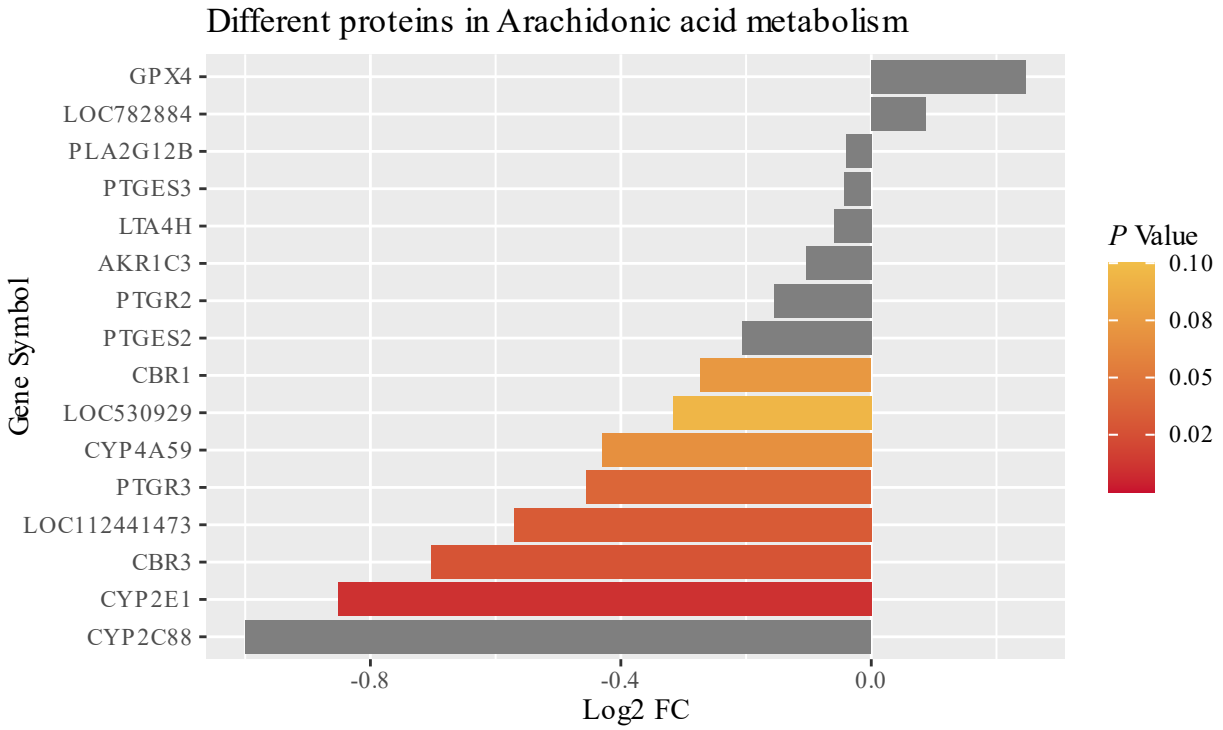

Figure 134. *Post hoc* analysis of proteins involved in arachidonic acid metabolism in failed liver abscess (LAIP-N) relative to control (CON).

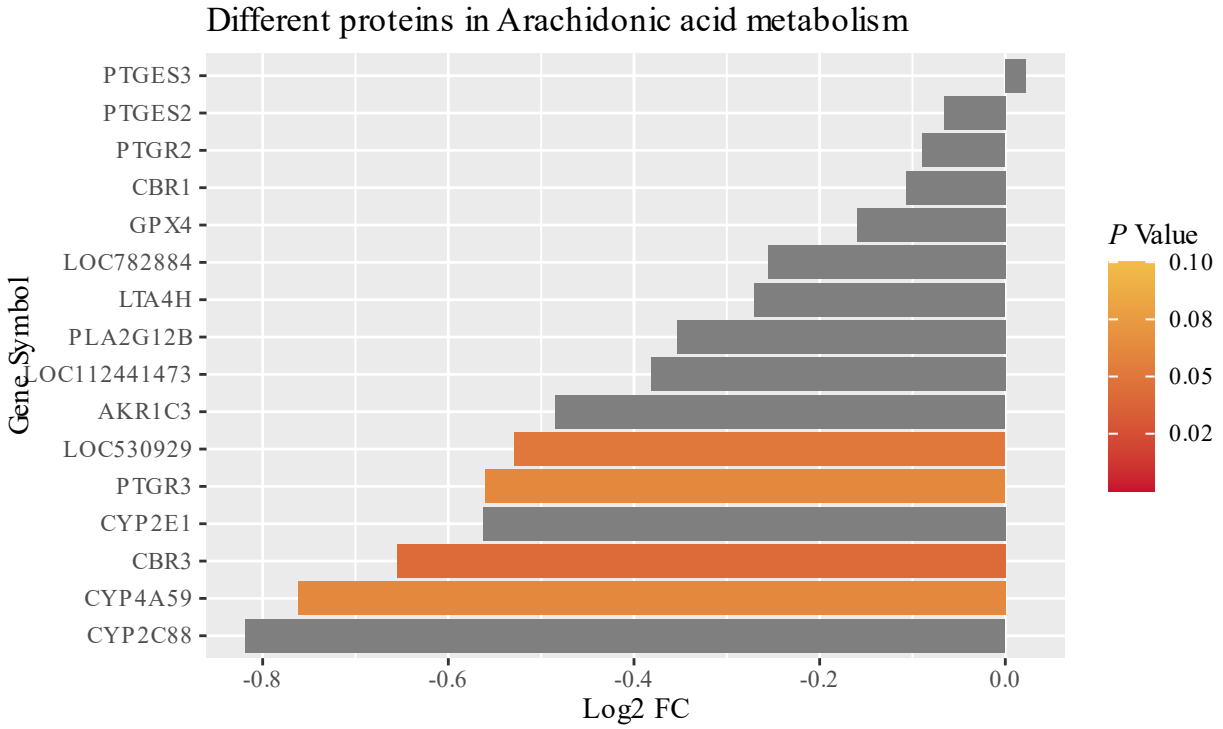

Figure 135. *Post hoc* analysis of proteins involved in arachidonic acid metabolism in successful liver abscess induction (LAIP-Y) relative to control (CON).

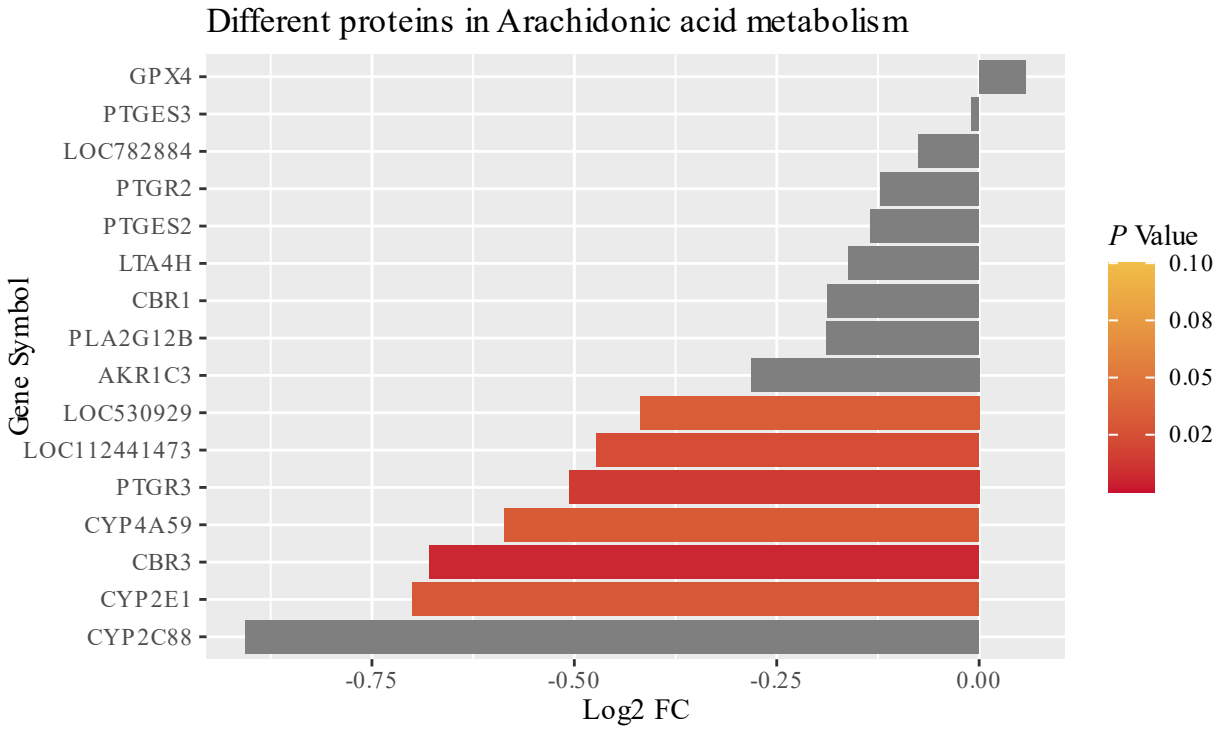

Figure 136. *Post hoc* analysis of proteins involved in arachidonic acid metabolism in liver abscess induction protocol (LAIP) relative to control (CON).

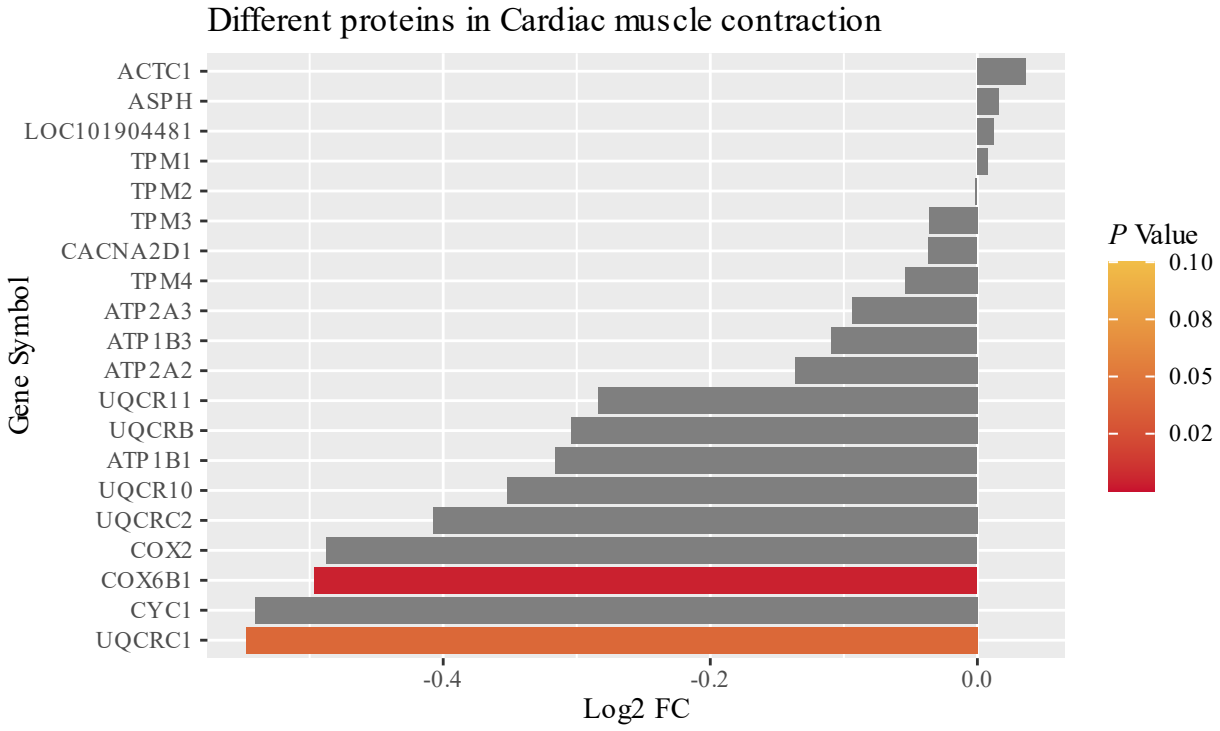

Figure 137. *Post hoc* analysis of proteins involved in cardiac muscle contraction in failed liver abscess (LAIP-N) relative to control (CON).

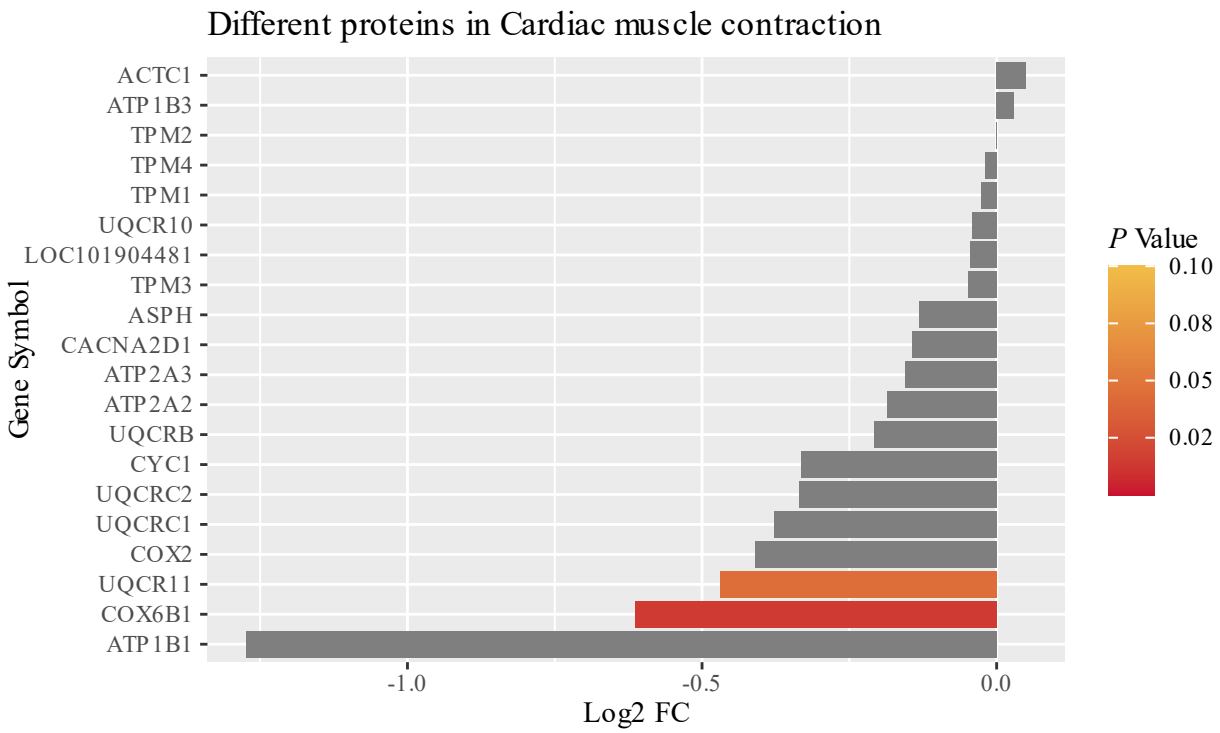

Figure 138. *Post hoc* analysis of proteins involved in cardiac muscle contraction in successful liver abscess induction (LAIP-Y) relative to control (CON).

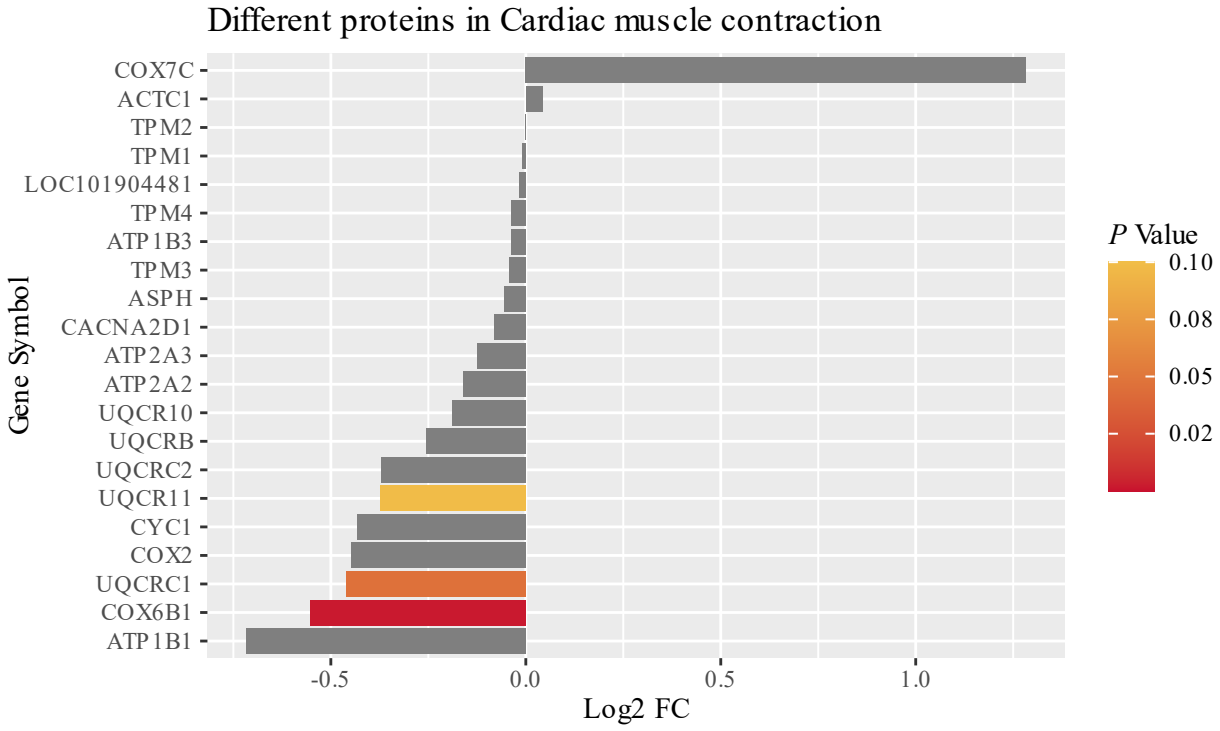

Figure 139. *Post hoc* analysis of proteins involved in cardiac muscle contraction in liver abscess induction protocol (LAIP) relative to control (CON).

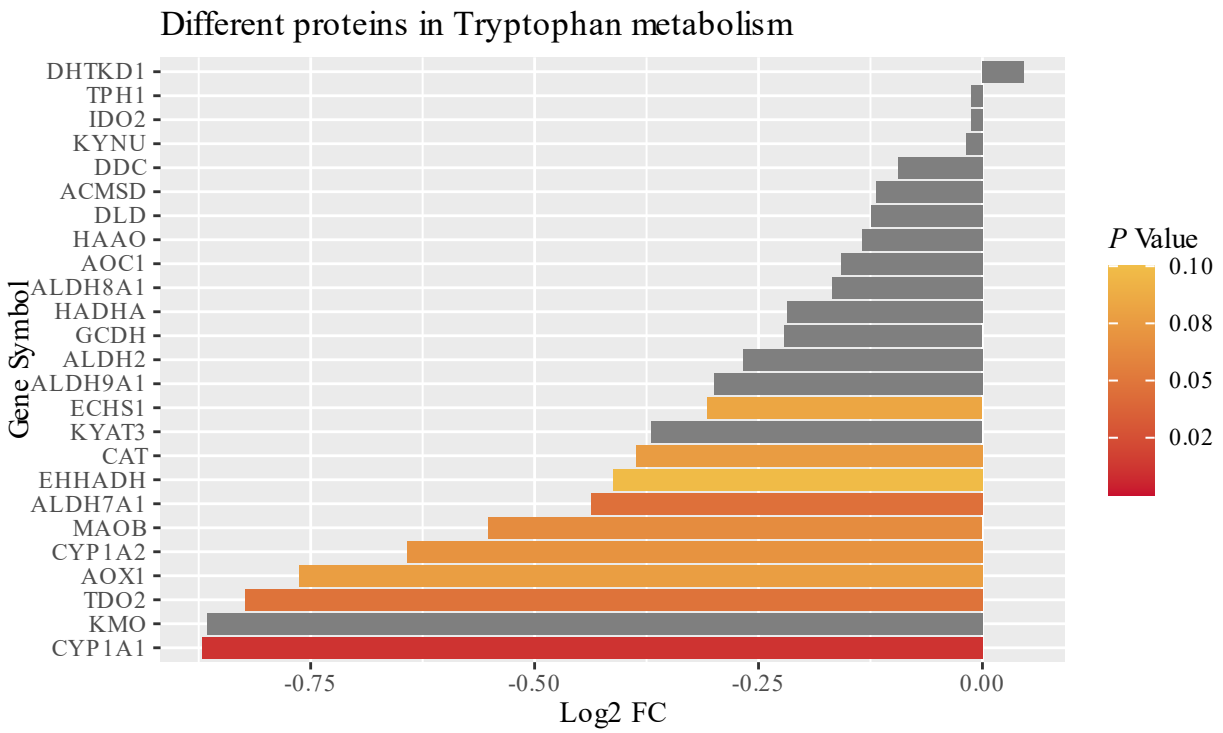

Figure 140. *Post hoc* analysis of proteins involved in tryptophan metabolism in failed liver abscess (LAIP-N) relative to control (CON).

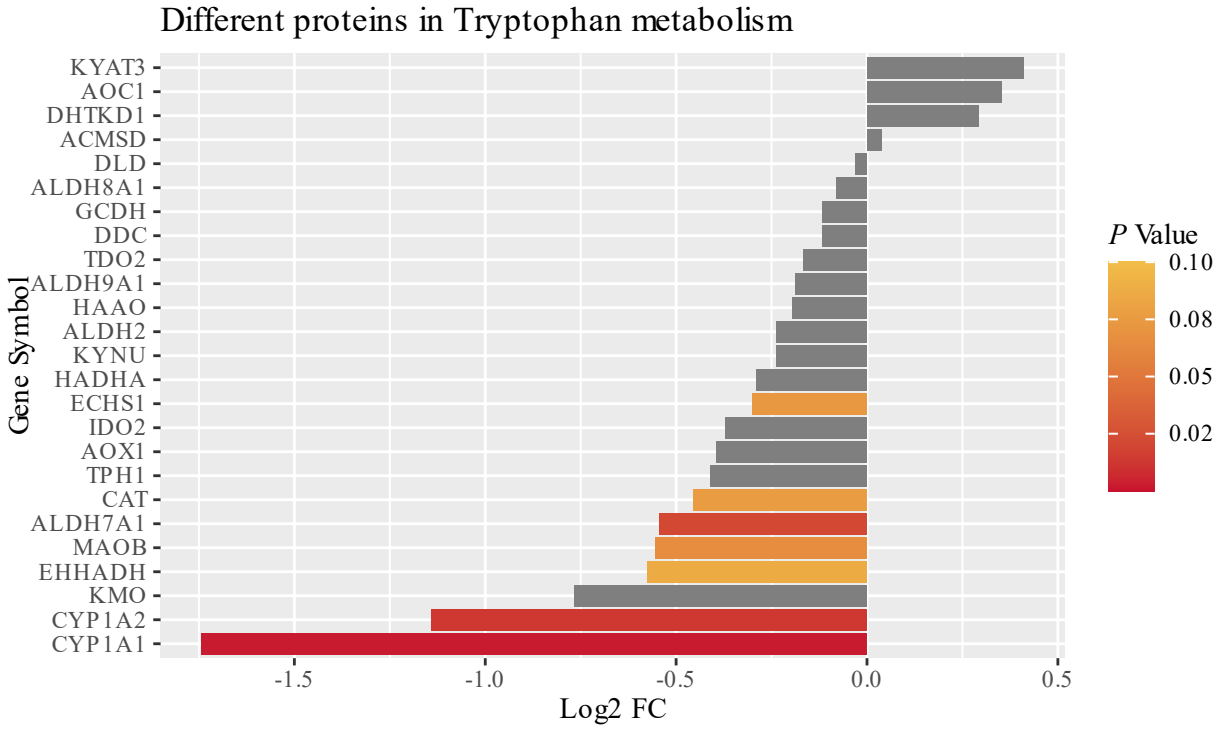

Figure 141. *Post hoc* analysis of proteins involved in tryptophan metabolism in successful liver abscess induction (LAIP-Y) relative to control (CON).

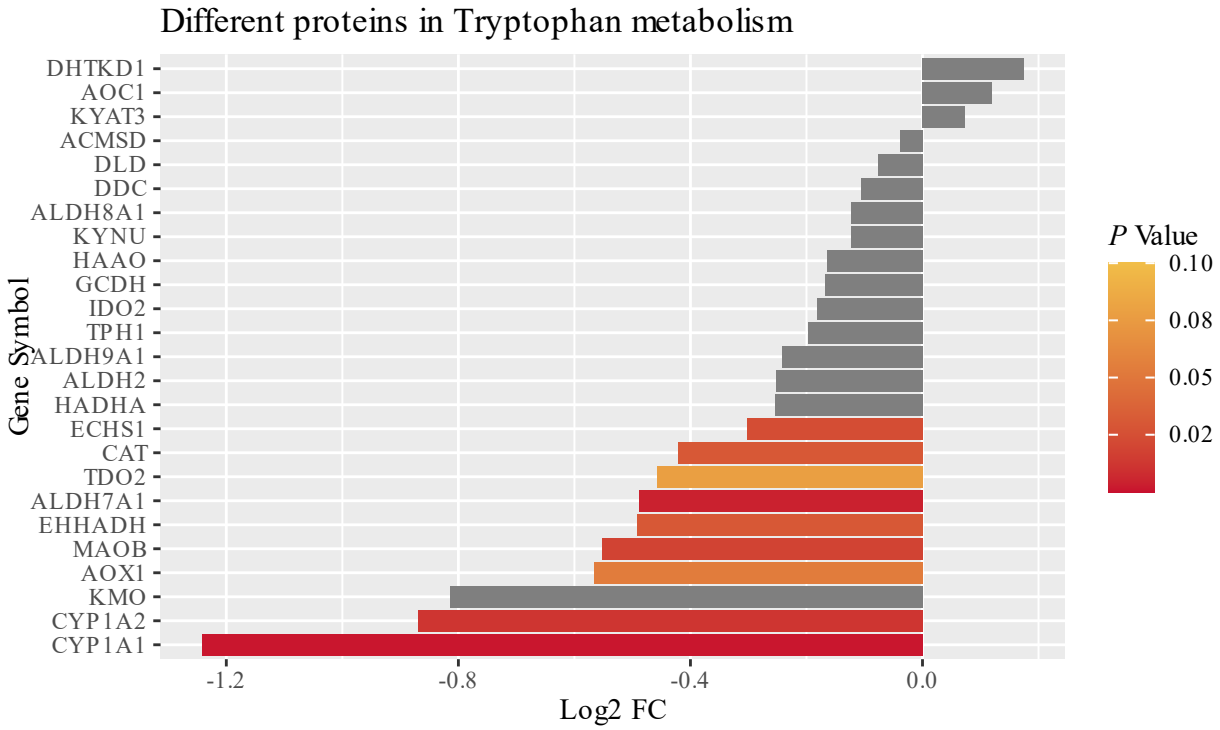

Figure 142. *Post hoc* analysis of proteins involved in tryptophan metabolism in liver abscess induction protocol (LAIP) relative to control (CON).

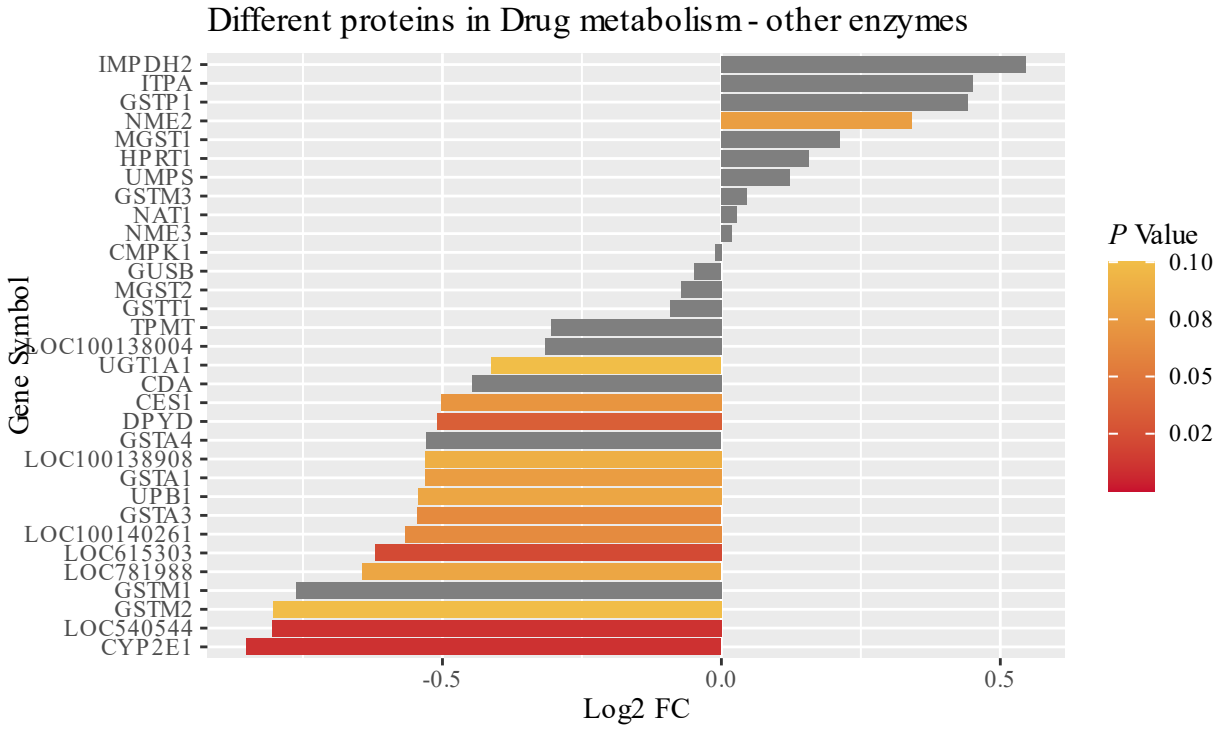

Figure 143. *Post hoc* analysis of proteins involved in drug metabolism - other enzymes in failed liver abscess (LAIP-N) relative to control (CON).

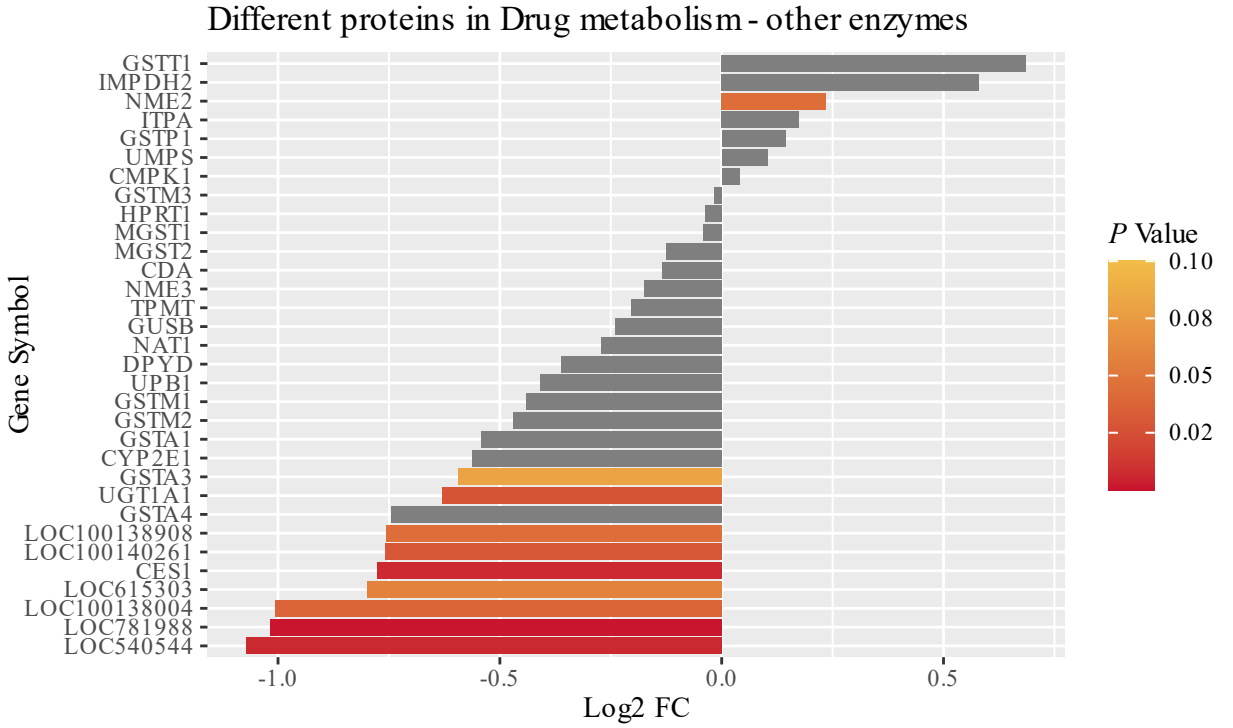

Figure 144. *Post hoc* analysis of proteins involved in drug metabolism - other enzymes in successful liver abscess induction (LAIP-Y) relative to control (CON).

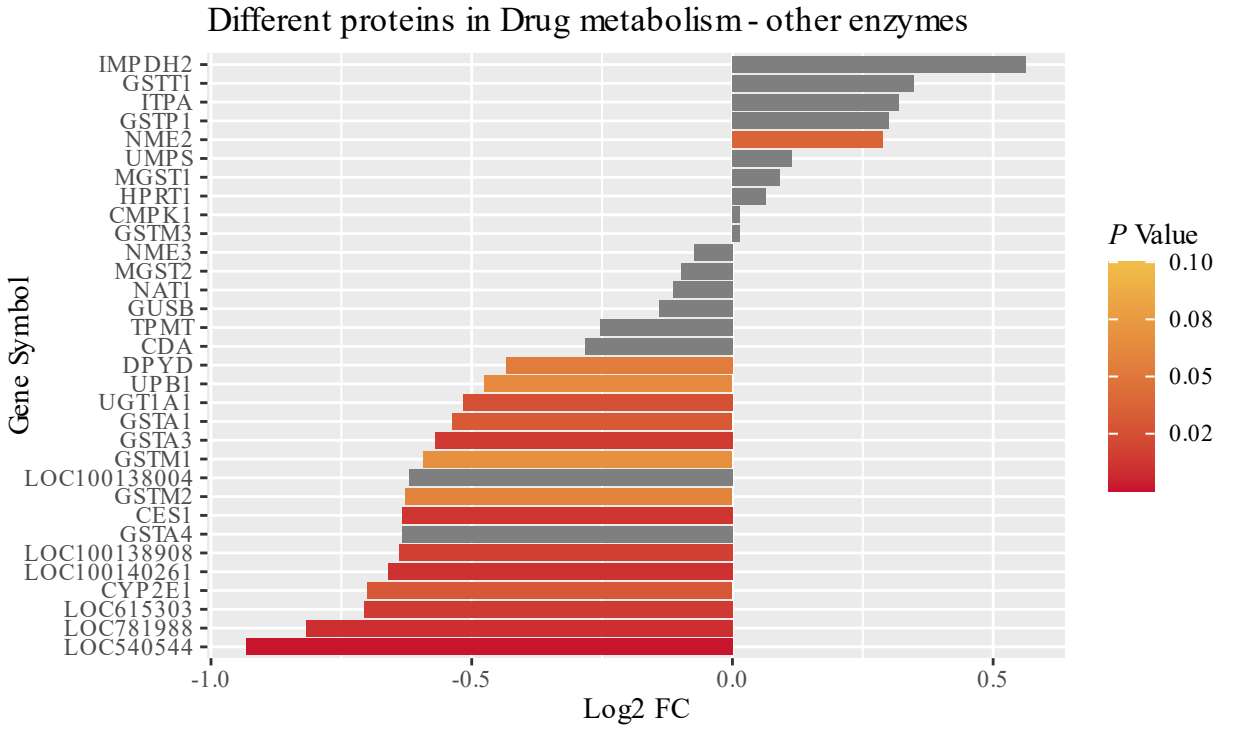

Figure 145. *Post hoc* analysis of proteins involved in drug metabolism - other enzymes in liver abscess induction protocol (LAIP) relative to control (CON).

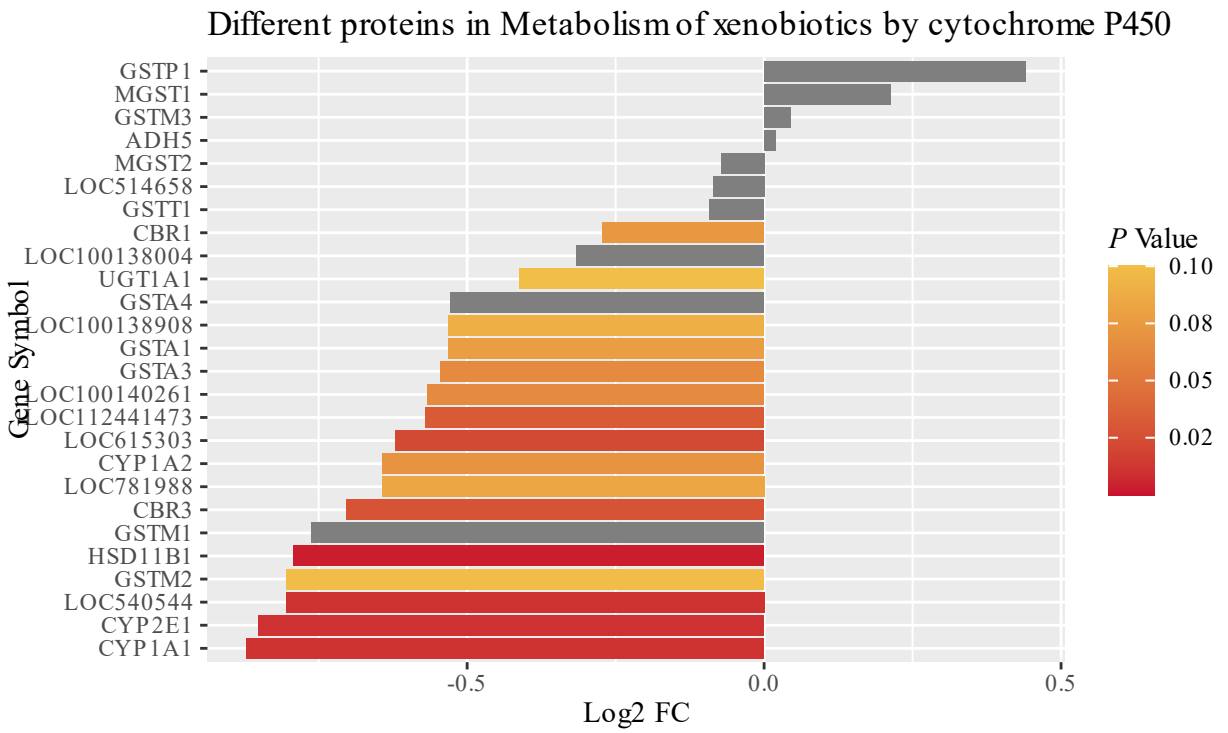

Figure 146. *Post hoc* analysis of proteins involved in metabolism of xenobiotics by cytochrome P450 in failed liver abscess (LAIP-N) relative to control (CON).

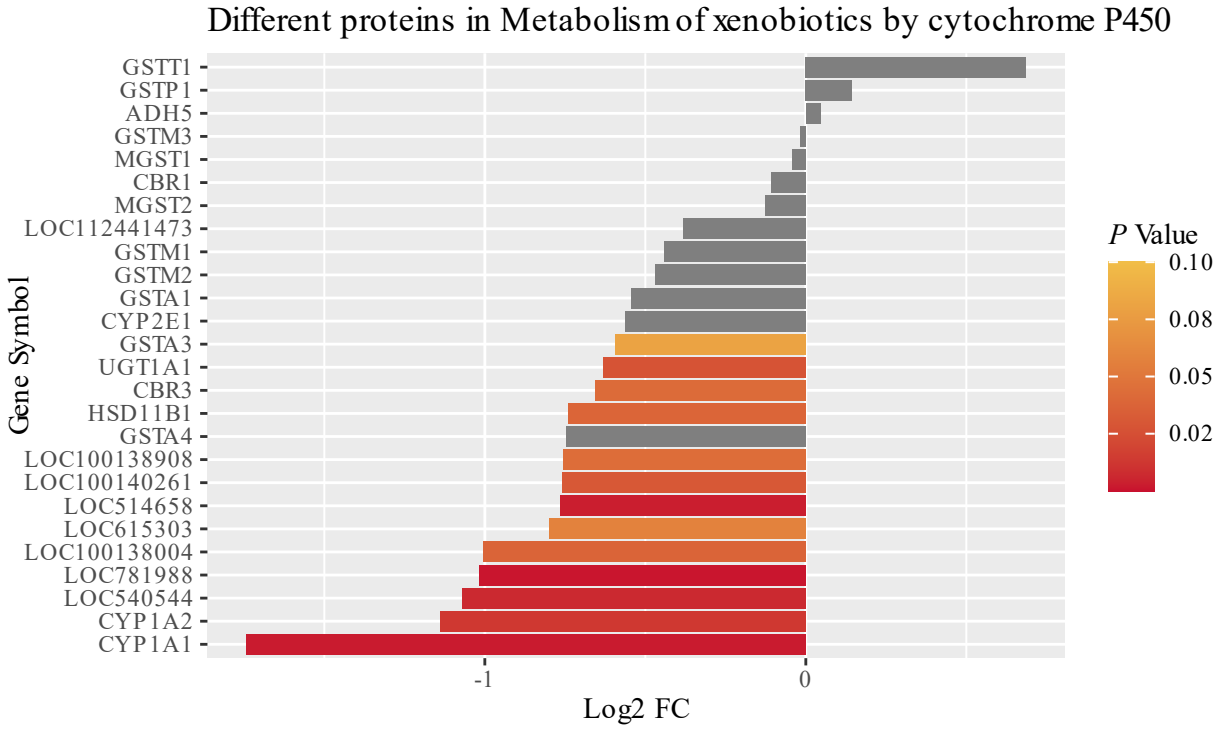

Figure 147. *Post hoc* analysis of proteins involved in metabolism of xenobiotics by cytochrome P450 in successful liver abscess induction (LAIP-Y) relative to control (CON).

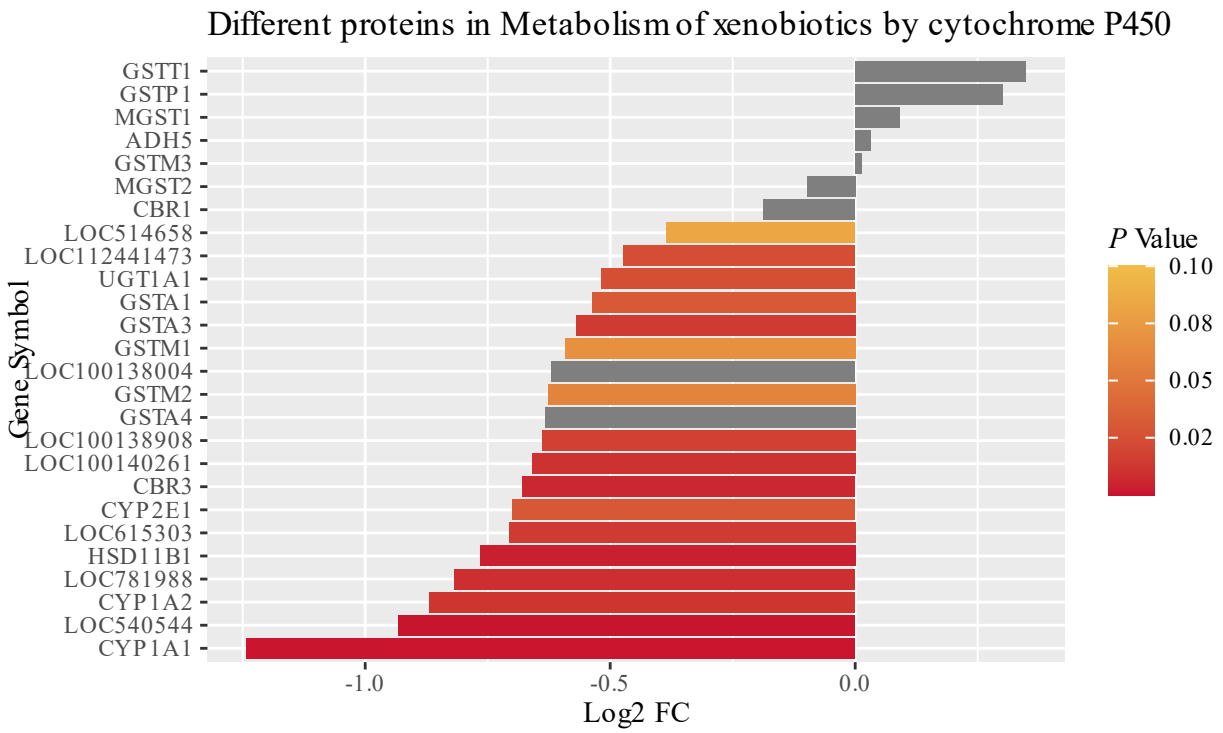

Figure 148. *Post hoc* analysis of proteins involved in metabolism of xenobiotics by cytochrome P450 in liver abscess induction protocol (LAIP) relative to control (CON).

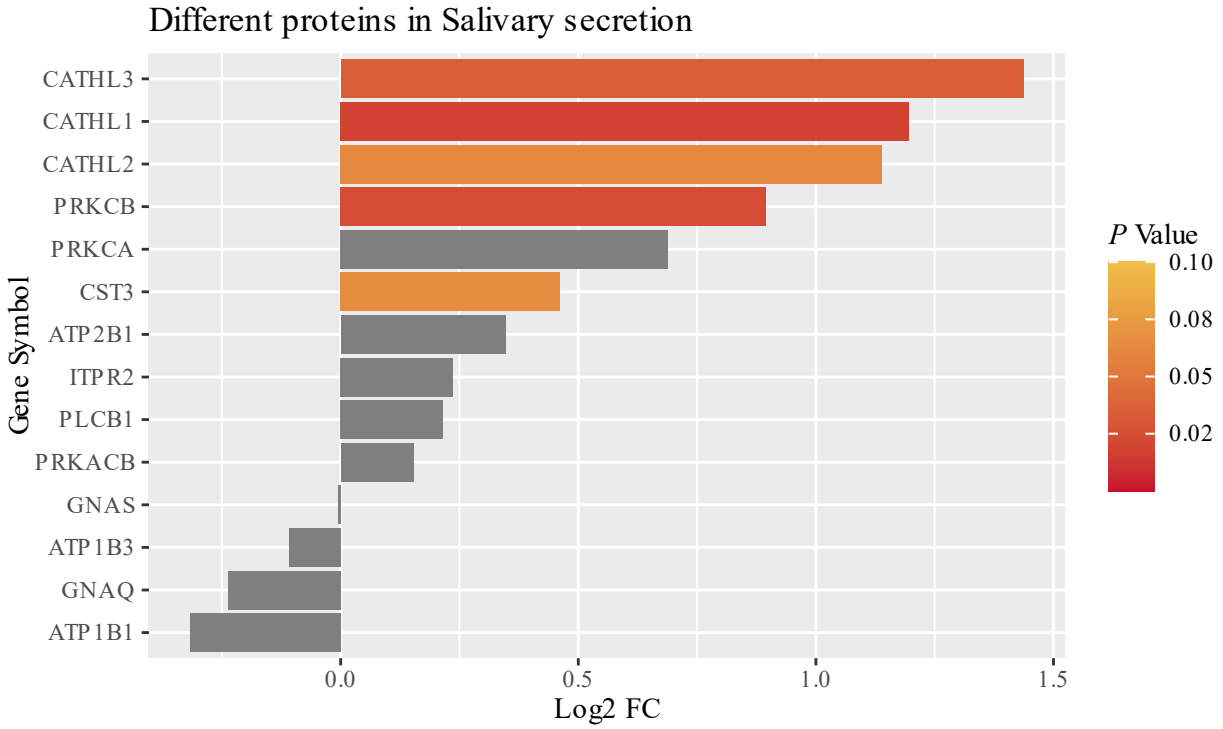

Figure 149. *Post hoc* analysis of proteins involved in salivary secretion in failed liver abscess (LAIP-N) relative to control (CON).

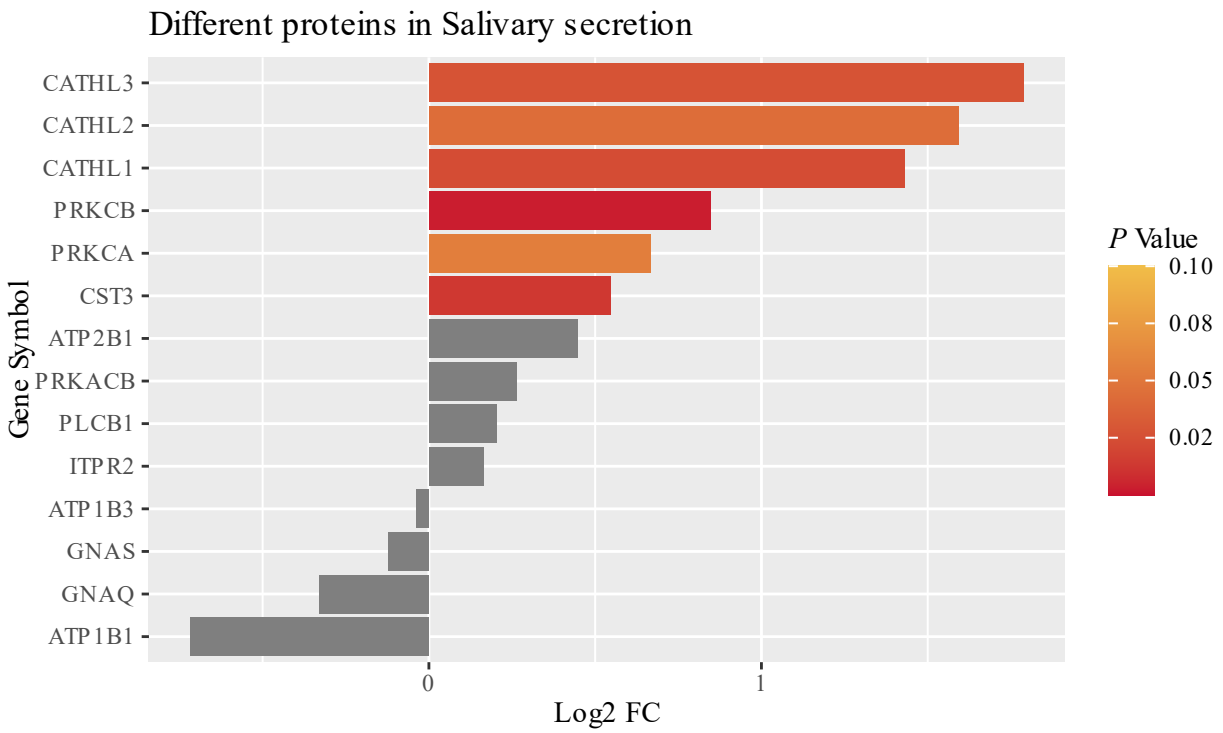

Figure 150. *Post hoc* analysis of proteins involved in salivary secretion in liver abscess induction protocol (LAIP) relative to control (CON).

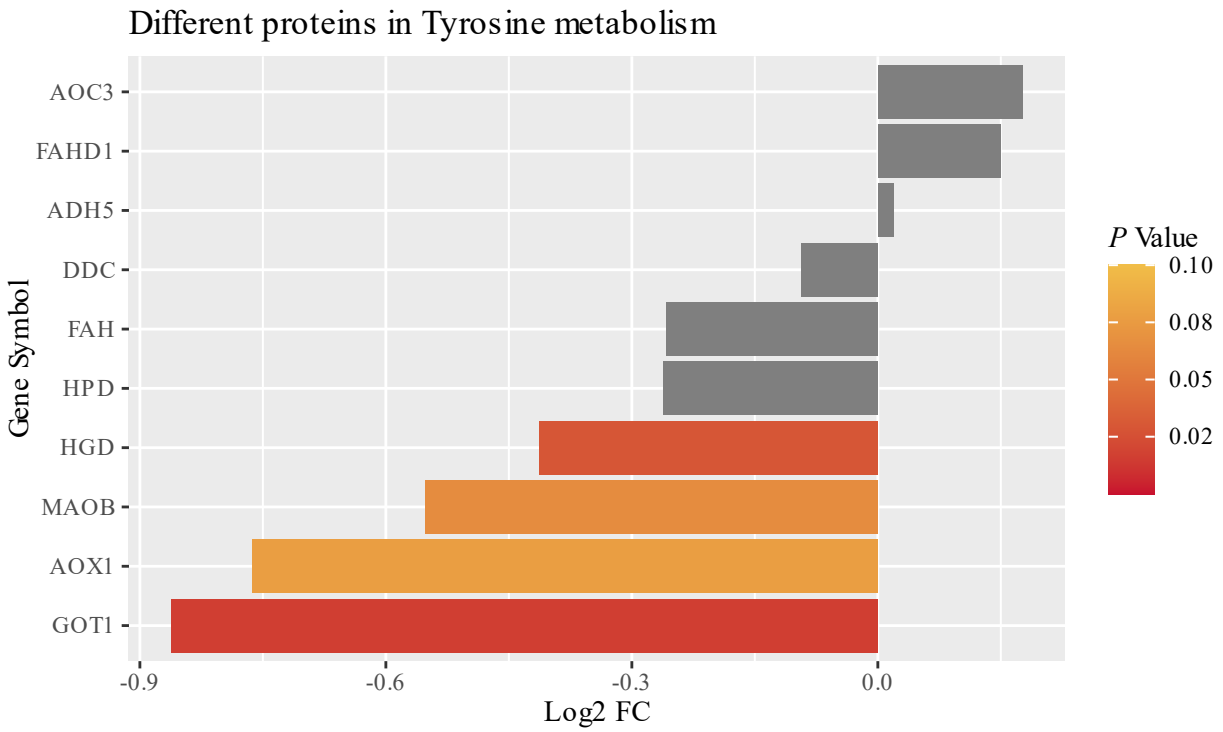

Figure 151. *Post hoc* analysis of proteins involved in tyrosine metabolism in failed liver abscess (LAIP-N) relative to control (CON).

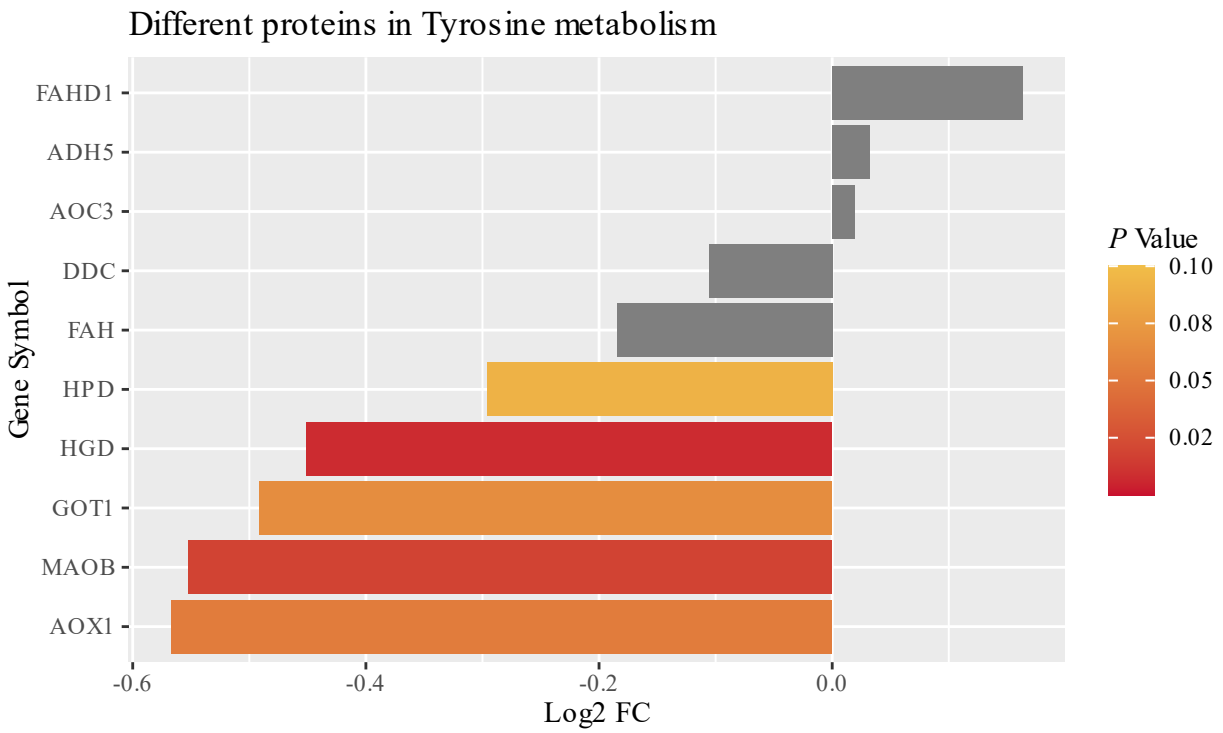

Figure 152. *Post hoc* analysis of proteins involved in tyrosine metabolism in liver abscess induction protocol (LAIP) relative to control (CON).

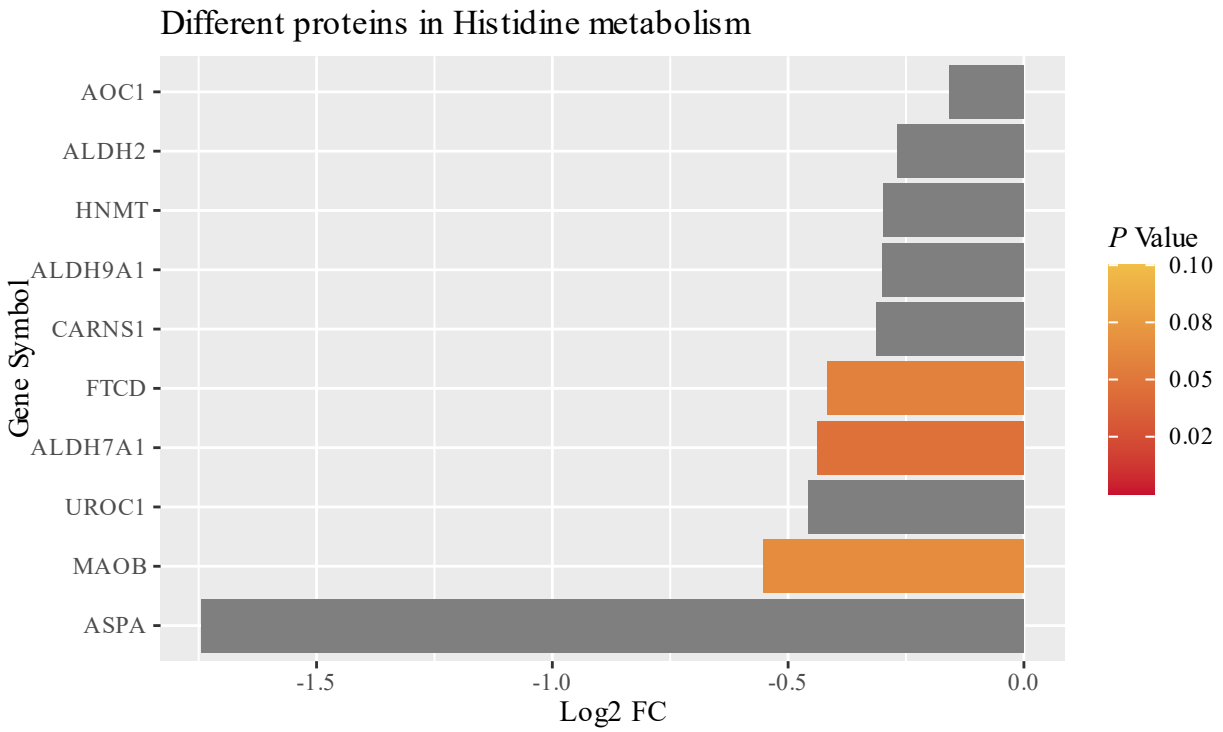

Figure 153. *Post hoc* analysis of proteins involved in histidine metabolism in failed liver abscess (LAIP-N) relative to control (CON).

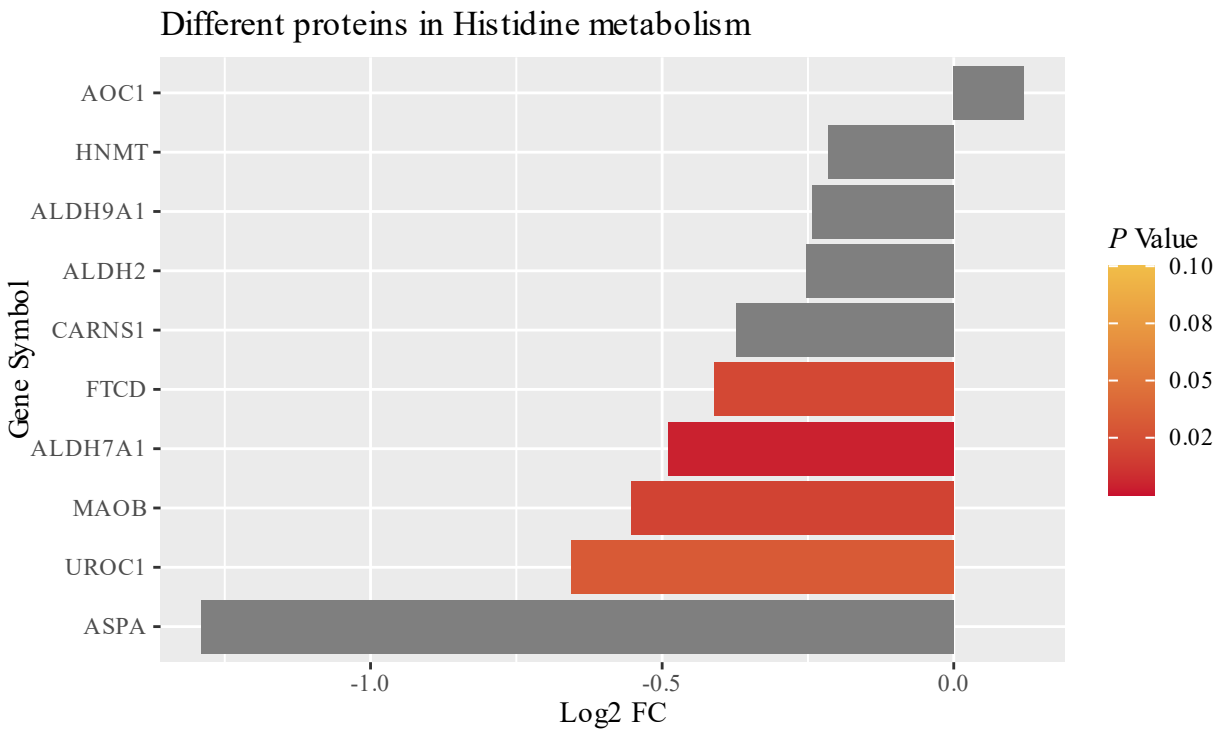

Figure 154. *Post hoc* analysis of proteins involved in histidine metabolism in liver abscess induction protocol (LAIP) relative to control (CON).

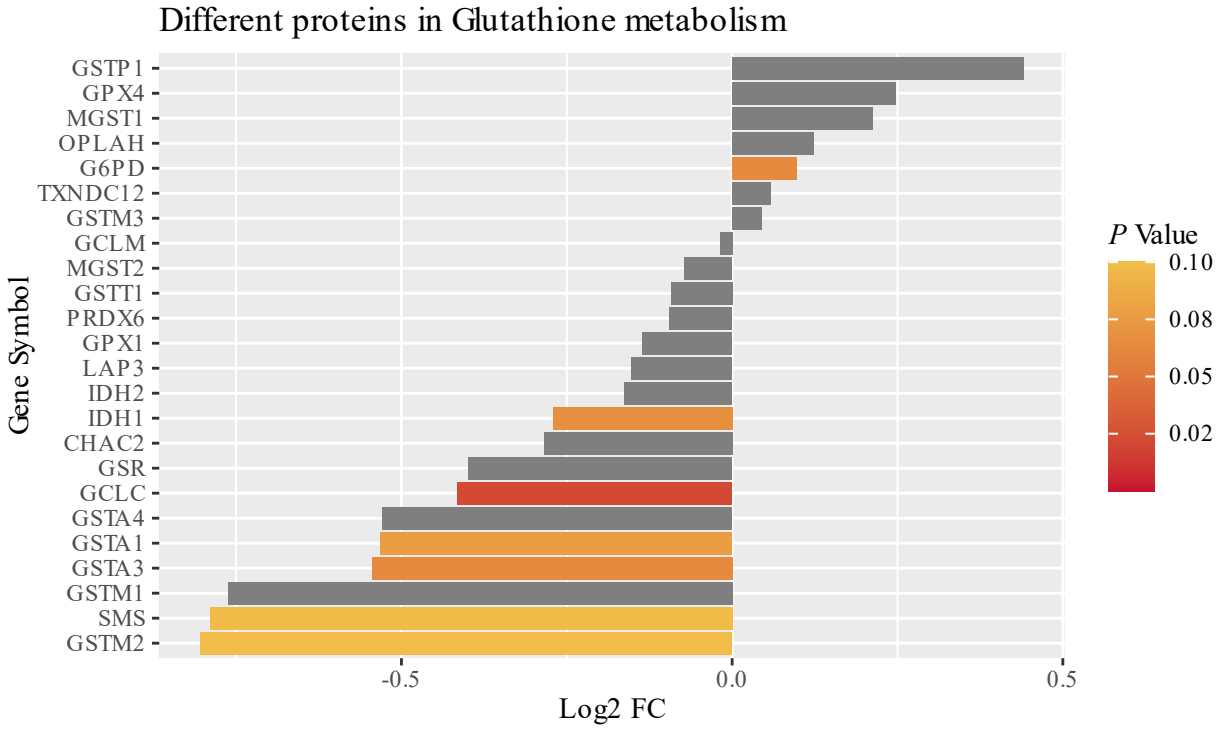

Figure 155. *Post hoc* analysis of proteins involved in glutathione metabolism in failed liver abscess (LAIP-N) relative to control (CON).

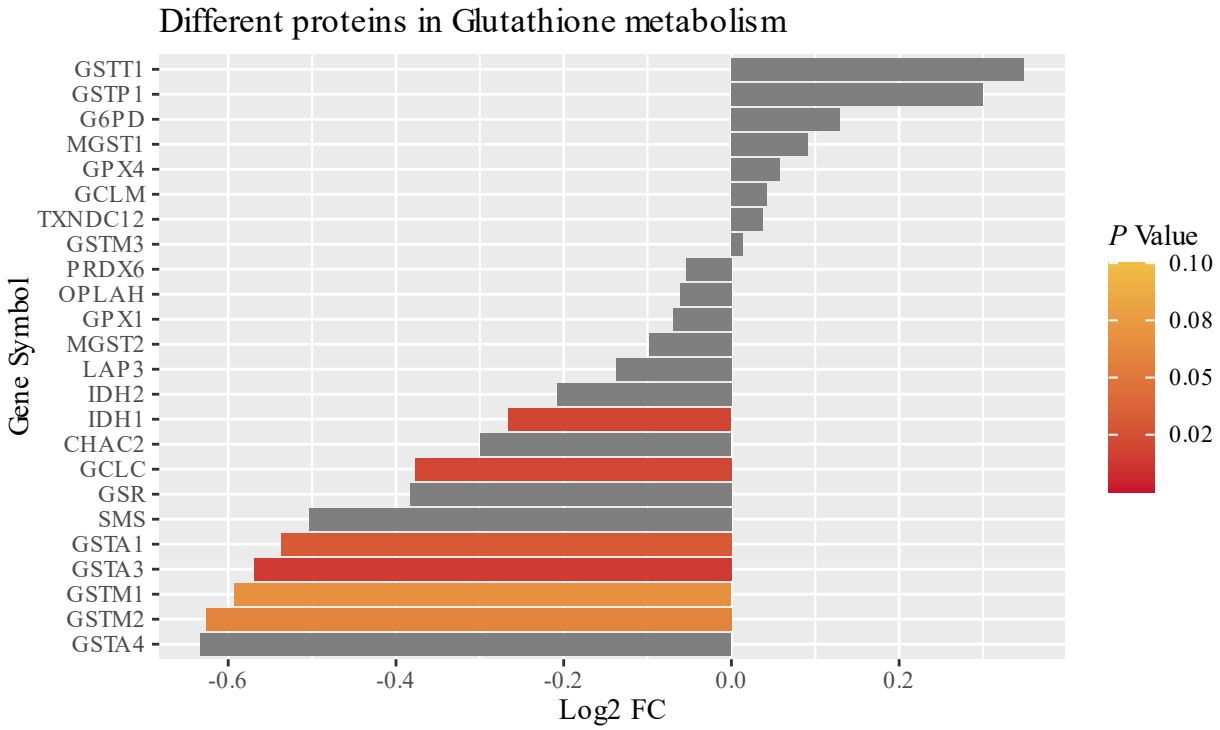

Figure 156. *Post hoc* analysis of proteins involved in glutathione metabolism in liver abscess induction protocol (LAIP) relative to control (CON).

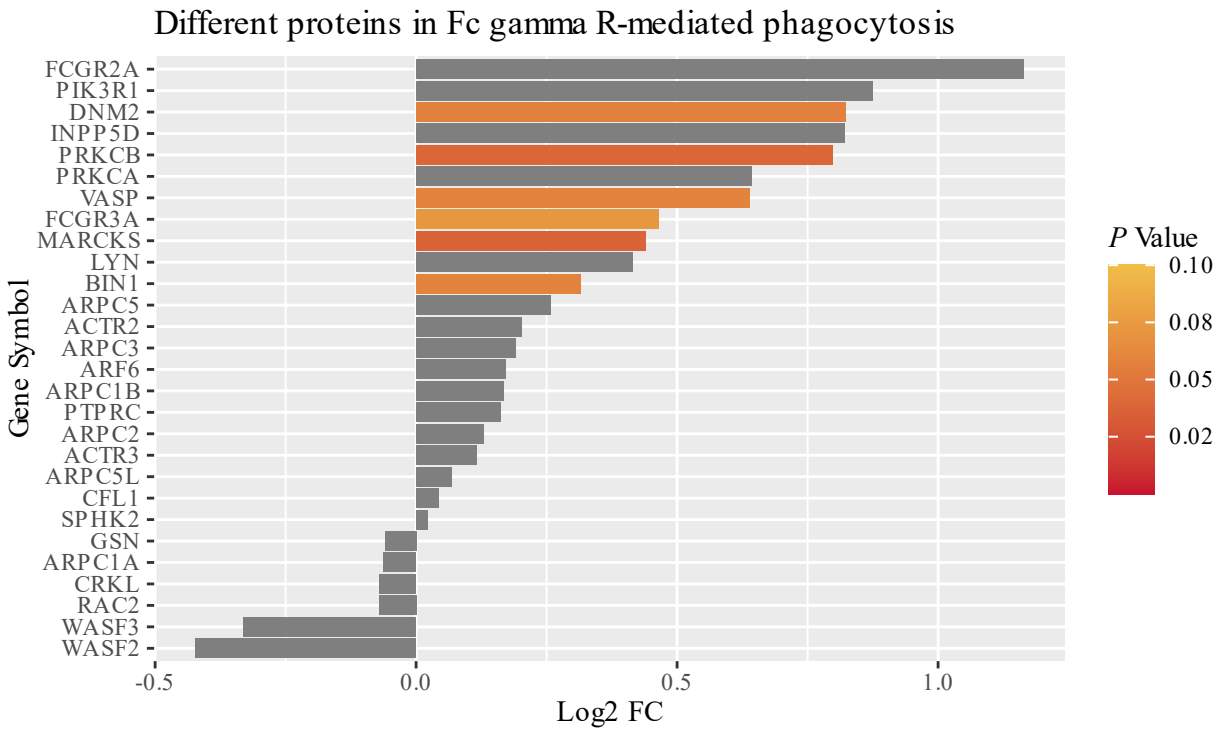

Figure 157. *Post hoc* analysis of proteins involved in Fc gamma R-mediated phagocytosis in successful liver abscess (LAIP-Y) relative to control (CON).

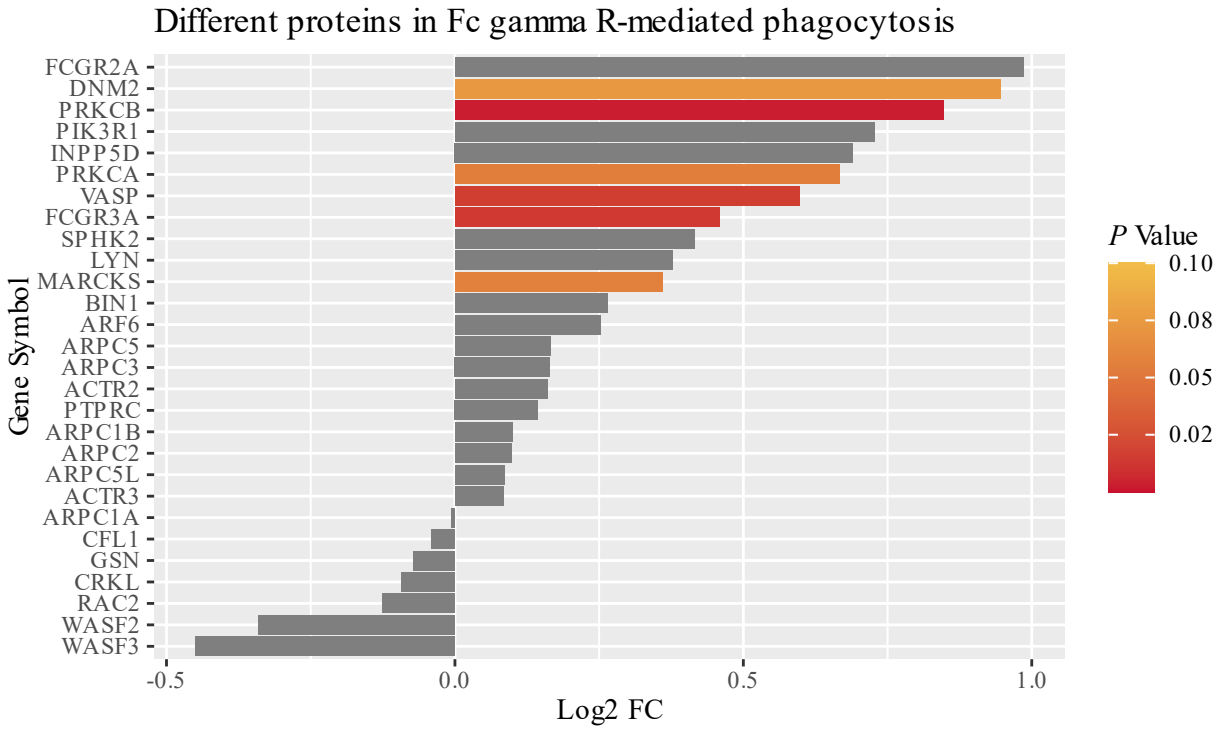

Figure 158. *Post hoc* analysis of proteins involved in Fc gamma R-mediated phagocytosis in liver abscess induction protocol (LAIP) relative to control (CON).

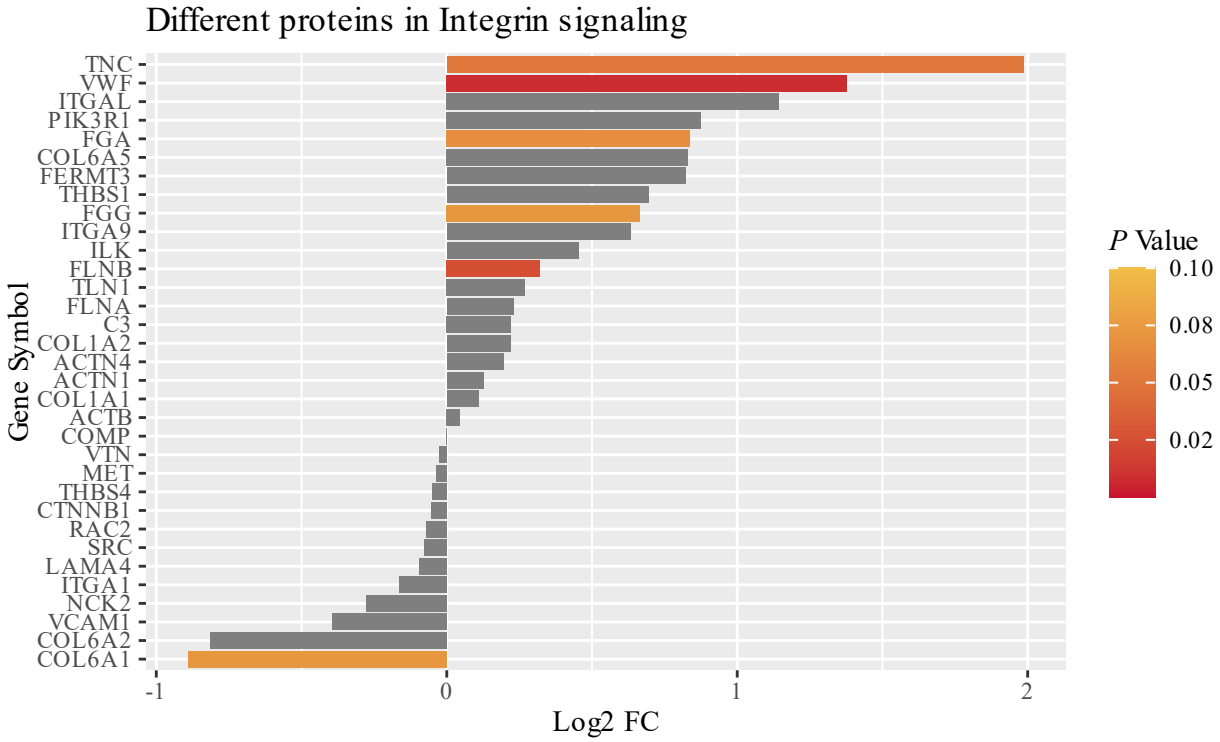

Figure 159. *Post hoc* analysis of proteins involved in integrin signaling in successful liver abscess (LAIP-Y) relative to control (CON).

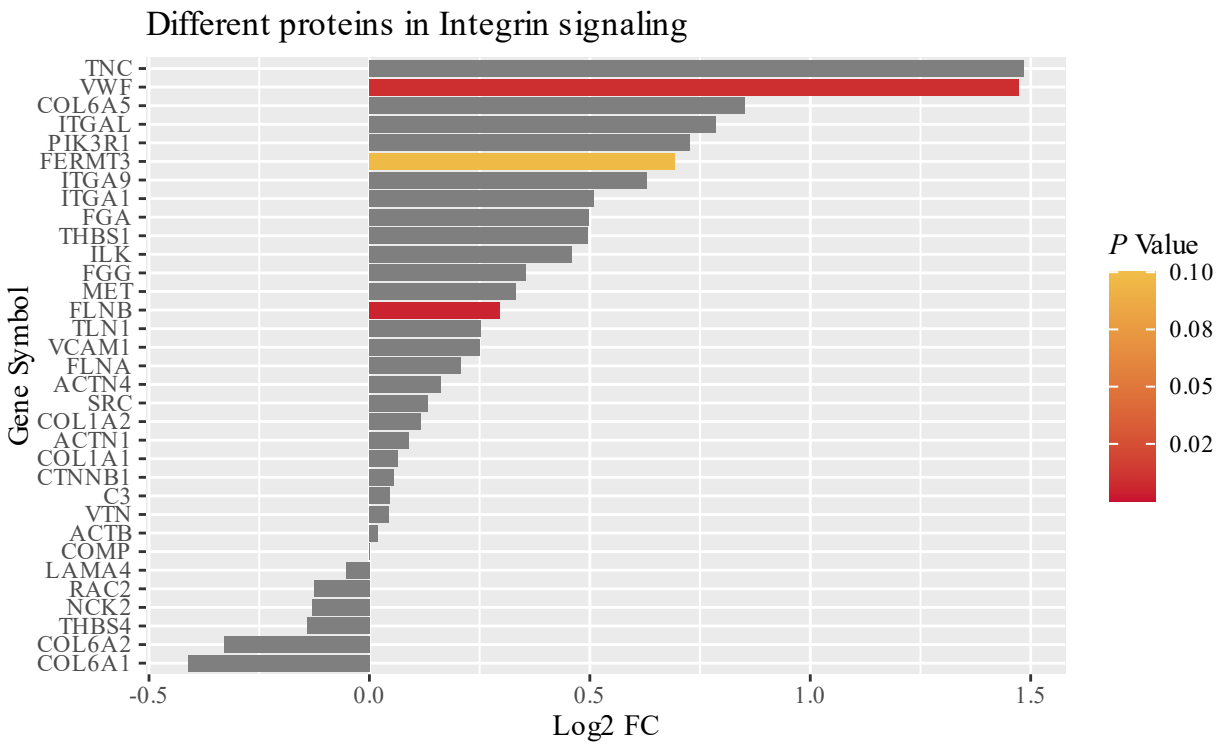

Figure 160. *Post hoc* analysis of proteins involved in integrin signaling in liver abscess induction protocol (LAIP) relative to control (CON).

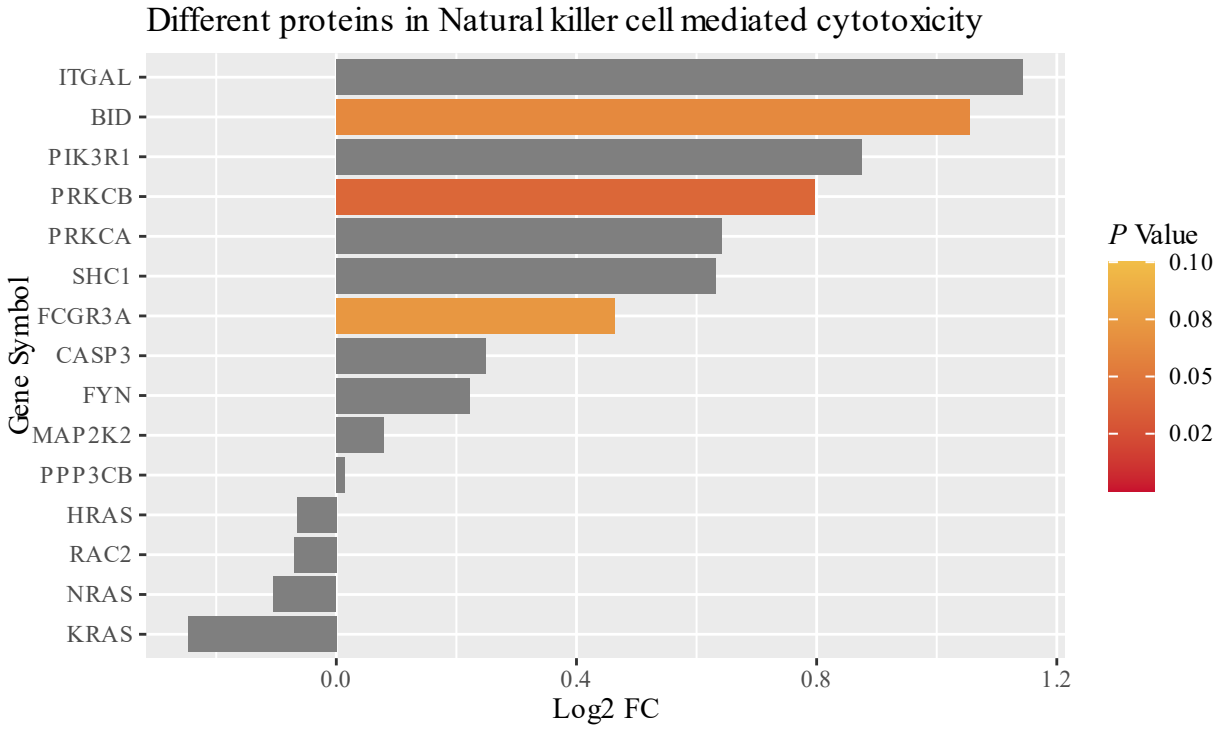

Figure 161. *Post hoc* analysis of proteins involved in natural killer cell mediated cytotoxicity in successful liver abscess (LAIP-Y) relative to control (CON).

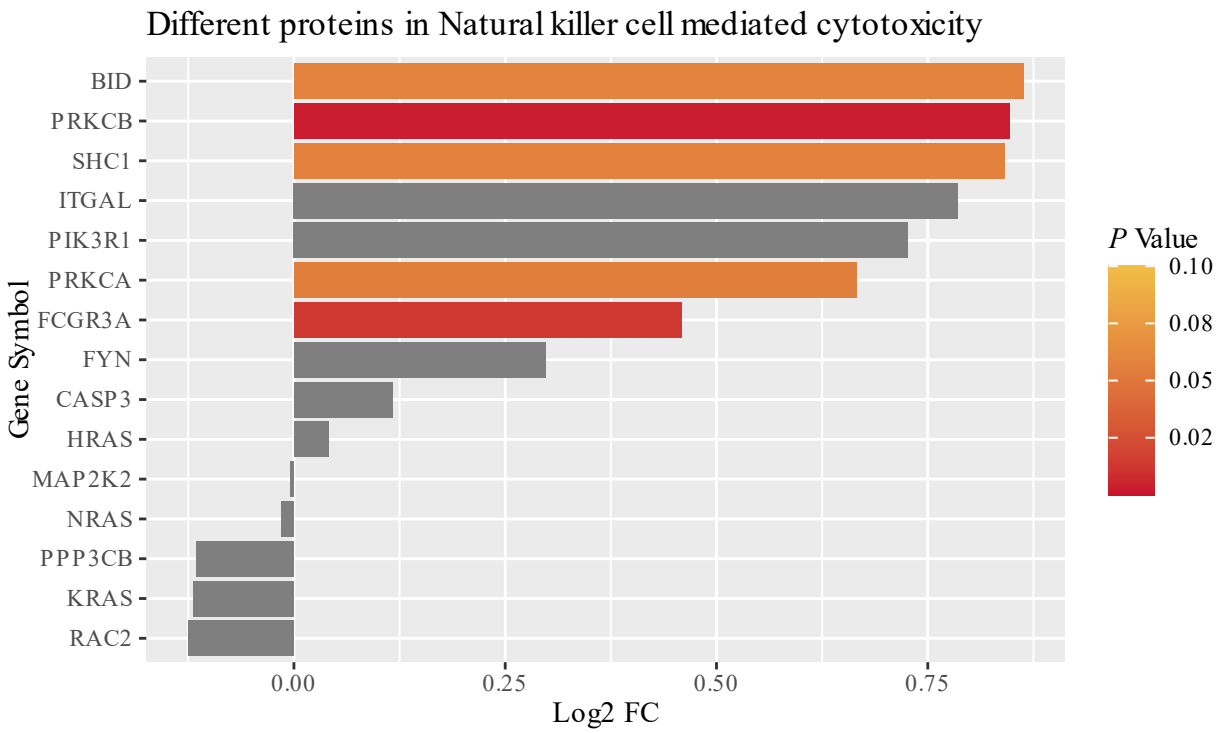

Figure 162. *Post hoc* analysis of proteins involved in natural killer cell mediated cytotoxicity in liver abscess induction protocol (LAIP) relative to control (CON).

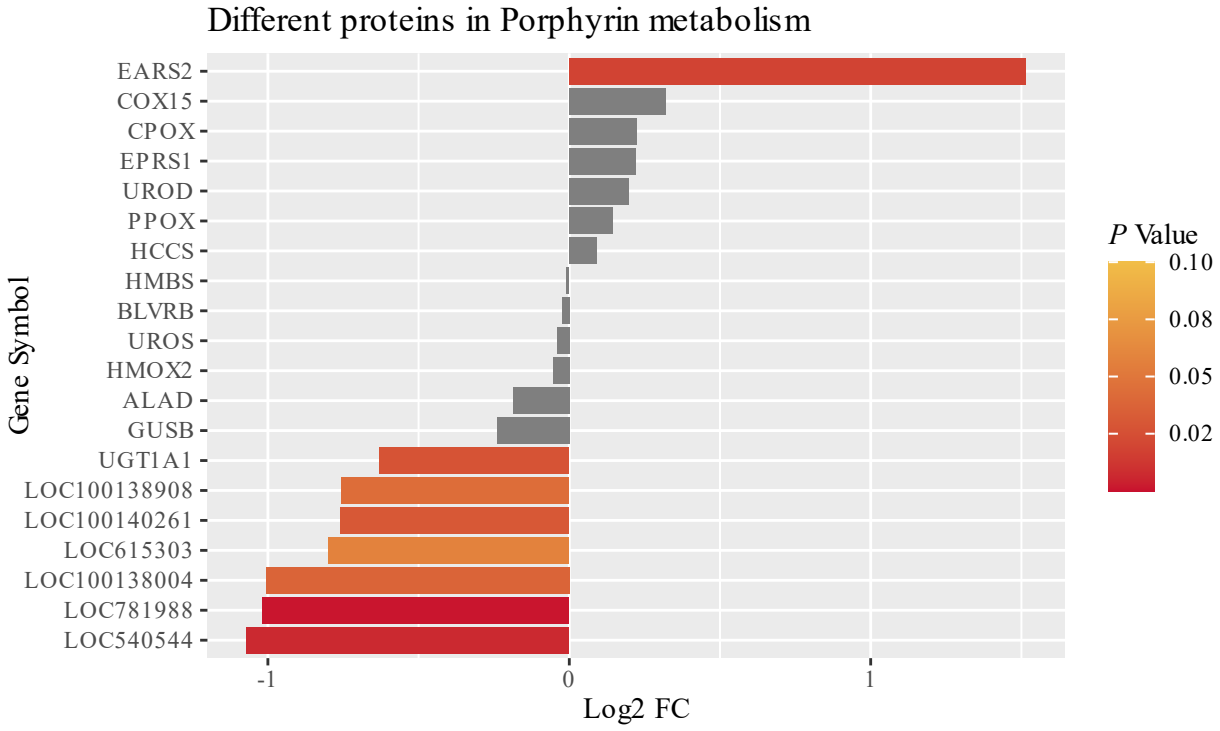

Figure 163. *Post hoc* analysis of proteins involved in porphyrin metabolism in successful liver abscess (LAIP-Y) relative to control (CON).

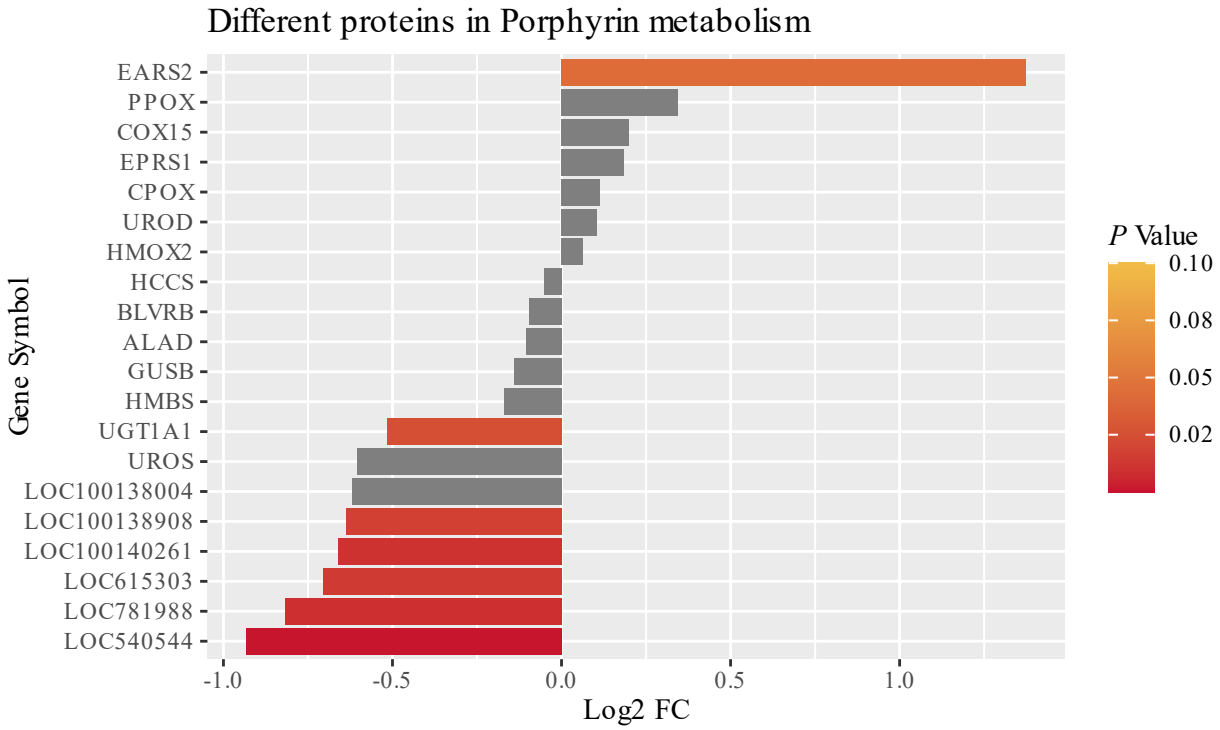

Figure 164. *Post hoc* analysis of proteins involved in porphyrin metabolism in liver abscess induction protocol (LAIP) relative to control (CON).

Figure 165. *Post hoc* analysis of proteins involved in fatty acid degradation in successful liver abscess (LAIP-Y) relative to control (CON).

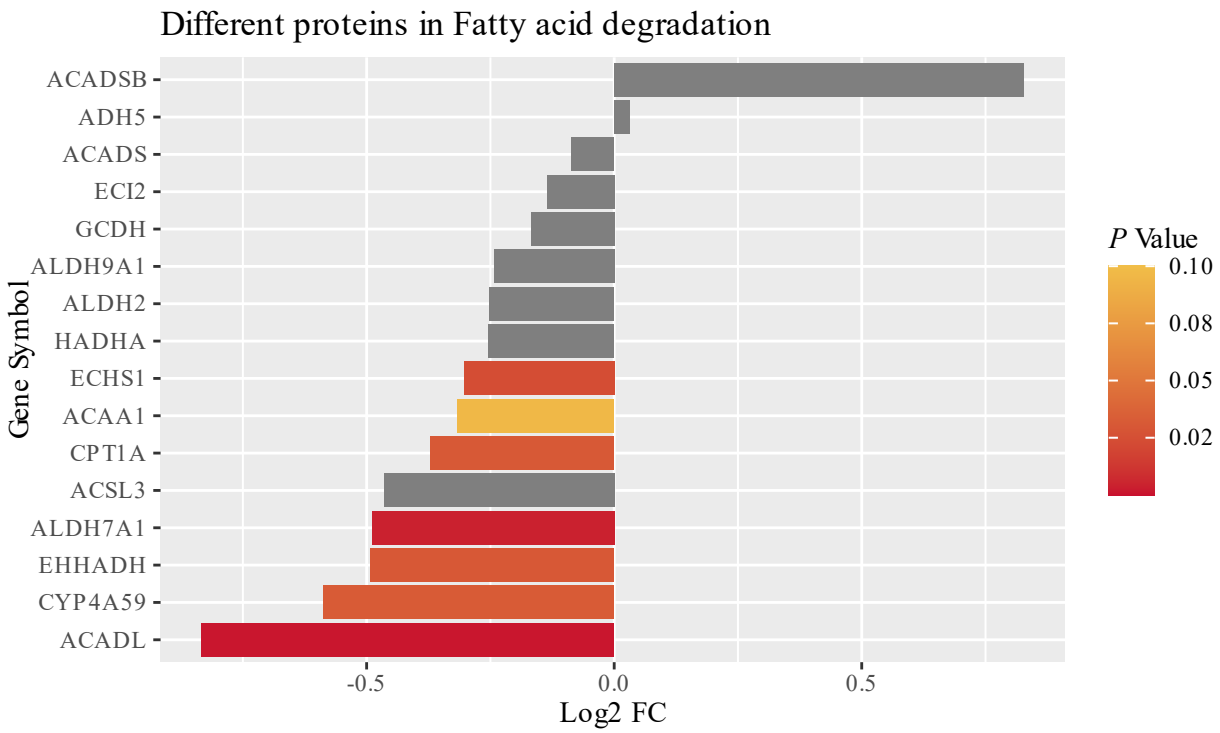

Figure 166. *Post hoc* analysis of proteins involved in fatty acid degradation in liver abscess induction protocol (LAIP) relative to control (CON).

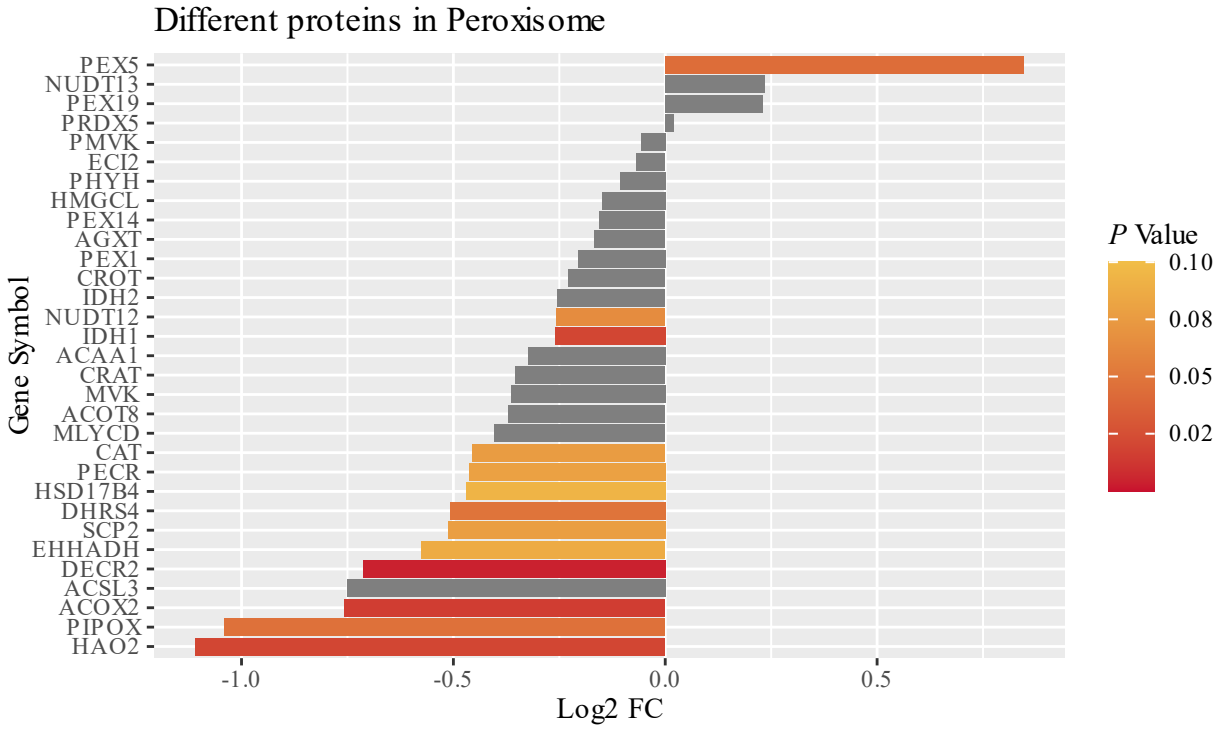

Figure 167. *Post hoc* analysis of proteins involved in peroxisome in successful liver abscess (LAIP-Y) relative to control (CON).

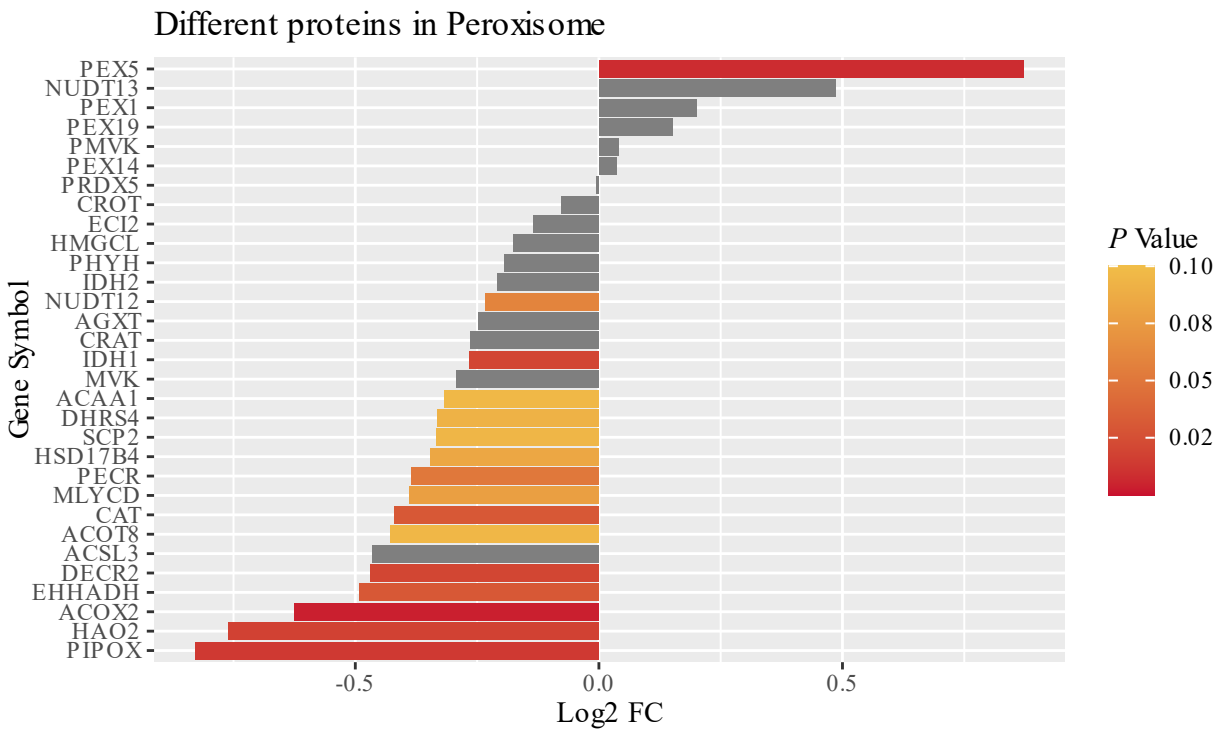

Figure 168. *Post hoc* analysis of proteins involved in peroxisome in liver abscess induction protocol (LAIP) relative to control (CON).

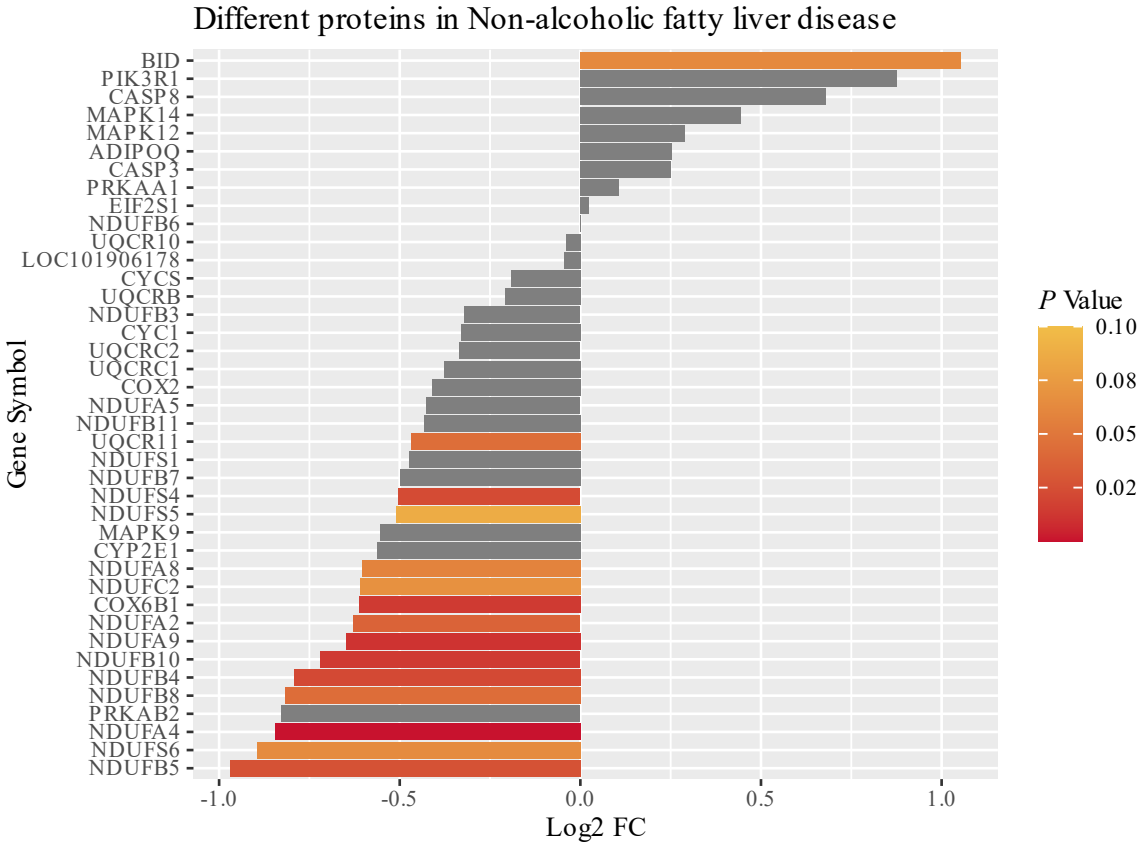

Figure 169. *Post hoc* analysis of proteins involved in non-alcoholic fatty liver disease in successful liver abscess (LAIP-Y) relative to control (CON).

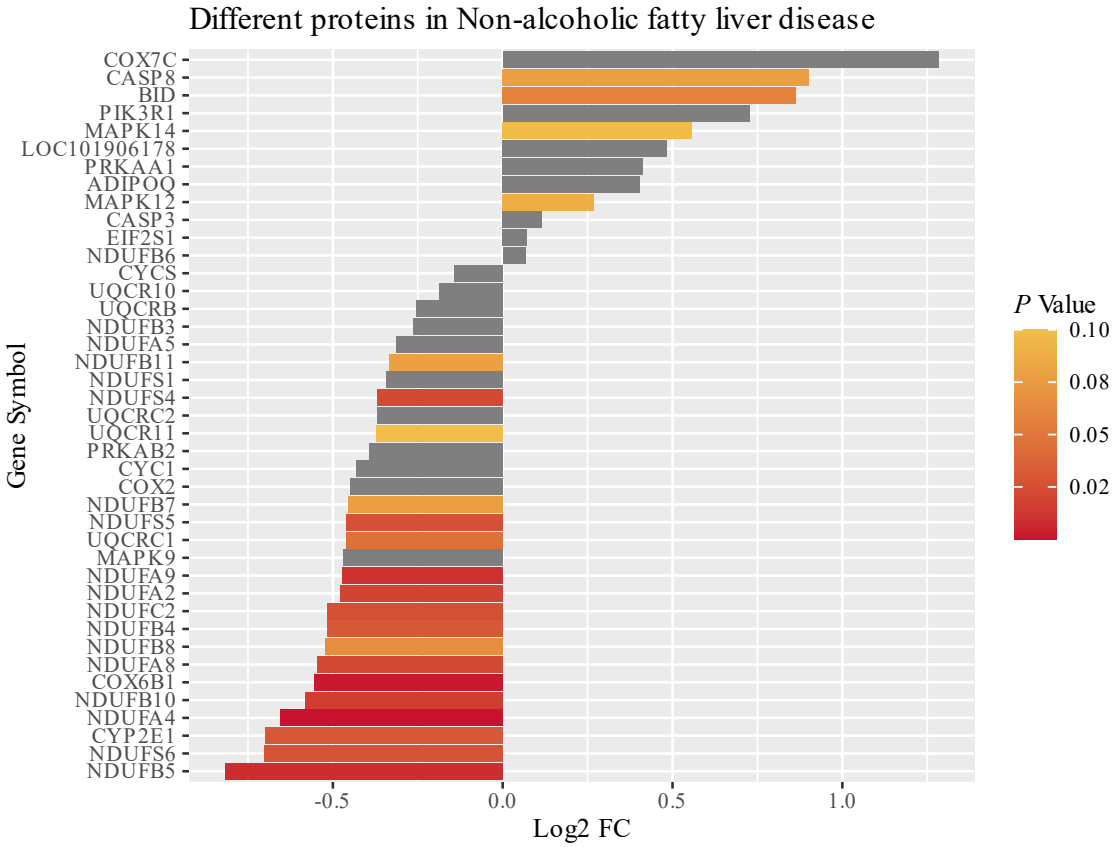

Figure 170. *Post hoc* analysis of proteins involved in non-alcoholic fatty liver disease in liver abscess induction protocol (LAIP) relative to control (CON).

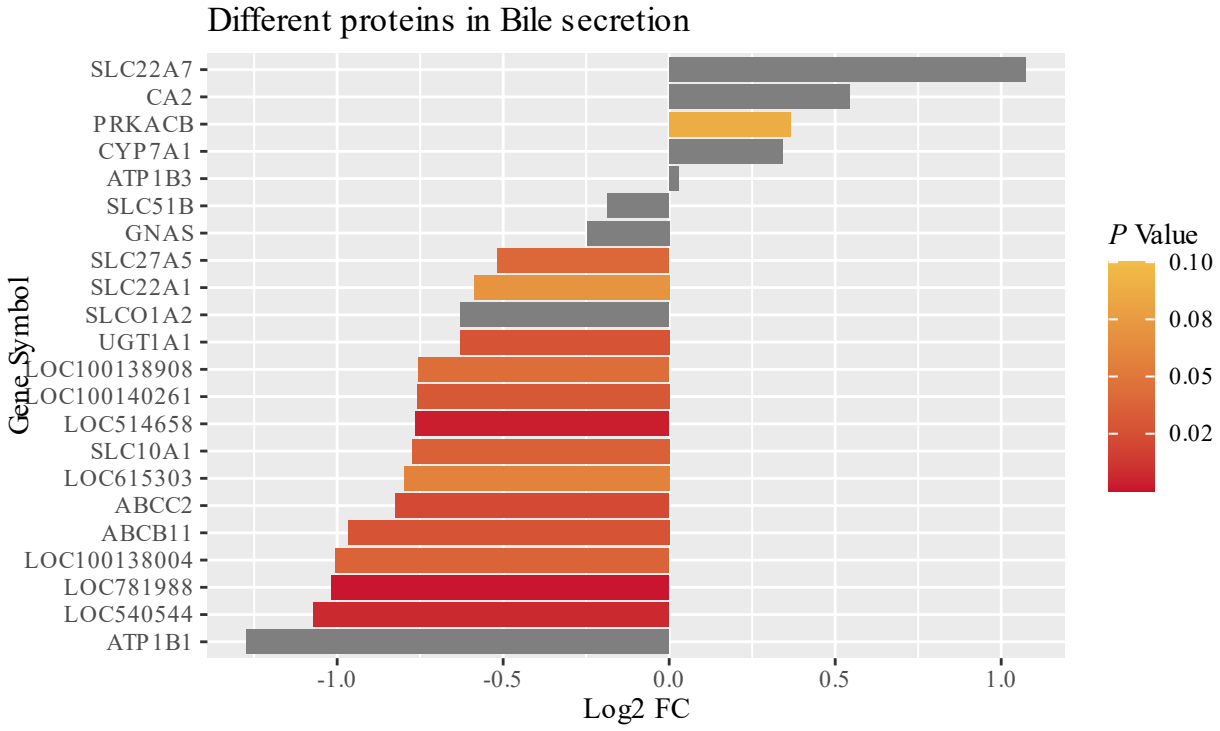

Figure 171. *Post hoc* analysis of proteins involved in bile secretion in successful liver abscess (LAIP-Y) relative to control (CON).

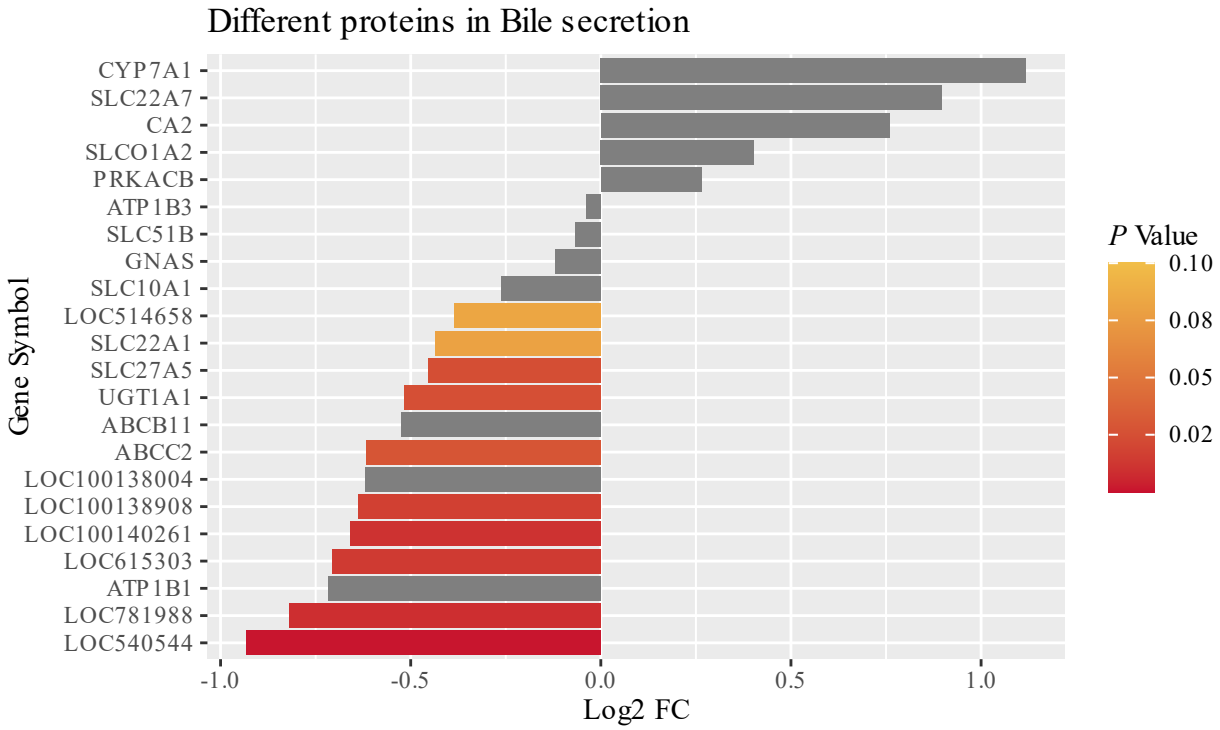

Figure 172. *Post hoc* analysis of proteins involved in bile secretion in liver abscess induction protocol (LAIP) relative to control (CON).

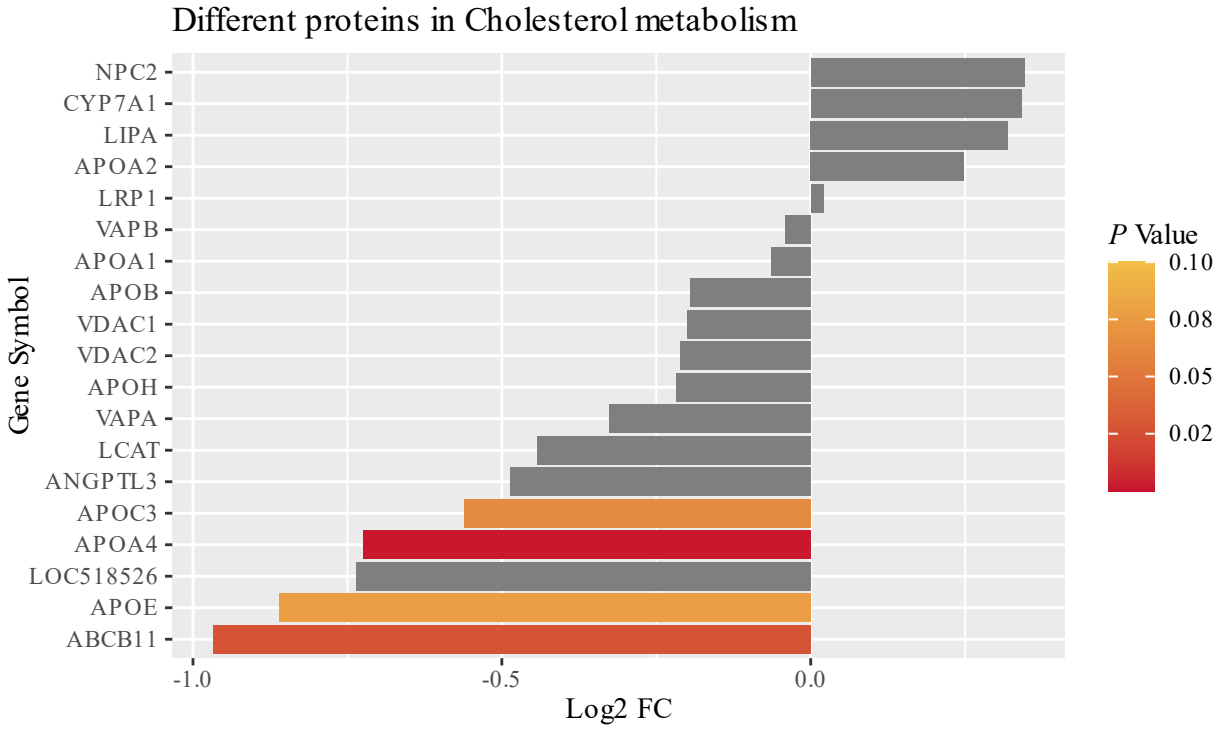

Figure 173. *Post hoc* analysis of proteins involved in cholesterol metabolism in successful liver abscess (LAIP-Y) relative to control (CON).

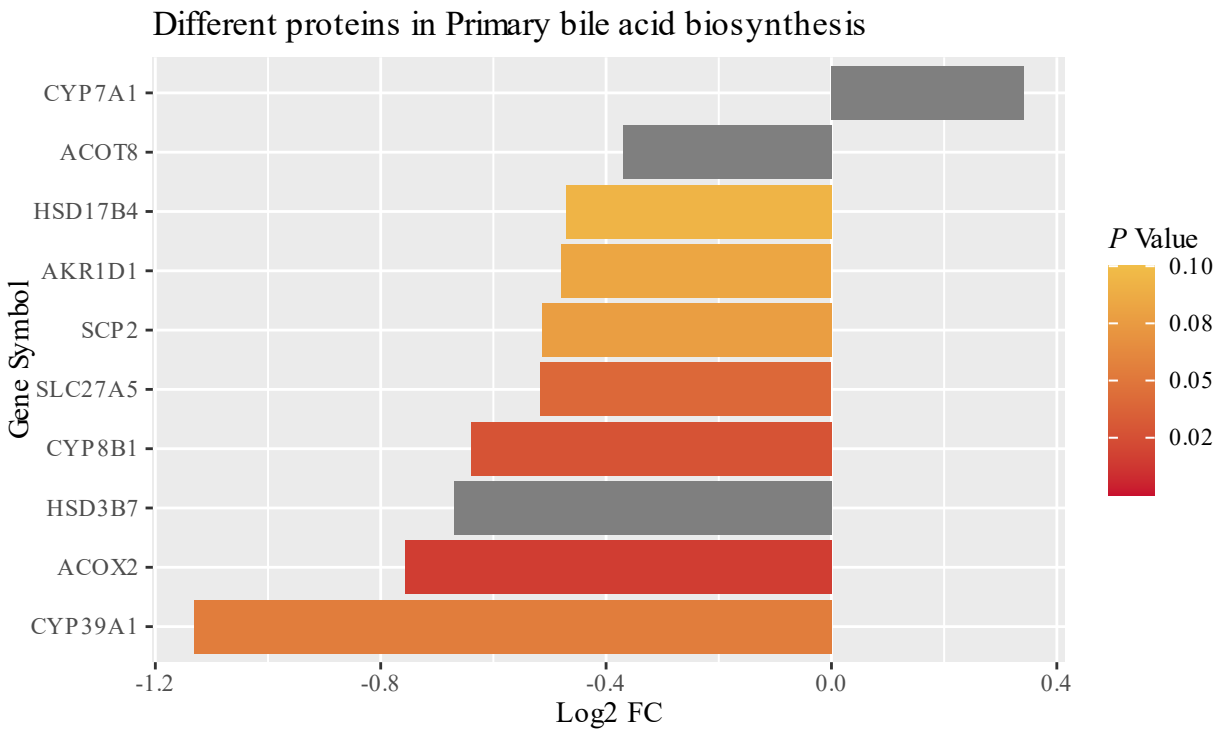

Figure 174. *Post hoc* analysis of proteins involved in primary bile acid synthesis in successful liver abscess (LAIP-Y) relative to control (CON).

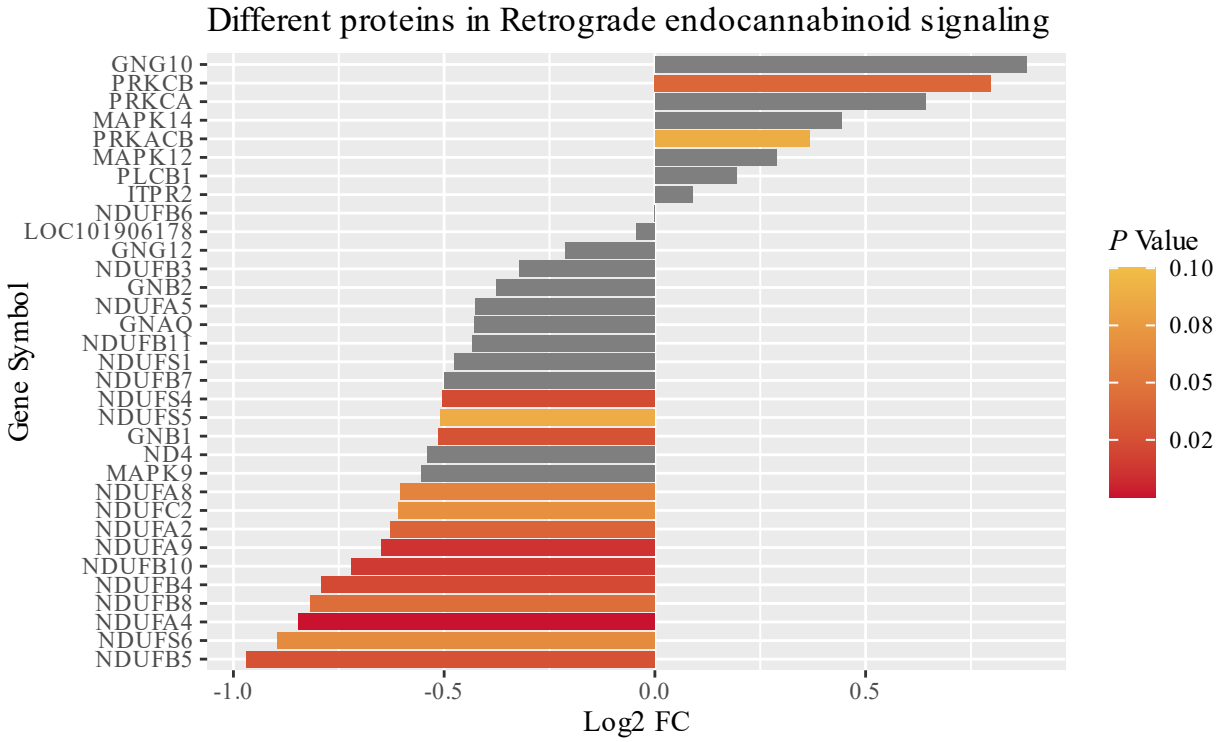

Figure 175. *Post hoc* analysis of proteins involved in retrograde endocannabinoid signaling in successful liver abscess (LAIP-Y) relative to control (CON).

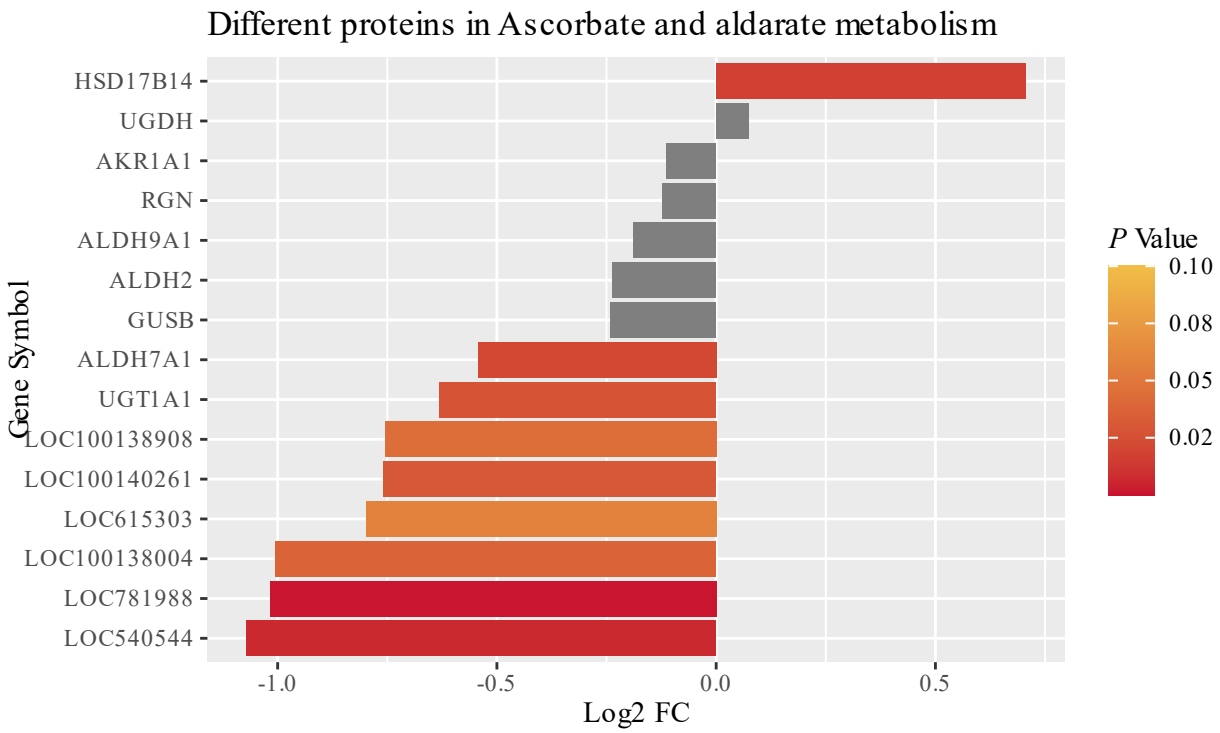

Figure 176. *Post hoc* analysis of proteins involved in ascorbate and aldarate metabolism in successful liver abscess (LAIP-Y) relative to control (CON).

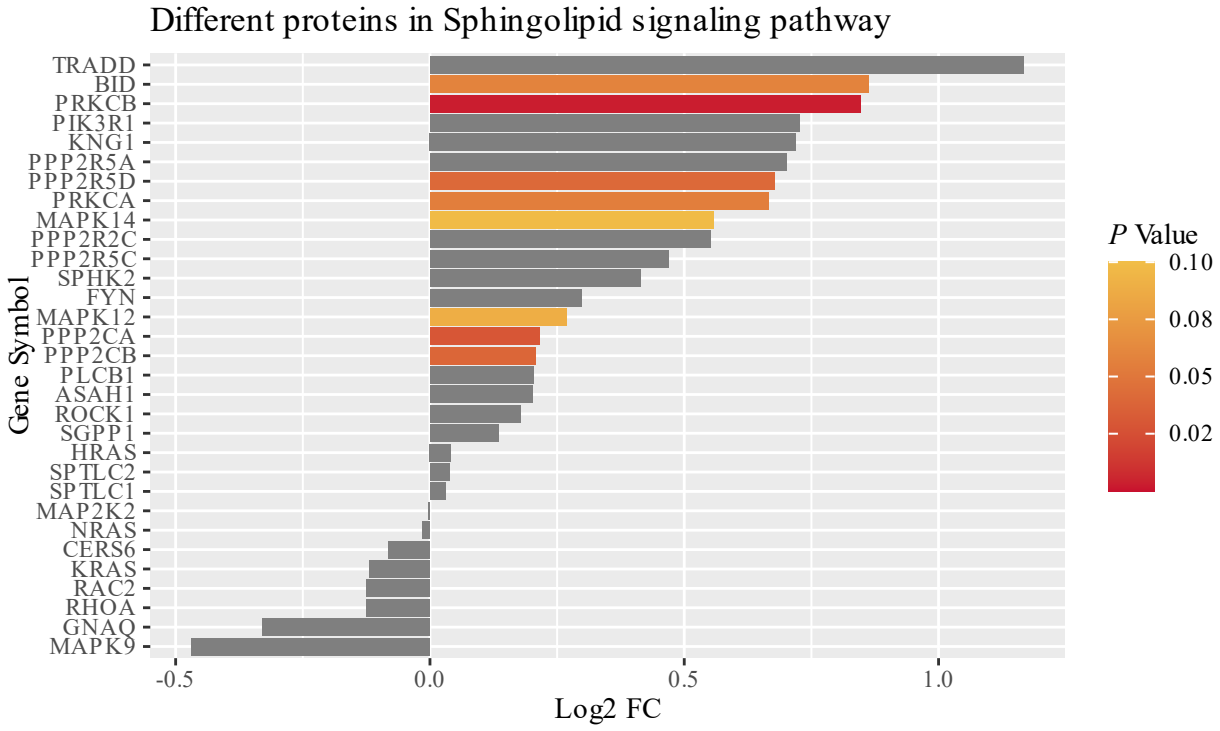

Figure 177. *Post hoc* analysis of proteins involved in sphingolipid signaling pathway in liver abscess induction protocol (LAIP) relative to control (CON).

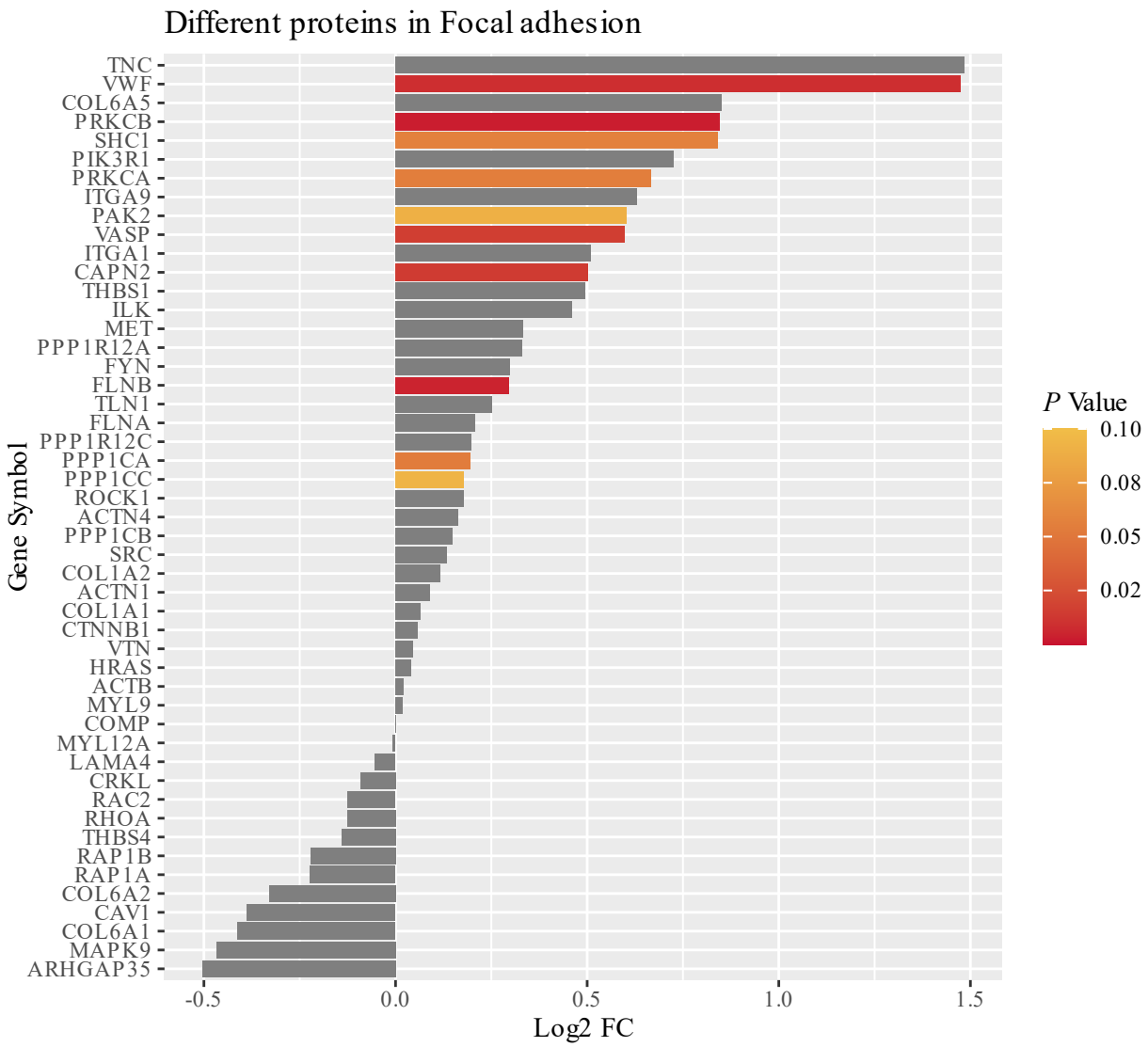

Figure 178. *Post hoc* analysis of proteins involved in focal adhesion in liver abscess induction protocol (LAIP) relative to control (CON).

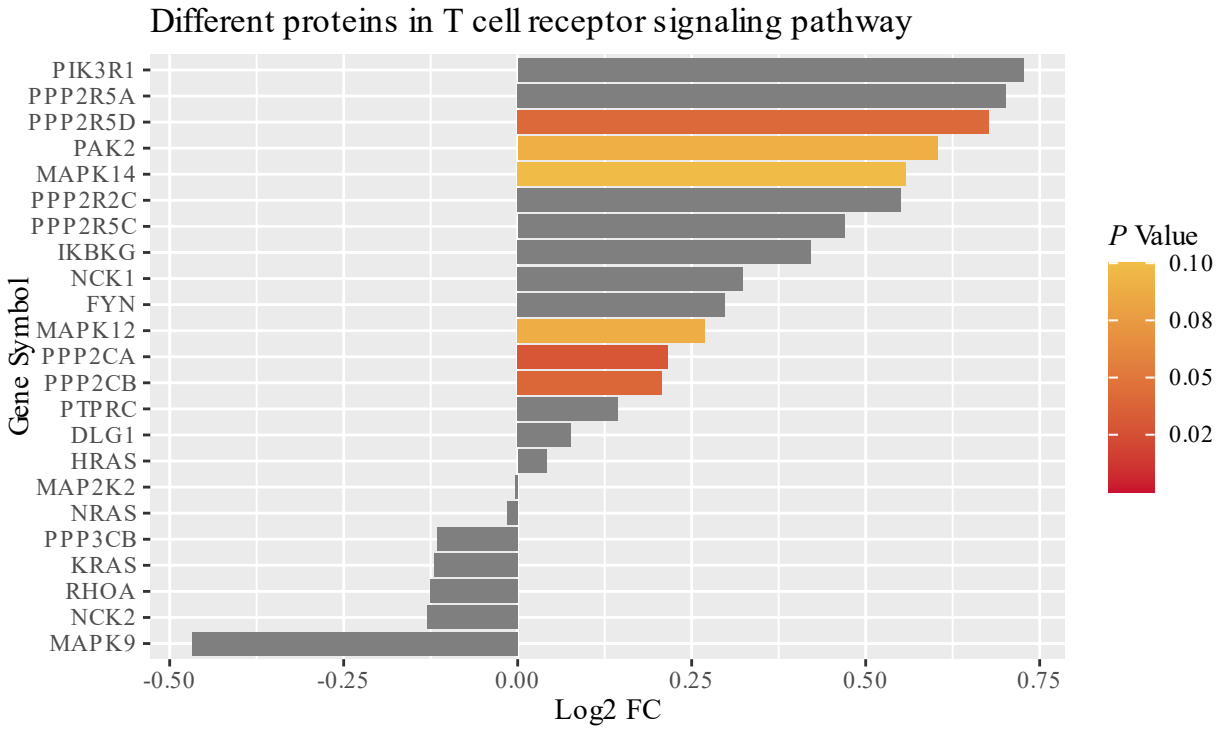

Figure 179. *Post hoc* analysis of proteins involved in T cell receptor signaling pathway in liver abscess induction protocol (LAIP) relative to control (CON).

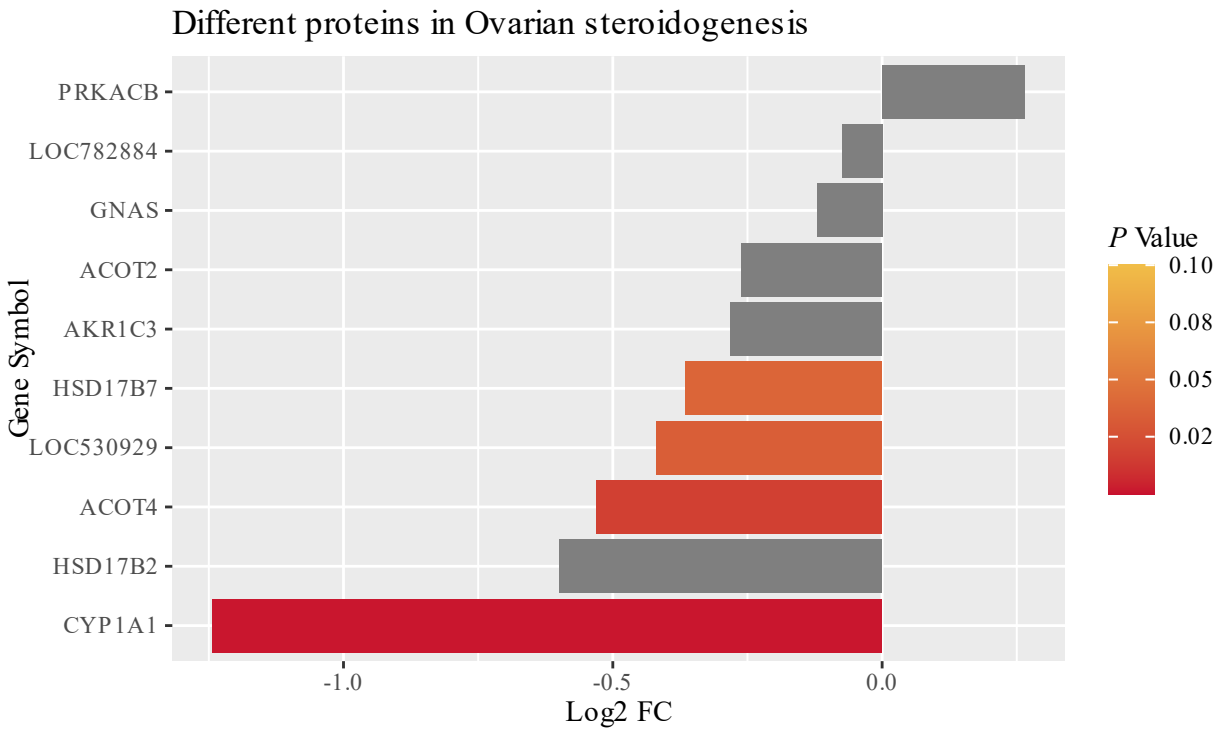

Figure 180. *Post hoc* analysis of proteins involved in ovarian steroidogenesis in liver abscess induction protocol (LAIP) relative to control (CON).

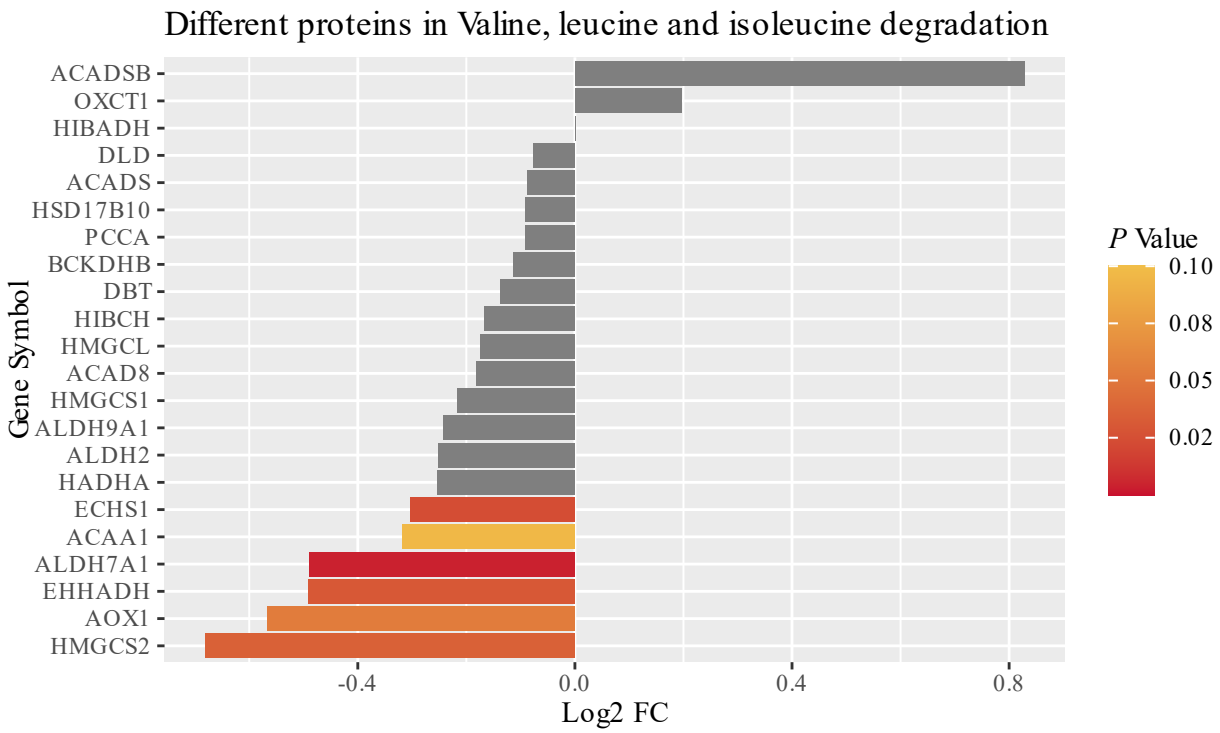

Figure 181. *Post hoc* analysis of proteins involved in valine, leucine, and isoleucine degradation in liver abscess induction protocol (LAIP) relative to control (CON).

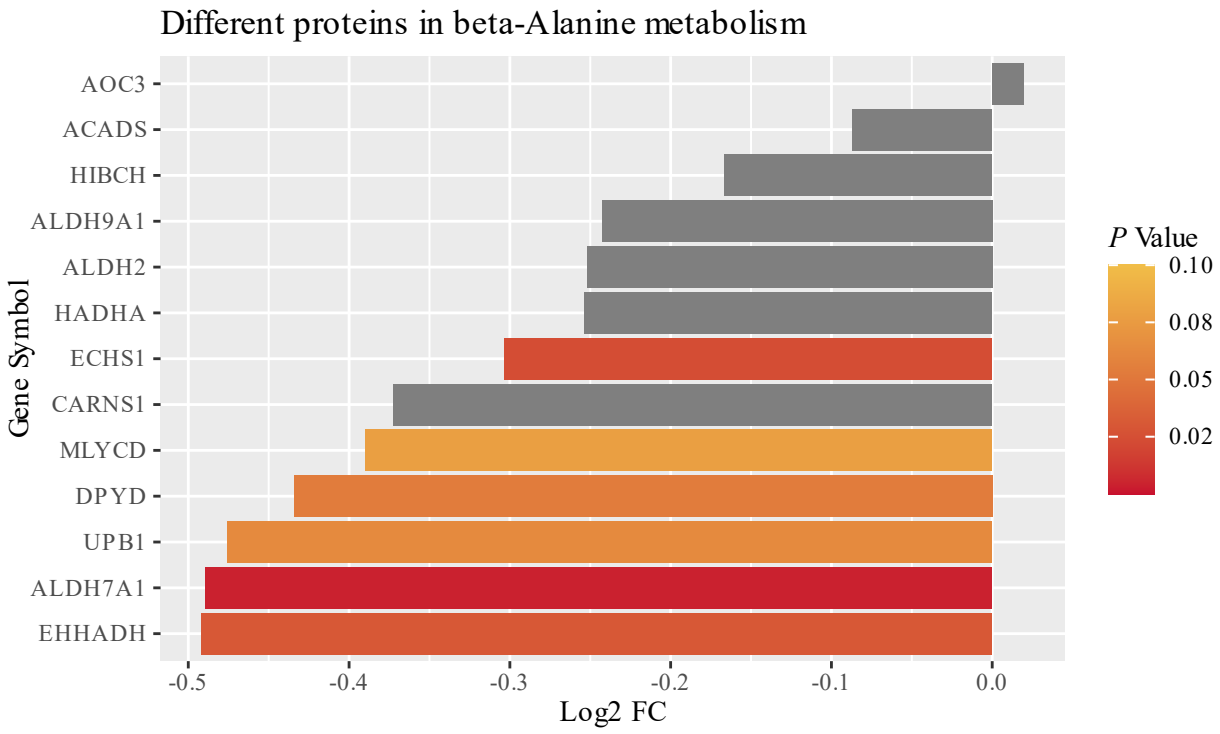

Figure 182. *Post hoc* analysis of proteins involved in β-alanine metabolism in liver abscess induction protocol (LAIP) relative to control (CON).

Liver Abscess Induction Model
Study Number: GJC-LHB-3

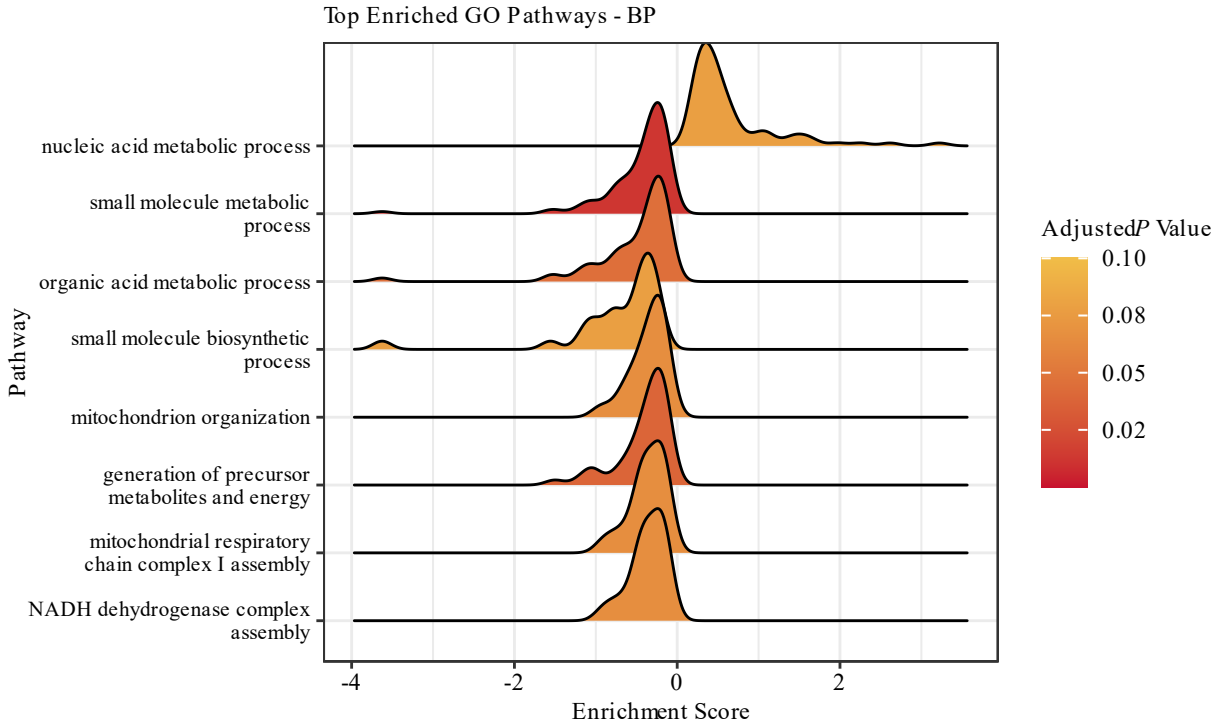

Figure 183. *Post hoc* ridge plot of enriched gene ontology biological process pathways in failed liver abscess induction (LAIP-N) relative to control (CON). Results limited to ≥4 proteins in core enrichment.

Liver Abscess Induction Model
Study Number: GJC-LHB-3

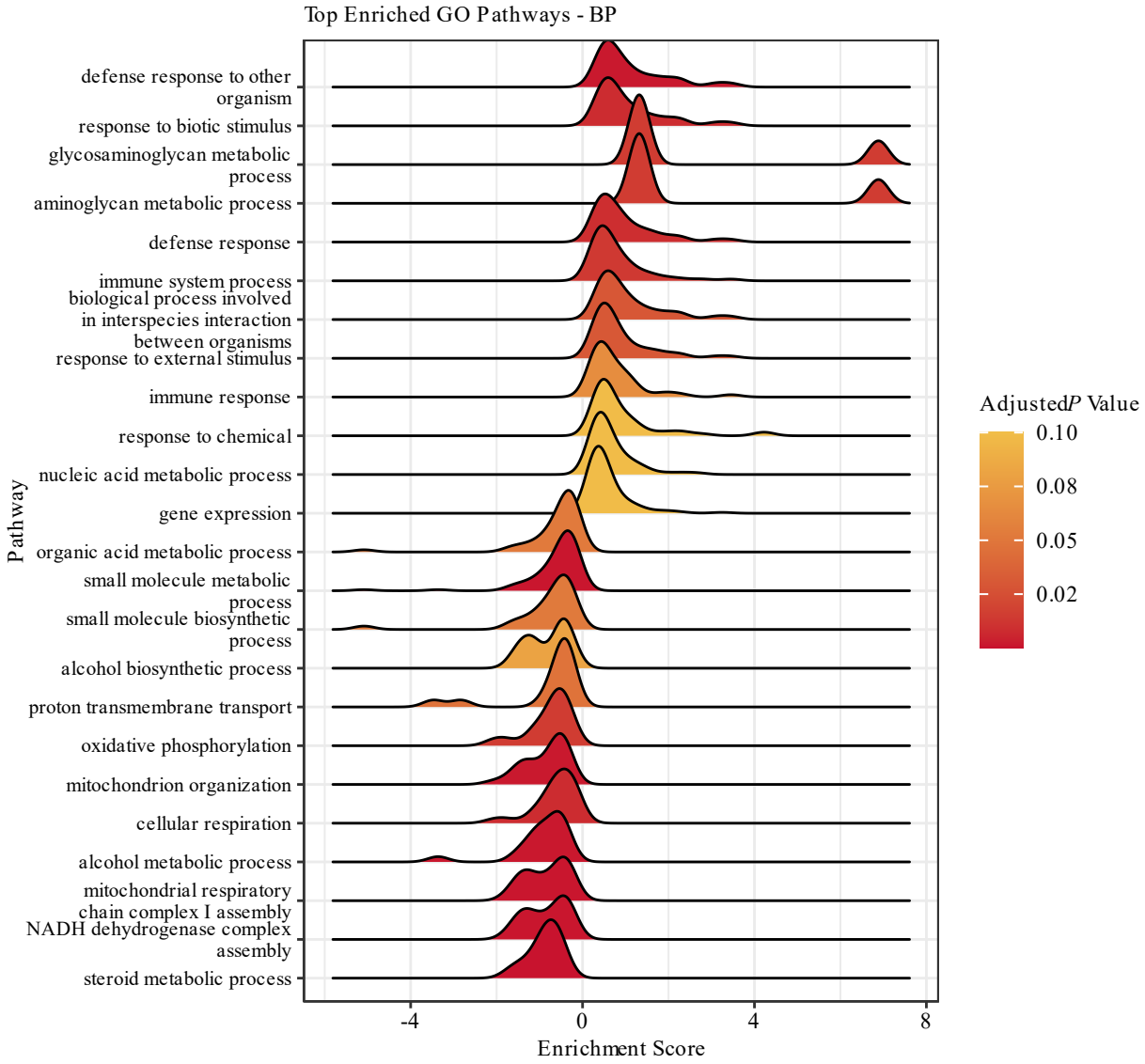

Figure 184. *Post hoc* ridge plot of enriched gene ontology biological process pathways in successful liver abscess induction (LAIP-Y) relative to control (CON). Results limited to ≥4 proteins in core enrichment.

Liver Abscess Induction Model
Study Number: GJC-LHB-3

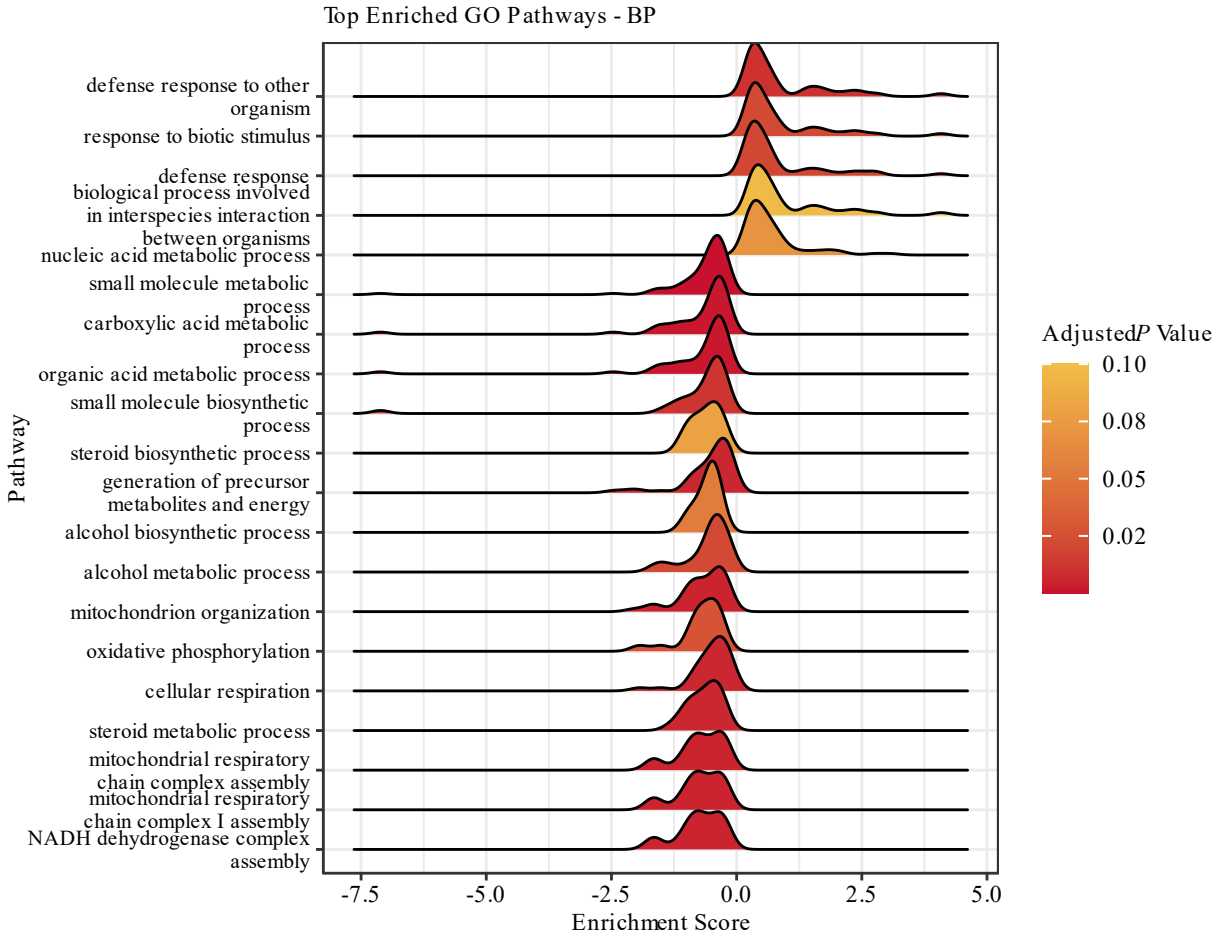

Figure 185. *Post hoc* ridge plot of enriched gene ontology biological process pathways in successful liver abscess induction protocol (LAIP-Y) relative to control (CON). Results limited to ≥4 proteins in core enrichment.

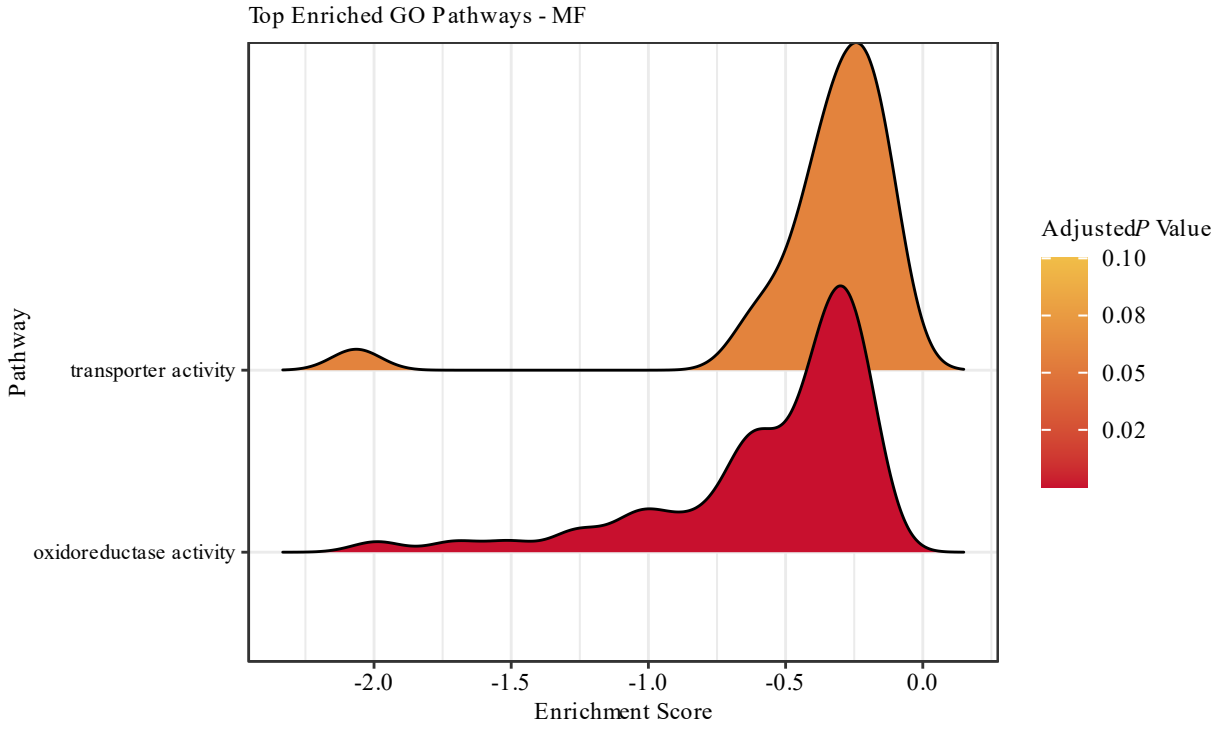

Figure 186. *Post hoc* ridge plot of enriched gene ontology molecular function pathways in failed liver abscess induction (LAIP-N) relative to control (CON). Results limited to ≥4 proteins in core enrichment.

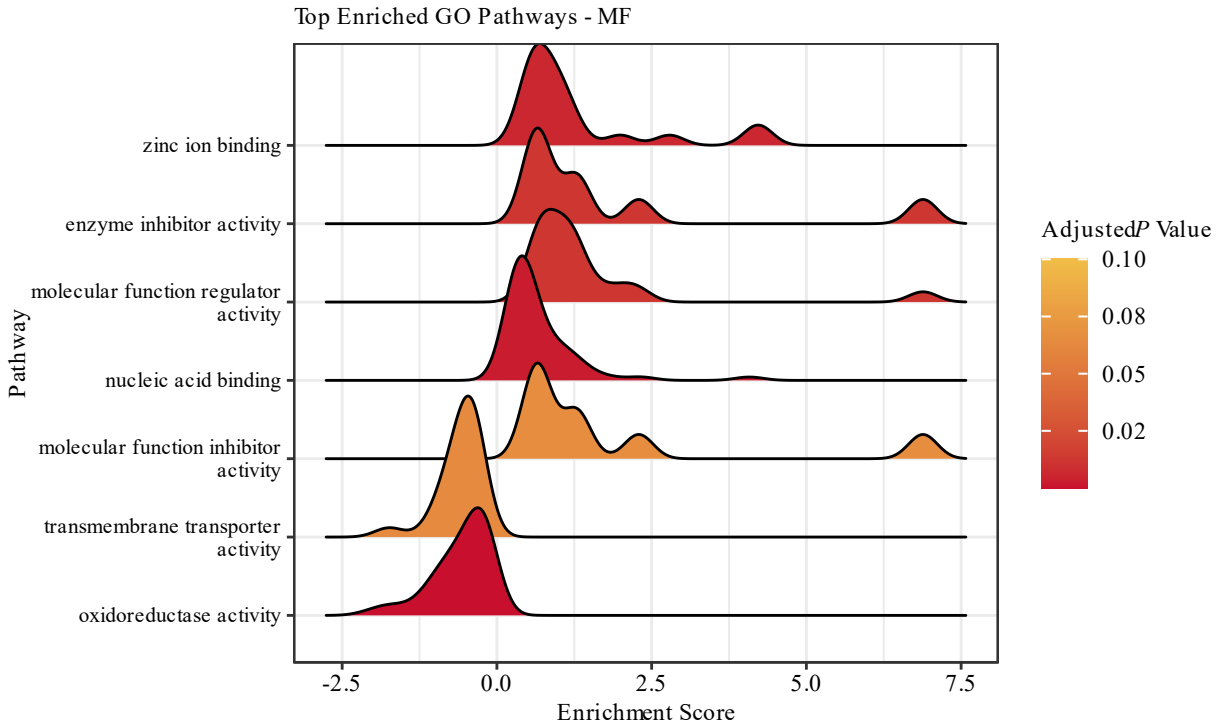

Figure 187. *Post hoc* ridge plot of enriched gene ontology molecular function pathways in successful liver abscess induction (LAIP-Y) relative to control (CON). Results limited to ≥4 proteins in core enrichment.

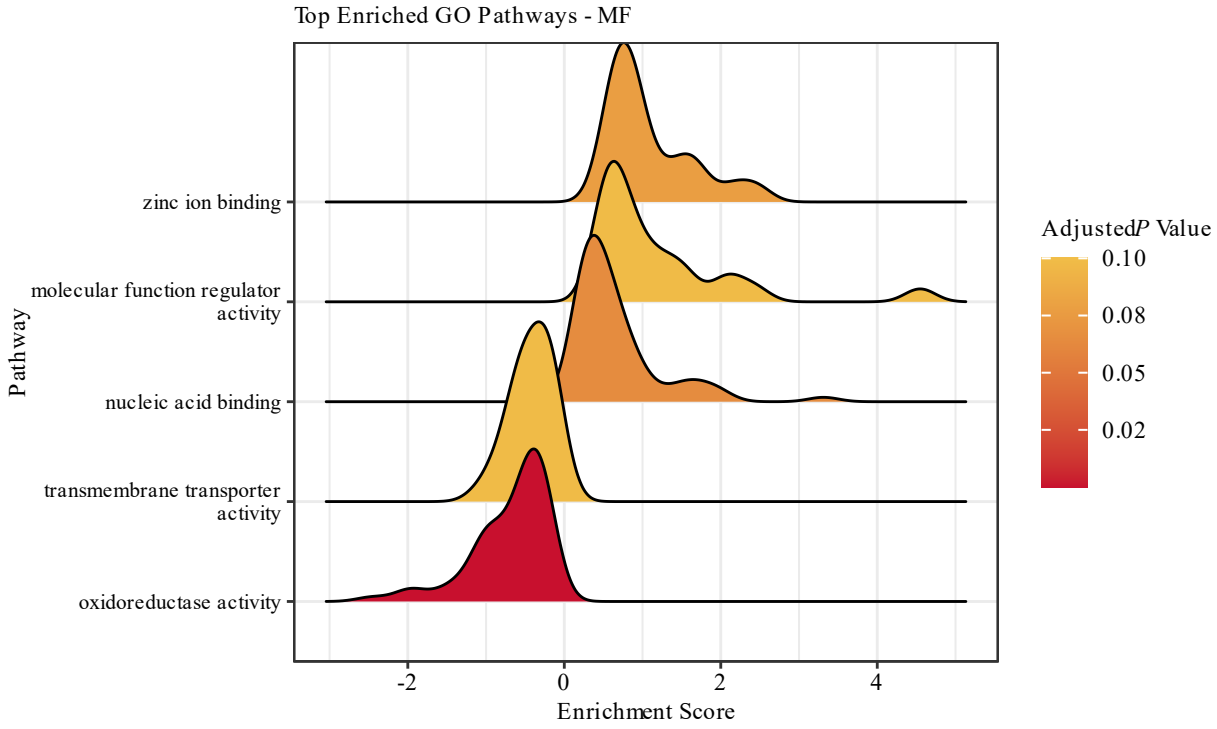

Figure 188. *Post hoc* ridge plot of enriched gene ontology molecular function pathways in successful liver abscess induction protocol (LAIP) relative to control (CON). Results limited to ≥4 proteins in core enrichment.

Liver Abscess Induction Model
Study Number: GJC-LHB-3

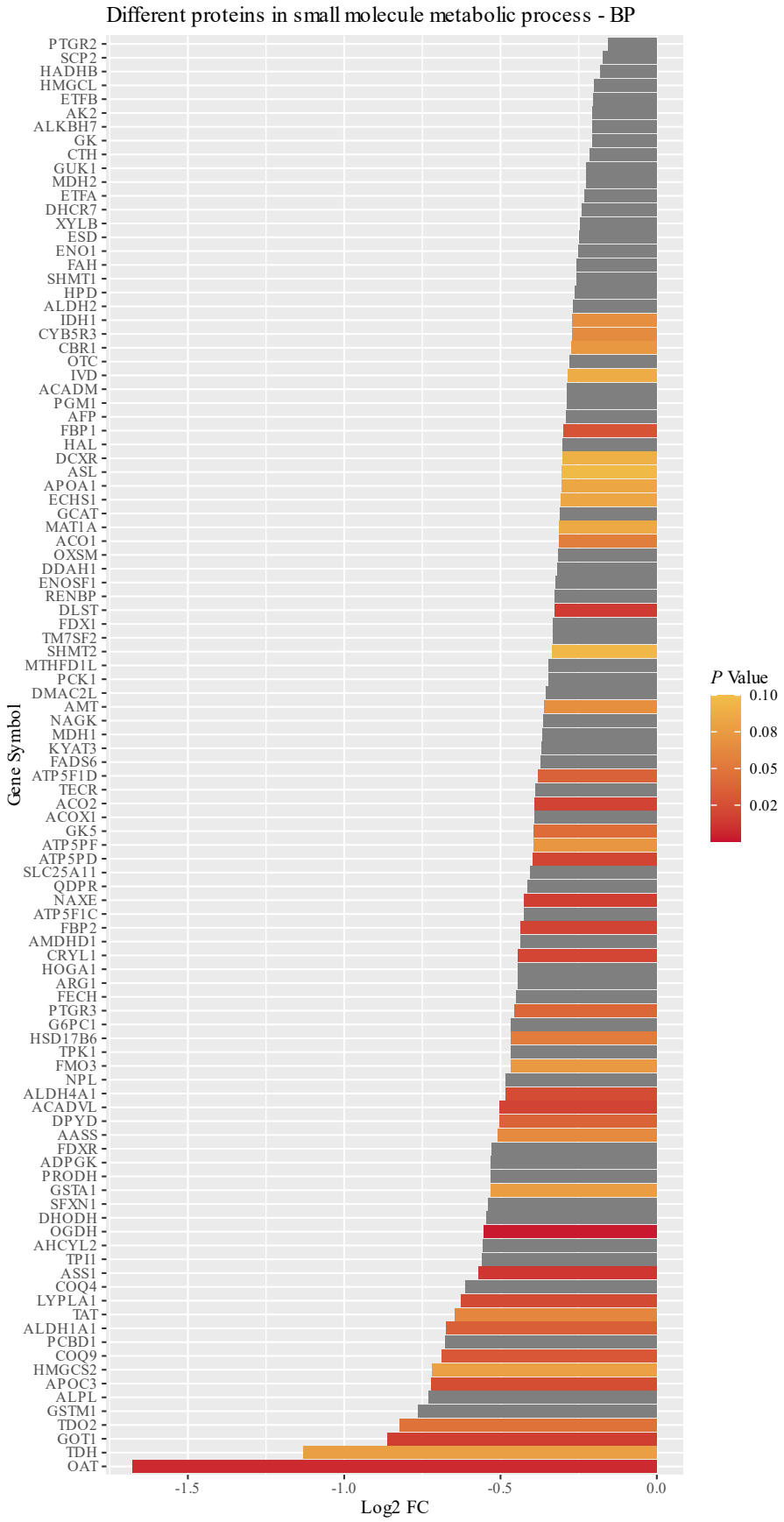

Figure 189. *Post hoc* analysis of proteins involved in small molecule metabolic process pathway in failed liver abscess induction (LAIP-N) relative to control (CON).

Liver Abscess Induction Model
Study Number: GJC-LHB-3

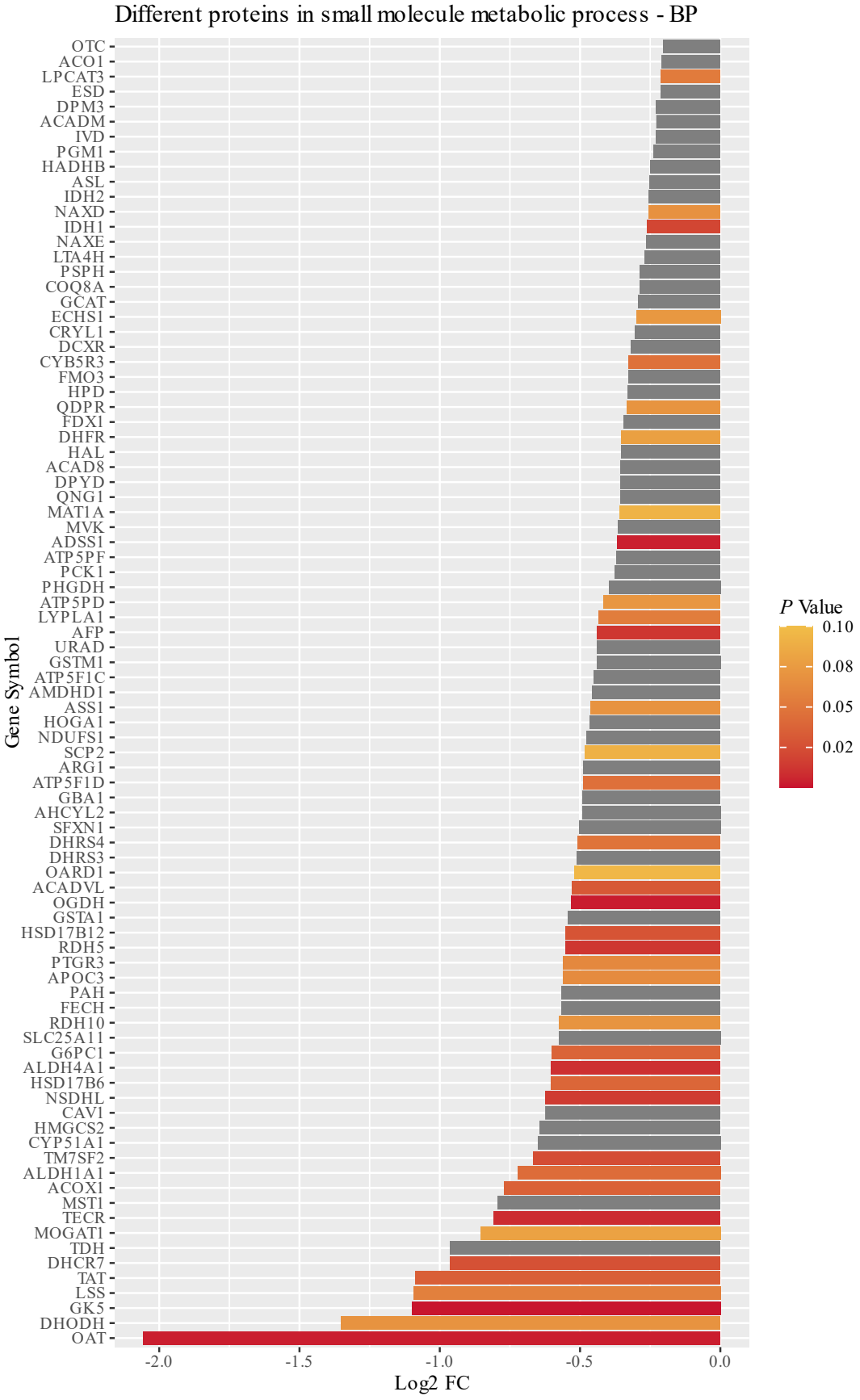

Figure 190. *Post hoc* analysis of proteins involved in small molecule metabolic process pathway in successful liver abscess induction (LAIP-Y) relative to control (CON).

Liver Abscess Induction Model
Study Number: GJC-LHB-3

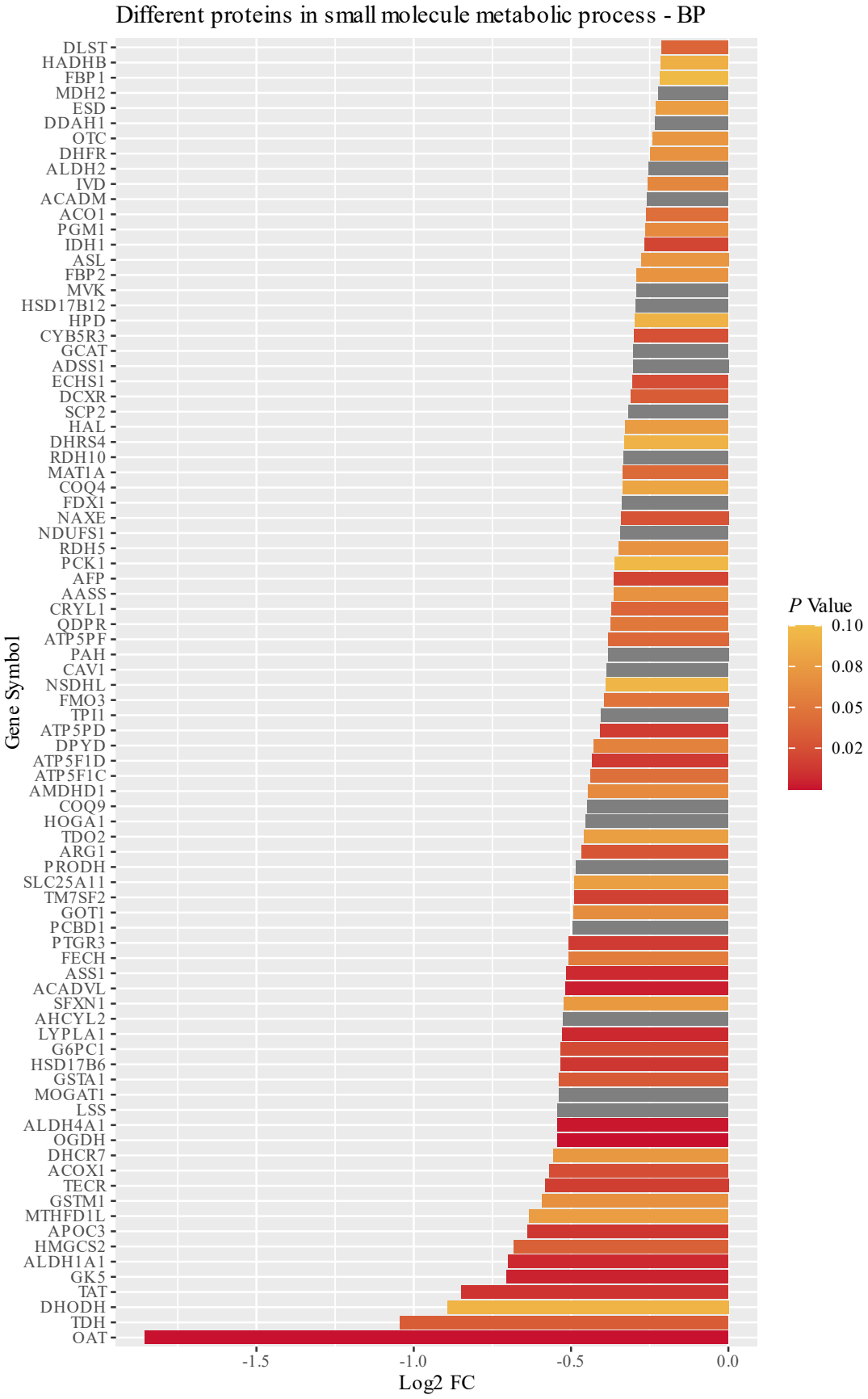

Figure 191. *Post hoc* analysis of proteins involved in small molecule metabolic process pathway in liver abscess induction protocol (LAIP) relative to control (CON).

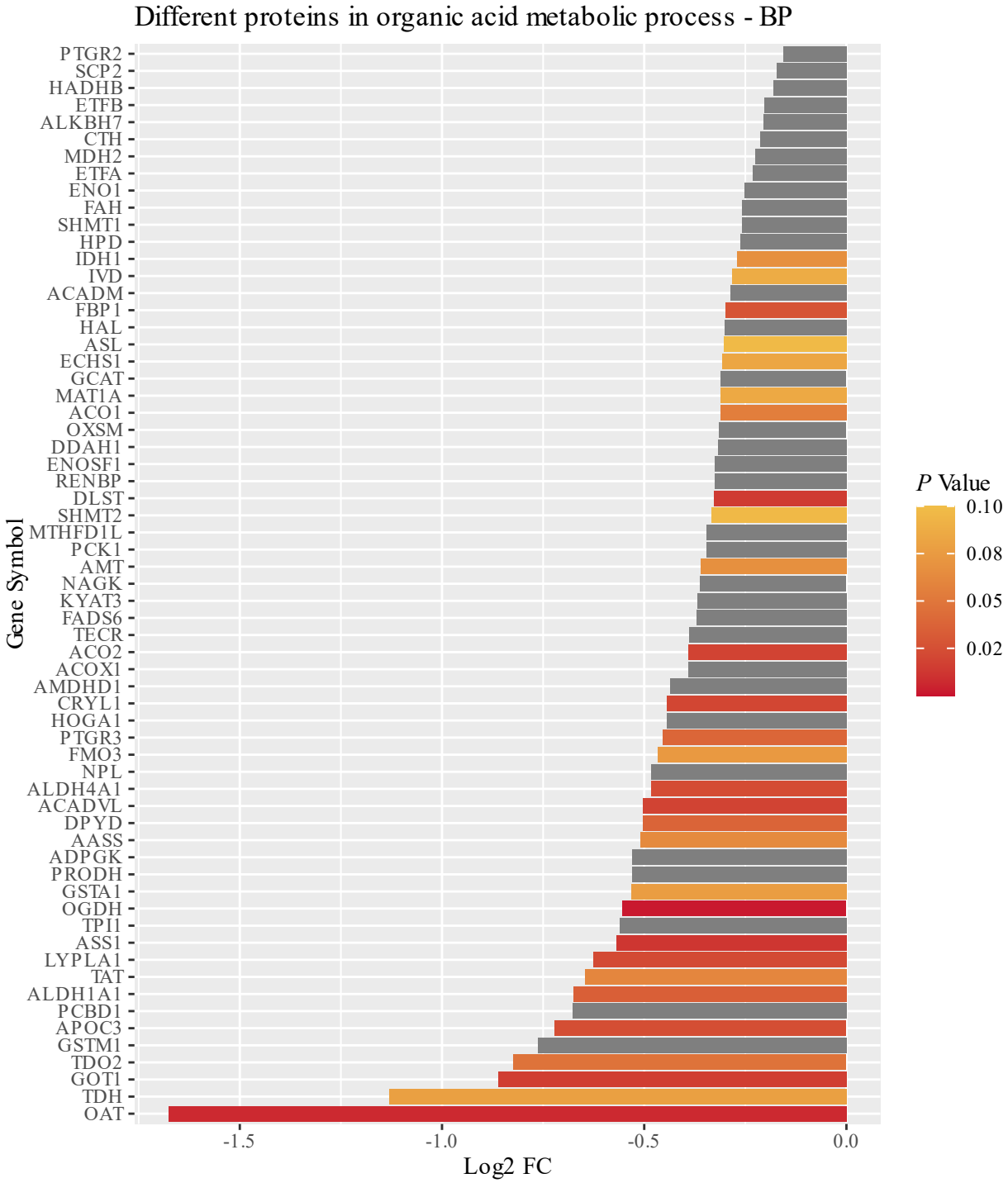

Figure 192. *Post hoc* analysis of proteins involved in organic acid metabolic process pathway in failed liver abscess induction (LAIP-N) relative to control (CON).

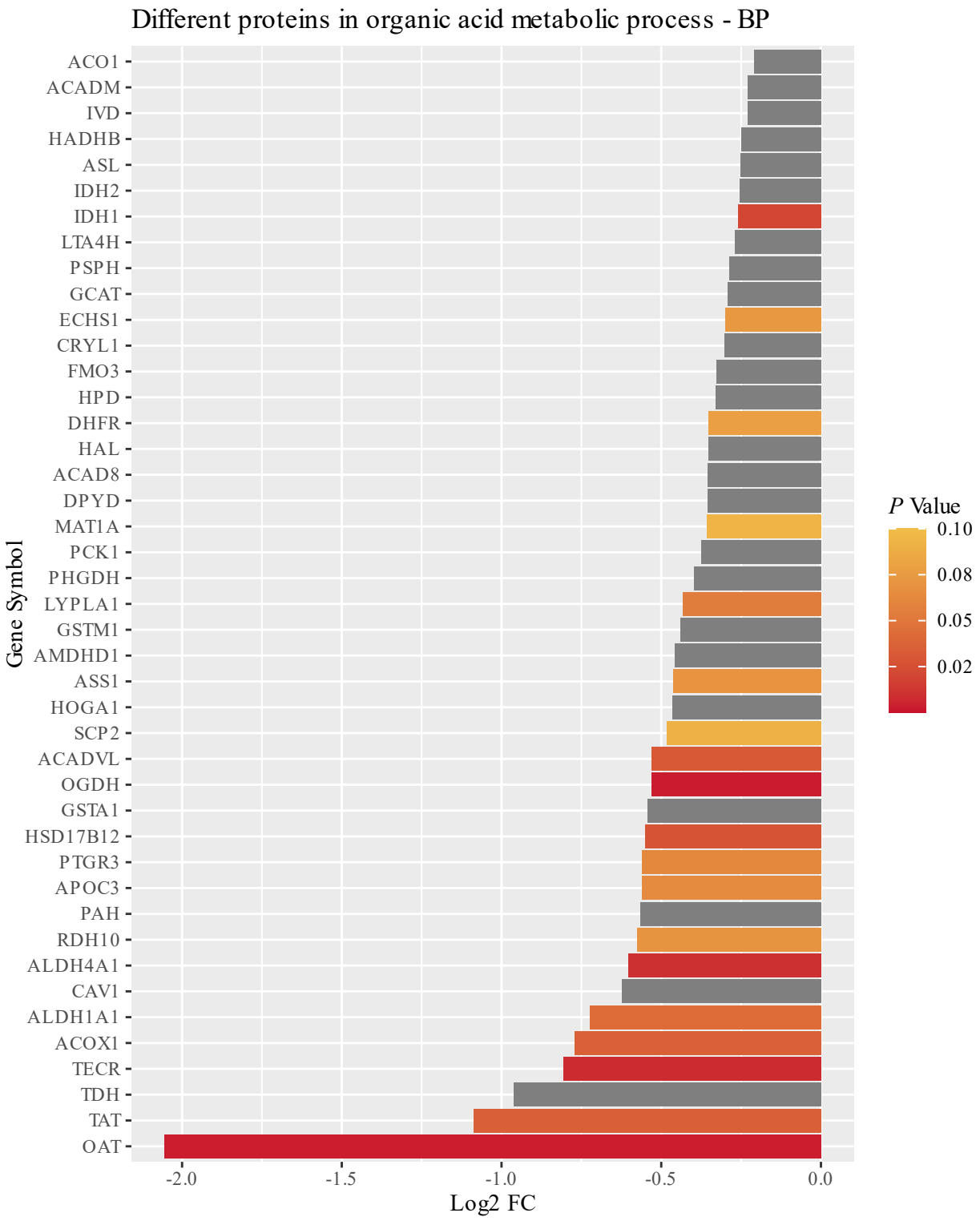

Figure 193. *Post hoc* analysis of proteins involved in organic acid metabolic process pathway in successful liver abscess induction (LAIP-Y) relative to control (CON).

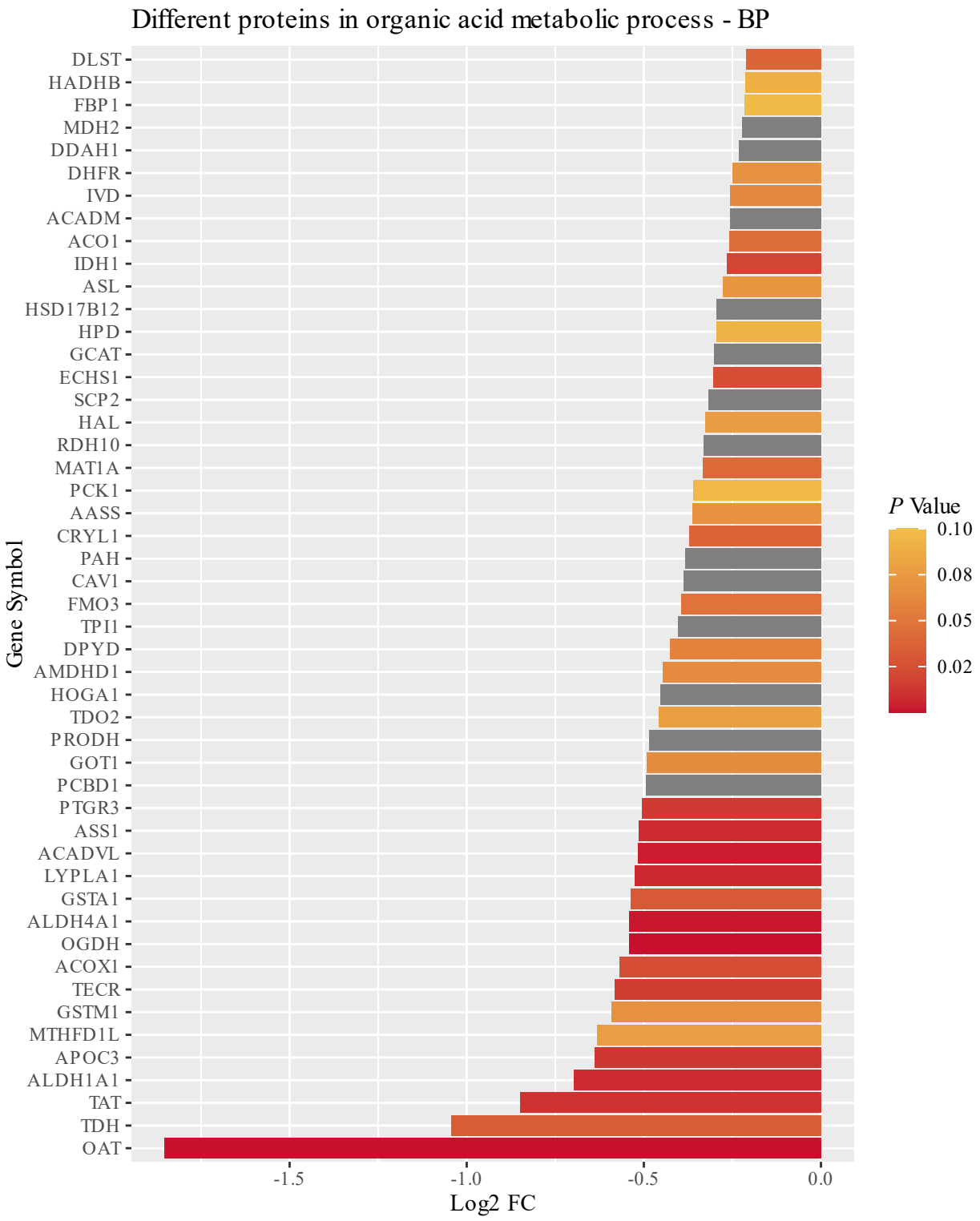

Figure 194. *Post hoc* analysis of proteins involved in organic acid metabolic process pathway in liver abscess induction protocol (LAIP) relative to control (CON).

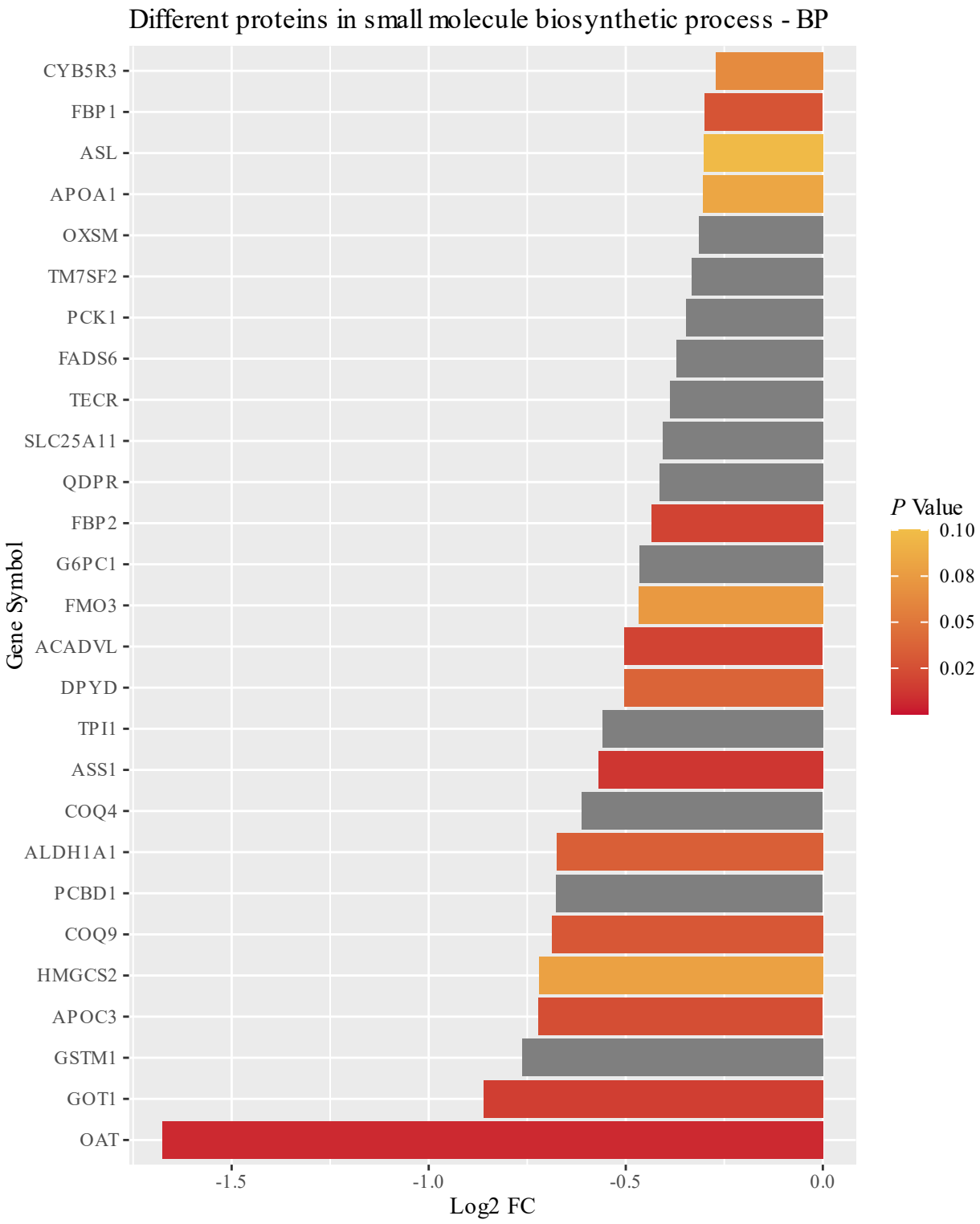

Figure 195. *Post hoc* analysis of proteins involved in small molecule biosynthetic process pathway in failed liver abscess induction (LAIP-N) relative to control (CON).

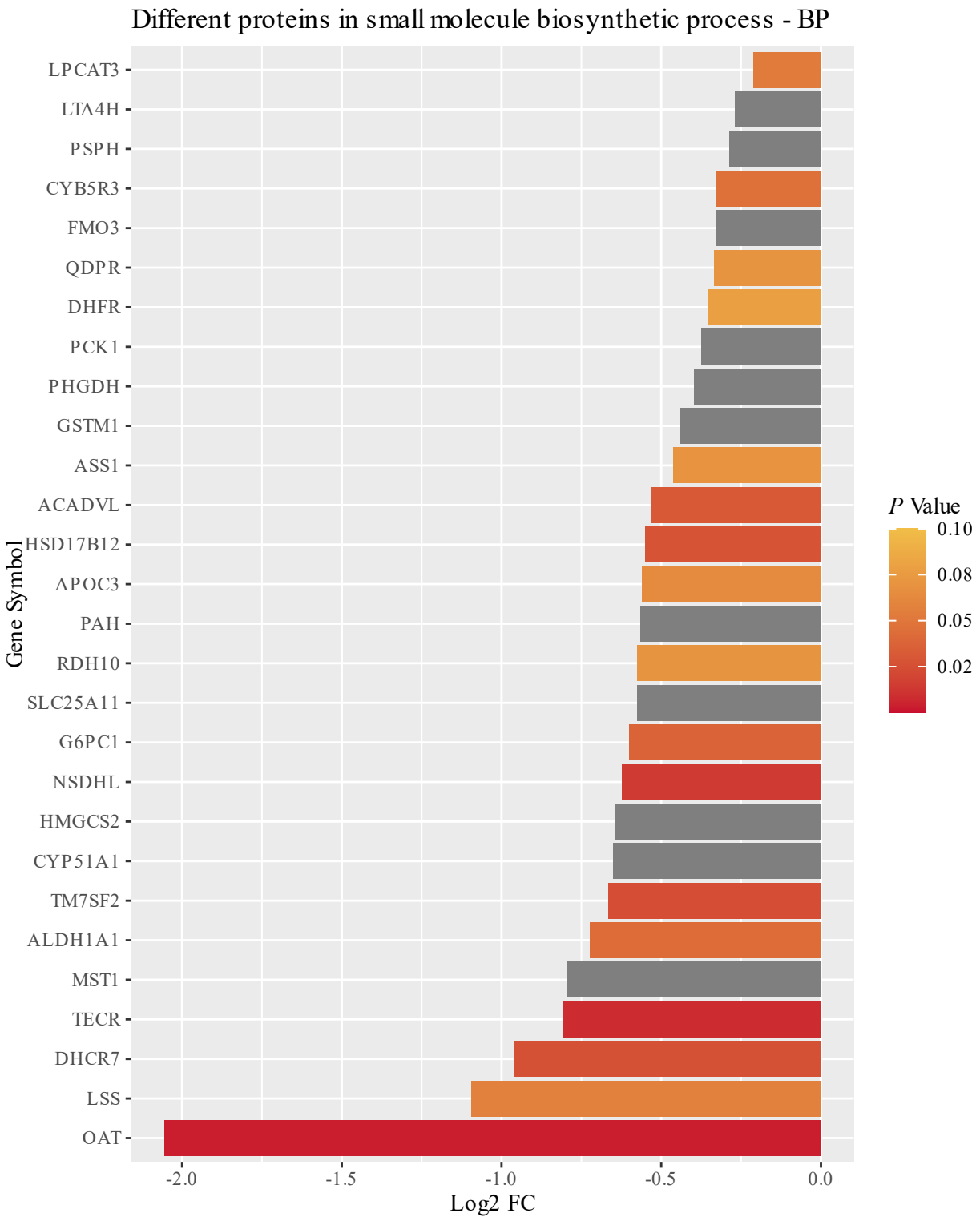

Figure 196. *Post hoc* analysis of proteins involved in small molecule biosynthetic process pathway in successful liver abscess induction (LAIP-Y) relative to control (CON).

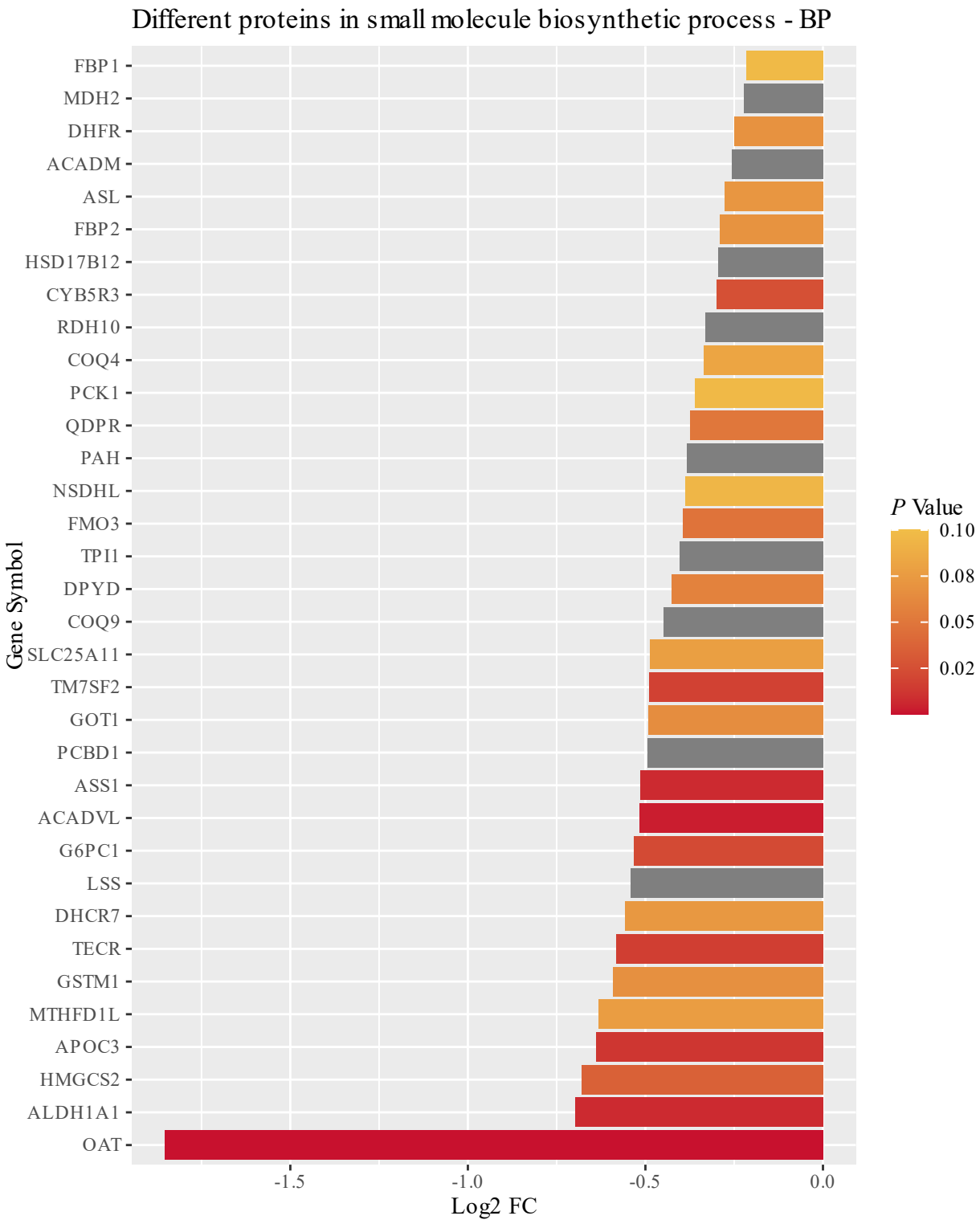

Figure 197. *Post hoc* analysis of proteins involved in small molecule biosynthetic process pathway in liver abscess induction protocol (LAIP) relative to control (CON).

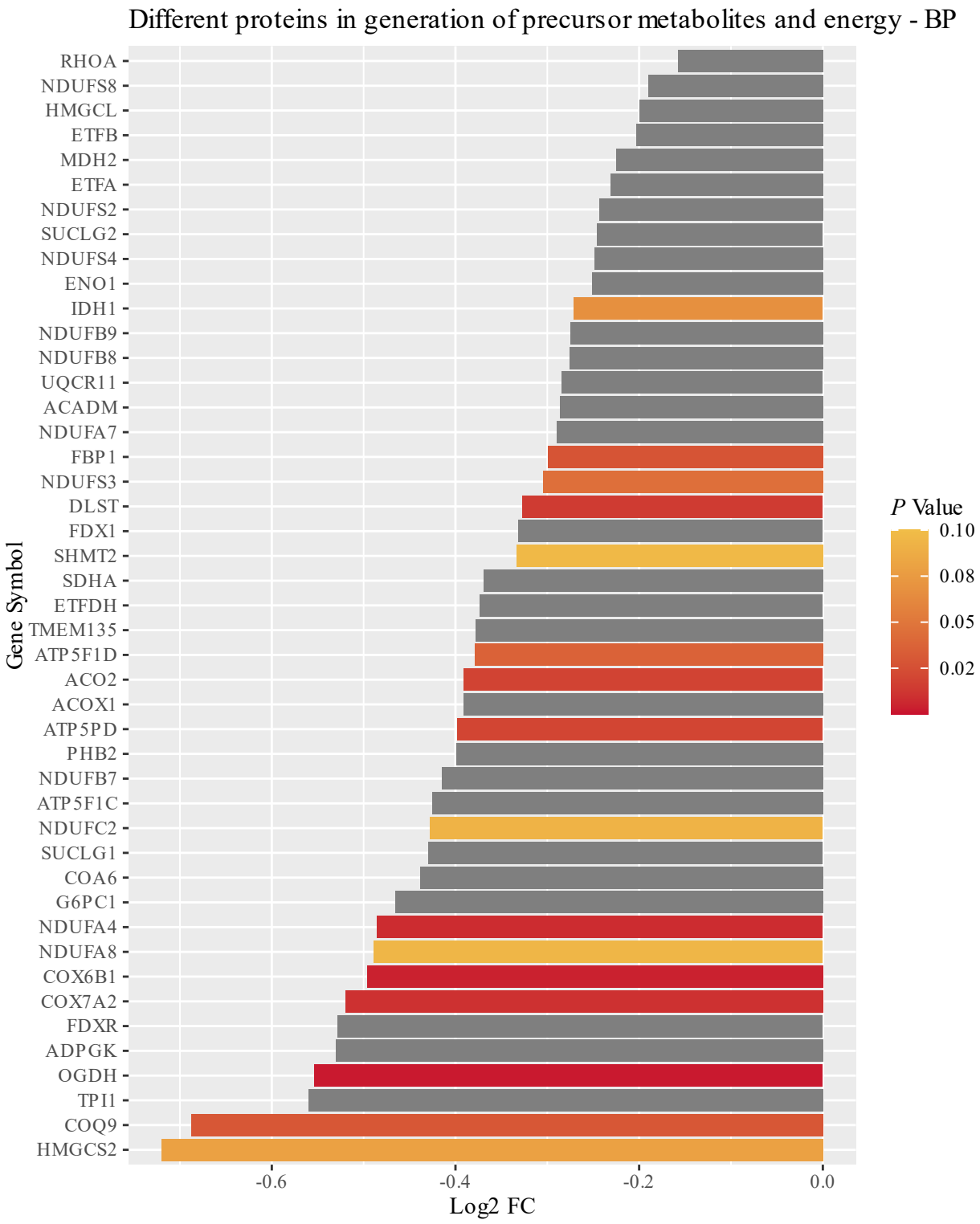

Figure 198. *Post hoc* analysis of proteins involved in generation of precursor metabolites and energy pathway in failed liver abscess induction (LAIP-N) relative to control (CON).

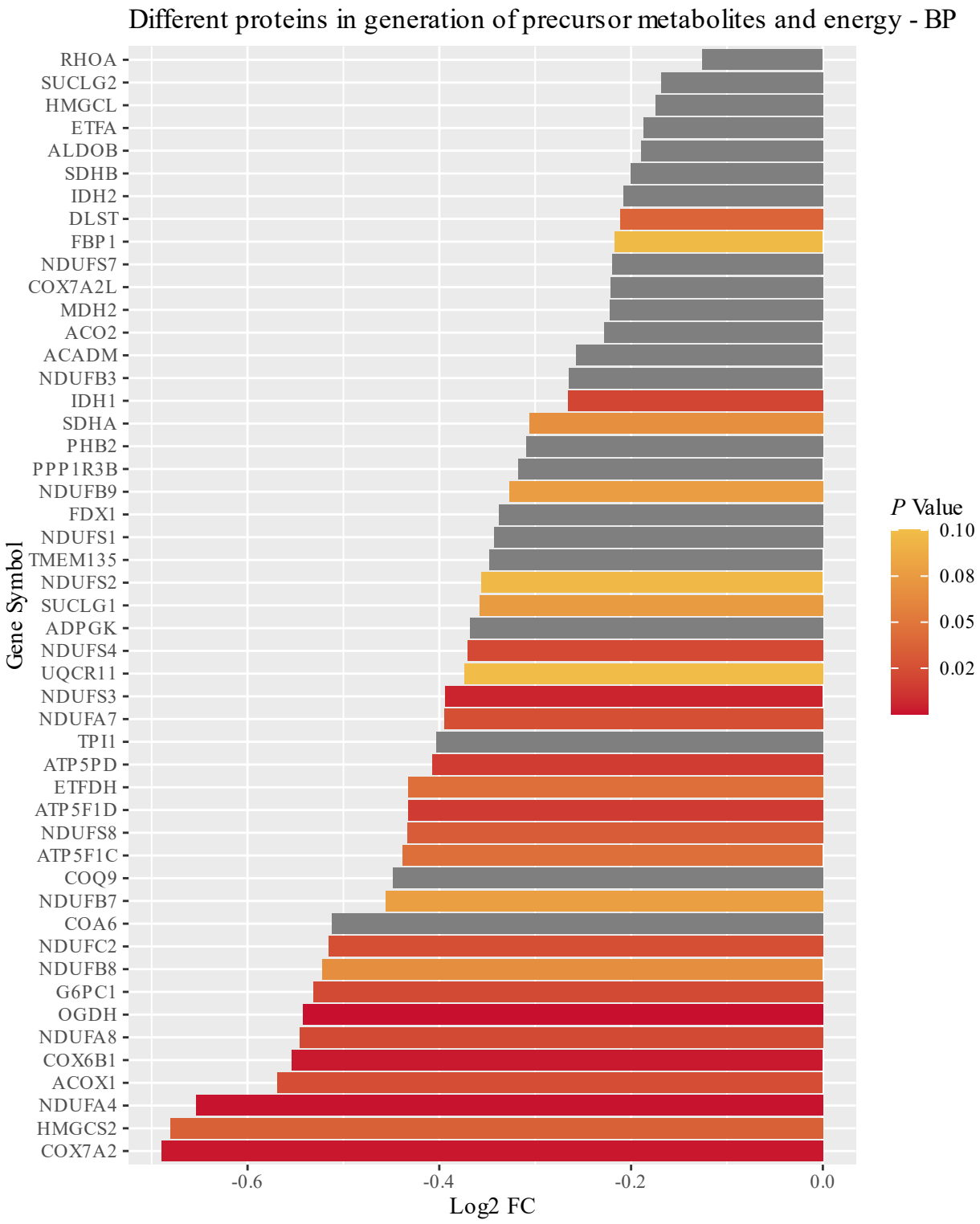

Figure 199. *Post hoc* analysis of proteins involved in generation of precursor metabolites and energy pathway in liver abscess induction protocol (LAIP) relative to control (CON).

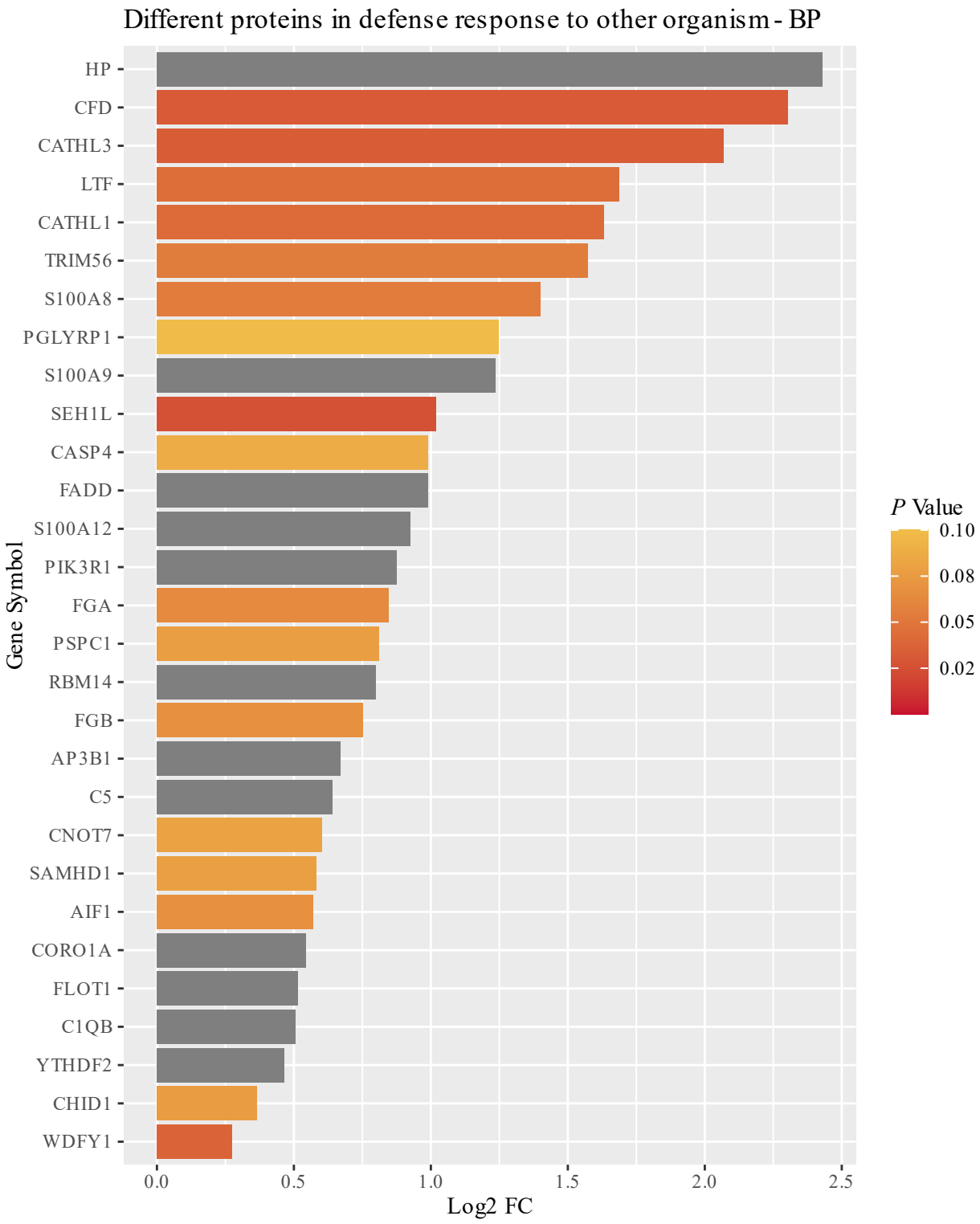

Figure 200. *Post hoc* analysis of proteins involved in defense response to other organism pathway in successful liver abscess induction (LAIP-Y) relative to control (CON).

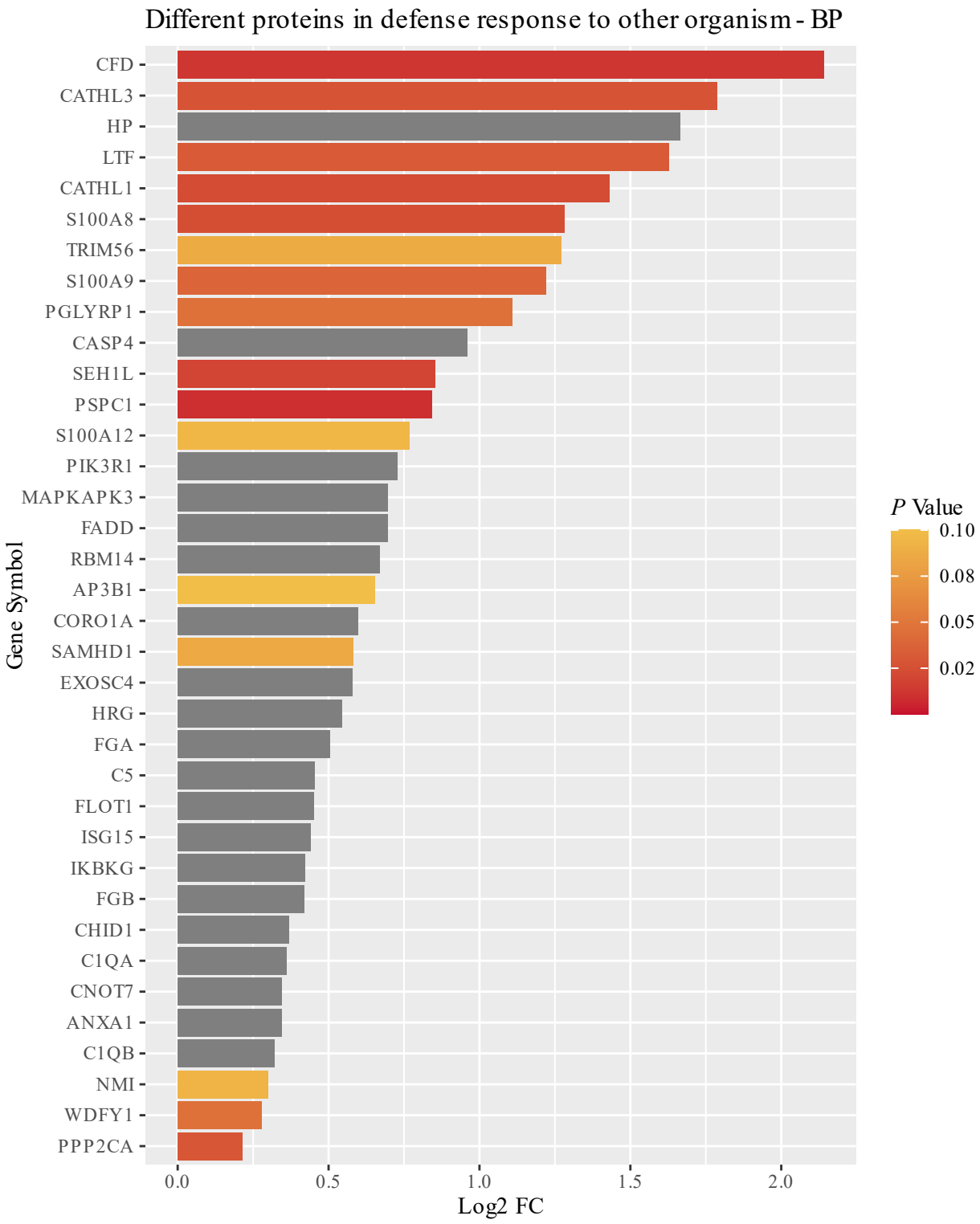

Figure 201. *Post hoc* analysis of proteins involved in defense response to other organism pathway in liver abscess induction protocol (LAIP) relative to control (CON).

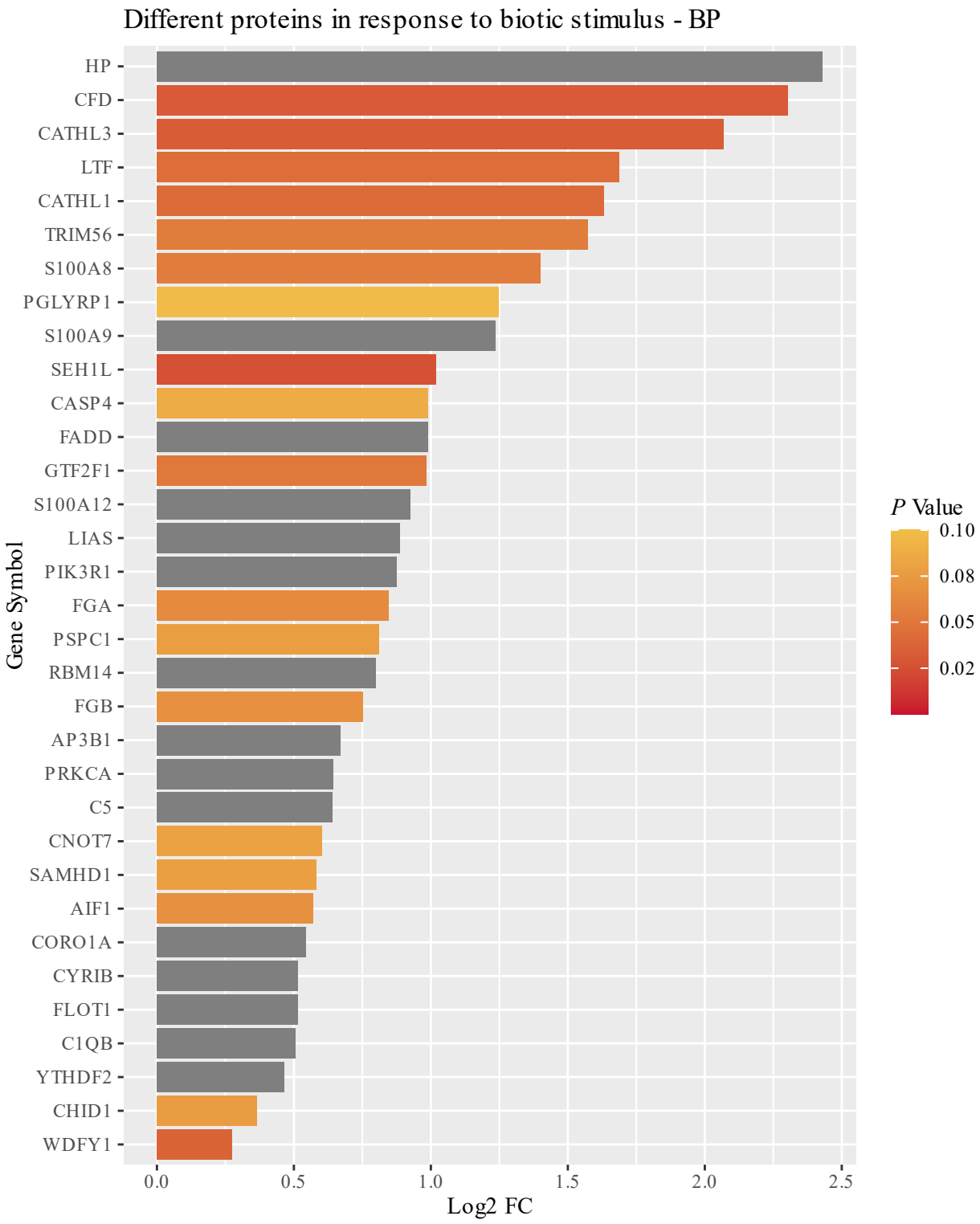

Figure 202. *Post hoc* analysis of proteins involved in response to biotic stimulus pathway in successful liver abscess induction (LAIP-Y) relative to control (CON).

Liver Abscess Induction Model
Study Number: GJC-LHB-3

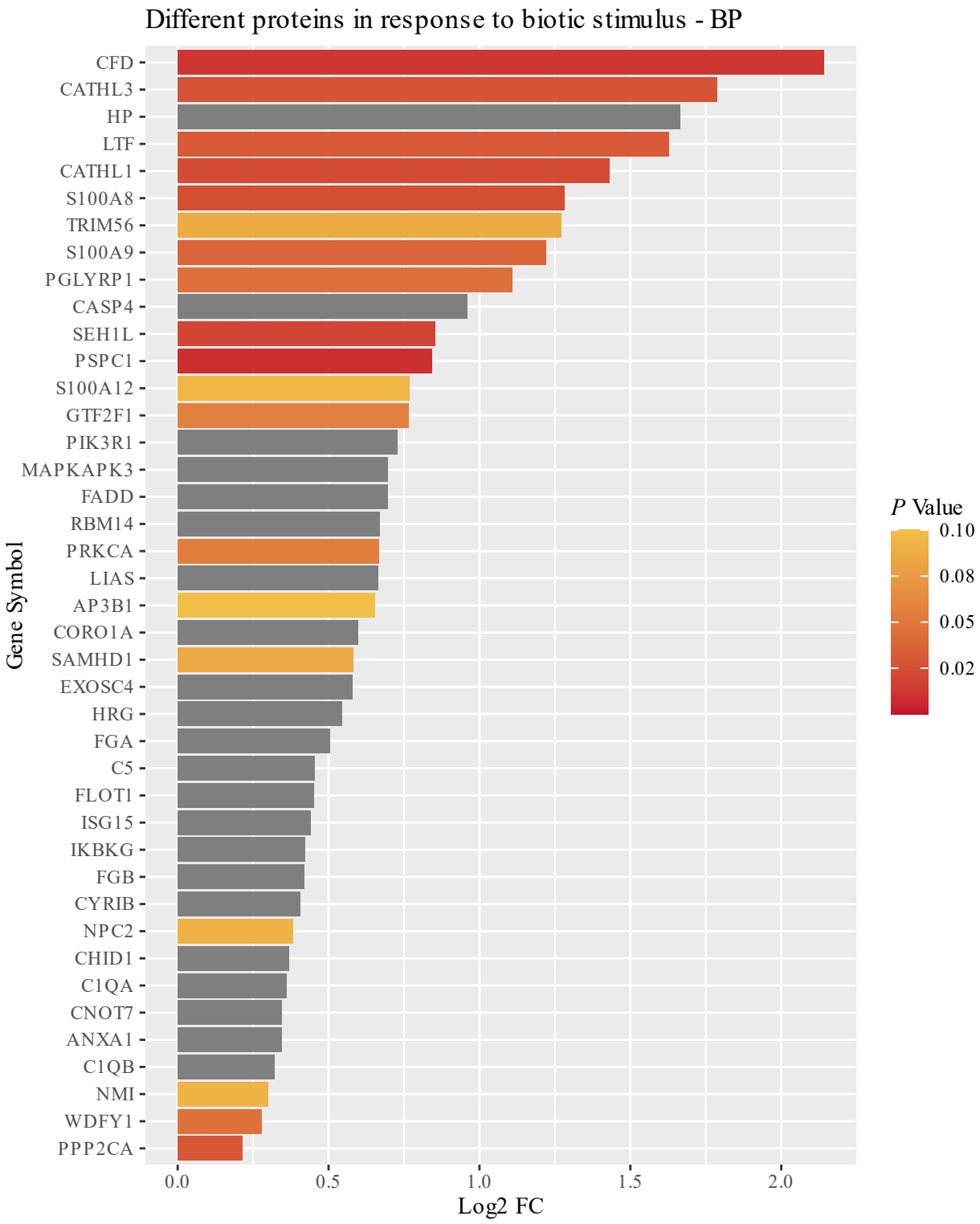

Figure 203. *Post hoc* analysis of proteins involved in response to biotic stimulus pathway in liver abscess induction protocol (LAIP) relative to control (CON).

Liver Abscess Induction Model
Study Number: GJC-LHB-3

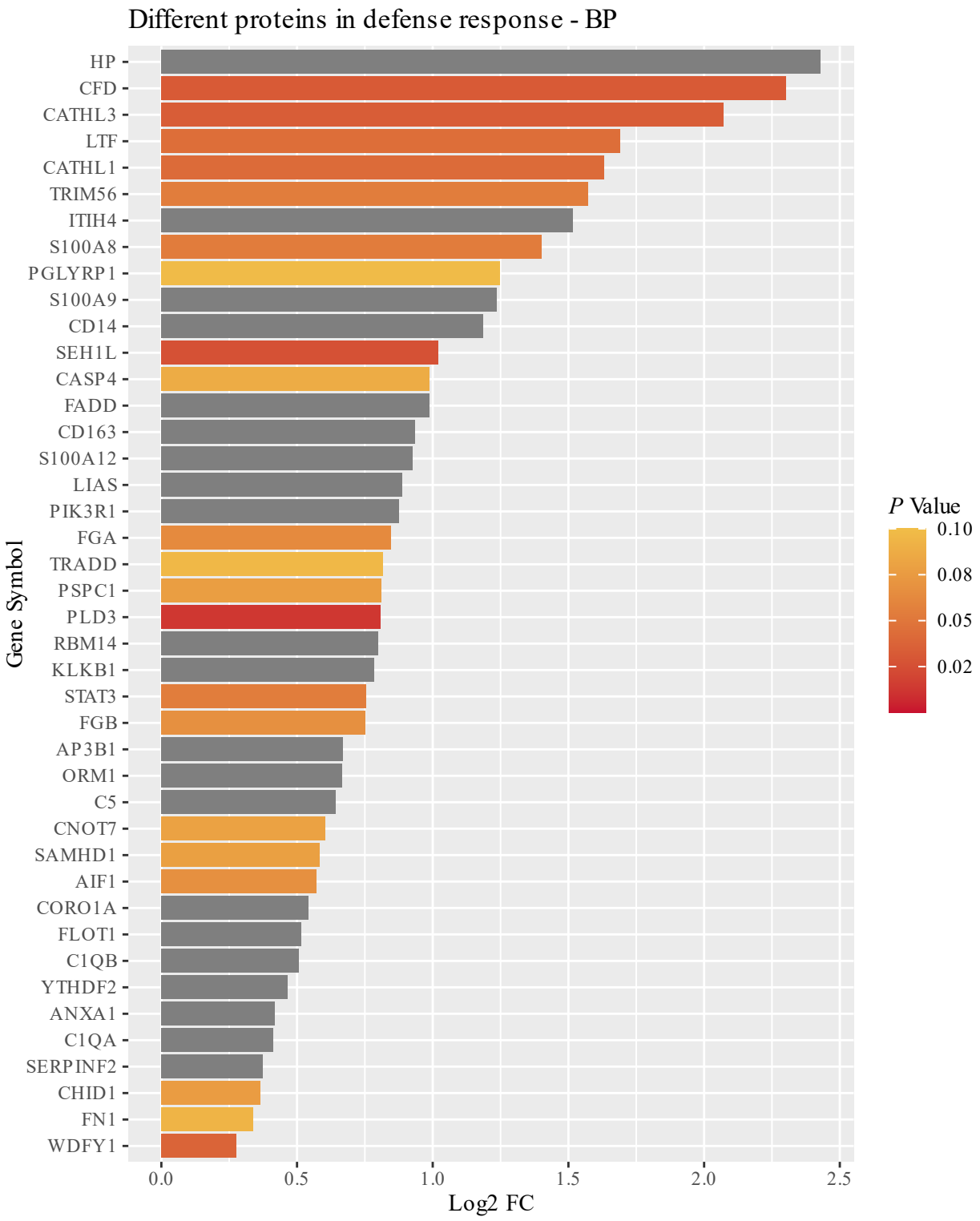

Figure 204. *Post hoc* analysis of proteins involved in defense response pathway in successful liver abscess induction (LAIP-Y) relative to control (CON).

Liver Abscess Induction Model
Study Number: GJC-LHB-3

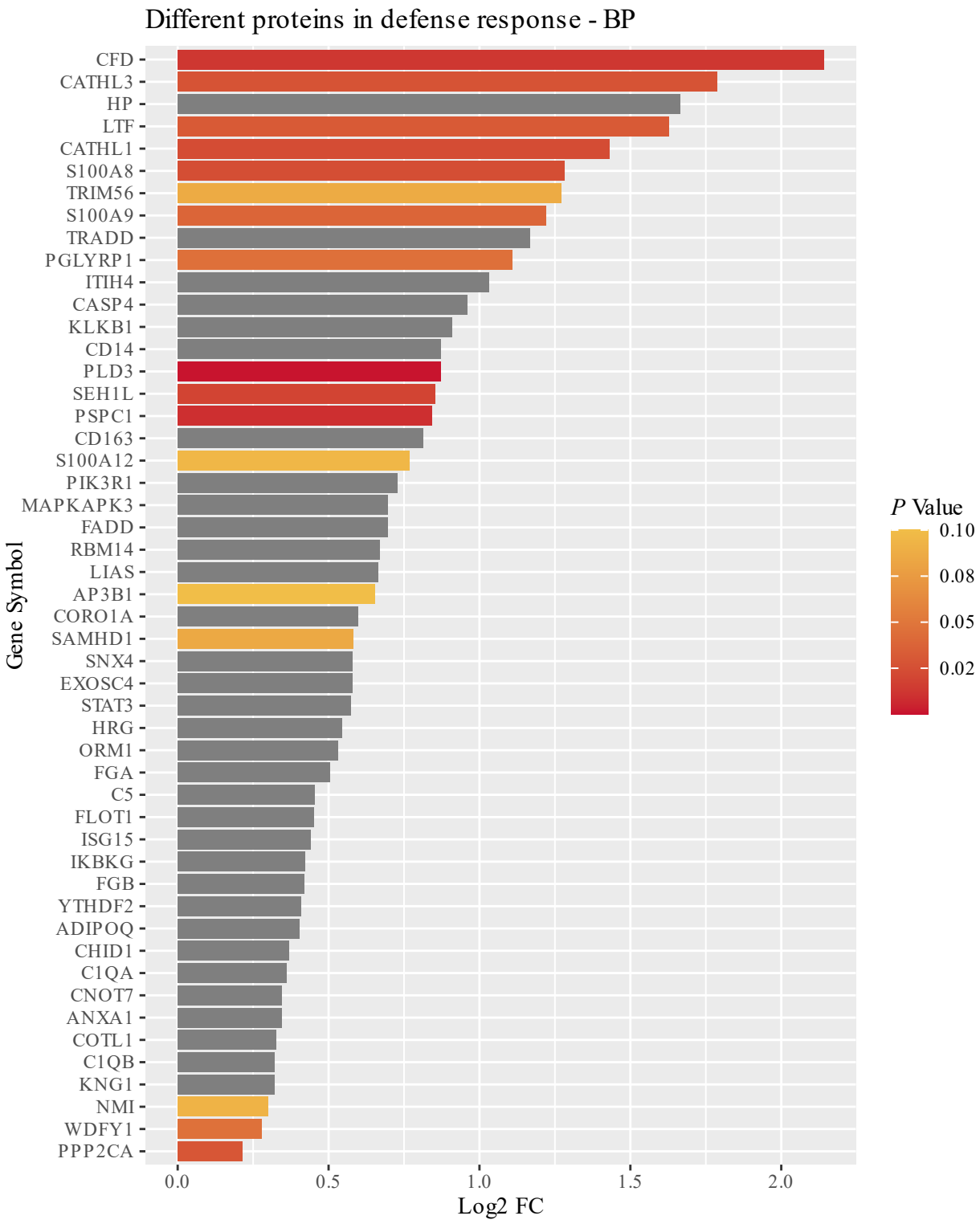

Figure 205. *Post hoc* analysis of proteins involved in defense response pathway in liver abscess induction protocol (LAIP) relative to control (CON).

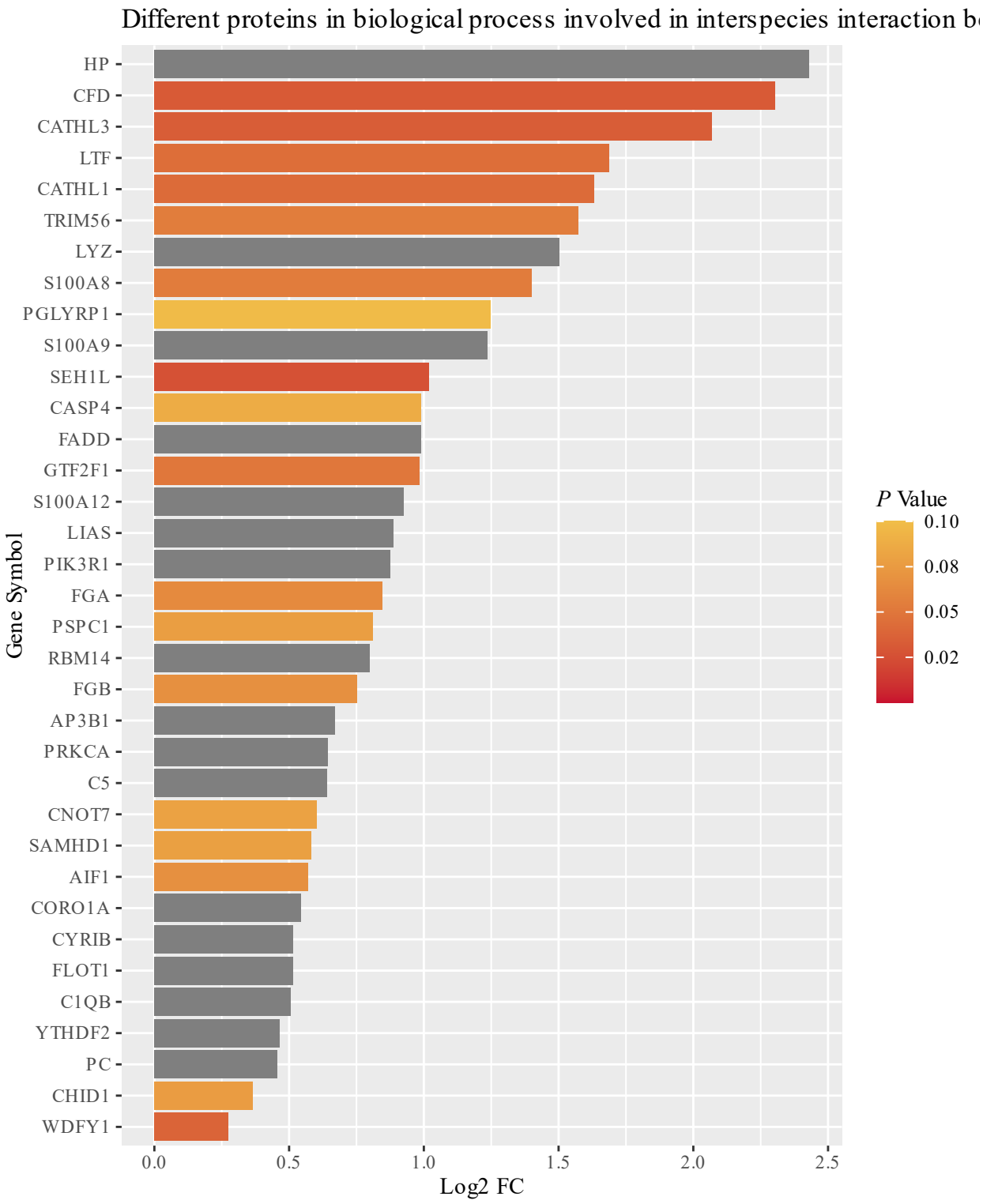

Figure 206. *Post hoc* analysis of proteins involved in biological process involved in interspecies interaction between organisms pathway in successful liver abscess induction (LAIP-Y) relative to control (CON).

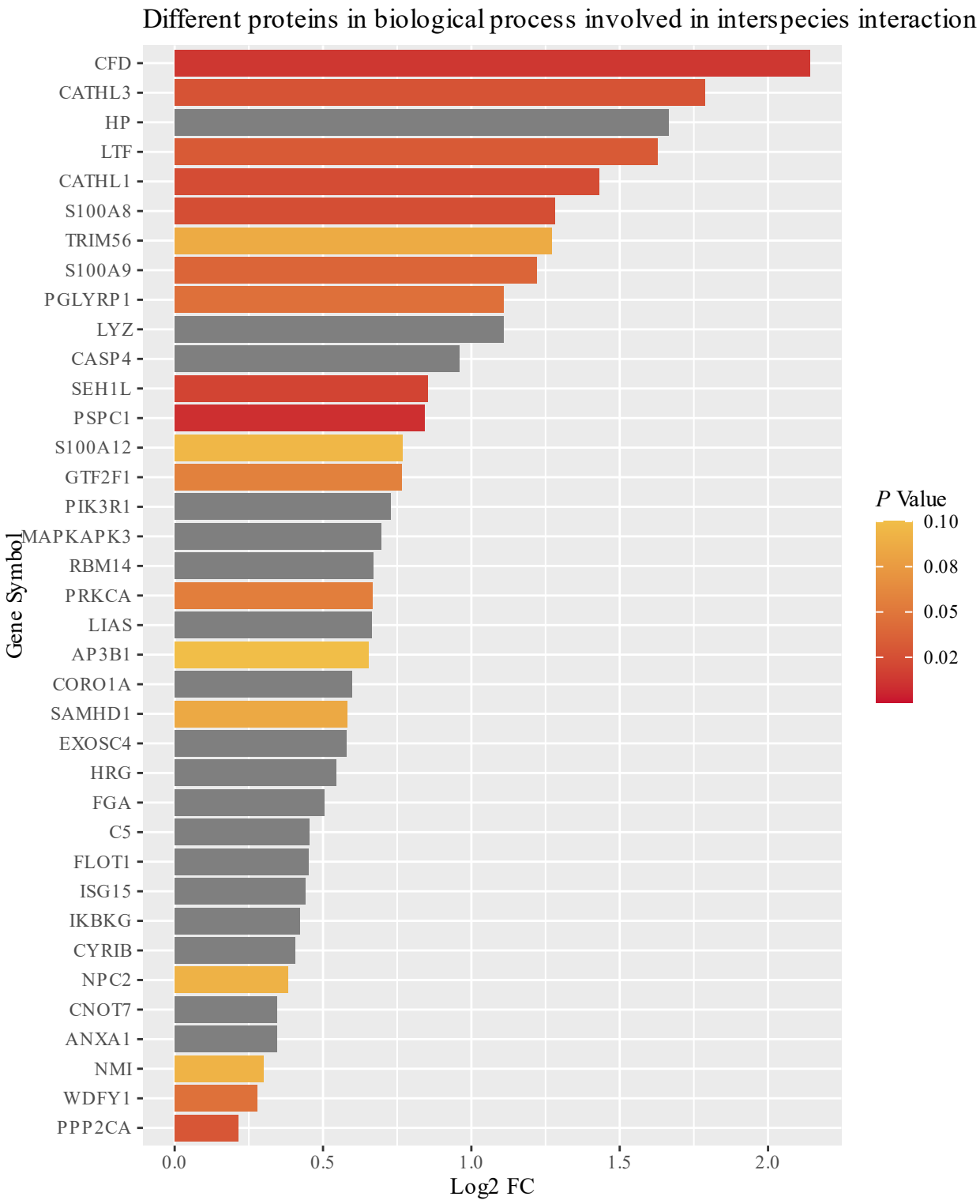

Figure 207. *Post hoc* analysis of proteins involved in biological process involved in interspecies interaction between organisms pathway in liver abscess induction protocol (LAIP) relative to control (CON).

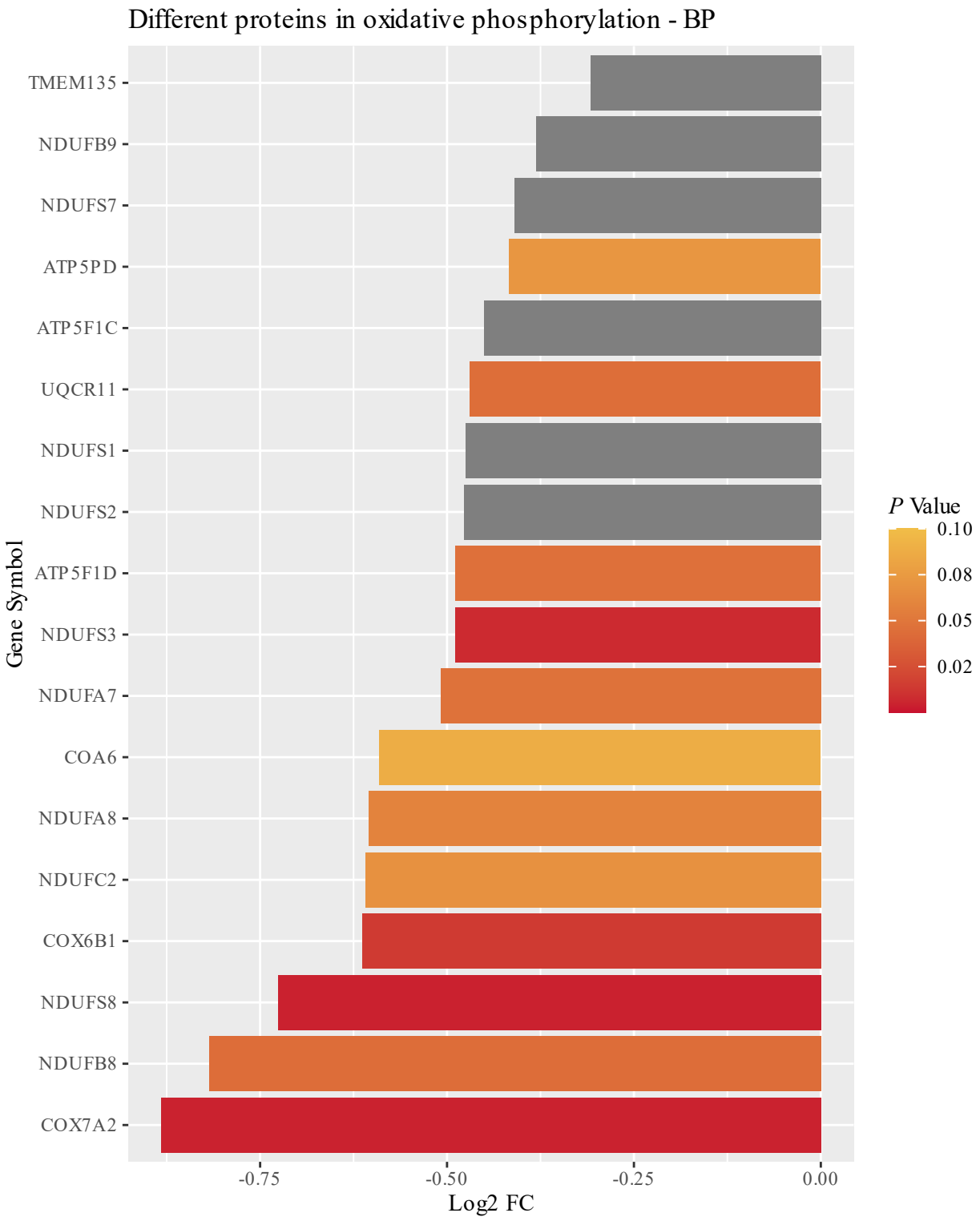

Figure 208. *Post hoc* analysis of proteins involved in oxidative phosphorylation pathway in successful liver abscess induction (LAIP-Y) relative to control (CON).

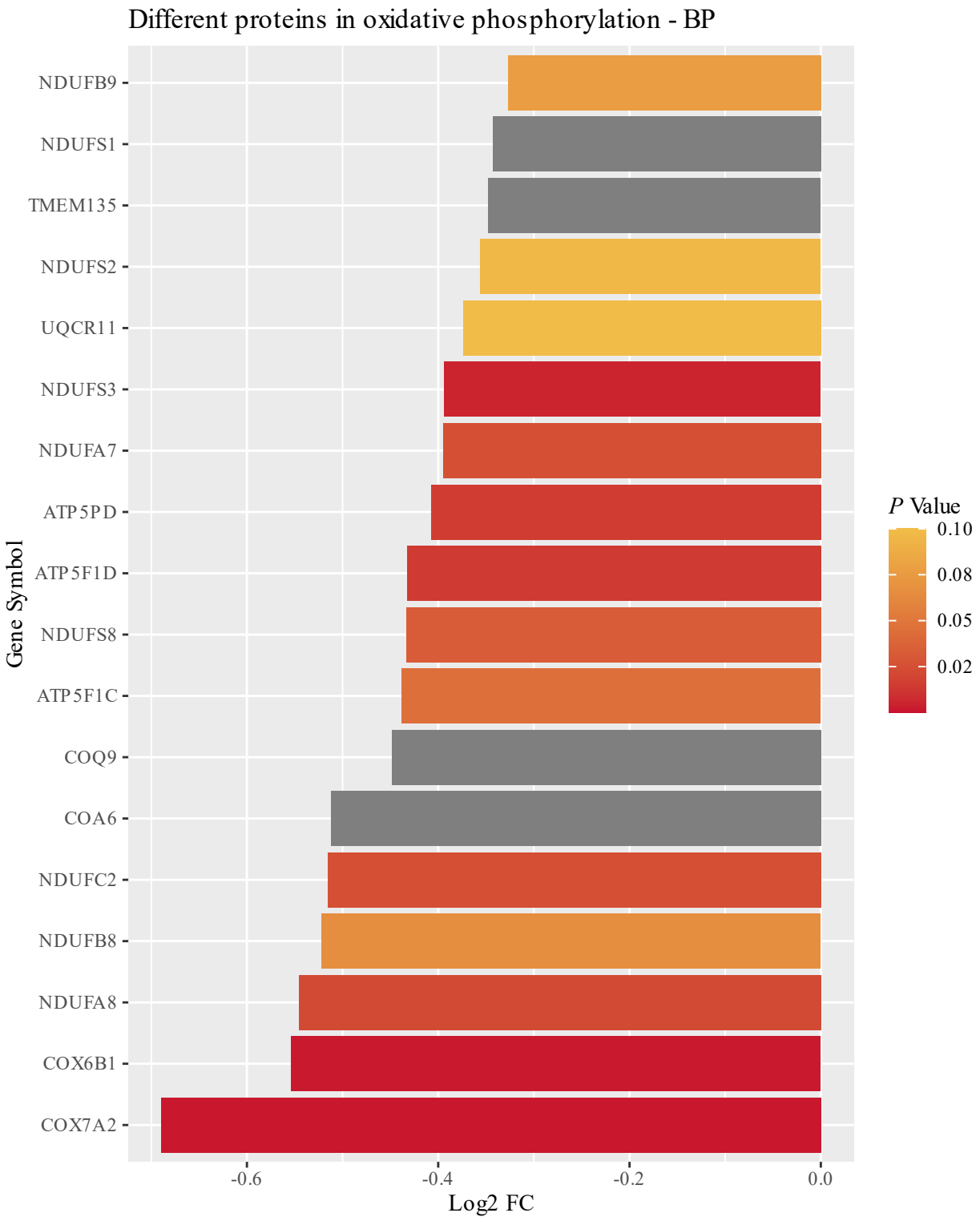

Figure 209. *Post hoc* analysis of proteins involved in oxidative phosphorylation pathway in liver abscess induction protocol (LAIP) relative to control (CON).

Liver Abscess Induction Model
Study Number: GJC-LHB-3

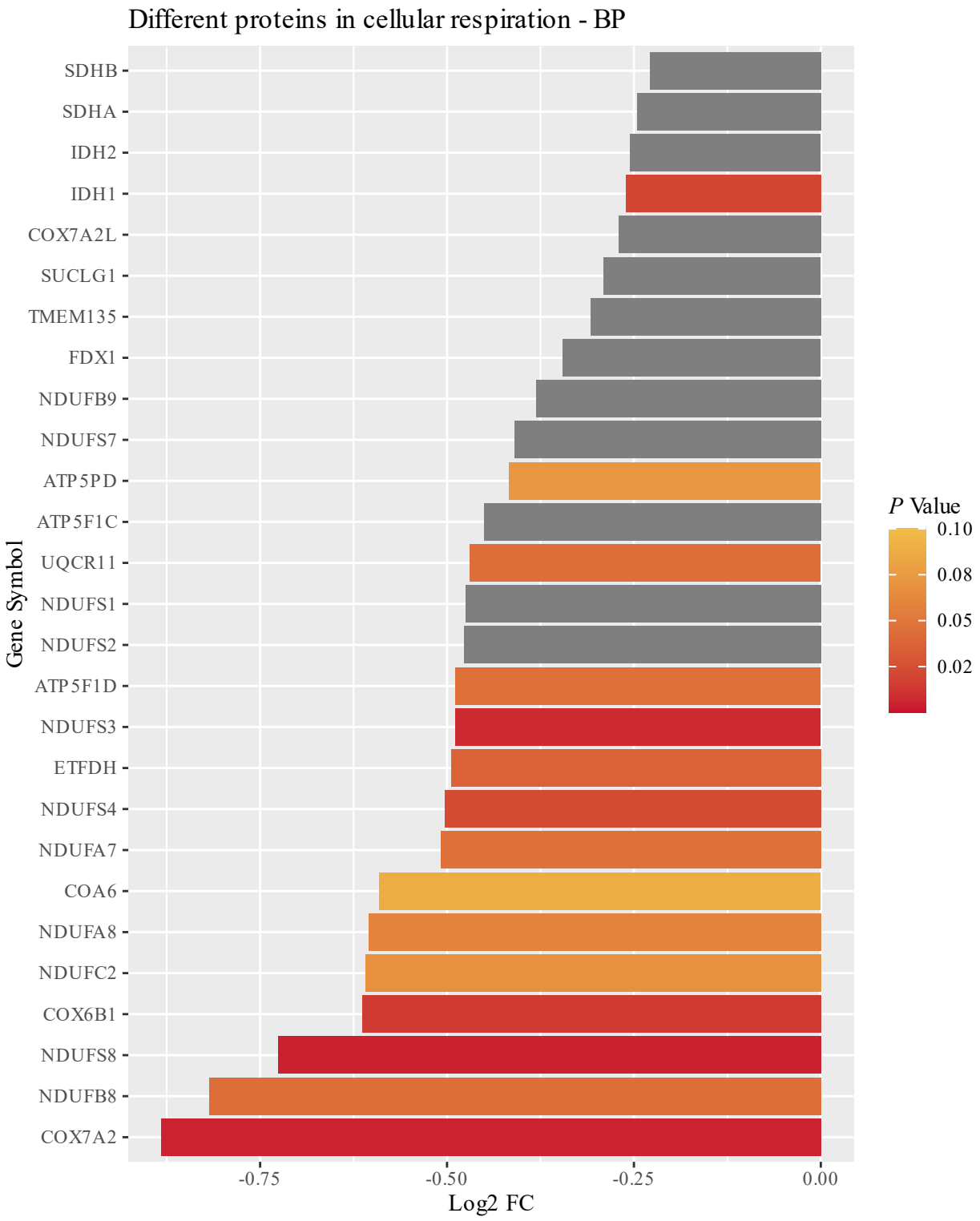

Figure 210. *Post hoc* analysis of proteins involved in cellular respiration pathway in successful liver abscess induction (LAIP-Y) relative to control (CON).

Liver Abscess Induction Model
Study Number: GJC-LHB-3

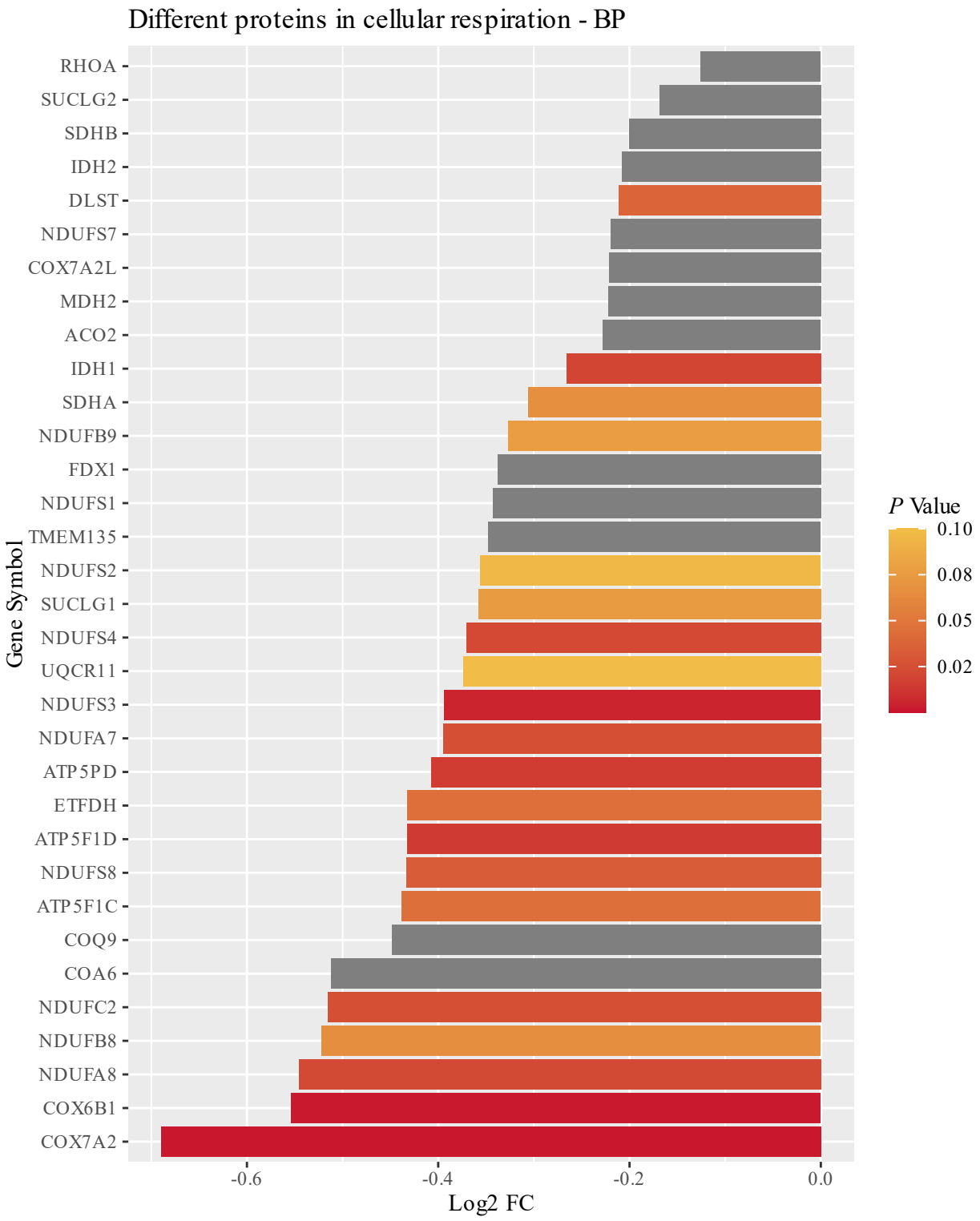

Figure 211. *Post hoc* analysis of proteins involved in cellular respiration pathway in liver abscess induction protocol (LAIP) relative to control (CON).

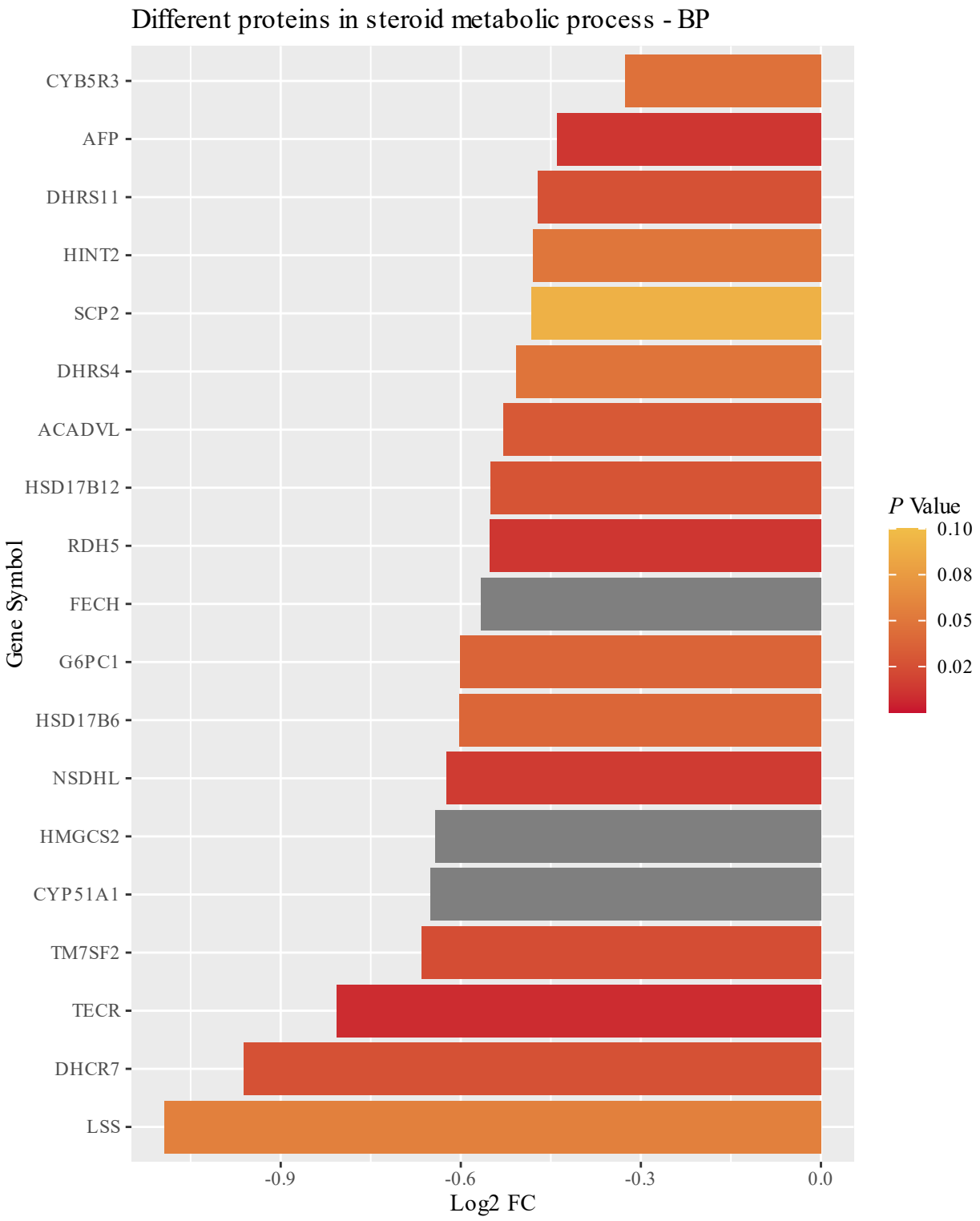

Figure 212. *Post hoc* analysis of proteins involved in steroid metabolic process pathway in successful liver abscess induction (LAIP-Y) relative to control (CON).

Liver Abscess Induction Model
Study Number: GJC-LHB-3

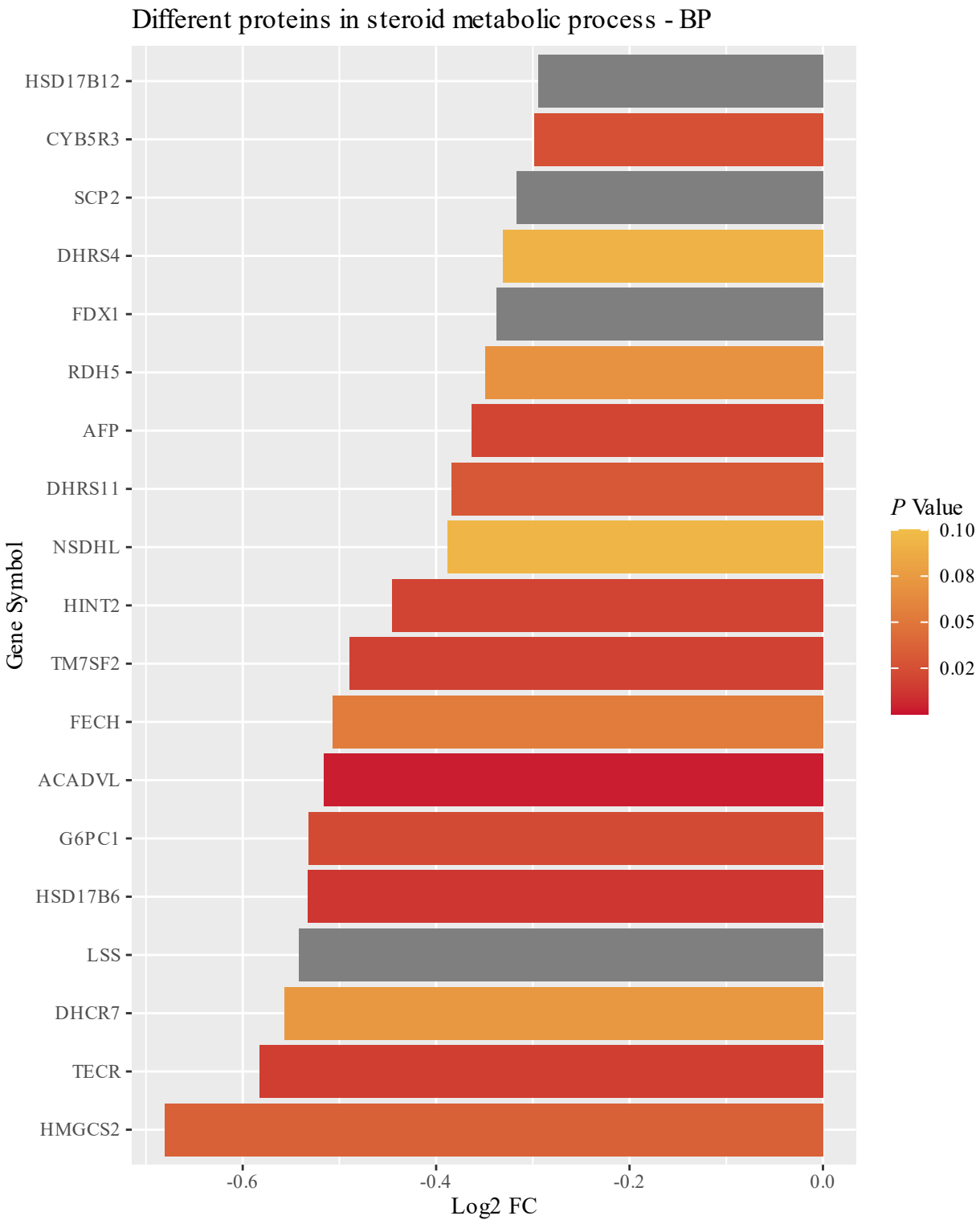

Figure 213. *Post hoc* analysis of proteins involved in steroid metabolic process pathway in liver abscess induction protocol (LAIP) relative to control (CON).

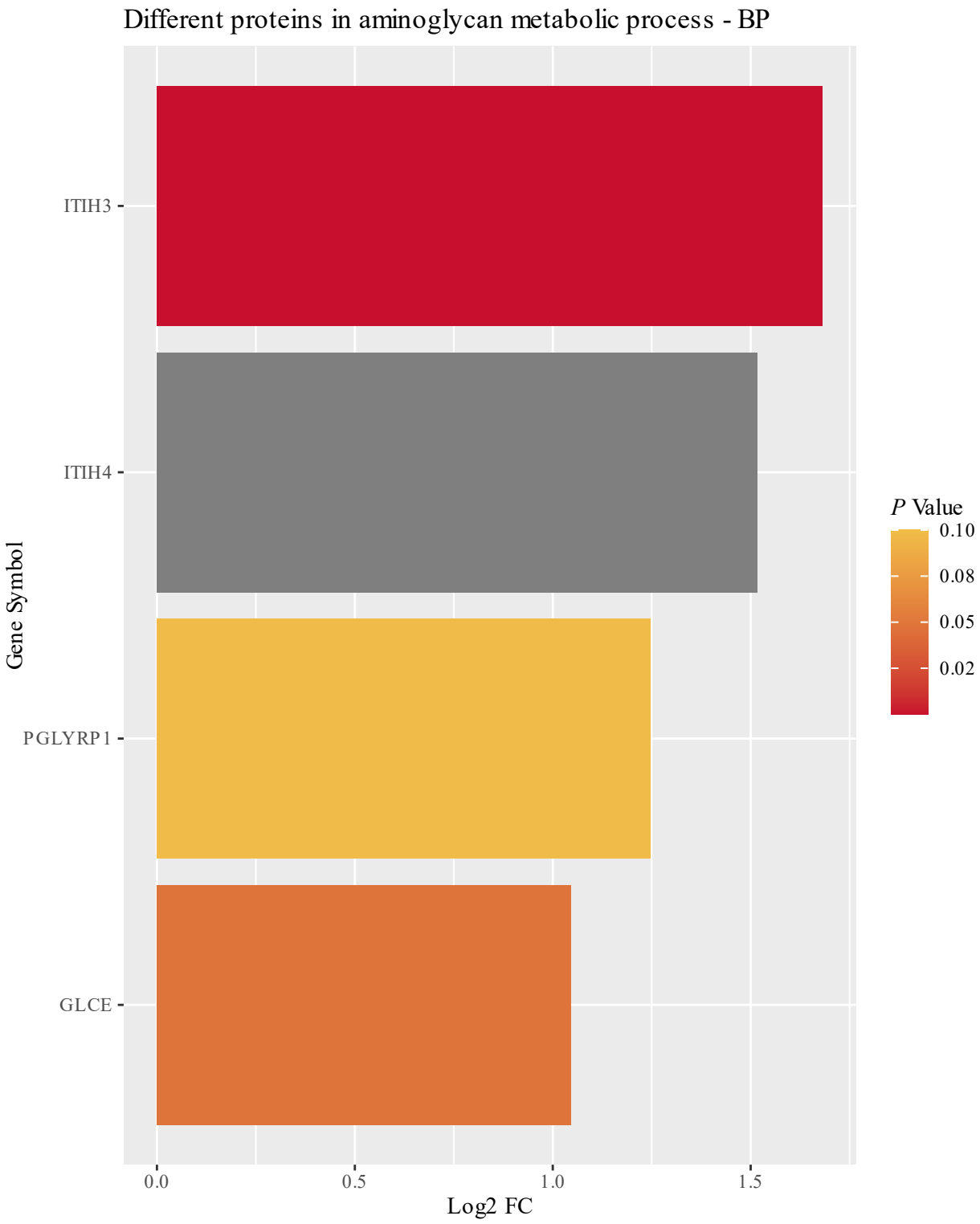

Figure 214. *Post hoc* analysis of proteins involved in aminoglycan metabolic process pathway in successful liver abscess induction (LAIP-Y) relative to control (CON).

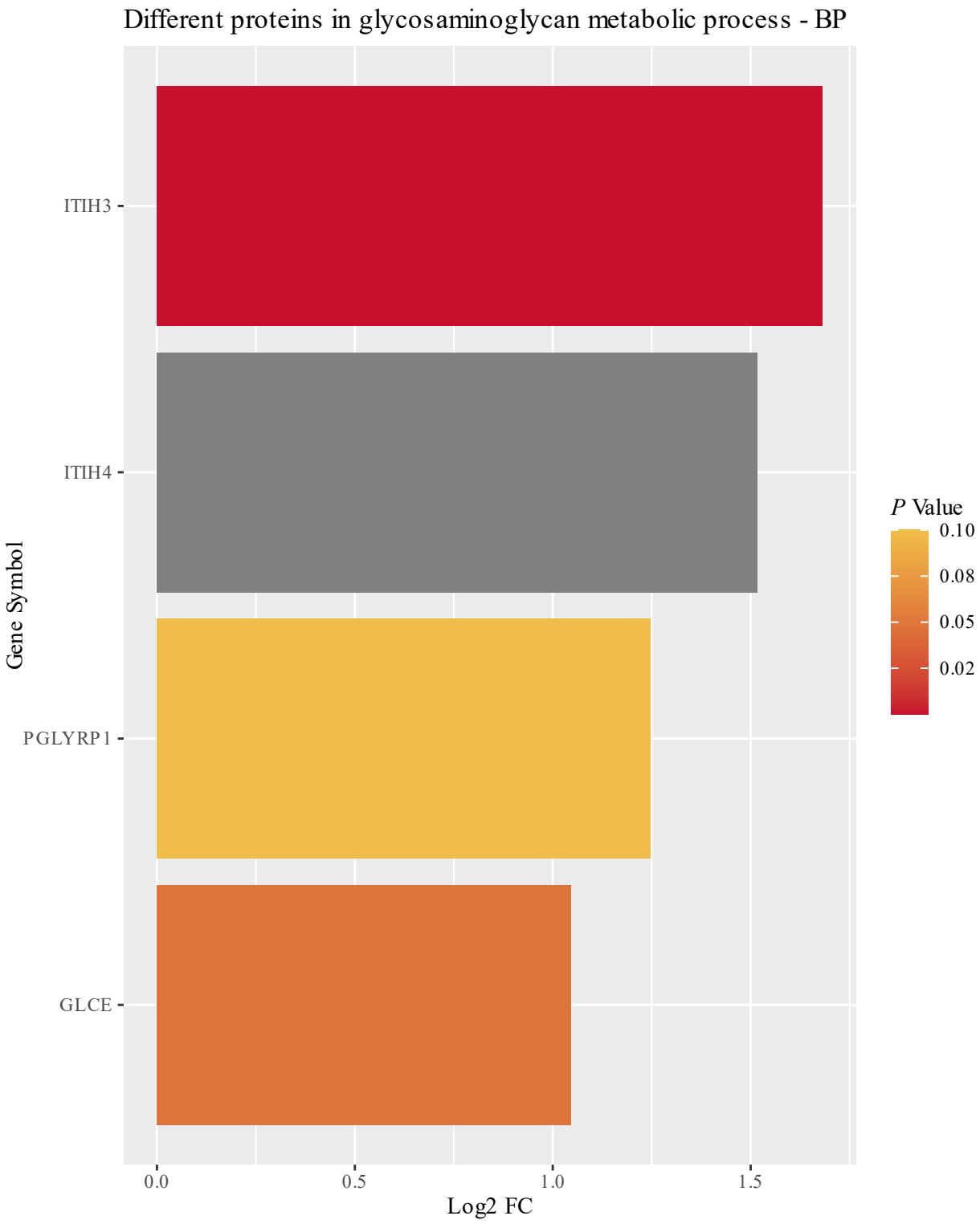

Figure 215. *Post hoc* analysis of proteins involved in glycosaminoglycan metabolic process pathway in successful liver abscess induction (LAIP-Y) relative to control (CON).

Liver Abscess Induction Model
Study Number: GJC-LHB-3

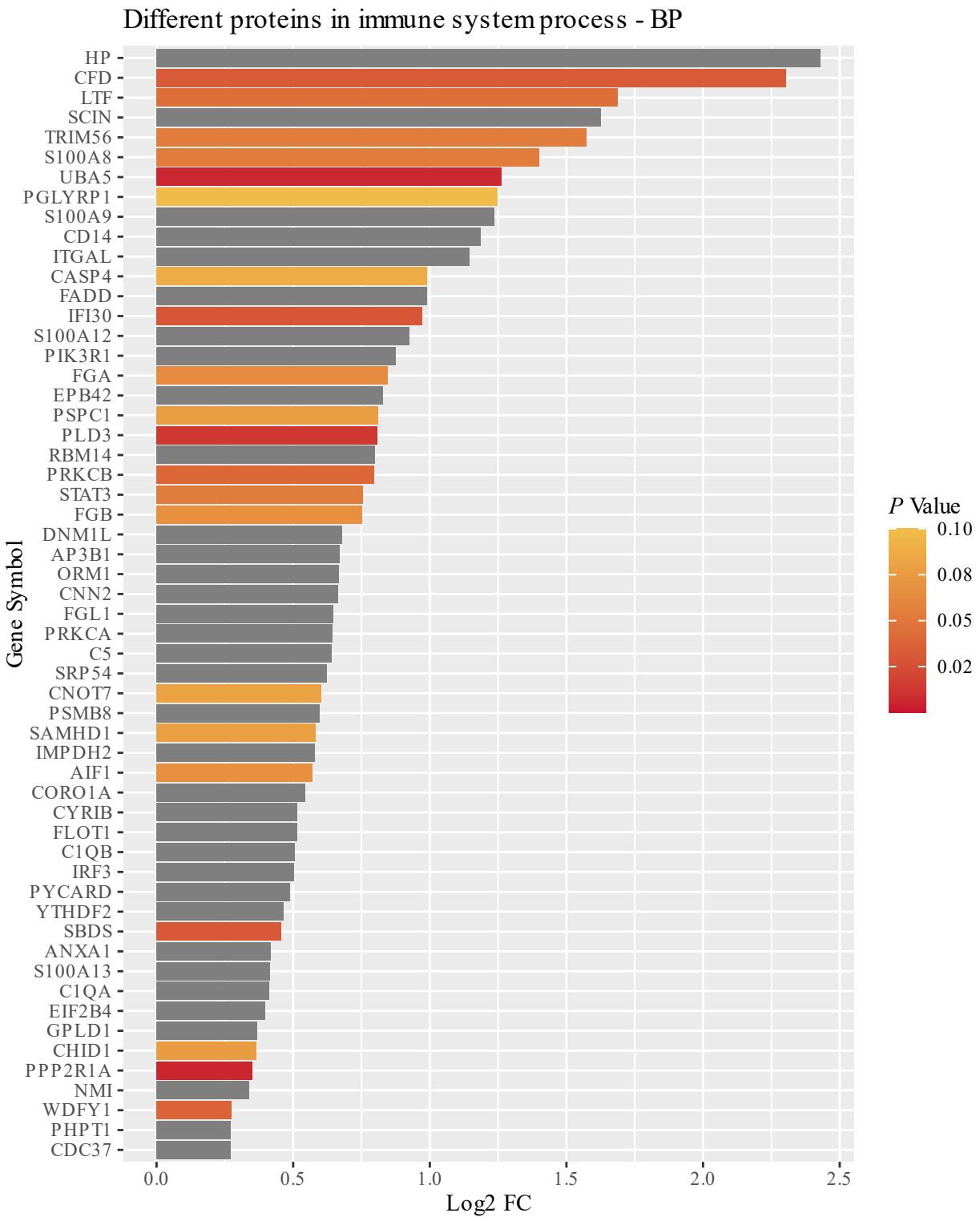

Figure 216. *Post hoc* analysis of proteins involved in immune system process pathway in successful liver abscess induction (LAIP-Y) relative to control (CON).

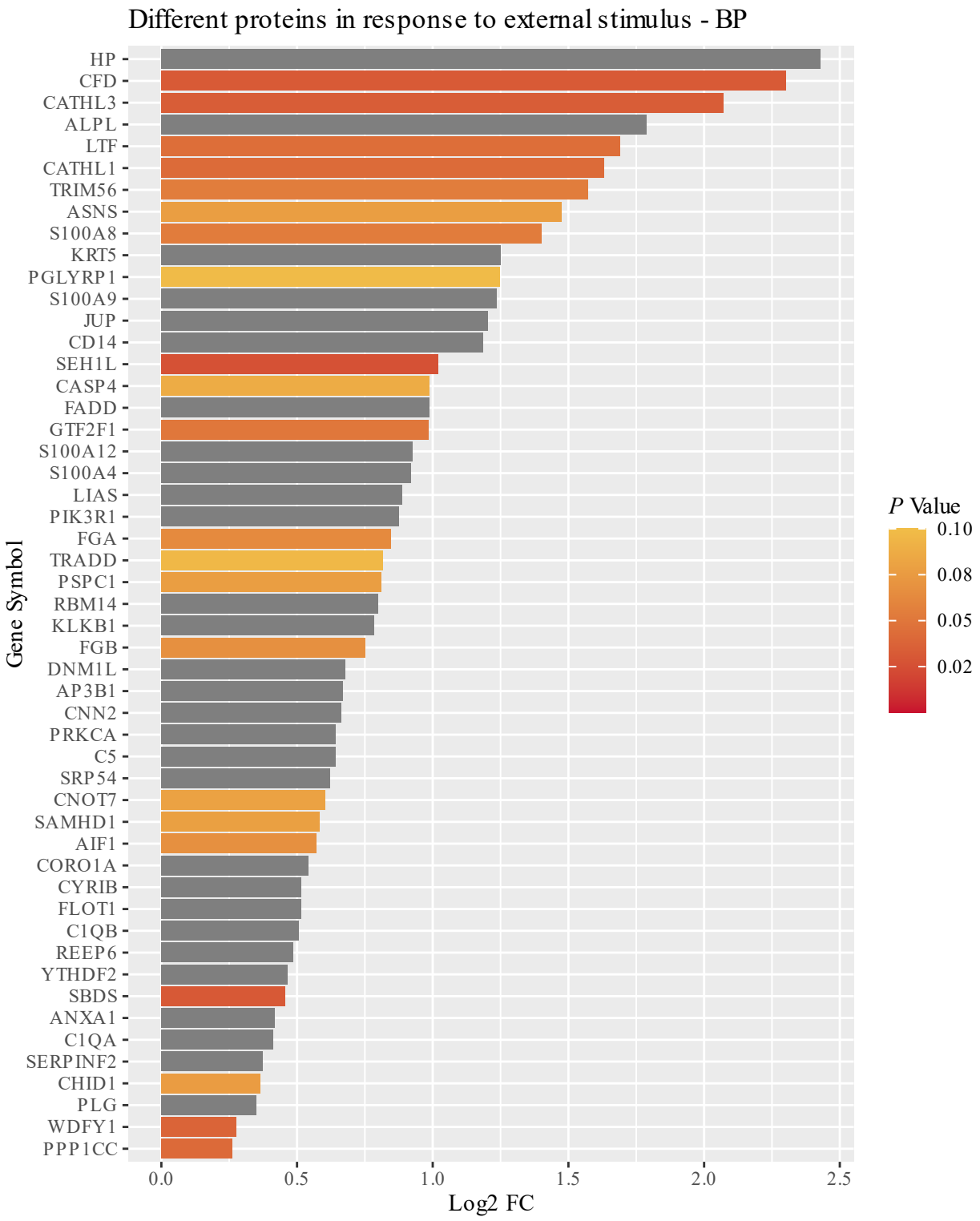

Figure 217. *Post hoc* analysis of proteins involved in response to external stimulus pathway in successful liver abscess induction (LAIP-Y) relative to control (CON).

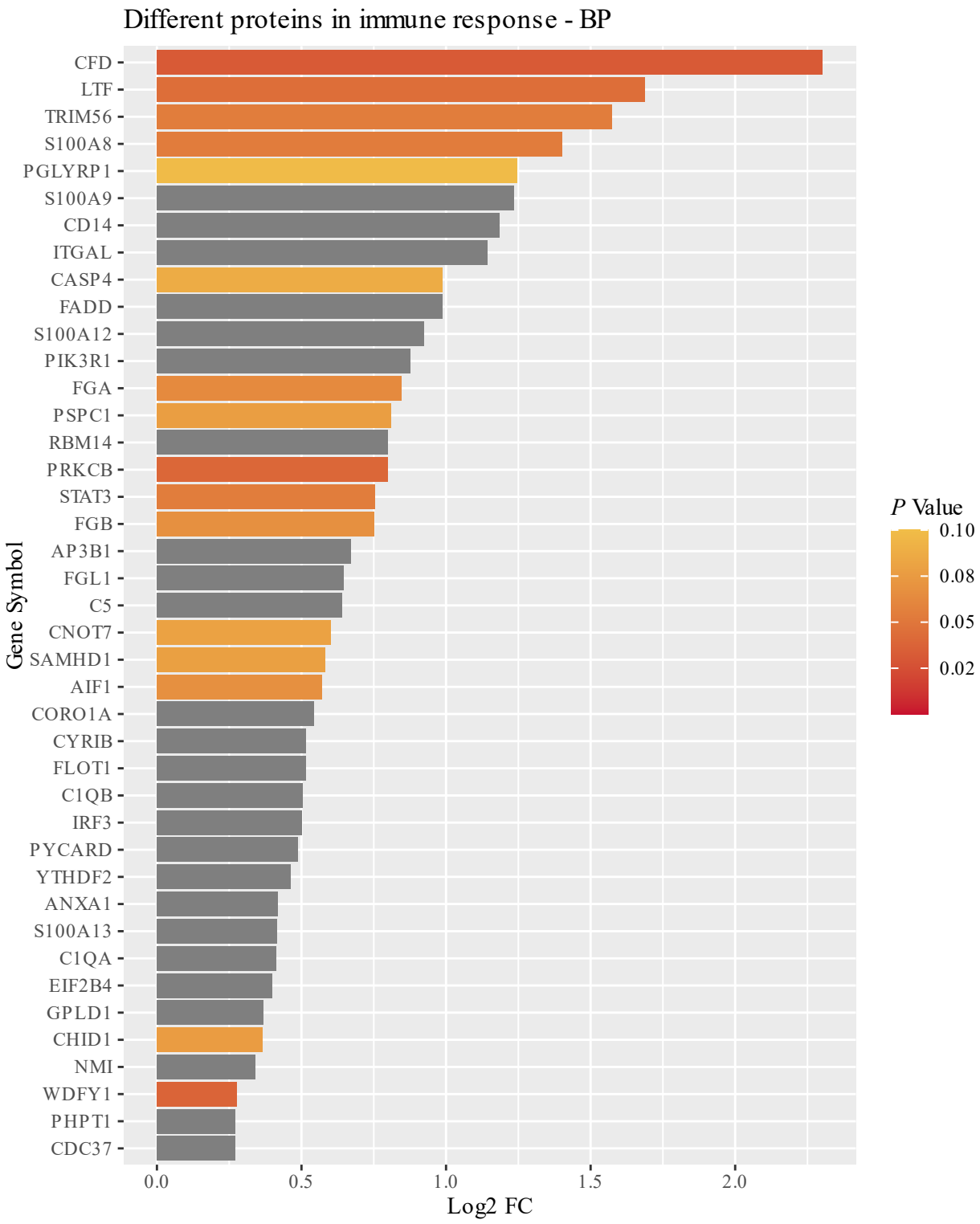

Figure 218. *Post hoc* analysis of proteins involved in immune response pathway in successful liver abscess induction (LAIP-Y) relative to control (CON).

Liver Abscess Induction Model
Study Number: GJC-LHB-3

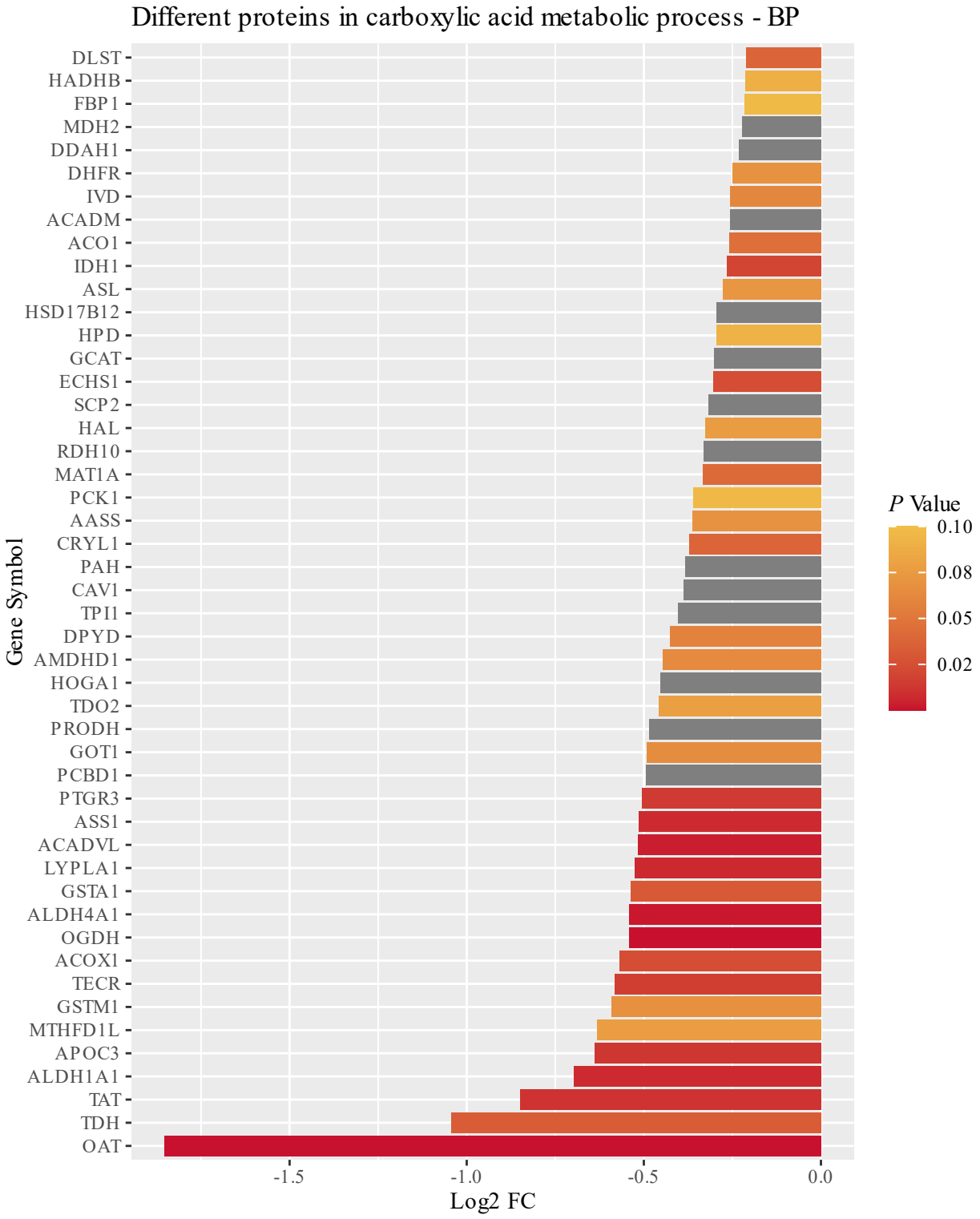

Figure 219. *Post hoc* analysis of proteins involved in carboxylic acid metabolic process pathway in liver abscess induction protocol (LAIP) relative to control (CON).

Liver Abscess Induction Model
Study Number: GJC-LHB-3

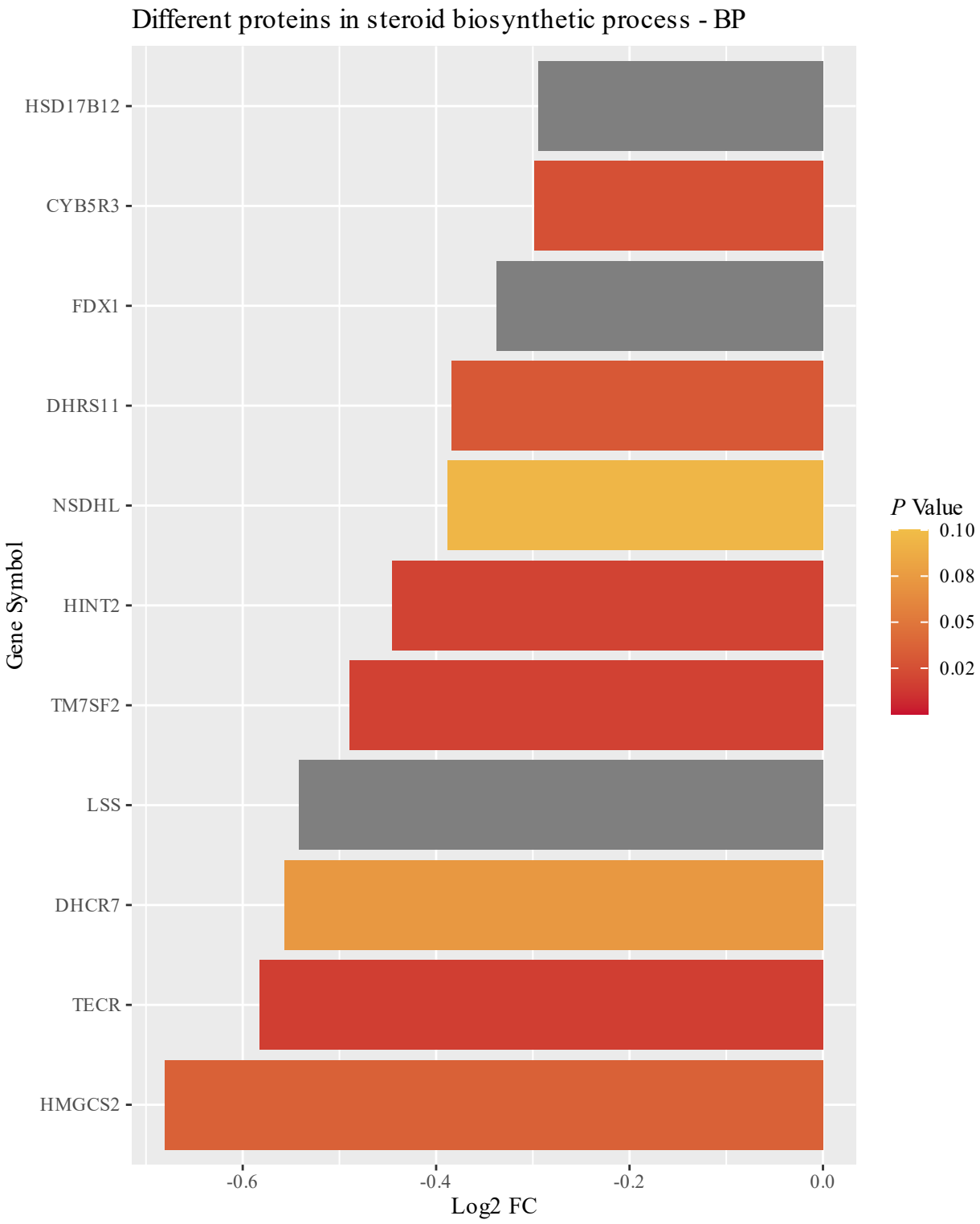

Figure 220. *Post hoc* analysis of proteins involved in steroid biosynthetic process pathway in liver abscess induction protocol (LAIP) relative to control (CON).

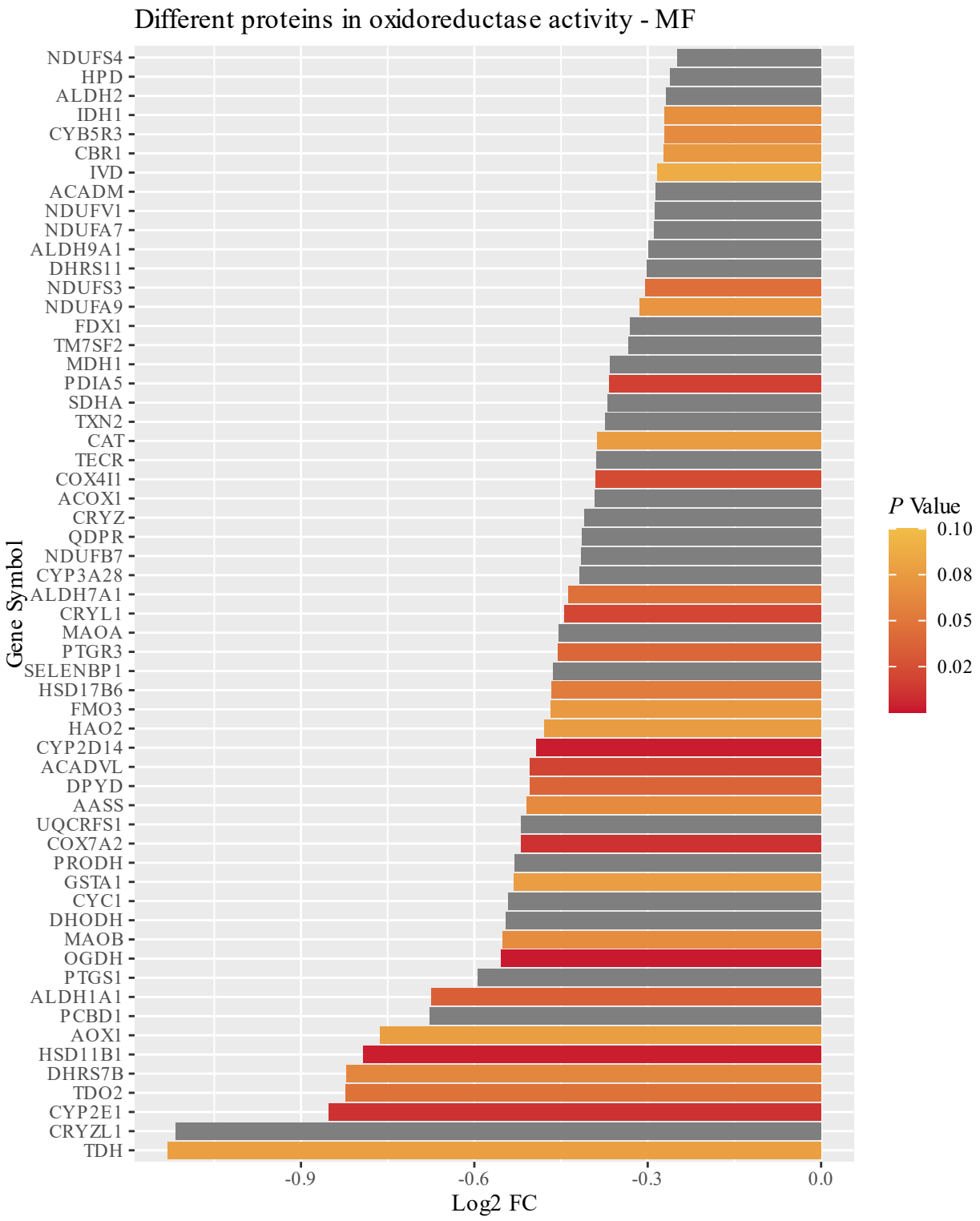

Figure 221. *Post hoc* analysis of proteins involved in oxidoreductase activity pathway in failed liver abscess induction (LAIP-N) relative to control (CON).

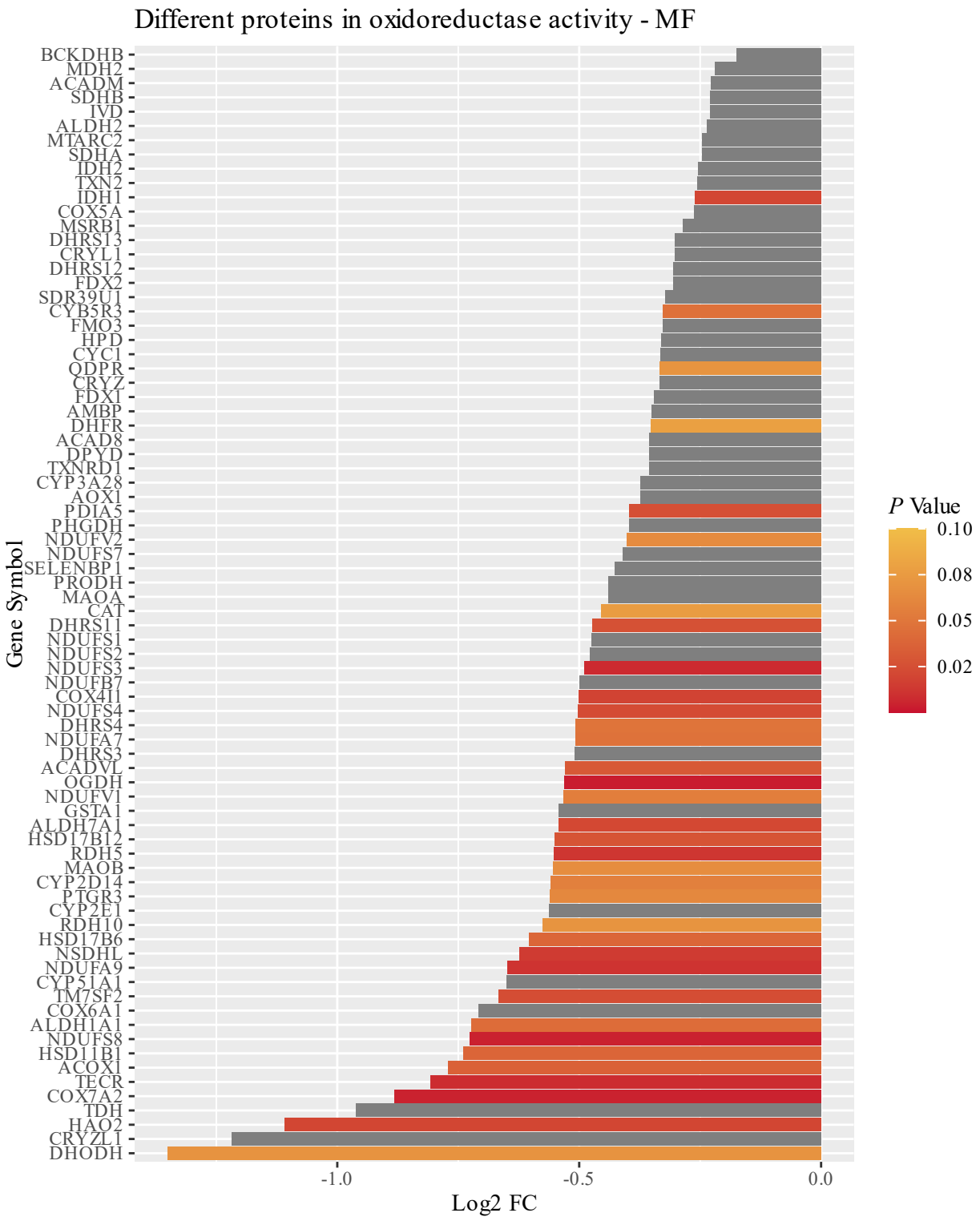

Figure 222. *Post hoc* analysis of proteins involved in oxidoreductase activity pathway in successful liver abscess induction (LAIP-Y) relative to control (CON).

Liver Abscess Induction Model
Study Number: GJC-LHB-3

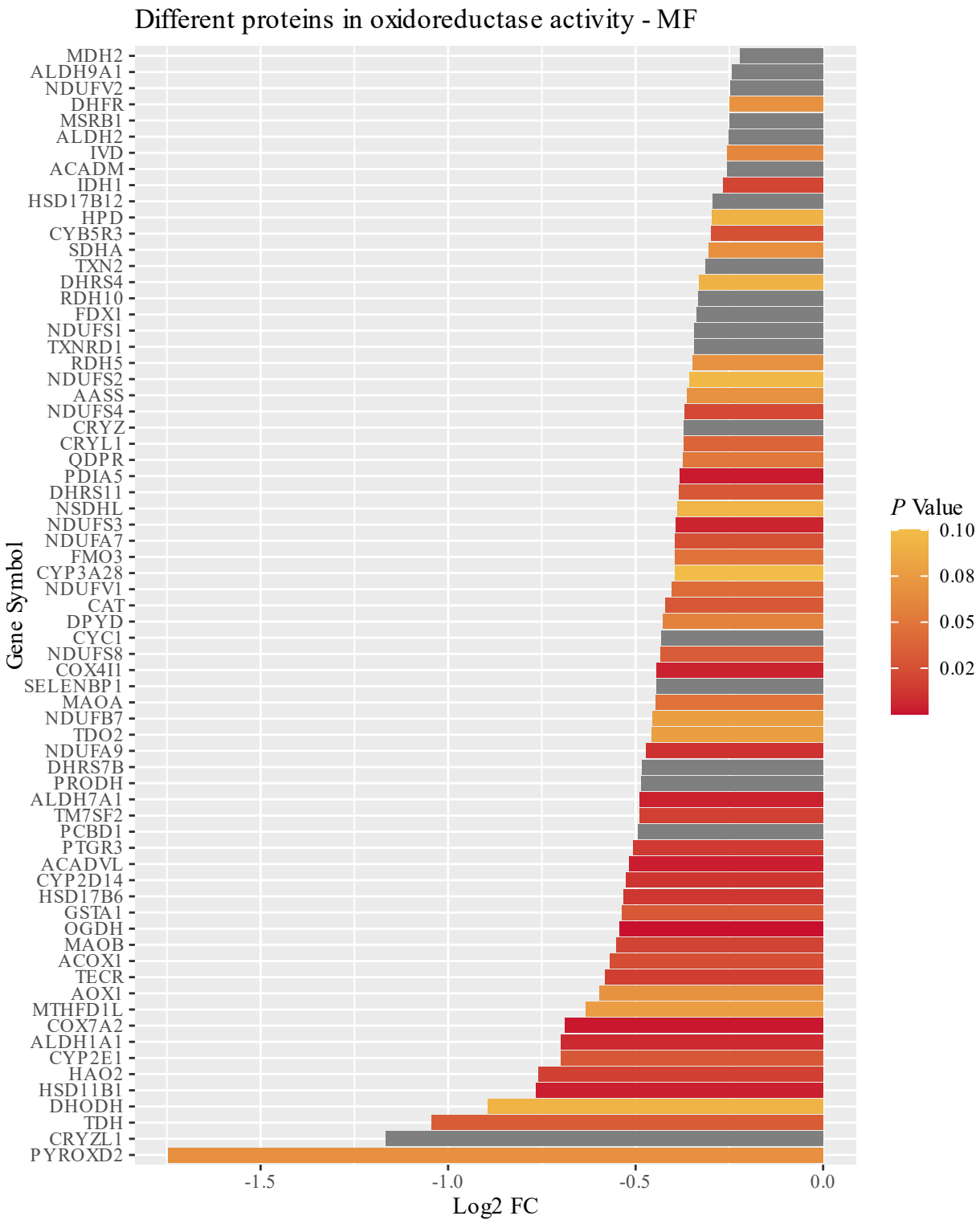

Figure 223. *Post hoc* analysis of proteins involved in oxidoreductase activity pathway in liver abscess induction protocol (LAIP) relative to control (CON).

Liver Abscess Induction Model
Study Number: GJC-LHB-3

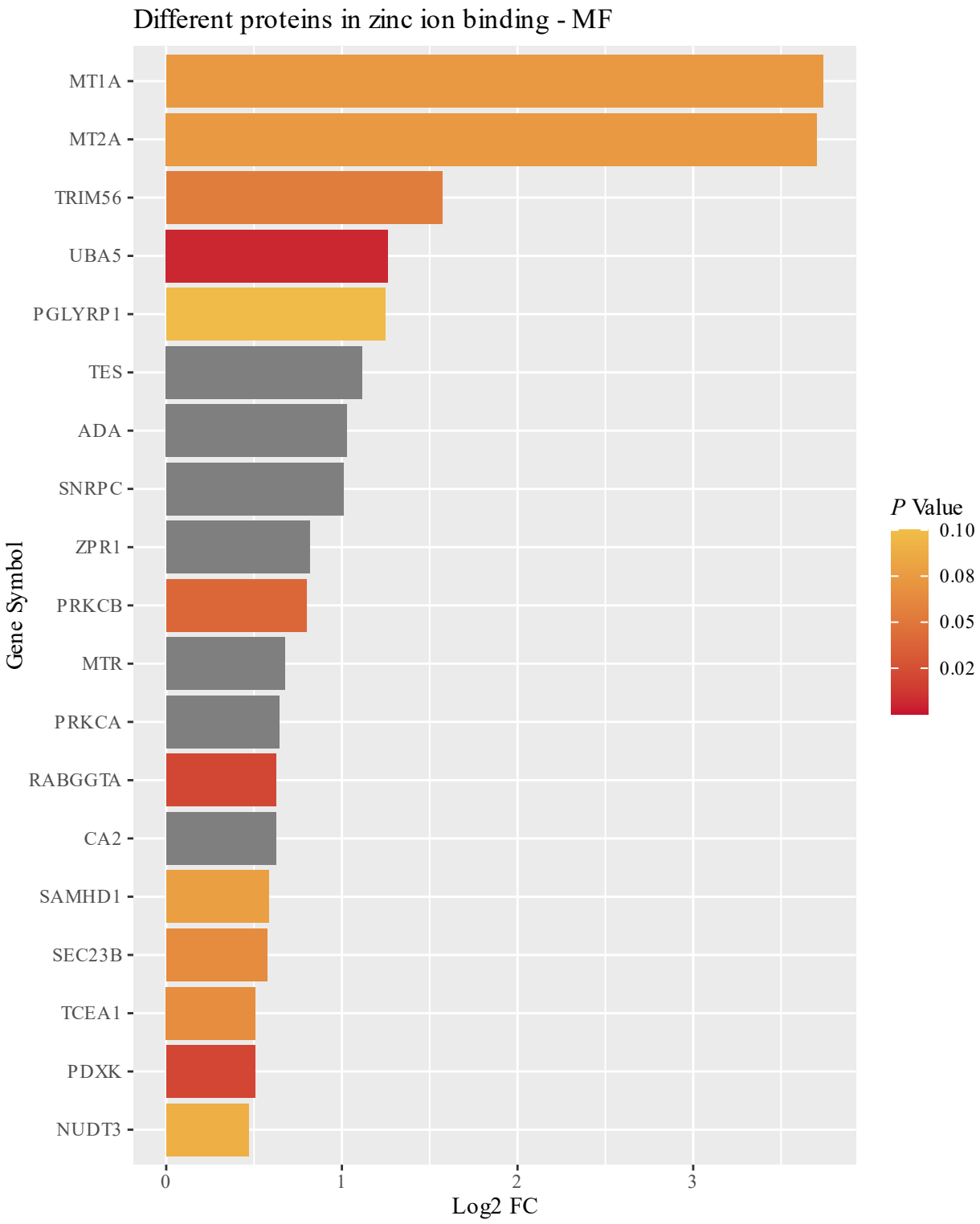

Figure 224. *Post hoc* analysis of proteins involved in zinc ion binding pathway in successful liver abscess induction (LAIP-Y) relative to control (CON).

Liver Abscess Induction Model
Study Number: GJC-LHB-3

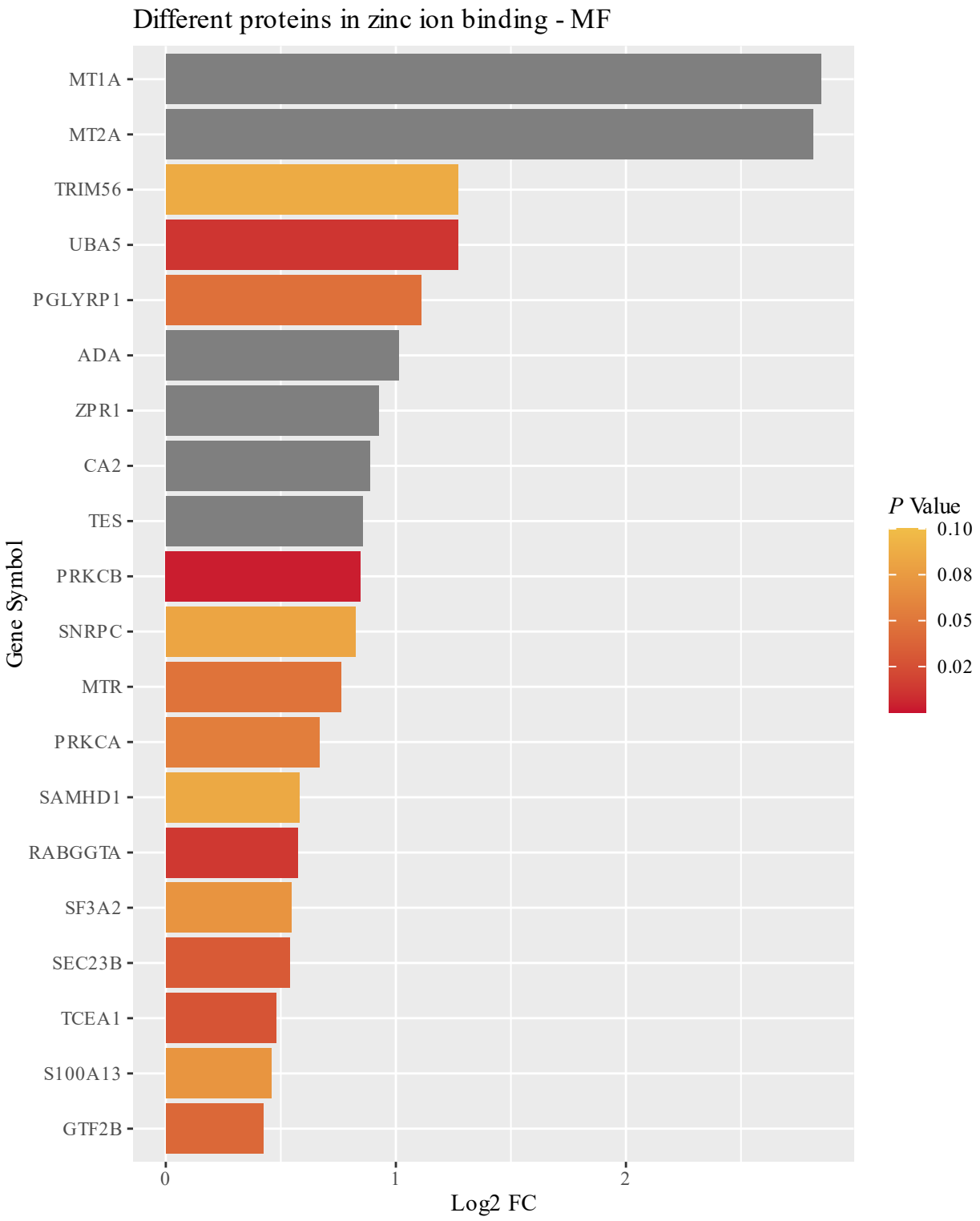

Figure 225. *Post hoc* analysis of proteins involved in zinc ion binding pathway in liver abscess induction protocol (LAIP) relative to control (CON).

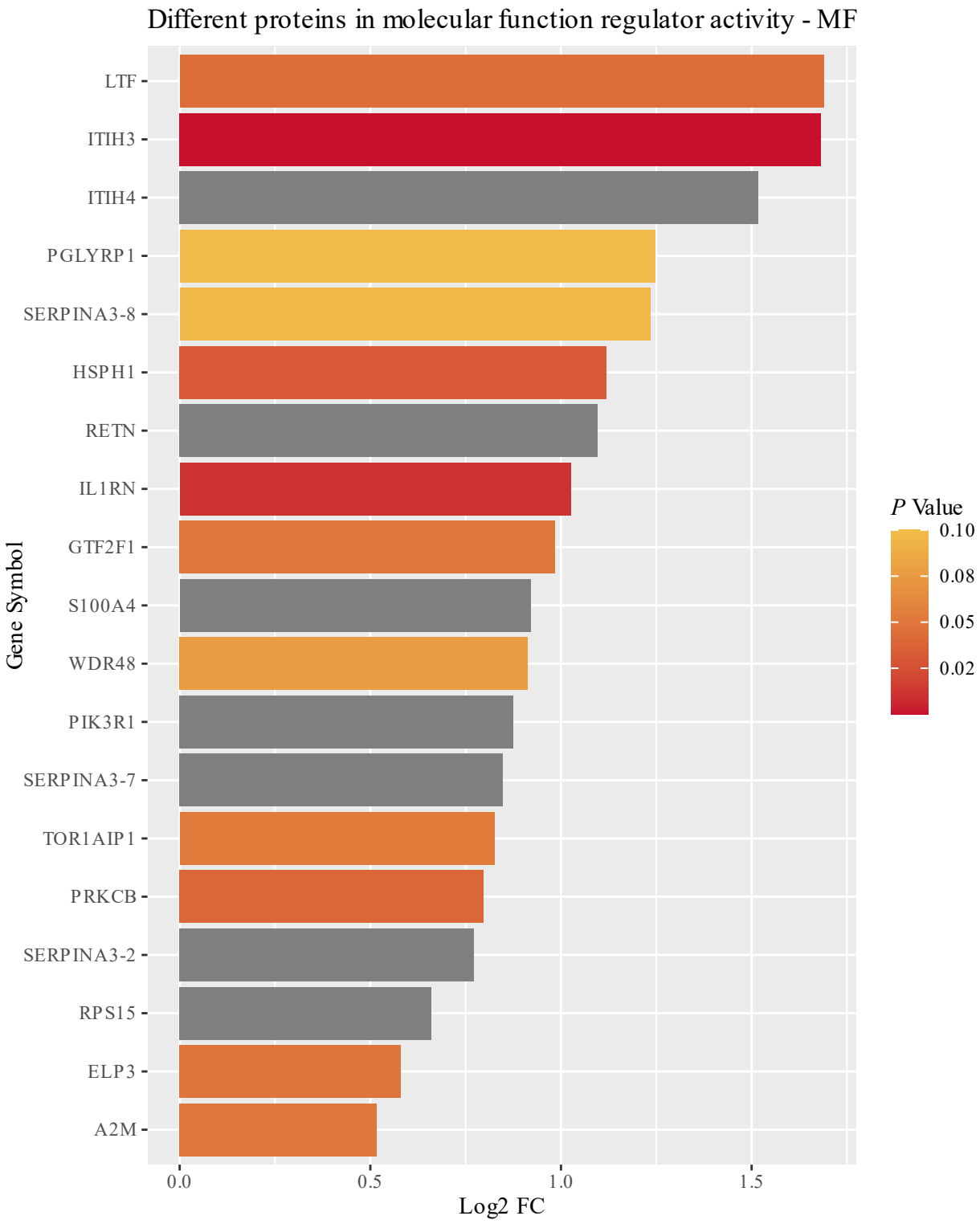

Figure 226. *Post hoc* analysis of proteins involved in molecular function regulator activity pathway in successful liver abscess induction (LAIP-Y) relative to control (CON).

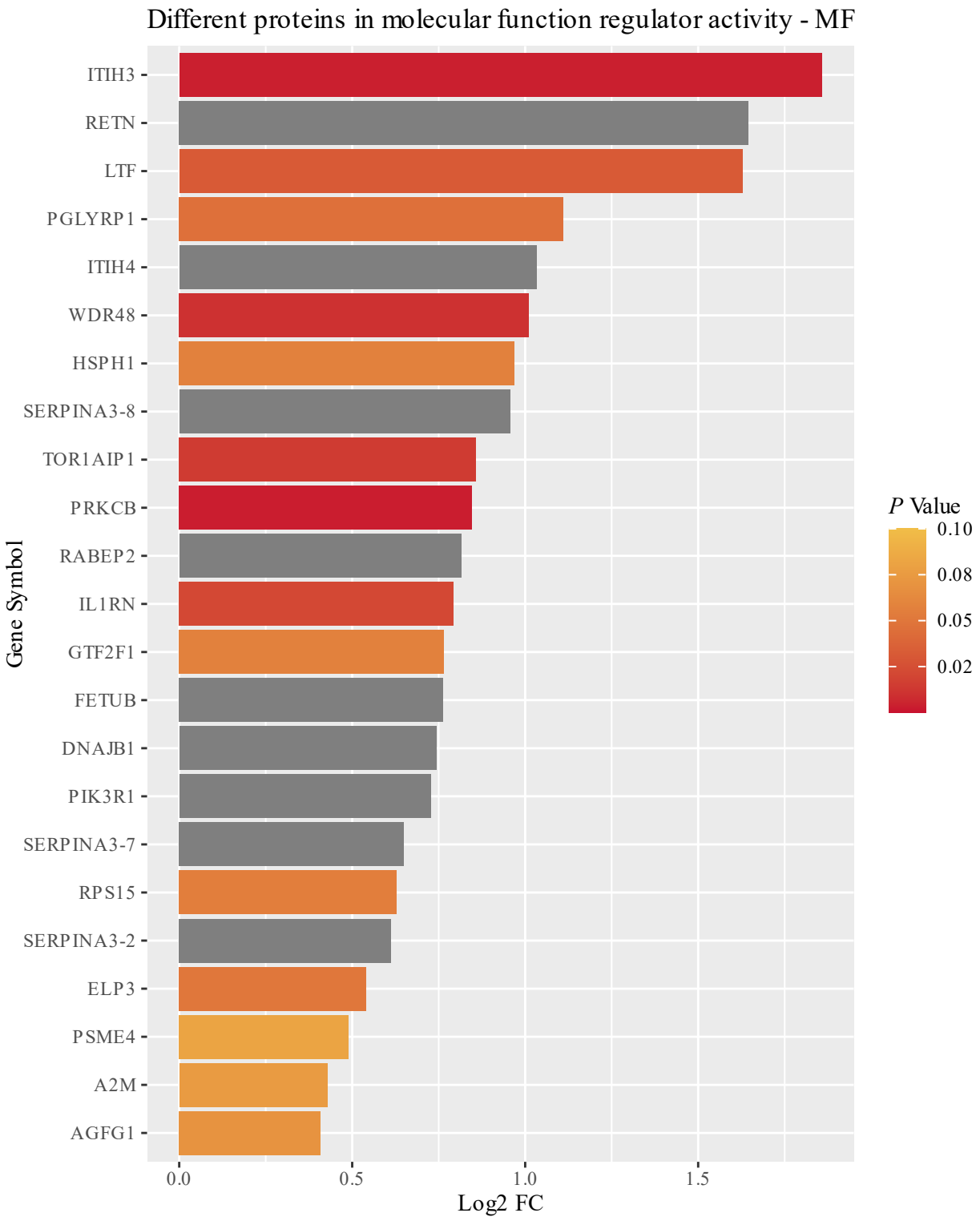

Figure 227. *Post hoc* analysis of proteins involved in molecular function regulator activity pathway in liver abscess induction protocol (LAIP) relative to control (CON).